

VARIABILITY OF BLADE VIBRATION
IN MISTUNED BLADED DISCS

A thesis submitted to the University of London
for the degree of Doctor of Philosophy

By
Yum Ji Chan

Department of Mechanical Engineering
Imperial College London

October 2009

Abstract

The huge variation in forced vibration response levels of mistuned bladed discs, which are bladed discs with slightly different blades, is investigated in this thesis. The issue is known as the blade mistuning problem. A mistuning management strategy is proposed and assembled to manage the high vibration response levels of mistuned bladed discs. This strategy involves (i) evaluation of the range of the response level, (ii) achieving a better bladed disc design, and (iii) monitoring the status of the actual hardware.

The severity of the vibration problem of a mistuned bladed disc is usually quantified by the “amplification factor”, which is clearly defined in this thesis to remove inconsistency among previous definitions. A new procedure is proposed to estimate the small probabilities of high amplification factors more accurately and more efficiently than is possible with typical Monte Carlo simulations.

By casting the blade mistuning problem as a robust design problem, parameter design and tolerance design concepts are used to find methods of improving robustness of bladed discs. The design parameters of the bladed disc design are changed in parameter design while, in contrast, the mistuning parameter distribution on a bladed disc is controlled in tolerance design.

If the blades and the disc form a single component (also known as a blisk), the uncertainties of joint properties are removed and the responses of the bladed disc can be predicted. A response-prediction procedure proposed previously is validated experimentally, and the quality of experimental data required is evaluated.

The investigation in this thesis has shown that a mistuning management strategy is viable. A new procedure is developed to fulfil (i), design guidelines are formed to facilitate (ii), and the monitoring in (iii) is practical in the foreseeable future.

Acknowledgments

I am grateful to Prof. D. J. Ewins for his commitment after his end of full-time service at Imperial College London. His guidance demonstrated good research practices, and his advice in concise technical writing can be seen everywhere in this thesis. The feedback from Prof. M. Imregun on my research is acknowledged.

I enjoy the professional and social discussions with my colleagues in the Dynamics Section, including Dr. E. P. Petrov, Dr. C. Zang, Dr. C. Schwingshackl, Dr. M. Nikolic, Dr. Sen Huang, Dr. D. Di Maio, Mr. A. Gondhalekar and the ERASMUS students. Special acknowledgment is given to Dr. D. Di Maio for his help in setting up the experimental rig, on which the results in Chapter 7 of this thesis is based. The help of Ms. N. Hancock on the administrative work is appreciated.

My thanks is also due to several staff members from the Department of Mathematics. The discussion with Dr. G. Moore was constructive, and the content in Appendix E is based on the advice of Dr. R. Jacobs. The pastoral care from Dr. G. Stephenson is exceptional, and his support went as far as reading my thesis voluntarily.

My studies at Imperial College would be much less enjoyable, or even impossible, without the support of several persons outside the College. Dr. M. G. Sainsbury stimulated my interest in structural dynamics and recommended me reading a doctoral degree at his *alma mater*. My parents, Fu-Chai Chan and Yuen-Yee Lai, have provided the finances and encouraged my intellectual explorations, and my sisters, Wancy and Mancy, have advised on my well-being with their expertise. Last but not least, I wish to express my gratitude to Leonie Lee, who has been understanding, supportive and caring throughout my academic adventures in Europe.

Contents

Nomenclature	vii
Abbreviations	xi
List of Figures	xii
List of Tables	xvi
1 Introduction	1
1.1 Overview	1
1.2 A Mistuning Management Strategy	3
1.3 Objectives of the current research	4
1.4 An overview of the thesis	4
2 Literature review	6
2.1 Introduction	6
2.2 Current developments in the blade mistuning problem	7
2.2.1 Our ability of analysing mistuned bladed discs	8
2.2.2 Range of response levels in mistuned bladed discs	11
2.2.3 Sensitivity studies	17
2.2.4 Intentional mistuning approach	18
2.2.5 Blisks and the need of mistuning identification	19
2.3 Questions to be answered in this thesis	20
2.4 A brief review of robust design concept	21
2.5 Summary	23
3 Evaluation of the range of the amplification factor	24
3.1 Introduction	25

3.2	Evaluation of the worst scenario: the quest to find a realistic maximum amplification factor	29
3.2.1	Upper bound of the amplification factor	29
3.2.2	Numerical search of the maximum amplification factor	33
3.3	Current approach of amplification factor distribution prediction	36
3.4	A new procedure to predict the probabilities of occurrence of extreme amplification factors	39
3.4.1	Introduction to the importance sampling method . . .	40
3.4.2	Importance sampling method in the blade mistuning problem	43
3.4.3	Demonstration	44
3.5	Summary	48
4	Application of robust design concepts to the blade mistuning problem	49
4.1	Introduction	50
4.2	Terminology	51
4.3	Introduction to major robust design methods	53
4.3.1	The Taguchi method	53
4.3.2	The Robust Optimisation method	57
4.4	Casting the blade mistuning problem as a robust design problem	59
4.4.1	Input parameters to the amplification factor function .	59
4.4.2	Robustness functions to be investigated	61
4.4.3	Outline and approach of investigation	64
4.5	Summary	66
5	Improving robustness of bladed discs by parameter design	67
5.1	Introduction	68
5.2	Significance of the blade mistuning problem in high cycle fatigue	68
5.3	Dependence of robustness on bladed disc design parameters .	70
5.3.1	Models to be used in the analyses	71
5.3.2	Maximum adjusted amplification factor of a 6-DOF model	74
5.3.3	Maximum adjusted amplification factors of four 64-sector models	76
5.3.4	Maximum amplification factors of six 24-sector blisks	80

CONTENTS

5.4	Robustness of bladed disc designs in previous research	82
5.5	Amplification factor distribution in special situations	87
5.5.1	Amplification factor distribution in bladed discs with damping mistuning	87
5.5.2	Amplification factor distribution with excitation of modes in veering regions	88
5.5.3	Amplification factor distribution in apparently-tuned bladed discs	91
5.6	Summary	92
6	Improving robustness of bladed discs by tolerance design	94
6.1	Introduction	95
6.1.1	Issues related to the “large mistuning concept”	96
6.2	Maximum amplification factor sensitivity to mass mistune	97
6.2.1	Derivation	97
6.2.2	Analysis	99
6.2.3	Demonstration	100
6.3	A new definition of interblade coupling ratio	102
6.4	Managing blade responses using a small mistuning approach	104
6.4.1	Dependence of robustness on level of input variability	106
6.4.2	Excitation of mode shapes in the veering region	110
6.5	Feasibility of the intentional mistuning approach	111
6.5.1	Determination of the consequences of intentional mis- tuning using the importance sampling method	112
6.5.2	Evaluation of a linear intentional mistuning pattern	113
6.6	Summary	117
7	Predicting vibration response levels of integral bladed discs (blisks)	119
7.1	Introduction	119
7.2	Outline of a response level prediction procedure	121
7.3	Experimental demonstration of the proposed procedure	123
7.3.1	Mistuning pattern 1	126
7.3.2	Mistuning pattern 2	128
7.4	Robustness of the proposed procedure	132
7.4.1	Major sources of error in modal testing	133

CONTENTS

7.4.2	Robustness of the predicted response	135
7.4.3	Identification of the damping mistuning pattern	138
7.5	Recommendations for future experimental work	140
7.6	Summary	141
8	Conclusions	143
8.1	Conclusions	143
8.1.1	Efficient estimation of small probabilities	144
8.1.2	Reduction of the variability of responses in blades	145
8.1.3	Validation of a response-prediction procedure	148
8.2	Major contributions to knowledge	149
8.3	Recommendations for future research	150
A	Modal properties of bladed discs	151
B	Implementation of the cross entropy method	154
B.1	Outline of the algorithm	156
C	First-order derivatives of natural frequencies and mode shapes	158
C.1	Derivatives of non-repeated natural frequencies	158
C.2	Derivative of a mode shape	159
C.3	Natural frequency and mode shape derivatives of double modes	160
C.4	Summary	161
D	Sensitivity of the maximum adjusted amplification factor	162
D.1	Simplifying the vibration responses derivatives vector	162
D.2	Analysing the adjusted amplification factor sensitivity	165
E	Pdf of the sum of random numbers of different distributions	167
F	The Fundamental Mistuning Model (FMM) and FMM-ID algorithms	169
F.1	The Fundamental Mistuning Model (FMM) algorithm	169
F.2	The FMM-ID algorithm	173
G	Parameters of an intentionally-mistuned blisk test piece	177
	References	180

Nomenclature

$[\Phi]$	Multiple mode shapes of a vibration system, where double modes are arbitrarily assigned
$[\Psi]$	Multiple mode shapes of a vibration system, where double modes are specified
Ω	Forced harmonic excitation frequency (in $\text{rad}\cdot\text{s}^{-1}$ unless otherwise specified)
Ω_r	Rotation speed of bladed disc (in rev/min)
α	Scaling coefficient
$\{\beta\}$	Modal weighting factors vector
γ	The adjustment factor in the conjugate gradient optimisation method
γ	The pass ratio in the cross entropy method
δ	Degree of intentional mistune
η	Structural damping loss factor
θ	Phase angle
μ	The mean of a random variable
σ	The standard deviation of a random variable
$\Delta\sigma$	Alternating stress experienced on a component
$\{\psi\}$	A mode shape of a vibration system, and the mode shape of a double mode is specified
ω	Natural frequency (in $\text{rad}\cdot\text{s}^{-1}$ unless otherwise specified)
ω_M	Natural frequency of a mistuned blisk
A	Amplification factor

CONTENTS

A_0	Threshold amplification factor
\hat{A}	The maximum amplification factor found in an optimisation analysis
A_{99}	The 99 th percentile amplification factor
\hat{A}_{WH}	The Whitehead Factor = $\frac{1}{2} (1 + \sqrt{N})$
E_i	Energy input/output of Sector i
$E_f(h\{x\})$	Expectation of the function ($h\{x\}$), with the pdf of the random variables equals to ($f\{x\}$)
$H(\{z\}, \{x\})$	Robustness function
K	Characteristic intersector stiffness
$[K]$	Stiffness matrix
K_G	Characteristic stiffness of the grounding spring in a 2 degree-of-freedom (DOF) per sector model
L_f	Fatigue life of a component
M	Characteristic disc sector mass in a 2-DOF-per-sector model
$[M]$	Mass matrix
N	Number of sectors (or blades) in a bladed disc
R	Number of samples in a simulation
S	Mode splitting parameter
T	Period of vibration
$a(\{x\})$	Amplification factor function
b_l, b_η	Coefficients related to the mass mistuning pattern
c	Interblade coupling ratio
$\{f\}$	Forced excitation pattern vector
$f(\{x\})$	Probability density function
$\{g\}$	Gradient vector in optimisation analysis
$g(\{x\})$	Sampling density function
$\{h\}$	Line search direction in optimisation analysis

CONTENTS

$h(\{x\})$	An arbitrary function in demonstrations, unless otherwise specified
i	Indexing variable
j	$=\sqrt{-1}$, unless otherwise specified
k	Characteristic blade stiffness
l	Mode index
m	Characteristic blade mass
n	Number of nodal diameters or the engine order
p	Probability
p_{DMC}	Probability estimate from a Direct Monte Carlo simulation
p_{IS}	Probability estimate from an Importance Sampling simulation
Δp	Half-width of the confidence interval
s^2	Sample variance
t	Time, unless otherwise specified
u	Displacement / forced vibration response level
$w(\{x\})$	Likelihood ratio in the importance sampling method
$\{x\}$	Mistuning pattern vector
$\{z\}$	Design parameter vector
∇	Gradient operator
$[\cdot]$	A matrix quantity
$\{\cdot\}$	A vector quantity
$\{\cdot\}^T$	Matrix / vector transpose
$\angle\theta$	$e^{j\theta}$
$[\cdot]^H, \{\cdot\}^H$	Hermitian transpose of a matrix (or vector)
x'	Derivative of x
\bar{x}	Complex conjugate of x
\check{x}	The minimum value of x
\hat{x}	The maximum value of x

CONTENTS

$\{\tilde{x}\}$ Discrete Fourier transform of $\{x\}$

$\text{Re}(u)$ The real part of u

$\text{Im}(u)$ The imaginary part of u

Abbreviations

Blisk	Integral bladed disc
DMC	Direct Monte Carlo
DOF(s)	Degree(s) of freedom
EO	Engine order
FMM	Fundamental Mistuning Model
FRF	Frequency response function
LDV	Laser Doppler vibrometer
MAC	Modal assurance criterion
ND	Nodal diameter(s)
pdf	Probability density function

List of Figures

3.1	Blade responses in tuned and mistuned 64-bladed discs. . . .	26
3.2	Blade responses against blade-alone frequencies of a bladed disc.	26
3.3	Blade responses against blade-alone frequencies in many bladed discs.	28
3.4	Search paths of optimisation algorithms on a 2-D plane. . . .	35
3.5	Typical probability density functions of amplification factor and partial amplification factors.	36
3.6	Amplification factor pdf, with the highest values sought using various methods in a 24-bladed disc design.	38
3.7	A “bombing problem” proposed by Asmussen and Glynn [4].	40
3.8	Probability density function of being hit.	41
3.9	Integral bladed disc (blisk) under investigation.	45
3.10	Amplification factor pdf, with the highest values sought using various methods.	46
3.11	Local worst mistuning patterns found in optimisation analysis.	46
3.12	Probabilities of amplification factors exceeding given thresholds.	47
3.13	Dependence of efficiency of the new procedure over DMC simulations on probability estimate.	48
4.1	Schematic of a non-robust system.	50
4.2	Schematic of an improved system.	51
4.3	Two steps in parameter design, after Park et al [85].	54
4.4	Robust optimal design missed in discretisation.	56
4.5	Non-additivity of robustness improvements.	57

LIST OF FIGURES

4.6	A Campbell diagram, after Sever [117].	62
4.7	Relationship between input variability and output variability in the blade mistuning problem, according to approaches based on (a) probabilistics and (b) interval analysis.	65
5.1	Fatigue life of a coated superalloy, after Wright et al [144].	70
5.2	Layout of a 6-DOF cyclic lumped parameter model.	72
5.3	Layout of a 64-sector lumped parameter model.	72
5.4	Layout of a 24-sector blisk.	73
5.5	Cross sections of the disc part of 24-sector blisk models.	74
5.6	Natural frequencies of the first mode family in six blisk models.	75
5.7	Dependence of the maximum adjusted amplification factor on interblade coupling and damping under 1EO excitation.	76
5.8	Dependence of the maximum adjusted amplification factor on interblade coupling and damping under 3EO excitation.	77
5.9	Normalised natural frequencies of 64-sector models.	78
5.10	Magnified plot of Figure 5.9.	79
5.11	Dependence of the adjusted amplification factor on damping loss factor in 64-sector models.	80
5.12	Dependence of maximum vibration responses on damping loss factor in tuned and mistuned models.	80
5.13	Dependence of the maximum amplification factor on damping loss factors in 24-sector blisks.	82
5.14	Blisk PS, after Myhre [78].	83
5.15	Natural frequencies of the first four mode families of Blisk PS, both stationary and rotating, after Myhre [78].	84
5.16	Natural frequencies of the first four mode families of Blisk NS, both stationary and rotating, after Myhre [78].	84
5.17	Models analysed by Petrov and Ewins [89].	85
5.18	Selected normalised natural frequencies of models analysed by Petrov and Ewins [89].	85
5.19	Locations of four bladed disc designs adopted in previous research in the robustness map.	86
5.20	Adjusted amplification factor pdfs under various levels of damping mistuning.	88

LIST OF FIGURES

5.21	Selected normalised natural frequencies of Models 64C and 64E.	89
5.22	Tuned vibration response levels of Models 64C and 64E under various EO excitations.	90
5.23	Adjusted amplification factor pdfs of Models 64C and 64E.	90
5.24	Correlation between the adjusted amplification factor and the resonance frequency.	91
5.25	Adjusted amplification factor pdfs of all and selected samples.	92
5.26	Adjusted amplification factor pdfs of (a) apparently tuned bladed discs and (b) mistuned bladed discs.	93
6.1	Dependence of the maximum adjusted amplification factor on maximum allowable mistune in three 6-DOF examples.	101
6.2	A magnified plot of Figure 6.1.	101
6.3	Locations of selected bladed disc designs in the robustness map.	105
6.4	Small mistuning regions according to the approaches discussed in Section 4.4.2.	105
6.5	Dependence of 99.9 th percentile amplification factor on mistuning scatter.	107
6.6	Dependence of 99.9 th percentile amplification factor on mistuning scatter in various blisks.	107
6.7	Maximum adjusted amplification factors of Models 64A, 64B and 64D under various levels of mistune.	108
6.8	Maximum adjusted amplification factors under 6EO excitation, various levels of mistune and damping loss factors.	108
6.9	Maximum adjusted amplification factor under various levels of mistune.	111
6.10	Linear mistuning pattern with a mistuning strength of 2%.	114
6.11	Dependence of the 50 th , 99 th and 99.9 th percentiles amplification factor on level of intentional mistuning.	115
6.12	Amplification factor cumulative distribution functions under various levels of intentional mistuning.	116
6.13	A magnified plot of Figure 6.12.	116
6.14	Stairs and linear mistuning patterns.	117

LIST OF FIGURES

7.1	Amplification factors before and after perturbation.	121
7.2	Predicting the amplification factor of a mistuned blisk.	123
7.3	Experimental setup.	124
7.4	Selected mistuned blades of the blisk test piece.	125
7.5	Natural frequencies of the model and the test piece.	127
7.6	MAC function between identified mode shapes from Test 1A and travelling modes of the finite element model.	127
7.7	Argand diagram of an identified mode shape.	128
7.8	Identified mistuning patterns in Tests 1A and 1B.	128
7.9	Comparison of identified mode shapes.	129
7.10	MAC function between identified mode shapes from Tests 2A, 2B and 2C.	129
7.11	Identified mistuning patterns based on all identified modes. . .	130
7.12	MAC function between identified modes and selected recon- structed modes.	131
7.13	Identified mistuning patterns based on selected modes.	132
7.14	Measurement and excitation points in simulations.	134
7.15	Receptance FRFs under various excitation points.	134
7.16	Point receptance FRFs around a pair of natural frequencies. . .	136
7.17	Modal constants of a point receptance FRF.	136
7.18	Distribution parameters of identified frequency mistuning pat- terns using noisy modes.	140
7.19	Distribution parameters of identified damping mistuning pat- terns using noisy modes.	140
7.20	Improved response-prediction procedure.	142
A.1	Natural frequencies of a 24-sector blisk.	152
A.2	Two types of modes found on a bladed disc.	152
A.3	Effect of mistune on (a) natural frequencies of the bladed disc and (b) nodal diameter components of modes in a family. . .	153
G.1	Mistuning assemblies with (a) countersunk and (b) cap screws.	178

List of Tables

2.1	Major contributors to the blade mistuning problem since 1990.	7
3.1	Dependence of probability estimate on centre of sampling distribution.	42
4.1	Definitions of the signal-to-noise ratio, after Taguchi [129]. . .	54
5.1	Whitehead Factors and maximum amplification factors of bladed disc designs investigated by Petrov and Ewins [89]. . .	71
5.2	Ranges of parameters applied to the 6-DOF model.	75
5.3	Design parameters of 64-sector models analysed, and those of the 36-sector model after Afolabi [2].	78
5.4	Levels of interblade coupling and maximum (or 99 th percentile) amplification factors of bladed disc designs, after References [78] and [89].	86
5.5	Design parameters of Models 64C and 64E.	89
6.1	Interblade coupling ratios of bladed disc designs analysed in Sections 5.3.3 and 5.3.4.	104
7.1	Experimental tests presented in this thesis.	125
7.2	Comparison of key identified response parameters.	132
7.3	Impact of mode identification error on the predicted peak response level.	138
G.1	Masses of representative components installed at blade tips. .	177
G.2	Masses and components installed in Mistuning pattern 2. . .	179

Chapter 1

Introduction

The effects of small variations between blades, known as **mistuning**, on the vibration response levels of bladed discs in gas turbines are investigated in this thesis. Compared with that of a tuned bladed disc, which is a bladed disc with identical blades, the vibration response levels of a mistuned counterpart can be much higher. This issue is called the **blade mistuning problem**. Extensive knowledge on mistuned bladed discs has been gained in the past four decades of research, but there is still a shortfall in providing industry with adequate tools to reduce the costs related to the consequences of mistuning.

A **mistuning management strategy** is proposed in this thesis to manage the blade mistuning problem. The objective of this thesis is to assemble the strategy by reviewing the current tools available and developing new tools. The structure of this thesis is to be described at the end of this chapter.

1.1 Overview

All blades on a bladed disc in a gas turbine are assumed to be identical at the design stage. However, the blades on a given bladed disc are slightly different from each other due to manufacturing tolerances, variations in material properties and wear and tear. The issue to be investigated in this thesis is the effect of the existence of these small variations between the blades, known as mistuning, on the forced vibration response levels of blades in gas turbines. This is known in gas turbine design as the *blade mistuning problem*.

A bladed disc is designed to withstand two types of vibration: flutter and

resonance due to forced excitations. Forced excitation on rotating bladed discs comes from air and gas pressure variations around the annulus due to upstream vanes, and is unavoidable. While mistuning is generally believed to be beneficial for flutter, it is found that small mistuning can lead to a huge variation of peak vibration responses across blades under forced excitation, and the highest vibration response level in a mistuned bladed disc can be much higher than that experienced on a tuned counterpart. For example, a 5% variation in the blade cantilever frequencies on a 92-bladed high pressure turbine disc can lead to one blade suffering a response level of over 500% of that observed on every blade on a tuned bladed disc [89]. The potentially high response levels lead to much shortened fatigue lives on one or few blades due to high cycle fatigue (HCF), while the other blades exhibit good conditions at the same time.

Research in the blade mistuning problem began more than 40 years ago and extensive knowledge about the structural dynamics of mistuned bladed discs has been gained. However, the blade mistuning problem is considered unsolved because industry still faces risk of much shortened fatigue lives and unexpected failure due to high vibration response levels. The cost incurred by high cycle fatigue-related problems is reported to be around \$400 million each year [41], which corresponds to 30% of all jet engine maintenance costs [131].

On the one hand, researchers have tried to understand the forced vibration response level distribution of mistuned bladed discs and wished that the variation of vibration response levels can be greatly reduced by coming up with a better bladed disc design. Alas, there are no indications in the previous research of how this can be achieved. On the other hand, the possibility of mistuning-related failure is usually addressed after an early failure, and not much has been learnt from experience, not least because the mistuning pattern of a failed bladed disc is no longer obtainable.

Given our understanding of bladed disc properties, it is timely to consolidate the current research capability into a strategy suitable to industrial applications.

1.2 A Mistuning Management Strategy

Assuming bladed disc designs without the blade mistuning problem do not exist, a new strategy called the Mistuning Management Strategy (MMS) is proposed to manage, instead of to eliminate, the potentially high vibration response levels in mistuned bladed discs. Vibration response levels in bladed discs are managed by estimating the extent of the problem precisely, finding a best practical design and monitoring mistuning bladed discs in operation more closely. This strategy involves three steps:

Step 1: evaluation of the vibration problem. The potential locations of resonances are identified for a given initial design. The variation of the forced vibration response level at each resonance is calculated, either in terms of the upper bound of the vibration response or the level with an acceptable risk (e.g. the 99.9th percentile).

Step 2: achieving a better bladed disc design. If a significant portion of bladed discs experience unacceptable levels of vibration responses, or the highest response level possible exceeds the acceptable level, design changes are sought to reduce the response levels by a combination of methods. This can include (i) changing the design of the disc or the blade (ii) controlling the mistuning and (iii) adding damping. The benefits and issues related to these consequences are considered by taking these as factors in design optimisation.

Step 3: Monitoring the status of actual hardware. For integral bladed discs (also known as *blisks*), the vulnerability of any specific bladed disc to high cycle fatigue due to mistuning-related issue is checked regularly, both after manufacture and throughout the service life.

The blade mistuning problem is proposed to be considered as a robust design problem because the dependence of response variability on design parameters is required in this strategy. Robust design is a concept which aims to keep the output of a system close to a target (i.e. robust) under variability at input or design parameters. This approach has not been advocated partially because robust design is a new concept in structural dynamics research.

1.3 Objectives of the current research

In this thesis, the Mistuning Management Strategy is assembled using existing and additional tools and techniques. In particular, this thesis aims to achieve

1. *efficient estimation of small probabilities* compared with current Monte Carlo simulation-based methods
2. *reduction of the variability of responses in blades* by changing the design, controlling mistuning and/or adding damping
3. *validation of a response-prediction procedure* recently proposed by Griffin and Feiner [43]

1.4 An overview of the thesis

This thesis is divided into eight chapters.

The current state-of-the-art of the mistuning problem in structural dynamic aspects is reviewed in Chapter 2. The necessary but missing tools in the new mistuning strategy are identified. As the mistuning management strategy is based on robust design concepts, a brief review of available robust design methods is also presented.

The “amplification factor” is examined in Chapter 3. The amplification factor is used to measure the severity of the consequences of mistuning in the vibration response levels of the blades on a mistuned bladed disc, and it is a random variable. The maximum amplification factor, which indicates the worst scenario, and the amplification factor distribution are studied. A new procedure comprising a conjugate gradient-based optimisation analysis and the importance sampling method is presented to tackle industrial need for reliable estimates of the small probabilities related to high amplification factors.

In Chapter 4, the possibility of managing the blade mistuning problem by adopting a robust design concept is discussed. Common robust design methodologies are introduced, and the input variability and robustness in the blade mistuning problem are defined according to approaches either based on (i) probabilistics or (ii) interval analysis.

The robustness of bladed discs is studied in Chapters 5 and 6 following two robust design concepts, namely parameter design and tolerance design. At the beginning of Chapter 5, the dependence of the fatigue life of a superalloy to high cycle fatigue (HCF) failure on vibration response level is discussed. By reducing the variation in blade vibration responses related to blade mistuning, the fatigue lives of blades can be extended significantly and the variations of the fatigue lives of blades on the same bladed disc can be reduced. The potential for decreasing the maximum amplification factor by changing the design parameters, including the level of damping, is investigated using three representative models. The distribution of amplification factor in damping mistuned bladed discs, bladed discs excited in the veering region and apparently-tuned bladed discs are also investigated.

The amplification factor on a mistuned bladed disc is managed in Chapter 6 by controlling the mistuning pattern on a bladed disc either by (i) imposing tight tolerances on blade dimensions, known as the small mistuning approach or (ii) incorporating non-identical blades of specific patterns, known as the intentional mistuning approach. The maximum adjusted amplification factor sensitivity in single-DOF-per-sector systems is derived to provide a guide on the small mistuning approach and a theoretical basis to a new way to quantify the coupling between blades. A tool based on the importance sampling method is used to reduce the computational effort in determining the magnitude of intentional mistuning. The potential of a “linear” pattern to become an intentional mistuning pattern is evaluated.

In Chapter 7, the challenges and opportunities in managing the extreme vibration response levels in mistuned blisks are discussed. As the uncertainty and variability of friction properties related to joints are absent in blisks, the maximum vibration response level of a blisk test piece in operation can be predicted by testing that blisk under controlled conditions. A procedure proposed in previous research for such use is demonstrated experimentally on a test piece. The sources of error in the experiments are analysed and recommendations for future experiments are made.

Chapter 2

Literature review

The current state of the mistuning problem in structural dynamic aspects is reviewed in the current chapter. The necessary but missing tools in the new mistuning strategy are identified. As the mistuning management strategy is based on the robust design concepts, a brief review on available robust design methods is also presented.

2.1 Introduction

Given the amount of the literature related to the blade mistuning problem, the literature review is carried out in a dedicated chapter.

Although the blade mistuning problem is considered unsolved, the forced vibration behaviour of mistuned bladed discs are much better understood. The current state-of-the-art of the blade mistuning problem in structural dynamic aspects is reviewed in Section 2.2 categorically, and the research output in each category is presented in a chronological order. Research related to aeroelastic aspects of mistuned bladed discs is included where appropriate, and the modal properties of bladed discs are explained separately in Appendix A. The previous achievements in understanding the vibration responses of mistuned bladed discs are compared with the needs of the mistuning management strategy proposed in Chapter 1, and the missing components are identified in Section 2.3.

Besides the blade mistuning problem, a brief review of the robust design concept is presented in Section 2.4 to provide a background for the discussion in Chapter 4.

2.2 Current developments in the blade mistuning problem

The origins of vibration analyses of bladed discs and non-symmetric discs can be traced to the work carried out by Armstrong in 1955 [3] and Tobias and Arnold in 1957 [132], respectively. The study of the forced vibration response behaviour of mistuned bladed discs, which is known as the blade mistuning problem, started by Whitehead in 1966 [140], Ewins in 1969 [31] and Dye and Henry in 1969 [30]. Since then, more than 400 papers have been published in topics related to the blade mistuning problem. This review intends to discuss the key research papers in the blade mistuning problem published after 1990. Readers are referred to the literature surveys presented by Ewins [33] and Castanier and Pierre [23] for the earlier developments of the blade mistuning problem, and Srinivasan [127] for an overview of blade vibrations in gas turbines.

The research in the blade mistuning problem is mainly carried out in a handful of research groups around the world. The major contributors to the structural dynamic aspects of the blade mistuning problem after 1990 are listed in Table 2.1, such that the names appearing in the review can be connected to their respective research groups.

Affiliation	Principal investigator	Members
Imperial College London	Ewins	Imregun, Nikolic, Petrov, Sever, Sanliturk, Yiu
Arizona State University	Whitehead	
Carnegie Mellon U.	Mignolet	Choi, Lin, Rivas-Guerra, Xiao
	Griffin	Ayers, Feiner, Kenyon, Rossi, Yang
Duke University	Kielb	Miyakozawa
Pennsylvania State U.	Sinha	
Polish Academy of Sciences	Rzadkowski	
United States Air Force	Cross	Jones
University of Michigan	Pierre	Bladh, Castanier, He, Judge, Lim, Kruse, Óttarsson, Song

Table 2.1: Major contributors to the blade mistuning problem since 1990.

2.2.1 Our ability of analysing mistuned bladed discs

Provision of accurate mistuned bladed disc models

The improved understanding of the vibration response levels of mistuned bladed discs relies on geometrically and physically accurate bladed disc models. The earliest bladed disc models were lumped parameter models [30] and beam-disc assemblies [32], and the vibration response levels were found using receptance methods. The lumped parameter and beam-disc models are still applied occasionally, because these models are small in sizes. Rzadkowski used a beam-disc model in 1994 [108] and added the torsion and warping effects to the beam elements. In the 21st century, Sinha in 2006 [121] and Beirow et al in 2007 [9] used lumped parameter models for statistical study and aerodynamic analysis, respectively.

As computing capabilities in the past 40 years have been dramatically improved, the geometry and material properties of bladed discs can be modelled accurately with the finite element method. However, these models, which can contain as many as 15 million degrees of freedom (DOFs) [89], are not suitable to the blade mistuning problem because the system matrices are too large for Monte Carlo simulations (Section 3.3). To run Monte Carlo simulations using accurate models, methods known as reduced order model (ROM) algorithms have been developed to (i) reduce the sizes of stiffness and mass matrices of a finite element model without losing the key features and (ii) consider the mistuning pattern, which has far fewer parameters than the number of DOFs in a finite element model, as an input parameter instead of a system parameter.

Two major “families” of ROM algorithms have been developed by the research groups at the University of Michigan and Carnegie Mellon University. At the University of Michigan, Castanier et al [19] proposed one of the first ROM algorithms called REDUCE in 1997, and REDUCE was extended to cover shrouded bladed discs in 1999 by Bladh et al [12]. The REDUCE algorithm is refined by Bladh et al in 2001 [13] to become the SMART algorithm, and the most recent version of the ROM algorithm presented by this research group is the component mode mistuning (CMM) method by Lim et al [65] in 2003.

At Carnegie Mellon University, Yang and Griffin [149] began their investigation in ROM algorithms in 1997, and Yang and Griffin [150] proposed

the “subset of nominal modes” (SNM) algorithm in 2001. The SNM algorithm was refined to become the fundamental mistuning model (FMM) in 2002, and the current format of the FMM was published by Feiner and Griffin in 2004 [35]. The FMM algorithm has been applied to reduce the finite element models in investigating the aeroelastic effects of mistuned bladed disc by Kielb et al in 2004 [59] and the effects of intentional mistuning on vibration response levels by Jones in 2008 [52]. Martel et al at Universidad Politécnica de Madrid developed the asymptotic mistuning model (AMM) in 2009 [71] to improve the accuracy of the FMM algorithm in flexible bladed discs.

Several other ROM algorithms have been proposed, for example, Bah et al [6] proposed an algorithm to find the mode shapes of mistuned bladed discs, and an exact reduced order model was developed by Petrov et al in 2002 [94].

In typical ROM algorithms, mistuning is represented either by nodal components like point masses, springs and dampers, as in Petrov et al’s algorithm [94], or by scaling the strain potential energy in blades, as in the FMM [35]. However, the commonest form of mistuning in blades is the variations in blade dimensions. The small differences between ways of representing mistuning can be significant, if the responses are contributed by more than one mode family. Characterisation of geometric mistuning was discussed by Capiez-Lernout et al in 2005 [18]. ROM algorithms taking account of global and local geometric mistuning were proposed by Sinha in 2009 [123] and by Ganine et al in 2009 [40], respectively.

Incorporation of all related physical phenomena

All related physical phenomena have to be included in a blade disc model to predict the vibration response levels of a bladed disc specimen under operating conditions accurately. The physical phenomena considered in previous mistuned bladed disc analysis include

1. the variation of the level of damping between sectors (also known as damping mistuning) in tuned and mistuned bladed discs, which were studied by Muszynska and Jones in 1983 [77] and Lin and Mignolet in 1996 [68], respectively,
2. stress stiffening due to centrifugal forces by Rzadkowski in 1994 [108],

3. spin softening by Petrov and Ewins in 2003 [89],
4. the coupling between multiple bladed discs, also known as multistage coupling, investigated by Bladh et al in 2003 [14], Sinha in 2007 [122] and Song et al in 2007 [126], and
5. Coriolis effects on mode localisation and mode splitting, by Huang and Kuang in 2001 [48] and Nikolic et al in 2007 [81], respectively. This issue was previously overlooked in analysing mistuned bladed discs.

Non-linear vibrations in bladed discs have to be considered to construct accurate models. Vakakis et al [135] studied the non-linear stiffness in bladed discs in 1992, and the non-linear vibration related to gaps in shrouds was studied by Yang and Griffin in 1995 [148] and by Song et al in 2007 [126] in tuned and mistuned bladed discs, respectively. However, the most significant form of non-linearity comes from friction damping. The two-dimensional properties of friction contacts were studied by Sanliturk and Ewins in 1996 [113], and the multi-harmonic vibration due to friction was studied by Petrov and Ewins in 2005 [90]. The friction model was refined by Petrov in 2007 [92] by considering the masses and stiffnesses of friction dampers. While friction dampers are commonly used to provide damping in bladed discs, other concepts of damping, such as a piezoelectric network [130], have been proposed.

The forced vibration response levels of bladed discs are strongly influenced by the additional coupling and damping caused by the air flow around the blades, which are known as the aeroelastics. The aeroelastics of bladed discs is usually treated as a separate research topic, but aeroelastic effects can be included in structural dynamic analysis of mistuned bladed discs either (i) by incorporating an extra forced excitation vector according to Kielb et al [59] and Kahl [54], or (ii) by adding extra structural components in structural dynamic models according to Sladojević [125] and Beirow et al [9], or (iii) by adding extra modal stiffness and mass matrices according to He et al [46], or (iv) by replacing the structural modal damping ratios by the aeroelastic counterparts, which are found by running a computational fluid dynamics-fluid structure interaction (CFD-FSI) code on a tuned bladed disc model, as Sladojević [125] carried out.

Responses of mistuned blades are sometimes assumed to be contributed by a single blade-alone mode shape [140, 35]. This assumption is valid except in the veering region, where the natural frequencies of two mode

shapes with the same number of nodal diameters but different blade mode shapes are close to each other. The veering region was singled out as a physical phenomenon in 1992 by Afolabi and Alabi [1] and the responses of mistuned bladed discs excited in a veering region were studied in various papers between 2002 and 2005 [15, 8, 58].

With the variety of bladed disc designs applied to gas turbines, researchers tried to represent every bladed disc design using a small number of dimensionless parameters, such that the vibration response level distributions due to mistuning can be compared between different designs. The common dimensionless parameters used in previous research are number of blades, N , the level of damping, η , blade-to-sector mass ratio (see [32]) and the interblade coupling ratio. While the highest vibration response level of a mistuned bladed disc with N sectors is known (Section 2.2.2), the relationship between the range of vibration response levels and other dimensionless parameters is not clear. Moreover, there is no agreed definition of interblade coupling ratio. The three groups of definitions [137, 127, 78] are introduced in Section 6.3.

Many physical phenomena related to bladed discs have been considered in mistuned bladed disc analysis individually. However, accurate forced vibration response level estimates can be found only if *all* the above-mentioned effects are included in the model, which has not been carried out yet. In addition to this, we lack the ability to predict the response behaviour of a new bladed disc design under mistuning, based on that of existing bladed disc designs.

2.2.2 Range of response levels in mistuned bladed discs

Since the beginning of research into the blade mistuning problem, we know the vibration response levels of mistuned bladed discs are almost always higher than that of the tuned bladed disc design. We would like to know

1. the highest vibration response level possible in a mistuned bladed disc (i.e. the worst case), and
2. the distribution of the response levels of blades, given the distribution of mistune in blades.

A term called the “amplification factor” has been introduced in previous research to quantify the increase of the response level. While this term is defined in Section 3.1, for the moment it will suffice to be treated as the maximum response level of a mistuned bladed disc with respect to the tuned counterpart.

Three previous research papers indicated that the amplification factor of bladed discs can be smaller than unity (i.e. mistuning can *reduce* the forced vibration response level in blades). Óttarsson in 1994 [84] reported that a small portion of mistuned bladed discs have amplification factors smaller than unity under very small damping loss factors, and Jones [52] explored such a phenomenon to design an intentional mistuning pattern. Petrov argued in 2009 [87] that the maximum amplification factor can be smaller than unity if unequal aerodynamic modal damping ratios are considered. However, these are usually considered as exceptions.

Explanation of variation of forced vibration response levels

It was discovered in the early history of the blade mistuning problem (e.g. Ewins in 1969 [31]) that the maximum responses of blades on a mistuned bladed disc vary greatly. By plotting the maximum response of mistuned blades from 100 random bladed discs against the corresponding blade-alone natural frequencies, Griffin and Hoosac [44] further observed in 1984 that the highest maximum responses under an n EO excitation would occur on blades with blade-alone natural frequencies near to the natural frequency of the n ND-mode of the bladed disc.

Previous research has attempted, using localisation analysis [10], to explain the variability of vibration response levels in mistuned bladed discs. An early study of localisation in mistuned bladed discs was carried out by Wei and Pierre in 1988, who studied the localisation of modes [137] and responses [138] in mistuned assemblies with cyclic symmetry. Afterwards, the studies of response localisation and mode localisation divided into two groups.

Castanier and Pierre in 1993 [20] studied the spatial decay (i.e. localisation) of vibration response level in a nearly-periodic structure by exciting only one sector harmonically. In 1996, Óttarsson and Pierre [83] studied the blade mistuning problem using a transfer matrix approach. In 1997, Castanier and Pierre [22] introduced Lyapunov exponent, which is a quantity

related to the study of chaos [47], to investigate the localisation of vibration response level in disordered cyclic structures. The idea of spatial decay of vibration studied by Castanier and Pierre in 1993 was developed by Mignolet et al in 2000 [73] into the partial mistuning concept. However, all previous studies in response localisation dealt with lumped parameter models only, and did not provide methods to reduce the extent of response localisation.

Besides response localisation, mode localisation was also studied after 1990. Pierre and Murthy in 1992 [97] and Pierre et al in 1994 [98] studied the localisation of the aeroelastic modes. Afterwards, Xie and Ariaratnam in 1996 [147] and Klauke et al in 2009 [60] believed that mode localisation contributes to the high forced vibration response levels on mistuned bladed discs significantly. However, as Nikolic et al [82] pointed out, the high vibration response levels on mistuned bladed discs are usually contributed by more than one mode, and those modes are not necessarily localised.

Upper bound (or maximum) of the amplification factor

Finding the upper bound of the amplification factor is one of the earliest topics discussed in the blade mistuning problem, because such a value can inform gas turbine designers of the “worst case”. Surprisingly, the most-often cited upper bound is the first research output in the blade mistuning problem presented by Whitehead in 1966 [140]. Based on aeroelastic coupling, and assuming the responses being contributed by a single blade-alone mode shape, he proposed that the upper bound of the amplification factor depends on N , the number of sectors in a bladed disc, only:

$$\hat{A}_{\text{WH}} = \frac{1}{2} (1 + \sqrt{N}) \quad (2.1)$$

The expression shown in Equation (2.1) is called the Whitehead Factor. Based on a structural dynamic analysis and the balance of vibration energy in a single sector, Lim et al in 2004 [67] proposed that the Whitehead Factor is an upper bound of the amplification factor in a single-DOF-per-sector system, if the maximum vibration response level in a mistuned bladed disc is normalised against the peak vibration response level of a tuned cantilever blade.

Other upper bounds of the amplification factor have been proposed. Whitehead proposed an alternative upper bound in 1976 [141] for n , the

order of excitation, being not equal to 0 or $N/2$:

$$\hat{A}_{\text{WH}} = \frac{1}{2} \left(1 + \sqrt{\frac{N}{2}} \right) \quad (2.2)$$

However, Whitehead retracted Equation (2.2) in 1998 [142]. Although Kenyon et al [57] proposed in 2003 that the expression in Equation (2.2) is the maximum amplification factor due to mode distortion only, abundant simulation results in previous research has shown that the amplification factor can be higher than the expression in Equation (2.2).

Amplification factors close to the Whitehead Factor were seldom encountered. According to their refined highest amplification factor expression, Rivas-Guerra and Mignolet [101] in 2003 showed that the maximum amplification factor of any single-DOF-per-sector lumped parameter system is lower than the Whitehead Factor. Martel et al [71] also proposed an upper bound of the amplification factor lower than the Whitehead Factor in 2009.

As mentioned above, the derivation of the Whitehead Factor assumes either a system where the blade responses are dominated by one blade-alone mode shape [140] or a single-DOF-per-sector system [67]. Kenyon et al [58] showed that the amplification factor can exceed the Whitehead Factor if the bladed disc is excited in the veering region, and Xiao [145] proposed that the maximum amplification factor of a finite element-based bladed disc model depends on the bladed disc design, and is a value between the Whitehead Factor and \sqrt{N} .

While there were attempts of refining the upper bound of amplification factor expression by incorporating other design parameters other than N , the Whitehead Factor remains the most popular upper bound used in analysis because

1. the Whitehead Factor is simple
2. amplification factors exceeding the Whitehead Factor rarely occur in practice
3. significant extra computational effort is needed
4. some maximum amplification factor expressions, like the one proposed by Rivas-Guerra and Mignolet in 2003 [101], have not been validated in finite element models

Besides the theoretical approach, the maximum amplification factor of a specific bladed disc design can be found by carrying out an optimisation analysis. The only information required in this approach is the relationship between amplification factor and mistuning pattern in that design. The blade mistuning problem was first modelled as an optimisation problem by Petrov et al [93] in 1999, and Petrov and Ewins [89] used a gradient-based optimisation analysis in 2003 to find the maximum amplification factors of a 26-bladed fan bladed disc design and a 92-sector shrouded turbine disc design. Scarselli and Leece carried out optimisation analyses based on genetic algorithms and the neural network algorithm in 2005 to find the maximum amplification factor of a bladed disc design [115]. While all methods discussed above use random initial mistuning patterns, Rivas-Guerra and Mignolet in 2003 [101] carried out optimisation analysis according to the partial mistuning model. Their proposal involves finding an initial highest amplification factor by allowing only 3 neighbouring blades to be mistuned, and the maximum amplification factor is approached by allowing more blades to be mistuned gradually.

The introduction of optimisation analysis solved the problem of evaluating accurate maximum amplification factors of particular designs, and the results show that the maximum amplification factor can be much lower than the Whitehead Factor in some designs. For example, the maximum amplification factors in two designs analysed by Petrov and Ewins in 2003 [89] are very different - 62% of the Whitehead Factor in a 26-bladed fan but nearly 95% of the Whitehead Factor in a 92-bladed high pressure turbine disc! The combination of design parameters leading to this discrepancy is not well understood, let alone the reason.

The amplification factor as a random variable

The amplification factor is a random variable because of the random nature of blade mistuning. The amplification factor is sensitive to changes in mistuning parameters and, as shown by Petrov and Ewins in 2002 [88] and Ayers et al in 2005 [5], the order in which a given set of N mistuned blades is arranged. In light of the Whitehead Factor, the amplification factor distribution is dependent on the number of sectors N , but Myhre in 2003 [78] showed that the amplification factor distribution also depends on other design parameters as well.

Monte Carlo simulations are commonly used to find the amplification factor pdf and, more importantly, the probabilities of extremely high amplification factors, which are related to early failure of blades. The probabilities of high amplification factors are usually small. Because a Monte Carlo simulation run with R samples cannot evaluate probabilities smaller than $1/R$, many samples have to be taken to find a reliable estimate of a small probability p . Monte Carlo simulations of those sizes are time-consuming to run and sometimes not possible at all. Previous research tried to avoid large-scale Monte Carlo simulations using one of the two approaches below:

- Research has been carried out to find the blade response level pdf without running simulations in 1989 by Sinha and Chen [124]. Lin and Mignolet [68] used a similar method in 1996 in studying the response distribution of damping mistuned bladed discs. This approach is attempted recently by Bah et al in 2003 [7] and Sinha in 2006 [121] using the stochastic reduced basis approach and the polynomial chaos-based stochastic finite element method [42], respectively. However, no research based on this approach is capable of finding the amplification factor distribution. A likely reason for this blank is the highly non-linear relationship between the N values of normalised maximum responses on a mistuned bladed disc and the amplification factor, which is the single maximum of those N values.
- By assuming the tail of the amplification factor pdf following a reverse Weibull distribution, Castanier et al [21] developed a method in 1997 to find the small probabilities of extremely high amplification factors using Monte Carlo simulation runs with as few as 50 samples. However, the method does not guarantee those extreme amplification factors would happen, as the mistuning patterns related to those amplification factors are not sought. Also, the maximum amplification factors estimate used in the method can be lower than true counterpart (see Reference [66] for an example).

Although Monte Carlo simulations have been carried out extensively, the dependence of the maximum amplification factor on design parameters is not well understood as simulations were usually carried out on selected bladed disc designs. Moreover, the current approach based on Monte Carlo simulations is not efficient. The statistical methods of finding the peak responses pdf are not considered further in this thesis because such an approach fails

to find the amplification factor distribution, which is important in analysing the response distribution of mistuned bladed discs. More efficient sampling approaches are needed to find the small probabilities and example mistuning patterns related to extremely high amplification factors.

2.2.3 Sensitivity studies

It has been found that the transition from the tuned bladed disc, where the response levels experienced on all blades are equal, to the situation where one or few blades suffer very high responses is gradual by increasing the degree of mistune. As a result, the sensitivity of blade responses to the degree of mistune is studied, including

- deriving the analytical relationship between the amplification factor and the degree of mode splitting, which is a function of the degree of mistune. MacBain and Whaley implemented such an approach in 1984 [69] by assuming the mode shapes of a mistuned bladed disc being identical to the mode shapes in the tuned counterpart
- deriving the response level distribution sensitivity to mistuning parameters distribution, as Kaneko et al carried out in 1994 [55]
- finding the maximum allowable mistune given a threshold maximum amplification factor by an inverse method, as Sanliturk and Imregun [114] presented in 1994
- finding the modes of a mistuned bladed disc by the perturbation method, as Watson and Kamat [136] carried out in 1995
- deriving the sensitivity of the response of every blade in the Fourier domain. The sensitivity expression presented by Shapiro in 1999 [118] is k/η , where k and η are the blade stiffness and damping loss factor, respectively. He claimed that the sensitivity does not depend on the level of interblade coupling.

There is relatively little research in finding the sensitivity of the amplification factor to the degree of mistune, but the potential and limitation of the approach have been shown. On the one hand, the sensitivity approach can explain why the vibration response levels of some bladed discs reach their maximum at a much lower degree of mistune than others, as asked by

Nikolic [80]; on the other hand, the highly non-linear relationship between the amplification factor and the degree of mistune restricts the valid range of first-order approximations. Besides the sensitivity analysis carried out in previous research, the maximum amplification factor sensitivity to design parameters has not been studied.

2.2.4 Intentional mistuning approach

The intentional mistuning approach means incorporating non-identical blades in a bladed disc design. The relatively low amplification factors of particular mistuning patterns were briefly mentioned in 1984 by Imregun and Ewins [51] and 1994 by Rzadkowski [109]. An intentional mistuning scheme of installing two types of blades alternatively, also known as “alternate mistuning”, was described *inter alia* by Griffin and Hoosac in 1984 [44]. In more recent research, the increased robustness of intentionally mistuned blisks was demonstrated by Castanier and Pierre in 1997 [21]. Research after that date attempted to find the optimal mistuning pattern. Current candidates of intentional mistuning patterns include a harmonic (i.e. sinusoidal) pattern [72, 56] and a linear pattern. Jones proposed the latter in 2008 [52] after a theoretical study.

A mistuning pattern can be taken as an intentional mistuning pattern only if the amplification factor variation is small under additional, random mistuning. Besides Castanier and Pierre, Choi et al [25] and Lim et al [66] have carried out related studies in 2003 and 2004, respectively. Also, Ayers et al [5] incorporated experimental data in showing the effect of intentional mistuning in 2005.

There were other proposals to avoid high amplification factors. In 2008, Nikolic et al [82] suggested using a large mistuning strategy to reduce the likelihood of encountering extremely high amplification factors.

While it is generally agreed that the intentional mistuning approach can improve the robustness of a bladed disc design, further research work has to be carried out to find an optimal intentional mistuning pattern, determine the optimal strength of the intentional mistuning pattern and evaluate the non-structural dynamic consequences of bladed discs due to intentional mistuning patterns.

2.2.5 Blisks and the need of mistuning identification

Bladed discs are traditionally assemblies of blades and rotors connected by fir-tree joints (other types of joints existed in the early history of gas turbines [102].) While blades can be replaced easily in a bladed disc assembly, extra weight is needed to support the fir-tree joints. Moreover, the properties of a bladed disc assembly are unpredictable because the uncertainties of contact conditions at root joints are significant, as investigated by Petrov and Ewins in 2006 [91]. This means the mistuning pattern measured on individual blades is not relevant to the behaviour of a mistuned bladed disc assembly comprising those blades.

An alternative of using a bladed disc assembly is to use an integral bladed disc, such that the friction surfaces at joints can be eliminated. Blisks were first incorporated into military helicopter engines, with the power turbines of Bristol Siddeley Nimbus engines in 1969 and the low pressure compressors of General Electric T700 engines in the early 1980s [49] as two examples. Blisks are gradually introduced to compressors in EJ200 Eurofighters and the Joint Strike Fighter [107]. In addition, blisks will be used in civil aviation applications in the near future, such as Rolls-Royce BR725 [103] and Trent XWB [104] engines.

While there are advantages in incorporating blisks into aero engines, it poses challenges to investigate the mistuning pattern of a blisk as blades are no longer detachable from the disc. In such a situation, a mistuning identification algorithm is needed to extract the mistuning parameters from mode shapes of a mistuned blisk. Mistuning identification is a focus of research in the blade mistuning problem since Mignolet and Lin published their work in 1997 [74]. Four additional research groups have proposed their mistuning identification algorithms for blisks in aero engines. Research groups at the University of Michigan and Carnegie Mellon University have presented mistuning identification algorithms based on the component mode mistuning (CMM) model [70] and the fundamental mistuning model (FMM) [35], respectively. Pichot et al [96] and Laxalde et al [62] have also presented their mistuning identification algorithms. In 2007, Griffin and Feiner [43] claimed their FMM-based method is capable of extrapolating the mistuning pattern on a rotating blisk test piece using that identified on the test piece while it is stationary.

The application of mistuning identification algorithms are not limited to

gas turbines, as Sheng [119] designed an mistuning identification algorithm to identify mistuning parameters of turbocharger bladed wheels.

The quality of the identified mistuning pattern depends heavily on the experimental procedure taken. The mainstream of previous research in mistuning identification used Laser Doppler Vibrometers (LDV) to measure the vibration response, while Salhi et al in 2008 [110] proposed extracting the modal parameters by using tip-timing data on rotating bladed discs. In contrast, the bladed disc can be excited by at least five different methods according to previous research. These include mechanical excitation by an electromagnetic shaker by Laxalde et al [62], acoustic excitation by Judge et al [53], electromagnetic excitation using multiple electromagnets by Rossi [105], magnetic excitation using a single DC magnet by Di Maio [28] and a electromagnetic excitation using a single AC electromagnet, also by Di Maio [28].

Although many mistuning identification algorithms have been proposed, there is much work to be carried out in finding the best experimental procedure, refining the mistuning identification algorithms and predicting the accurate vibration response levels of blades under operating conditions.

2.3 Questions to be answered in this thesis

Much knowledge on the forced vibration response properties of mistuned bladed discs has been gained after 40 years of research. However, as mentioned in the introduction, the blade mistuning problem is considered as unsolved, and the mistuning management strategy is not feasible with the current available tools. In particular, the following questions have to be answered:

1. Can we find the small but significant probabilities of extreme amplification factors with less computational effort than running Monte Carlo simulations?
2. What is the amplification factor distribution under damping mistuning?
3. Does the Whitehead Factor represent the upper bound of the amplification factor if the modes in the veering region are excited?

4. How are the amplification factor distribution and the maximum amplification factor influenced by with the design parameters of a bladed disc design?
5. Does the maximum amplification factor sensitivity to the degree of mistune depend on the design parameters of a bladed disc design? If so, how?
6. If the intentional mistuning approach can lead to more robust bladed discs, how can we determine the optimal level of intentional mistuning at the design stage?
7. How well can we predict the responses of real bladed discs with tools currently available? How can this capability be improved?
8. What are the options available to manage the potentially high vibration response levels of mistuned bladed discs?

2.4 A brief review of robust design concept

The core issue of the blade mistuning problem is that small variations of the system parameters, known as mistuning parameters, lead to huge variations at the output in terms of vibration response levels of blades. The same problem is experienced in many other engineering systems, and these are called non-robust systems. The robust design concept attempts to reduce the variations at the output, preferably without putting additional constraints at input or at system parameters.

Although some components in robust design were developed in the 1920s [37], it is generally agreed that the foundation of robust design was first laid down by Genichi Taguchi [153, 11]. Besides the brief overview presented below, the robust design concept has been surveyed by Park et al [85] and Bayer and Sendhoff [11]. A sample robust design problem in structural dynamics was presented by Zang et al [153].

If the output variation of a system is a function of design parameters, the output variation can be reduced by carrying out a normal design optimisation analysis, as Han and Kwak did in 2001 [45]. Otherwise, one of the two robust design methods - namely the Taguchi method and the Robust Optimisation method - has to be adopted. The two robust design methods were developed independently until 1997 [133], and still, little research in

robust design methods nowadays addresses the two methods equally except in literature surveys.

The Taguchi method. Taguchi developed his method of robust design, known as the Taguchi method, after the Second World War to design reliable telecommunication equipments in a systematic manner. The first components of the Taguchi method appeared in 1957 [128], and the Taguchi method was fully developed in the 1980s [27]. Readers interested in the overview of the Taguchi method are recommended to read Reference [129], which outlines the Taguchi method and its application in various disciplines. Another demonstration of the Taguchi method was provided by Lee et al in 1996 [63]. In 1996, Chen et al [24] adjusted the Taguchi method by introducing the response surface methodology, before the relationship between the robust optimisation method and the Taguchi method was established.

However, the popularity of the Taguchi method does not mean that it gains unequivocal praise. A debate was carried out in 1992 [79] on the statistical techniques used in the parameter design stage of the Taguchi method and Taguchi's approach to condense robustness into a single parameter (i.e. the signal-to-noise ratio). According to the critics of the Taguchi method, the parameter design stage is statistically either inefficient [139] or too simplistic [79]. Also, Chen et al [24] argued that multiple robustness parameters are needed to fulfil multiple design objectives. At the extreme end, Pease opposed the application of the Taguchi to analogue electronic circuits manufacture in a 2-part critique published in 1992 [86].

The Robust Optimisation method. The term “robust optimisation method” was first proposed by Murphy et al in 1995 [75], but the need of taking into account of parameter uncertainties in operational optimisation was addressed earlier. The first applications of the robust optimisation method were in operational science [75] and topological optimisation of structures [111]. Previous research to the robust optimisation method can be divided into three areas, which are (i) determining the input variation, (ii) determining the output variation, and (iii) improving existing optimisation algorithms.

Determining the output variation is the most important research area because it can only be evaluated by stochastic methods in many prob-

lems, and Monte Carlo simulations are not computationally efficient. The importance sampling method has been proposed on several occasions to improve the efficiency of Monte Carlo simulations: Du and Chen [29] proposed a Most-Probable-Point (MPP)-based importance sampling method in 2001, Fonseca et al [38] designed an importance sampling-based method in 2007 to reuse samples in design iterations, and Rubinstein and Kroese [106] developed the cross entropy method in 2008 to find the optimal importance sampling parameters.

Although all optimisation algorithms available in the robust optimisation method can be classified into three groups - namely deterministic methods, randomised methods and genetic algorithms, there were numerous attempts to improve the optimisation algorithms. For example, Lee and Park proposed a simplified sensitivity analysis in 2001 [64] and Sandgren and Cameron improved the efficiency of the genetic algorithms in 2002 [111].

2.5 Summary

The recent research in the structural dynamic aspects of the blade mistuning problem has been reviewed and our understanding in the vibration response levels in mistuned bladed discs is presented. However, there are still outstanding questions to be answered before the mistuning management strategy can be implemented. As the mistuning management strategy in Chapter 1 treats the blade mistuning problem as a robust design problem, the available robust design methods have been introduced as well.

Chapter 3

Evaluation of the range of the amplification factor

The **amplification factor** is a number used by the majority of the mistuning research community to measure the severity of the consequences of mistuning in the maximum vibration response level of a mistuned bladed disc. The amplification factor is normally defined as the ratio of the highest forced vibration response level found in a given mistuned bladed disc to the highest forced vibration response level found in a tuned counterpart, under the same excitation pattern. New names are given to alternative definitions introduced in previous research for specific purposes.

The amplification factor is bounded from above by the **maximum amplification factor** which depends on number of blades on a disc, the detailed design and the damping loss factor. In previous research, the term “maximum amplification factor” has been used to refer to any of the three different quantities: firstly, it has been referred to a theoretical upper bound of the amplification factor (e.g. the Whitehead Factor); secondly, the term has been applied to describe the maximum found in optimisation, or thirdly, it can mean the highest amplification factor found in a simulation involving many samples (i.e. Monte Carlo simulation). In this thesis, only the second quantity is called the “maximum amplification factor”.

Because mistuning patterns (i.e. the arrangement of the mistuning on a mistuned bladed disc) are random, the amplification factor is also a random variable having a probability density function (pdf). The consequences of mistuning can be quantified by the 99.9th (or any other) percentile of the pdf, and this value is usually found by Monte Carlo simulation. The 99.9th percentile

amplification factor is often significantly lower than the maximum amplification factor, and amplification factors between these two values seldom occur, i.e. these are *rare events*. These small probabilities are of practical interest because the rare events are associated with extreme amplification factors and short fatigue lives, and industry is interested to assess the risk of their occurrences in practice.

A new procedure is developed in this chapter to tackle industrial interest in rare events. Because Monte Carlo simulation fails to give reliable prediction of the probabilities in that range, importance sampling is applied to close the gap between the maximum amplification factor provided by optimisation analysis and the 99.9th percentile amplification factor given by Monte Carlo simulation. The new procedure is demonstrated on a 24-bladed integral bladed disc.

3.1 Introduction

From structural dynamics principles, the forced vibration response of Blade i in a bladed disc, expressed as u_i , is controlled by the design parameters of the bladed disc design (including damping), mistuning pattern, the excitation pattern and the excitation frequency, which are denoted $\{z\}$, $\{x\}$, $\{f\}$ and Ω respectively:

$$u_i = u_i(\{z\}, \{x\}, \{f\}, \Omega) \quad (3.1)$$

The potentially high forced vibration response is of interest in the blade mistuning problem, because the blades experiencing high response levels are likely to fail earlier than others. To investigate the severity of the consequences of mistuning, the response levels of a mistuned bladed disc are first normalised against the peak response level of every blade on a hypothetical tuned bladed disc of the same design, under the same excitation pattern. The response levels of blades on a particular mistuned bladed disc over a resonance region are plotted in Figure 3.1.

After that, the maximum response level of each blade over a resonance region is sought, and it is customary to plot the N maximum responses of the N blades on a mistuned bladed disc against the corresponding blade-alone natural frequencies. Figure 3.2 is such a plot corresponding to the responses shown in Figure 3.1.

At last, the maximum normalised response level of all blades is sought to

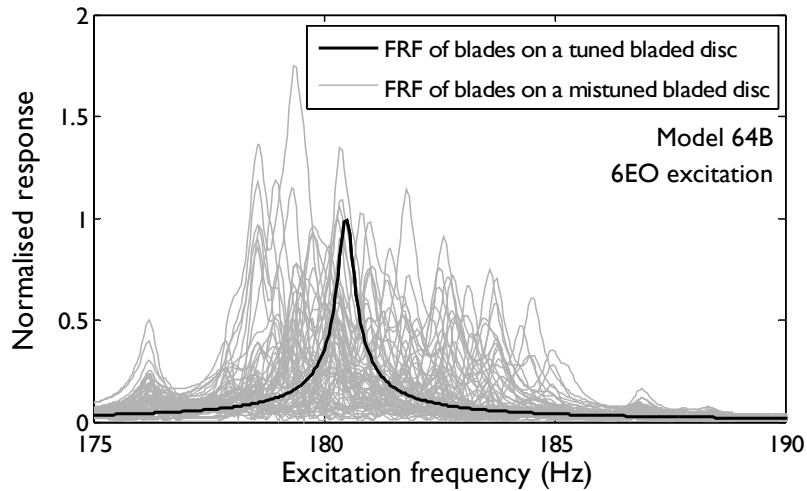


Figure 3.1: Blade responses in tuned and mistuned 64-bladed discs.

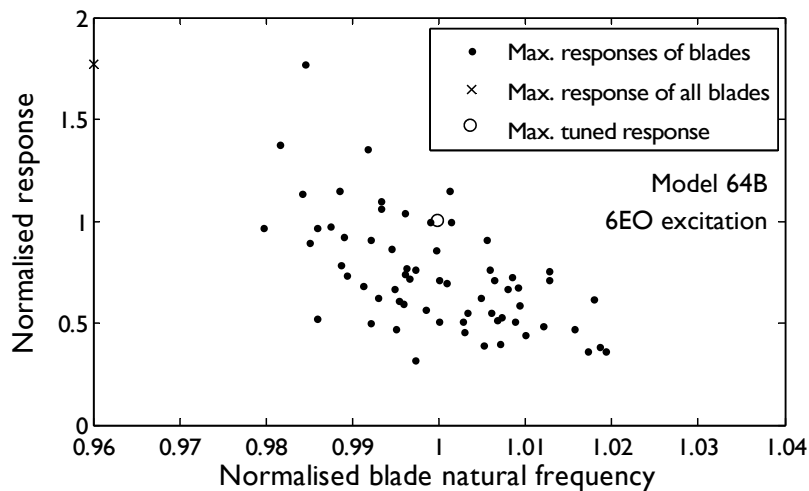


Figure 3.2: Blade responses against blade-alone frequencies of a bladed disc.

show the highest vibration response level possible in a particular mistuned bladed disc, which is plotted as a cross on the left hand side of Figure 3.2. This value is called the amplification factor. The amplification factor has been used in research since 1966, but no names were given before it was called “magnification” in 1994 [84], and finally “amplification factor” in 2003 [101]. It is more appropriate to call this ratio “amplification factor” than “magnification factor” because the highest vibration responses in mistuned bladed discs are actually, instead of apparently, higher than the highest vibration response of a tuned bladed disc.

Mathematically, the amplification factor can be defined as the output of the *amplification factor function* (a) as shown in Equation (3.2):

$$\begin{aligned} A &= \frac{\max_{i=1,2,\dots,N} \max_{\Omega} |u_i(\{z\}, \{x\}, \{f\}, \Omega)|}{\max_{i=1,2,\dots,N} \max_{\Omega} |u_i(\{z\}, \{0\}, \{f\}, \Omega)|} \\ &= a(\{z\}, \{x\}, \{f\}) \end{aligned} \quad (3.2)$$

The definitions of the inputs to the amplification factor function will be discussed in Section 4.4.1. The vectors $\{z\}$ and $\{f\}$ can be omitted from the written expression if the amplification factors of only one design under a particular excitation pattern is considered.

While the traditional definition of the amplification factor is widely used in research related to the blade mistuning problem, the term “amplification factor” has been used in two other ways described, and more precisely defined, below.

Partial amplification factor. In some previous experimental studies, the responses were not measured in all blades (e.g. 23 out of 64 in Reference [54]), and the ratio of the highest measured response to the tuned peak response is found. It is called the *partial amplification factor* in this thesis.

Adjusted amplification factor. Lim et al [67] defined the amplification factor as the ratio of the highest response found in a given mistuned bladed disc to the peak cantilever response of the mistuned blade where the highest response is found, such that the energy flow in a mistuned bladed disc can be studied. In this thesis, the amplification factor derived from this definition is called the *adjusted amplification factor*. The adjusted amplification factor of a tuned bladed disc is not equal to 1 due to the existence of interblade coupling.

The adjusted amplification factor apparently introduces complexities but there are two advantages: (i) the adjusted amplification factors of different bladed disc designs are comparable as long as the same blade design is used, and (ii) the adjusted amplification factor can quantify the response increase in bladed discs with unequal damping ratios across blades (also known as *damping mistuning*).

Obviously, the maximum blade responses and all variants of the ampli-

fication factor are random variables as mistuning means random changes of blade properties. For example, the maximum blade responses of 1,000 randomly-picked mistuned bladed discs are plotted in Figure 3.3. From the 64,000 data points, it can be seen that the blade responses are scattered between 0.2 and 2.5 times the tuned peak response level. In addition, the maximum blade response is apparently bounded from above, so is the amplification factor.

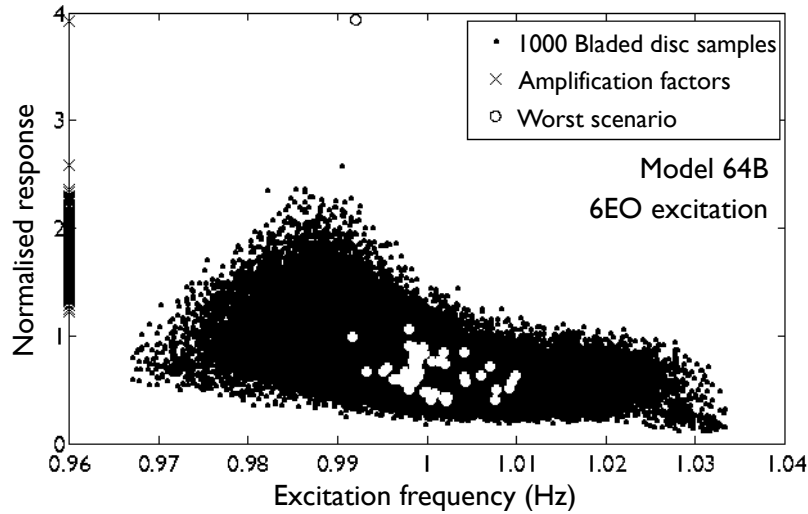


Figure 3.3: Blade responses against blade-alone frequencies in many bladed discs.

While it is true that the blade response cannot be infinite due to existence of damping, the amplification factor can be much higher than the highest amplification factor found in the 1,000 mistuned bladed discs. One extreme situation is also plotted in Figure 3.3: in such a situation, the natural frequency of the blade experiencing the highest response level ($0.9922\omega_b$) is close to the 6ND natural frequency of the bladed disc ($0.9916\omega_b$).

The discussion in the rest of this chapter is focused on the extremely high amplification factors: the maximum possible amplification factor, called the maximum amplification factor, is discussed in Section 3.2, and Sections 3.3 and 3.4 discuss the methods to evaluate the small probabilities of occurrence of extremely high amplification factors.

3.2 Evaluation of the worst scenario: the quest to find a realistic maximum amplification factor

Because a conservative estimate of the amplification factor is needed in bladed disc design, much of the previous research effort has been concentrated in finding the *maximum amplification factor*. The maximum amplification factor has been referred to as any of the three quantities below:

1. a theoretical upper bound of the amplification factor. This value, called “the upper bound of the amplification factor”, is discussed in Section 3.2.1;
2. the maximum output of the amplification factor function (Equation (3.2)) under a given set of design parameters and a known excitation pattern. This approach, together with a new optimisation algorithm introduced to the blade mistuning problem, is discussed in Section 3.2.2.

The maximum amplification factor only refers to this value in this thesis because every maximum amplification factor found in this approach corresponds to a mistuning pattern, which means it can occur in practice; or

3. the highest amplification factor found in a numerical simulation involving many random samples (e.g. Monte Carlo simulation). This approach is not discussed further in this section because Monte Carlo simulations are not designed to find maxima or minima. Instead, the Monte Carlo simulation approach is analysed in Section 3.3.

3.2.1 Upper bound of the amplification factor

Some researchers have tried to find an analytical upper bound of the amplification factor (i) to avoid dealing with an infinite amount of possible mistuning patterns and (ii) to gain insight into the causes of high amplification factors in mistuned bladed discs. The most well-known research outcome in this topic is called *the Whitehead Factor* [140], named after the person who first derived such an expression in 1966. While Whitehead derived the factor by considering aeroelastic coupling between blades, it has also been proven to be the upper bound of the adjusted amplification factor in a single-DOF-per-sector system using structural dynamics principles [67].

The Whitehead Factor involves only N , the number of blades on a bladed disc:

$$\hat{A}_{\text{WH}} = \frac{1}{2} \left(1 + \sqrt{N} \right) \quad (3.3)$$

In practice, the Whitehead Factor is a conservative upper bound of the adjusted amplification factor. The results from attempts [101, 146] to include other design parameters of bladed discs into Equation (3.3) are not widely used because of the complexities involved.

Whitehead derived the upper bound of the amplification factor by assuming the modal damping ratio of all modes being equal, and Lim et al assumed the damping loss factor being constant throughout a bladed disc. However, bladed discs with unequal damping on the blades, also known as damping-mistuned bladed discs, have recently been included in the analysis of frequency mistuned bladed discs [68]. If the stiffness mistuning is small compared with damping mistuning, an upper bound of the adjusted maximum amplification factor in a single-DOF-per-sector system can be found by taking a very similar approach to that adopted by Lim et al [67].

Finding an upper bound of the adjusted amplification factor in damping mistuned bladed discs

It is assumed that every sector on the single-DOF-per-sector system is excited under an EO-type excitation with the magnitude being equal to unity. The forced harmonic excitation on Sector i , f_i , equals to

$$f_i = \sin(\Omega t + \theta_i) \quad (3.4)$$

where θ_i is the phase angle of the excitation on Sector i . Under steady-state vibration with a period T , the displacement and the velocity of Sector i are, respectively,

$$u_i = |u_i| \sin(\Omega t + \theta_i + \Delta\theta_i) \quad (3.5)$$

$$u'_i = |u_i| \Omega \cos(\Omega t + \theta_i + \Delta\theta_i) \quad (3.6)$$

Suppose structural damping exist on the system and the damping loss factor on Sector i is η_i , the damping force experienced on Sector i is $f_i^d = \eta_i k_i u_i$. Under steady-state sinusoidal vibration with a period of 2π , the average energy dissipation on Sector i due to structural damping over one

vibration cycle, E_i^d , is

$$E_i^d = \frac{1}{2\pi} \int_0^{2\pi} f_i^d u_i' d\theta = \frac{1}{2\pi} \int_0^{2\pi} \eta_i k_i u_i u_i' d\theta = \frac{1}{2} \Omega \eta_i k_i |u_i|^2 \quad (3.7)$$

The average energy input to Sector i through forced harmonic excitation E_i^f , with the magnitude of excitation normalised to unity, is calculated using Equations (3.4) and (3.6)

$$E_i^f = \frac{1}{2\pi} \int_0^{2\pi} f_i u_i' d\theta = \frac{1}{2} \Omega |u_i| \sin \Delta\theta \quad (3.8)$$

where $\Delta\theta$ is the phase angle between the forced excitation and response on Sector i . To maintain the energy balance of energy in a steady-state vibration, the inter-sector coupling energy, E_i^c , is introduced to account for the difference between E_i^d and E_i^f :

$$E_i^c = \frac{1}{2} \Omega \left(\eta_i k_i |u_i|^2 - |u_i| \sin \Delta\theta \right) \quad (3.9)$$

The response amplitude $|u_i|$ is divided by the peak cantilever response of that sector, $|u_i^b| = 1/(\eta_i k_i)$ to give the normalised response a_i :

$$a_i = |u_i| \eta_i k_i \quad (3.10)$$

$$E_i^c = \frac{1}{2} \frac{\Omega}{\eta_i k_i} (a_i^2 - a_i \sin \Delta\theta) \quad (3.11)$$

As the variation of the damping loss factor across blades can be of several orders of magnitude, mistuning of blade stiffnesses can be neglected (i.e. $k_i \approx k$ in every sector). Also, because $-1 \leq \sin \Delta\theta \leq 1$, the inequality of Equation (3.11) is created:

$$\frac{1}{2} \frac{\Omega}{\eta_i k_i} (a_i^2 - a_i) \leq E_i^c \leq \frac{1}{2} \frac{\Omega}{\eta_i k_i} (a_i^2 + a_i) \quad (3.12)$$

E_i^c is then normalised by $\Omega/2k$ to give \bar{E}_i^c , the normalised inter-sector coupling energy:

$$\frac{1}{\eta_i} (a_i^2 - a_i) \leq \bar{E}_i^c \leq \frac{1}{\eta_i} (a_i^2 + a_i) \quad (3.13)$$

By knowing the minimum value of $a_i^2 - a_i$, the minimum value of \bar{E}_i^c is

found to be

$$\min(\bar{E}_i^c) = -\frac{1}{4\eta_i} \quad (3.14)$$

The minimum value of \bar{E}_i^c is the maximum energy drain possible from Sector i . Suppose such an amount of energy is drained from every sector from 2 to N and transferred to Sector 1, where the maximum amplification factor is observed. The normalised interblade coupling energy in Sector 1 is

$$\bar{E}_1^c = \sum_{i=2}^N \frac{1}{4\eta_i} \quad (3.15)$$

To maximise the energy input in Sector 1 under forced excitation, $(\Delta\theta)_1 = \pi/2$. Therefore,

$$\bar{E}_1^c = \frac{1}{\eta_i} \left(a_i^2 - a_i \sin \frac{\pi}{2} \right) = \frac{1}{\eta_i} (a_i^2 - a_i) \quad (3.16)$$

Equations (3.15) and (3.16) are combined to form a quadratic equation (Equation (3.17)), and the solution of such a quadratic equation is shown in Equation (3.18):

$$a_1^2 - a_1 - \eta_1 \sum_{i=2}^N \frac{1}{4\eta_i} = 0 \quad (3.17)$$

$$a_1 = \frac{1}{2} \left(1 + \sqrt{1 + \sum_{i=2}^N \frac{\eta_1}{\eta_i}} \right) = \frac{1}{2} \left(1 + \sqrt{\sum_{i=1}^N \frac{\eta_1}{\eta_i}} \right) \quad (3.18)$$

If the maximum allowable deviation of the damping loss factor any blade is $\Delta\eta$, the upper bound of a_1 can be found by assuming $\eta_1 = (1 + \Delta\eta)\eta$ and the damping ratios on all other blades as $\eta_i = (1 - \Delta\eta)\eta$. The upper bound of the maximum amplification factor becomes

$$a_1 \approx \frac{1}{2} \left(1 + \sqrt{1 + (N-1) \frac{1 + \Delta\eta}{1 - \Delta\eta}} \right) \quad (3.19)$$

Suppose $\Delta\eta > 0$, the upper bound of the amplification factor of a damping-mistuned bladed disc is higher than the Whitehead Factor, which is derived by assuming the modal damping ratios of all modes being equal.

3.2.2 Numerical search of the maximum amplification factor

Besides the theoretical approach, the maximum amplification factor in a bladed disc design under a specific excitation pattern can also be found by maximising the output of the amplification factor function (Equation (3.2)). As the relationship between a mistuning pattern and the corresponding amplification factor is not simple, no analytical means to calculate the maximum amplification factor have been found.

Nevertheless, the maximum amplification factor can be searched for using an optimisation analysis. The optimisation analysis was developed as a numerical strategy to find the “optimal design” vector which leads to a function (called a *goal function* in optimisation terminology) giving the minimum output. With minor adjustments, the same analysis can also be used to find the maximum output of the goal function.

Given the bladed disc design parameters, $\{z\}$, and the forced excitation pattern, $\{f\}$, the optimisation analysis is used in the blade mistuning problem to maximise the output of the amplification factor function (Equation (3.2)), such that the maximum amplification factor, \hat{A} , and the mistuning pattern that leads to that maximum, $\{x_0\}$, known as the *worst mistuning pattern*, can be found:

$$\begin{aligned}\hat{A} &= \max_{\{x\}} a(\{z\}, \{x\}, \{f\}) \\ &= \max_{\{x\}} a(\{x\}) = a(\{x_0\})\end{aligned}\tag{3.20}$$

The resulting mistuning pattern $\{x_0\}$ is related to a particular combination of bladed disc design and excitation pattern only. It is noted that $\{x_0\}$ is called the “optimal design” in optimisation terminology.

There are numerous references (e.g. [99, 143]) introducing the possible ways of carrying out optimisation analysis, also known as *optimisation algorithms*. Optimisation algorithms can be classified into two types, and both types have been applied to find the maximum amplification factor in previous research. The first type of algorithm requires the gradient vector of the amplification factor function, $\nabla a(\{x\})$, with entries

$$\nabla a(\{x\}) = \left\{ \frac{\partial a}{\partial x_1} \quad \frac{\partial a}{\partial x_2} \quad \dots \quad \frac{\partial a}{\partial x_N} \right\}^T\tag{3.21}$$

Examples of the first type of applied algorithms include Quasi-Newton [89] and response surface methods [95]. In these, the gradient of the amplification factor function is found by assuming the excitation frequency and the location of the worst blade are kept constant. The second type of optimisation algorithms, which includes genetic algorithms and neural network (both in Reference [115]), does not require gradient information. In a problem with many dimensions such as the blade mistuning problem, optimisation can be carried out more efficiently if gradient information is used. Therefore, a gradient-based optimisation algorithm is used to find the maximum amplification factor of every design discussed in this thesis.

An introduction to two gradient-based optimisation algorithms

The basic gradient-based optimisation algorithm is the steepest descent method. To find the maximum value of $a(\{x\})$ using the steepest descent method, an initial mistuning pattern $\{x_1\}$ is chosen and the following four steps are carried out:

1. By evaluating the derivatives of $a(\{x\})$ with respect to individual mistuning parameters, the gradient of the function at the selected point $\{g_i\} = \nabla a(\{x_i\})$ (where $i \geq 1$) is found, and $\{g_i\}$ becomes a search direction $\{h_i\}$.
2. The function is evaluated at points along the line passing $\{x_i\}$ in the direction of $\{h_i\}$, i.e.

$$\{x\} = \{x_i\} + \alpha \{h_i\} \quad (3.22)$$

where α is a variable determined either by a geometric progression [89] or the Golden section method (if the maximum possible value of α is known).

3. The location where the maximum of $a(\{x\})$ is found is marked as $\{x_{i+1}\}$.
4. i is increased by 1 and the four steps are repeated until convergence is reached.

Although the steepest descent method is very easy to understand, the method converges poorly if the contour lines of the function form elongated

ellipses (Figure 3.4). This problem can be solved by employing the *conjugate gradient method*, with nearly no additional computational effort.

The conjugate gradient method can achieve comparable results to the Newton-Raphson method [99]: theoretically, the optimum can be reached in N iterations in an N -dimensional optimisation problem by the conjugate gradient method if the contours are perfectly ellipsoidal. A two-dimensional example is shown in Figure 3.4.

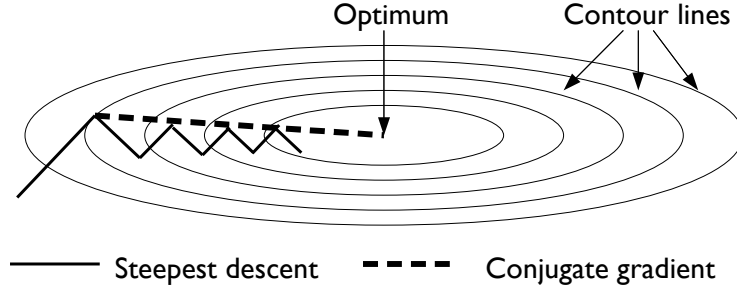


Figure 3.4: Search paths of optimisation algorithms on a 2-D plane.

The only difference between the conjugate gradient method and the steepest descent method is in the selection of the search direction (i.e. Step 1 of the procedure above) in the second iteration and thereafter. In the conjugate gradient method, the searching direction of Step i , $\{h_i\}$, is determined by three variables: the gradients at $\{x_i\}$ and $\{x_{i-1}\}$, and the previous search direction $\{h_{i-1}\}$. In mathematical terms,

$$\{g_i\} = -\nabla f(\{x_i\}) \quad (3.23)$$

$$\{h_i\} = \{g_i\} + \gamma_i \{h_{i-1}\} \quad (3.24)$$

There are two methods for finding the coefficient γ_i , namely the Polak-Ribiere and Fletcher-Reeves approaches (both described in [143]), and these are shown in Equations (3.25) and (3.26) respectively. After comparing the performances of the two approaches, the conjugate gradient method based on the Fletcher-Reeves approach is adopted in this thesis.

$$\gamma_i = \frac{(\{g_i\} - \{g_{i-1}\}) \cdot \{g_i\}}{\{g_{i-1}\} \cdot \{g_{i-1}\}} \quad \text{Polak-Ribiere approach} \quad (3.25)$$

$$\gamma_i = \frac{\{g_i\} \cdot \{g_i\}}{\{g_{i-1}\} \cdot \{g_{i-1}\}} \quad \text{Fletcher-Reeves approach} \quad (3.26)$$

3.3 Current approach of amplification factor distribution prediction

As mentioned in Section 3.1, the amplification factor is a random variable, and it has its own probability density function (pdf). Typical pdfs of the amplification factor and the partial amplification factors are shown in Figure 3.5. The thin tails on the right hand side of the pdfs show that the probabilities of extremely high levels of amplification factors are low. The tail of the partial amplification factor pdf is even thinner than that of the amplification factor because the blade with the highest response is not always included.

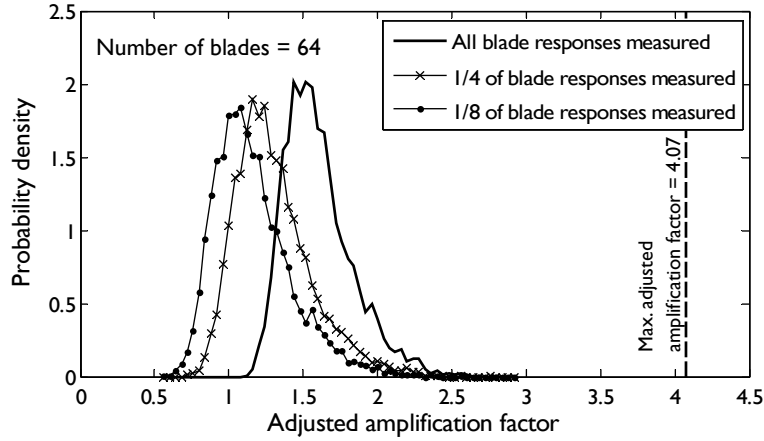


Figure 3.5: Typical probability density functions of amplification factor and partial amplification factors.

Although there have been attempts to find the responses distribution by analytical means, numerical simulations like the Monte Carlo simulations are usually used to find the amplification factor pdf. The Monte Carlo simulation is sometimes referred to any stochastic computer simulation [106], but a narrower definition proposed by Law [61] is adopted in this thesis: the Monte Carlo (also known as *Direct Monte Carlo*, DMC) simulation refers to a numerical method of evaluating the probability p of an event function, $h(\{x\})$, with $f(\{x\})$ being the pdf of the N -element random parameter vector $\{x\}$:

$$p = E_f(h(\{x\})) = \int_{\hat{x}_N}^{\hat{x}_N} \cdots \int_{\hat{x}_1}^{\hat{x}_1} h(\{x\}) f(\{x\}) dx_1 \cdots dx_N \quad (3.27)$$

In a Direct Monte Carlo simulation trial, the integral in Equation (3.27) is approximated by p_{DMC} , which is found by calculating the event function $h(\{x\})$ for R selected samples $\{x_i\}$. These samples are created by a (pseudo-) random number generator such that distribution of samples is as close to $f(\{x\})$ as possible:

$$p \approx p_{\text{DMC}} = \frac{1}{R} \sum_{i=1}^R h(\{x_i\}) \quad (3.28)$$

In the blade mistuning problem, the probability of the amplification factor lying above a given threshold A_0 in a design $\{z\}$ and an excitation pattern $\{f\}$ is sought. Therefore the event, $h(\{x\})$, to be evaluated in a DMC simulation is the function $a_t(\{x\})$ shown in Equation (3.29):

$$a_t(\{z\}, \{x\}, \{f\}) = \begin{cases} 1 & a(\{z\}, \{x\}, \{f\}) \geq A_0 \\ 0 & a(\{z\}, \{x\}, \{f\}) < A_0 \end{cases} \quad (3.29)$$

There are two major weaknesses associated with using the DMC simulation in the blade mistuning problem to estimate the small probabilities:

1. A Direct Monte Carlo simulation run with R samples cannot predict probabilities smaller than $1/R$ directly. For example, 10,000 samples are used to produce the pdf shown in Figure 3.6. The highest amplification factor among the samples is 1.9, while the maximum amplification factor is known to be 2.8 from the results obtained in optimisation. As a result, the probability of the amplification factor exceeding any threshold between 1.9 and 2.8 cannot be evaluated. This is a serious deficiency because a difference of 32% in the amplification factor corresponds to a 500-time difference in the fatigue life, as the correlation between the vibration amplitude and fatigue life is discussed in Chapter 5.
2. Any probability estimate p_{DMC} in the order of $1/R$ found in a Direct Monte Carlo simulation is unreliable due to sampling error. The uncertainty of the estimate can be quantified by the concept of the *confidence interval*. The “100(1 - α)% confidence interval” means there is a 100 (1 - α)% chance that the true probability, p , lies within a

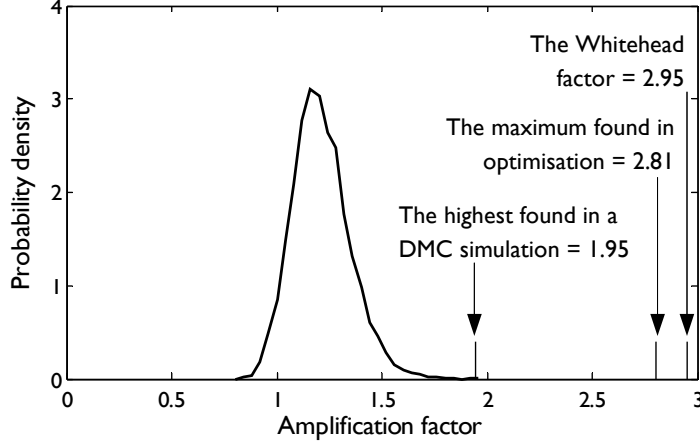


Figure 3.6: Amplification factor pdf, with the highest values sought using various methods in a 24-bladed disc design.

specified interval:

$$\Pr(p_{\text{DMC}} - \Delta p \leq p \leq p_{\text{DMC}} + \Delta p) = 1 - \alpha \quad (3.30)$$

The quantity Δp is called the *half-width* of the confidence interval, and is calculated using Equation (3.31) after knowing the sample variance, s^2 , by using Equation (3.32).

$$\Delta p = z_{R-1, 1-\frac{\alpha}{2}} \sqrt{\frac{s_{\text{DMC}}^2}{R}} \quad (3.31)$$

$$\begin{aligned} s_{\text{DMC}}^2 &= \frac{1}{R-1} \sum_{i=1}^R (h(\{x_i\}) - p_{\text{DMC}})^2 \\ &\approx p_{\text{DMC}} (1 - p_{\text{DMC}}) \end{aligned} \quad (3.32)$$

The factor z in Equation (3.31) is the “degrees of freedom” in Student’s t -distribution and is dependent on the number of samples in the Monte Carlo simulation and the confidence level [106]. Typically, the “95% confidence level” is taken, such that $z_{\infty, 0.975} = 1.960$ [61]. By substituting Equation (3.32) into Equation (3.31), it can be seen in Equation (3.33) that the half-width of the confidence interval associated with the estimated probability of $1/R$ is higher than $1/R$. The result means that the probability estimate is highly unreliable.

$$(\Delta p)_{p_{\text{DMC}}=\frac{1}{R}} = 1.96 \sqrt{\frac{p_{\text{DMC}}(1-p_{\text{DMC}})}{1/p_{\text{DMC}}}} \approx 1.96 p_{\text{DMC}} \quad (3.33)$$

More samples could have been used to improve the range and the accuracy of a CMC simulation, but such an approach is inefficient because the half-width of the confidence interval (Equation (3.31)) is proportional to $1/\sqrt{R}$. For example, 100 times as many samples is needed in a Direct Monte Carlo simulation to reduce the order of the width of the confidence interval by one (e.g. from $0.1p$ to $0.01p$).

3.4 A new procedure to predict the probabilities of occurrence of extreme amplification factors

Figure 3.6 shows that a huge gap can exist between the highest amplification factor found in a Direct Monte Carlo simulation run and the maximum amplification factor. As industry is interested in knowing the probabilities associated with the rare events, a better method is needed to predict the probabilities of extreme amplification factors occurring, and one is introduced below. The procedure comprises four steps:

Step 1: DMC simulation. A small-scale Direct Monte Carlo simulation finds an estimate amplification factor pdf.

Step 2: search for the worst mistuning patterns. The worst mistuning patterns are searched for using optimisation analysis.

Step 3: importance sampling. The importance sampling method is carried out around the worst mistuning patterns to find the probabilities of amplification factors exceeding certain thresholds.

Step 4: interpolation. The tail of the amplification factor pdf is drawn by interpolating the probabilities found in Step 3.

The second and third steps in the procedure are uncommon in previous mistuning research. While optimisation analysis has been introduced in Section 3.2.2, the importance sampling method is explained in Section 3.4.1 below. The importance sampling concept is then applied to the blade mistuning problem in Section 3.4.2. Lastly, the 4-step procedure above is demonstrated in Section 3.4.3 on a 24-bladed integral bladed disc.

3.4.1 Introduction to the importance sampling method

Because the probabilities of very high amplification factors occurring are low, the integral in Equation (3.27) is contributed by a small portion of the whole domain. The distribution density in that portion is usually low because some blades in those patterns are relatively heavily mistuned and are not very likely to occur. As a result, a large number of samples is needed in DMC simulations in dealing with the blade mistuning problem. Improvements can be made by adopting the *importance sampling* method.

A “bombing problem” suggested by Asmussen and Glynn [4], shown in Figure 3.7, is introduced to facilitate further discussion. In this problem, a bomb is aimed at a target at (0,0) on the xy -plane, and the actual hitting point is given as a bivariate normally-distributed pdf with the standard deviation of (1,1). The probability p of the bomb falling in within 1 unit of a sensitive object A with the southwest and northeast corners located at (4,-0.5) and (5,0.5) respectively (i.e. Area B in Figure 3.7), is sought.

The probability can be found analytically by solving p in Equation (3.34), where $h(x, y) = 1$ in Area B and 0 elsewhere:

$$p = E_f(h(x, y)) = \int_{-\infty}^{\infty} \int_{-\infty}^{\infty} h(x, y) f(x, y) dx dy \quad (3.34)$$

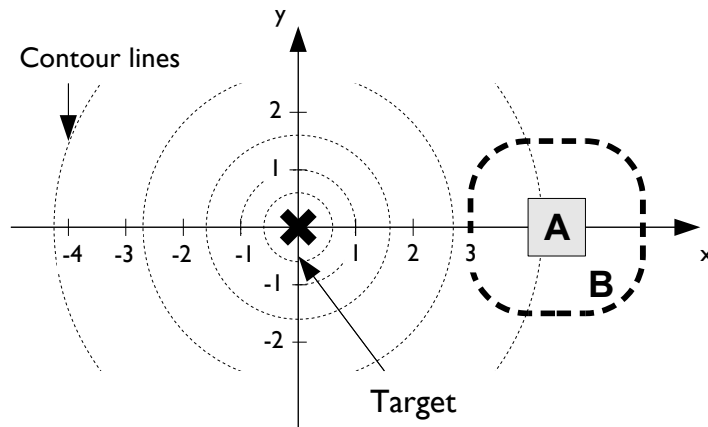


Figure 3.7: A “bombing problem” proposed by Asmussen and Glynn [4].

The straightforward method of finding p is to carry out a DMC simulation: samples are taken randomly around the target with a standard deviation of (1,1). However, the pdf $f(x, y)$ in Area B is very low (Figure 3.8), such that the majority of samples fall outside Area B. A large amount

of samples is required in a DMC simulation to ensure a reasonable amount of samples fall in Area B, and to estimate the integral in Equation (3.34) accurately.

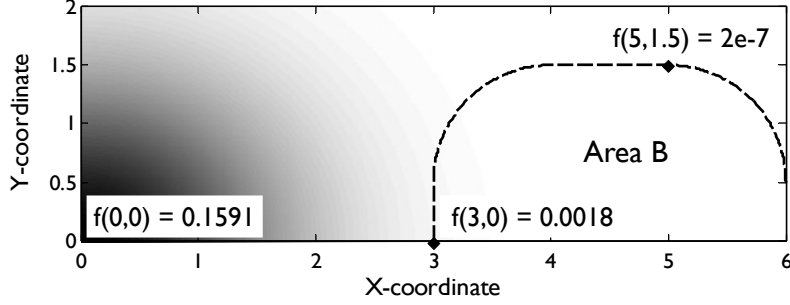


Figure 3.8: Probability density function of being hit.

In the importance sampling method, more samples are taken at regions which contribute most significantly to the integral (i.e. in the vicinity of Area B in the bombing problem) according to a sampling distribution $g(x, y)$, and the samples are reweighted to simulate the original problem. The sampling distribution is changed by rewriting Equation (3.27) into Equation (3.35):

$$p = E_g(h(\{x\})) = \int_{\hat{x}_N}^{\hat{x}_N} \cdots \int_{\hat{x}_1}^{\hat{x}_1} \underbrace{h(\{x\}) \frac{f(\{x\})}{g(\{x\})}}_{\text{function}} \underbrace{g(\{x\})}_{\text{pdf}} dx_1 \cdots dx_N \quad (3.35)$$

By using a similar approximative approach to that transformed Equation (3.27) into Equation (3.28), the probability p is estimated by calculating p_{IS} in Equation (3.36), with samples taken according to the sampling distribution $g(\{x\})$:

$$p \approx p_{\text{IS}} = \frac{1}{R} \sum_{i=1}^R h(\{x_i\}) \frac{f(\{x_i\})}{g(\{x_i\})} = \frac{1}{R} \sum_{i=1}^R h(\{x_i\}) w(\{x_i\}) \quad (3.36)$$

The ratio $w(\{x_i\})$ is called the *likelihood ratio*. To find the confidence interval associated with an importance sampling simulation using Equation (3.31), the sample variance is calculated according to Equation (3.37):

$$s_{\text{IS}}^2 = \frac{1}{R} \sum_{i=1}^R (h(\{x_i\}) w(\{x_i\}))^2 - (p_{\text{IS}})^2 \quad (3.37)$$

The confidence interval can be narrowed significantly by using importance sampling. Two simulation runs, with 100,000 samples in each run, were carried out to evaluate the bombing problem. The standard deviation of sampling distributions is kept at (1,1). By moving the centre of the sampling distribution from (0,0) to (3,0) (the edge of Area B), the half-width of the 95% confidence interval drops from $0.203p_{IS}$ to $0.0135p_{IS}$. The detailed results listed in Table 3.1 shows that importance sampling is a practical method to reduce the variance compared with that encountered in Direct Monte Carlo simulations.

Centre of sampling	Standard deviation	Probability estimate p_{IS}	Half-width Δp
(0,0) (DMC)	(1,1)	9.3×10^{-4}	1.889×10^{-4}
(3,0)	(1,1)	9.584×10^{-4}	0.129×10^{-4}

Table 3.1: Dependence of probability estimate on centre of sampling distribution.

An algorithm of finding the best sampling distribution automatically

To exploit the importance sampling method, an algorithm is needed to find a good sampling distribution automatically. Such an algorithm is crucial in applying the importance sampling method to the blade mistuning problem, because the number of samples taken is small compared with the dimension of the problem. Ideally, if the importance sampling distribution pdf, $g^* (\{x\})$, is in the form shown in Equation (3.38), the probability found is exact (Equations (3.39) and (3.40)):

$$g^* (\{x\}) = \frac{|h (\{x\}) f (\{x\})|}{p} \quad (3.38)$$

$$p_{IS} = \frac{1}{R} \sum_{i=1}^R \frac{h (\{x_i\}) f (\{x_i\})}{g^* (\{x_i\})} = \frac{1}{R} \sum_{i=1}^R p = p \quad (3.39)$$

$$s_{IS}^2 = \frac{1}{R} \sum_{i=1}^R \left(\frac{h (\{x_i\}) f (\{x_i\})}{g^* (\{x_i\})} \right)^2 - (p_{IS})^2 = p^2 - p^2 = 0 \quad (3.40)$$

However, it is impossible to obtain random samples with the pdf $g^* (\{x\})$ because the previous knowledge of p is needed to find $g^* (\{x\})$, but p is the variable we want to find. Also, $h (\{x\})$ is often geometrically irregular, thus

$g^* (\{x\})$ is geometrically irregular as well.

The *cross entropy method* provides an iterative procedure of choosing the best practical sampling distribution. The cross entropy method determines the quality of the distribution by minimising the “distance” D between the existing sampling distribution and the ideal counterpart (Equation (3.41)):

$$D (g^*, g) = E_{g^*} \left(\ln \frac{g^* \{x\}}{g \{x\}} \right) = \int_{\hat{x}_N}^{\hat{x}_N} \cdots \int_{\hat{x}_1}^{\hat{x}_1} g^* \{x\} (\ln g^* \{x\} - \ln g \{x\}) dx_1 \cdots dx_N \quad (3.41)$$

Readers are referred to Reference [106] for a detailed introduction of the theory related to the cross entropy method. If the sampling and the probability distributions are both multivariate exponential (e.g. normal), the Equation (3.41) can be transformed into a simple procedure presented in Appendix B.

3.4.2 Importance sampling method in the blade mistuning problem

The bombing problem example shows that the importance sampling method can reduce the width of the confidence interval significantly. The approach can be used in the blade mistuning problem to improve probability estimates of high amplification factors. Provided that the amplification factor function is continuous, more samples can be taken around the worst mistuning patterns initially, and the best sampling distribution is found by iterations using the cross entropy method. It is known to be more complicated to apply the importance sampling method to the blade mistuning problem than to the bombing problem due to two major issues, multidimensionality and multiple optima.

Multidimensionality. In problems with many dimensions like the blade mistuning problem, the variation of $w (\{x_i\})$ in Equation (3.36) is significant if the sampling distribution $g (\{x\})$ is vastly different from the probability distribution $f (\{x\})$. To control the variation of $w (\{x_i\})$, (i) the sampling distribution $g (x, y)$ has the same type of distribution as $f (x, y)$ and (ii) only *bottleneck elements*, the distribution parameters critical to the variance of the estimate, are different between the probability and sampling distributions. For example, the sampling

distribution in the bombing problem is bivariate normally distributed (same as the probability distribution) and the x -coordinate of the centre of sampling is the only bottleneck element.

Multiple optima. The cross entropy method does not work with multimodal distributions (i.e. distributions centred at more than one point), but more than one “worst mistuning pattern” exists in many bladed disc designs. Finding best-fit normal distribution parameters of a multi-modal distribution would result in a bad distribution.

There are two sources of multiple worst mistuning patterns, namely *multiple global optima* and *multiple local optima*. *Multiple global optima* arise from cyclic symmetry. The following mistuning patterns are physically identical on an N -bladed disc:

$$\begin{aligned} \{x_1\} &= \left\{ x_{11} \quad x_{21} \quad \cdots \quad x_{(N-1)1} \quad x_{N1} \right\}^T \\ \{x_2\} &= \left\{ x_{21} \quad x_{31} \quad \cdots \quad x_{N1} \quad x_{11} \right\}^T \\ &\vdots \\ \{x_N\} &= \left\{ x_{N1} \quad x_{11} \quad \cdots \quad x_{(N-2)1} \quad x_{(N-1)1} \right\}^T \end{aligned}$$

To facilitate the cross entropy method, all possible mistuning patterns are partitioned such that only one worst mistuning pattern exists in a partition. All mistuning patterns are first divided into N identical partitions to avoid multiple global optima, and each partition is further cut into qN subpartitions to avoid multiple local optima, if q local optima exist. Importance sampling is then carried out q times in the q subpartitions to find the true probability as all partitions are identical. The boundaries are drawn equidistantly to the neighbouring patterns according to the Euclidean distances.

3.4.3 Demonstration

The procedure described at the beginning of Section 3.4 is applied to finding the probabilities of amplification factors exceeding specific thresholds, such as $A_0 = 1.85 - 2.15$ in 0.05 steps for the 24-sector integral bladed disc, also known as a *blisk*, shown in Figure 3.9. The blisk is excited under 7EO excitation. The finite element model of the blisk is reduced by the Fundamental Mistuning Model (FMM) [35] algorithm using the first family

of modes, so that mistuning parameters of blades are determined by the fractional changes of the sector natural frequencies. (The FMM algorithm is outlined in Appendix F.) The standard deviation of mistuning parameters and maximum allowable mistune are 0.02 and 0.067 respectively. Structural damping is present in the model with a loss factor of 0.002.

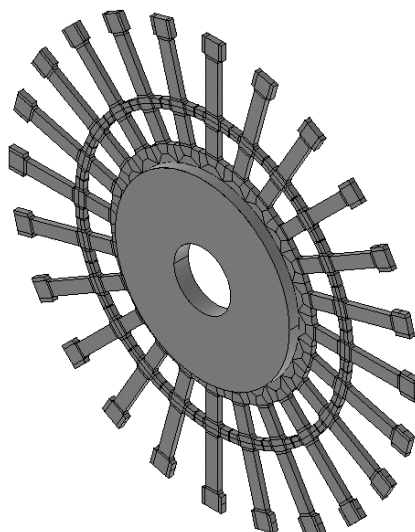


Figure 3.9: Integral bladed disc (blisk) under investigation.

Steps 1 and 2. A DMC simulation with 30,000 samples was carried out to provide a reference pdf for later comparison. The amplification factor pdf is shown in Figure 3.10 and the highest amplification factor found in the 30,000 samples is 1.952. Each of the 35 worst mistuning patterns among the Monte Carlo samples was subjected to an optimisation analysis. The conjugate gradient method was used with 120 iterations carried out in optimising each sample. The maximum amplification factor found in the optimisations (2.630) is also shown in Figure 3.10. The discrepancy of 26% between the highest amplification factor found in the DMC simulation and the maximum amplification factor found in optimisation shows that the DMC simulation performs poorly in finding the maximum amplification factor. Three local optima identified among the 35 optimised mistuning patterns are plotted in Figure 3.11.

Steps 3 and 4. Importance sampling was carried out according to the algorithm listed in Appendix B. Because 3 local optima exist, the mistuning domain was divided into $24 \times 3 = 72$ parts and importance

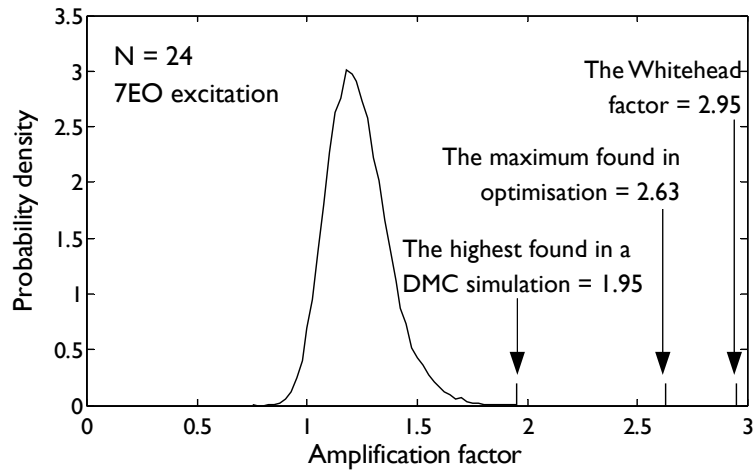


Figure 3.10: Amplification factor pdf, with the highest values sought using various methods.

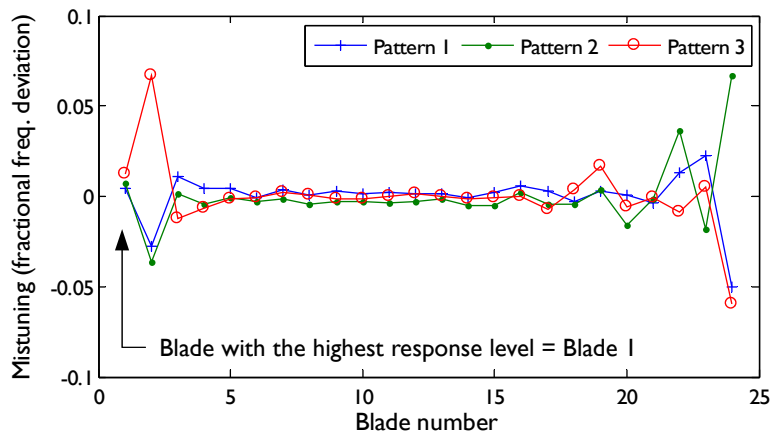


Figure 3.11: Local worst mistuning patterns found in optimisation analysis.

sampling was carried out 3 times. A total of 47,000 samples were used to evaluate each probability around each local optimum: 8,000 samples were used in each cross entropy iteration, and 15,000 samples were used in evaluating the probabilities. Between 5 and 15 mistuning parameters out of 24 were assigned bottleneck elements, where the distribution parameters were adjusted in the course of cross entropy iterations.

The probabilities found were joined to form a curve which resembles a cumulative distribution function. The probability curves with the associated 95% confidence intervals are shown in Figure 3.12. The results from the DMC simulation are provided as a reference.

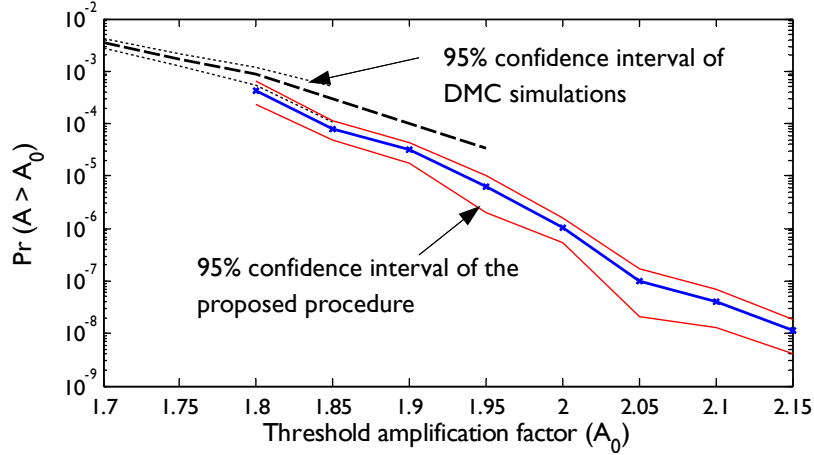


Figure 3.12: Probabilities of amplification factors exceeding given thresholds.

The results in Figure 3.12 show that the new procedure extends the possible range of evaluation well beyond that covered by DMC simulations of a similar number of samples. The discrepancy between the results found using the DMC simulations and the procedure is contributed to by two factors: (i) the results from DMC simulation are easily affected by sampling error. Only 3 and 1 DMC samples out of 30,000 have amplification factors exceeding 1.9 and 1.95, respectively; and (ii) the samples taken in importance sampling have average mistuning close to zero because the representative patterns have zero means. However, mistuning patterns with average mistuning below zero (i.e. more flexible blades) have slightly higher amplification factors. The discrepancy does not come from the inherent failure of the procedure as the importance sampling method shows that probability of the amplification factor higher than 0.5 is 1 (i.e. the amplification factor is always higher than 0.5).

The efficiency of the new procedure is measured in terms of the savings in computational time. By assuming a Direct Monte Carlo simulation with R_{eqv} samples can achieve the same accuracy as new procedure with R_{IS} samples, the efficiency is defined as the ratio R_{eqv}/R_{IS} . Figure 3.13 shows that the new procedure is more efficient compared with a Direct Monte Carlo simulation if a lower probability (i.e. the probability related to a higher threshold amplification factor) is estimated. However, the new procedure is not as efficient as Direct Monte Carlo simulations in estimating probabilities higher than 10^{-4} . Therefore, the new procedure and Direct Monte Carlo

simulations are useful in finding the shape of the amplification factor pdf in different regions.

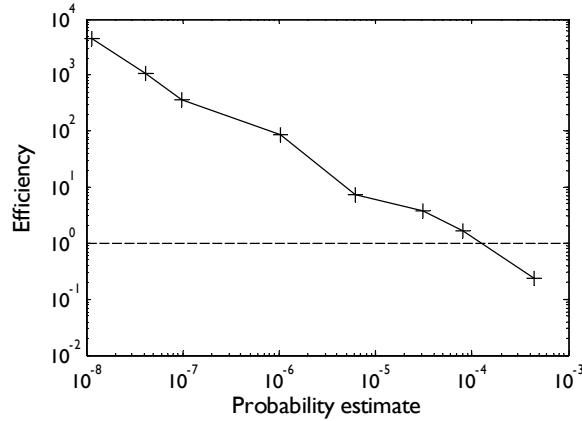


Figure 3.13: Dependence of efficiency of the new procedure over DMC simulations on probability estimate.

3.5 Summary

The terms *amplification factor* and *maximum amplification factor* are discussed in this chapter to facilitate further discussion in the blade mistuning problem. The various definitions of the amplification factor are introduced, and the maximum amplification factor is defined as the value obtained by optimisation. The conjugate gradient method is introduced to find an efficient method of finding the maximum amplification factor and the associated mistuning patterns.

By treating the amplification factor as a random variable, the tail of the pdf needs to be described accurately because it is associated with extremely high amplification factors. To overcome the weakness of Direct Monte Carlo simulations in evaluating small probabilities (also known as rare events), a new procedure based on the importance sampling method is presented. It is shown that the new procedure is more efficient than the Direct Monte Carlo simulation approach in determining small probabilities in terms of computational effort. The new procedure also extends the range of our ability in estimating the probabilities related to extremely high amplification factors.

Chapter 4

Application of robust design concepts to the blade mistuning problem

The blade mistuning problem can be managed by adopting a robust design concept. Robust design aims to keep the output of a system close to a target (i.e. robust) under *variability* at input or of design parameters. Variability refers to the irreducible scatter of a parameter, usually due to its physical nature. Variability is different to uncertainty, which is related to the possible level of error in measurements.

Two major robust design methods - namely, the **Taguchi method** and the **Robust Optimisation method** - exist. The Taguchi method seeks to improve robustness of a system in three steps in the following order: (i) in **system design**, the original system is replaced by a more robust alternative if possible, (ii) **parameter design** aims to improve the robustness of a system (or “make a system more robust”) without reducing the acceptable variability at input or that of design parameters and (iii) **tolerance design** determines the maximum permissible input variability to a system.

To use the Robust Optimisation method, the relationship between the input and output of a system is represented by a **goal function**. The method comprises two parts. Firstly, by incorporating variability at input or that of design parameters, the Robust Optimisation method transforms the goal function into a **robustness function**. The input and output of the robustness function are the input variability and robustness of the system function, respectively. Secondly, the Robust Optimisation method optimises the robustness function by

either a deterministic or a randomised approach.

By treating the blade mistuning problem as a robust design problem, the input variability and robustness are defined according to approaches either based on (i) probabilistics or (ii) interval analysis. If an approach based on **probabilistics** is adopted, the standard deviation of mistuning parameters and the 99.9th (or any other) percentile amplification factor are defined as the input variability and robustness, respectively. Alternatively, in an approach based on **interval analysis**, the input variability and robustness refer to the maximum allowable mistune on any blade on a bladed disc and the maximum amplification factor, respectively.

4.1 Introduction

The discussion in Chapter 3 has shown that small variations between blades in a bladed disc can lead to huge variations of forced vibration responses, and some of these are extremely high. Bladed discs can be described as non-robust systems, which are systems suffering from high variation at output due to small variations, also known as heterogeneity, at input and design parameters. A schematic of a non-robust system is shown in Figure 4.1.

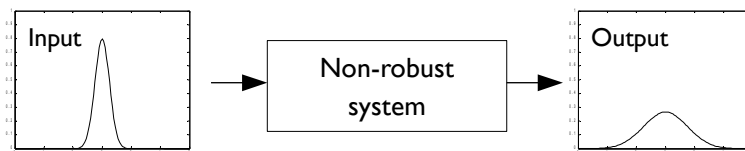


Figure 4.1: Schematic of a non-robust system.

Traditionally, the output variation of non-robust systems is controlled by imposing tight tolerances at input and design parameters, which is rather expensive. A robust design concept explores the possibility of designing a more robust system, which means a system producing reduced output variation without changing the variation at input and design parameters. For example, by using a robust design concept, the non-robust system shown in Figure 4.1 becomes the system shown in Figure 4.2, which is more robust.

In the current chapter, the two main robust design methods are introduced in Section 4.3. The issues related to casting the blade mistuning problem as a robust design problem and the approach to carry out robust design on mistuned bladed discs are presented in Section 4.4.

It should be noted that a more robust design is not always a better design

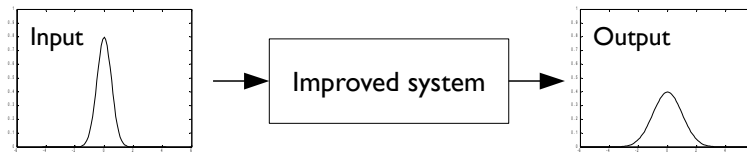


Figure 4.2: Schematic of an improved system.

in terms of manufacturing and operational costs. It may cost more to adopt a robust design than to tighten the tolerances in a non-robust design. For example, a robust bladed disc design may be too heavy to be applied to aero gas turbines.

4.2 Terminology

Many terms in the robust design concept mean slightly differently from usual. This discrepancy is critical if two apparently similar words refer to completely different meanings in robust design. Therefore, the words having apparently similar meanings are compared before further discussion.

Uncertainty and Variability. A measured parameter is non-deterministic on different samples of a product because uncertainty and variability exist. *Uncertainty* is the level of possible error in determining a quantity due to lack of knowledge, while *variability* reflects the stochastic nature of a parameter. Uncertainty can be reduced by having better knowledge of the parameter (e.g. by making better measurements), while variability is irreducible by better measurements.

If the blade-alone natural frequencies measured on a tuned bladed disc are non-identical, the scatter is due to uncertainty alone (e.g. measurement error). In contrast, mistuning parameters in a bladed disc are a source of variability because the scatter exists even if the parameters are measured accurately and precisely.

Sensitivity and Robustness. *Sensitivity* means “easily influenced, changed or damaged, especially by a physical activity or effect” in a non-technical sense [17]. However, in this thesis, sensitivity only means the ratio of the change of output to the change of input in a function. Sensitivity can be described by derivatives. *Robustness* refers to the relative output variability to input variability and design parameter

variability. Sensitivity parameters can be used to find robustness in some problems.

Robustness and Variability. Robustness refers to the relative output variability to input variability and design parameter variability. Given the level of variability at the input and of design parameters is constant, robustness is increased if the output variability is reduced.

Goal function and robustness function. The one-to-one or many-to-one relationship between input and output parameters in a system is called the *goal function*. If at least one of the input parameters, design parameters or output parameters in the goal function is scattered, the *robustness function* defines the relationship between input variability, design parameter variability and output variability. The robustness function is usually derived from the goal function.

Design parameters and noise parameters. In the robust design concept, robustness of a design is improved solely by controlling the *design parameters*, also called “control parameters” in some robust design texts. *Noise parameters* are not adjusted in robust design because of the difficulties involved. For example, the dimensions of the tuned bladed disc can be considered as design parameters, and mistuning parameters are treated as noise parameters.

Optimal design and robust optimal design. *Optimal design* is the parameter vector, $\{x_0\}$, that minimises the goal function (Section 3.2.2). If the parameter vector consists of random variables, as in the case of the blade mistuning problem, the *robust optimal design* is the design parameter vector, $\{z_0\}$, which minimises the output of the robustness function $H(\{z\}, \{x\})$ ¹ under input variability $\{x\}$:

$$\min_{\{z\}} H(\{z\}, \{x\}) = H(\{z_0\}, \{x\}) \quad (4.1)$$

The variants of the robustness function expressions are introduced in Sections 4.3.1 and 4.3.2.

¹To be precise, $H(\{z\}, \{x\})$ is the “non-robustness function”, because these measures are to be minimised in robust optimisation. However, it is called the robustness function in robust optimisation texts [11].

4.3 Introduction to major robust design methods

Two independent robust design methods - namely, the Taguchi method [129] and the robust optimisation method [11] - are available to implement the robust design concept, and are outlined in Sections 4.3.1 and 4.3.2, respectively.

It is noted that there is no agreed scheme to classify robust design problems. Previous research often classifies robust design problems by the source of variability or uncertainty. Chen et al [24] divided robust design problems into two types: variability exists in the noise parameters in Type I problems while that in Type II problems exists in the design parameters. Alternatively, Beyer and Sendhoff [11] classified robust design problems into four groups, where Groups A and B describe the sources of variability and Groups C and D describe the sources of uncertainty. In systems belonging to Groups A and B, variability exists in operating conditions and manufacturing tolerances, respectively, while uncertainty exists in output measurements in Group C systems and in fulfilment of the constraints in Group D systems. As a result, the blade mistuning problem is a Type II, Group B robust design problem according to References [24] and [11], respectively.

4.3.1 The Taguchi method

The development of the Taguchi method began in the 1950s [128] and the method took the current shape in the 1980s [27]. The Taguchi method was first developed by Genichi Taguchi in testing telecommunication product designs, but it is now used in many disciplines in engineering. Handbooks outlining the Taguchi method such as Reference [129] are available, on which the description below is based.

Robustness is defined by the signal-to-noise ratio (SNR) in the Taguchi method. The SNR is the ratio of signal output to noise output in terms of power. Because SNR is to be maximised in the Taguchi method, it is the reciprocal of the robustness function. The SNR of R pieces of output data Y , with the mean and standard deviation of Y being μ_Y and σ_Y respectively, can be defined by one of the equations listed in Table 4.1, depending on required output in particular problems:

The Taguchi method comprises three stages:

Required output	Signal-to-noise ratio
Smaller the better	$-10 \log \left(\frac{1}{R} \sum_{j=1}^R Y_j^2 \right)$
Larger the better	$-10 \log \left(\frac{1}{R} \sum_{j=1}^R \frac{1}{Y_j^2} \right)$
Nominal the best	$-10 \log \left(\frac{\mu_Y^2}{\sigma_Y^2} \right)$

Table 4.1: Definitions of the signal-to-noise ratio, after Taguchi [129].

- 1. System design.** The robustness of a system is improved by replacing the original system by a potentially more robust counterpart. For example, a simple voltage source-and-ammeter circuit can be replaced by a Wheatstone bridge to measure the resistance of a resistor.
- 2. Parameter design.** Parameter design aims to improve the robustness of a system by changing the design parameters. Parameter design involves (i) reducing the variability of the output without considering the mean of it and (ii) moving the mean of the output to the target value [85]. This two-step process is shown graphically in Figure 4.3.

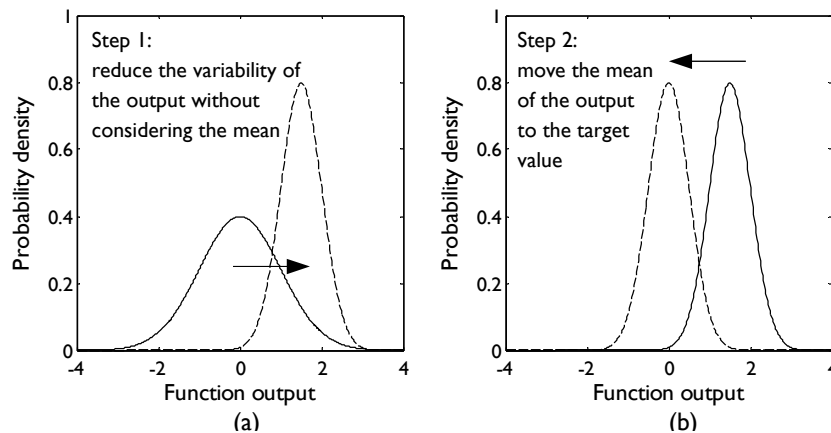


Figure 4.3: Two steps in parameter design, after Park et al [85].

The Taguchi method proposes a “Design of Experiment” scheme to reduce the variability of the output (Step (i) above). The scheme was first designed for finding optimal combinations of parameters in carrying out experiments, but this scheme can also determine parameters to be adopted in simulations. In the Design of Experiment scheme, every design or noise parameter is discretised into 2 or 3 levels. Then, a small number of experiments (up to 108 in problems with many

variables, but usually 36) are carried out [129], with the design and noise parameters determined by a specially-design array known as an orthogonal array, in which all combinations of any two design parameters are included. After the experiments, the dependence of robustness on individual design parameters is found by analysing the variance of the experimental output. Finally, the robust optimal design can be determined without considering the mean of the output.

3. Tolerance design. Manufacturing tolerances are specified by considering three factors: (i) the “quality level”, which is the cost paid by the customer to repair or replace a single faulty product. This cost is called the “social cost” in the Taguchi method; (ii) the additional cost of imposing tighter tolerances in manufacture and (iii) the maximum deviation allowable before the product fails to perform the required function, also known as the “function limit”. A safety factor is calculated in tolerance design based on the ratio of the “quality level” and the additional cost of imposing tighter tolerances.

The engineering design approach adopted in the Taguchi method is atypical. Although the Taguchi method is considered user-friendly by some engineers, the parameter design step of the Taguchi method has six shortcomings:

1. The robustness improvements in the first step may be reduced by moving the output to the target value in the second step.
2. Discretisation of design parameters restricts the scope of investigation. The robust optimal design may locate between two discrete levels of a design parameter, as shown in Figure 4.4.
3. Noise parameters are continuously-distributed parameters but the probability distribution information is removed by discretisation in the Design of Experiment scheme. Without knowing the distribution of the noise parameters, it is misleading to calculate the variance of the experimental outputs.
4. The results from the few experiments carried out according to the Design of Experiment scheme can give a false sense of safety in complex problems like the blade mistuning problem. In comparison, typical Monte Carlo simulations involve hundreds (if not thousands) of samples to give reliable output statistics.

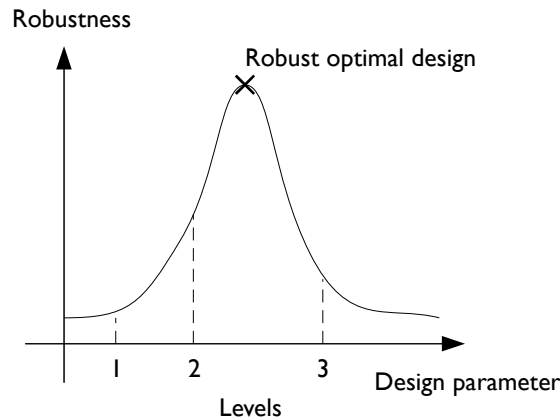


Figure 4.4: Robust optimal design missed in discretisation.

5. The interaction of multiple design parameters cannot be precisely determined in parameter design based on the Design of Experiments scheme. Although all combinations of any two design parameters are included in the experiments, those experiments are carried out without fixing other parameters. Therefore, the variance of the output is due to either the interaction of the two design parameters under consideration or that of multiple design parameters.
6. Robustness is assumed to be additive in the Taguchi method: the robustness improvement of changing several design parameters together can be approximated by the sum of robustness improvement of changing each design parameter separately. However, this assumption is not valid in some problems like the blade mistuning problem, or in the example shown in Figure 4.5. In such an example, the Taguchi method would give x_{1A} and x_{2A} as the optimal values of the design parameters x_1 and x_2 , respectively, if the dependence of robustness on the two parameters are considered separately. However, the design with parameters (x_{1A}, x_{2A}) is not robust because the robustness improvements are not additive.

Besides the shortcomings of parameter design, there are two issues related to tolerance design. Firstly, the term “social costs of quality” in the Taguchi method is overstated because it only refers to the costs related to the customer and the manufacturer, instead of the costs related to society at large (e.g. the impact of product quality on the environment). The “social costs of quality” cover repair and replacement costs of the product, which

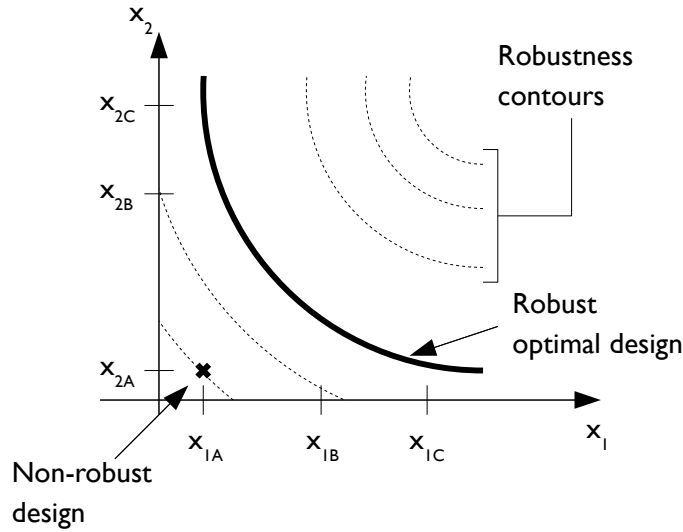


Figure 4.5: Non-additivity of robustness improvements.

are better described as life cycle costs. Also, the cost-based safety factor in tolerance design is not significantly better than the traditional safety factor. The traditional, well-documented, reliability-based safety factor is specified based on the probability of failure, which is related to the cost of failure.

4.3.2 The Robust Optimisation method

By assuming the relationship between input variability and output variability to be deterministic, the Robust Optimisation method [11] transforms the goal function $h(\{z\}, \{x\})$ into a robustness function $H(\{z\}, \{x\})$, and the minimum value of the robustness function is sought. The input variability and output variability of the goal function become input and output of the robustness function, respectively. Robust Optimisation is loosely related to parameter design in the Taguchi method. There are five different robustness functions available [11]. By writing the design parameter vector, noise parameter vector and the pdf of the noise parameter vector as $\{z\}$, $\{x\}$ and $f(\{x\})$ respectively, the three robustness functions related to the blade mistuning problem are listed below:

1. In the *robust counterpart measure*, the robustness of the system is quantified by the highest output due to all possible combinations of input, also known as the “worst case”.

2. By using the *expectancy measures*, the expectation and/or the variance is used to measure robustness:

$$H_{2a} = \int_{\hat{x}_N}^{\hat{x}_N} \cdots \int_{\hat{x}_1}^{\hat{x}_1} h(\{z\}, \{x\}) f(\{x\}) dx_1 \cdots dx_N \quad (\text{Expectation}) \quad (4.2)$$

$$H_{2b} = \int_{\hat{x}_N}^{\hat{x}_N} \cdots \int_{\hat{x}_1}^{\hat{x}_1} h^2(\{z\}, \{x\}) f(\{x\}) dx_1 \cdots dx_N \quad (\text{Variance}) \quad (4.3)$$

A multiple-objective robust design problem is created if both expectation and variance are to be minimised [76]. In this case, the robustness function becomes a linear combination of Equations (4.2) and (4.3):

$$H_{2c} = \alpha H_{2a} + (1 - \alpha) H_{2b} \quad (4.4)$$

3. The *probabilistic threshold measure* of robustness is the probability of the output being higher than a certain threshold, y_0 :

$$H_3 = p(h(\{z\}, \{x\}) \geq y_0) \quad (4.5)$$

This kind of problem can be transformed into one using expectancy measures by creating a function, h_3 , in the form of Equation (4.6), such that H_3 can be expressed in the form of Equation (4.7):

$$h_3(\{z\}, \{x\}) = \begin{cases} 1 & \text{if } h(\{z\}, \{x\}) \geq y_0 \\ 0 & \text{if } h(\{z\}, \{x\}) < y_0 \end{cases} \quad (4.6)$$

$$H_3 = \int_{\hat{x}_N}^{\hat{x}_N} \cdots \int_{\hat{x}_1}^{\hat{x}_1} h_3(\{z\}, \{x\}) f(\{x\}) dx_1 \cdots dx_N \quad (4.7)$$

If the robustness of a system is known to be entirely dependent on certain design parameters, robust optimisation is straightforward because the robustness optimisation problem is then equivalent to a normal optimisation problem. For example, the robustness of the performance of an MEMS component investigated in Reference [45] can be controlled by the spacing of natural frequencies. Otherwise, either a deterministic or a randomised approach can be adopted to tackle a robust optimisation problem:

- In the deterministic approach, the robustness function is optimised

using existing optimisation techniques. A deterministic approach is viable if the robustness function can be expressed analytically. The robustness function can be constructed either by using sensitivity information, if the goal function is differentiable, or by using more advanced methods (e.g. the spectral stochastic finite element method [42]).

- The randomised approach refers to direct search methods, which include Monte Carlo simulation, importance sampling and evolutionary algorithms. In direct search methods, a set of samples is provided to the original system function to simulate the input variability, and robustness is evaluated by analysing the output. In some cases, an approximate robustness function can be created by interpolating the robustness at certain points in the design space by using either a surrogate model [134] or the response surface methodology [24].

4.4 Casting the blade mistuning problem as a robust design problem

Following the discussion in Sections 4.1 and 4.3, the blade mistuning problem can be described as an acute robustness problem, because slightly mistuned bladed discs can generate extremely high amplification factors for their vibration response levels. The robust design concept can be applied to the bladed disc design process to reduce the likelihood of encountering high responses. The dependence of the amplification factor distribution on design parameters and mistuning distribution can be investigated according to parameter design and tolerance design concepts, respectively.

4.4.1 Input parameters to the amplification factor function

The system to be investigated in the blade mistuning problem is the amplification factor function (Equation (3.2)):

$$A = a(\{z\}, \{x\}, \{f\})$$

The variables $\{z\}$, $\{x\}$ and $\{f\}$ represent design parameters, mistuning pattern and the excitation pattern respectively. While the amplification

factor, A , has been extensively discussed in Chapter 3, the input parameters to the amplification factor function are introduced below.

Design parameters. From a designer’s point of view, the design parameters of a bladed disc design involve dimensions (and tolerances) of parts, the material properties of those parts and the properties of joints. For the sake of generality, the dimensions of a bladed disc design are often transformed into dimensionless design parameters in the blade mistuning problem, such that the findings on one bladed disc design can be used to predict the forced vibration response behaviours of other bladed discs under mistuning. Design parameters of bladed discs are often defined according to their modal properties, which are introduced in Appendix A. After 40 years of research, it is found that the design of a bladed disc can be condensed into three parameters: number of blades, interblade coupling, and the level of damping.

Interblade coupling describes the extent of influence of the motion of one blade on other blades. Generally speaking, a bladed disc design with a more flexible disc has a higher level of interblade coupling than that with a more rigid disc: for example, there is virtually no interblade coupling on a bladed disc with an infinitely heavy and rigid disc. This term is examined in further detail in Section 6.3.

The *level of damping* is sometimes treated separately because it can only be changed by adding dampers. However, it is considered as a design parameter in this thesis because it can be calculated from material properties. The variation of damping across blades (mainly due to joints) is called *damping mistuning* and is considered as a kind of mistuning pattern. The issue of damping mistuning is investigated in Section 5.5.1.

Mistuning parameter, mistune and mistuning pattern. The *mistuning parameter* of a blade is usually measured by fractional difference of the cantilever blade natural frequency of a mistuned blade with a tuned counterpart in previous research, including in the Fundamental Mistuning Model [35]. In addition, *mistune* refers to the magnitude (i.e. absolute value) of the mistuning parameter in this thesis. The order of mistuning parameters present on a mistuned bladed disc is called a *mistuning pattern*. The variation of damping across blades, also known as damping mistuning, is usually treated separately.

According to the definition above, any bladed disc with all blades having the same blade natural frequency is called a tuned bladed disc. However, the blades on a bladed disc can be physically different from each other, even if the blade natural frequencies are equal on all blades. This bladed disc is called an *apparently-tuned* bladed disc in this thesis. The distribution of amplification factor of apparently-tuned bladed discs is investigated in Section 5.5.3.

The forced excitation pattern. In the blade mistuning problem, the forced vibration responses of blades under *Engine order* (EO) type of excitation is considered. Bladed discs experience EO excitation because the pressure distribution around the annulus is not uniform. The excitation of a stationary pressure distribution around the circumference on a forward-rotating bladed disc can be approximated by putting a backward-travelling excitation pattern on a stationary bladed disc.

Besides the rotation speed, the frequency of such excitation depends on the number of cycles of the pressure variation around the annulus. For example, the existence of n upstream vanes would lead to an n^{th} EO (n EO) excitation, and the frequency of excitation is $n\Omega_r \cdot \left(\frac{2\pi}{60}\right)$ Hz, where Ω_r is the rotation speed of the bladed disc in rev/min. Resonance occurs if the n EO excitation frequency coincide a natural frequency of a mode with n -nodal-diameter (n ND) component. This relationship can be expressed clearly using an interference diagram, also known as a *Campbell diagram*, and an example is shown in Figure 4.6. In a Campbell diagram, the slanting and the (nearly) horizontal lines represent the frequencies of forced excitation and the natural frequencies of a bladed disc, respectively. The black dots indicate the locations where resonance occurs in a tuned bladed disc.

While an n EO excitation excites only one mode in a family (i.e. the mode with n nodal diameters) on a tuned bladed disc, all mode shapes in a family in a mistuned bladed disc are excited because every mode shape in mistuned bladed discs comprises multiple nodal diameter components (see Appendix A).

4.4.2 Robustness functions to be investigated

Although Equation (3.2) shows that the amplification factor of a mistuned bladed disc sample is a random variable, the relationship between the dis-

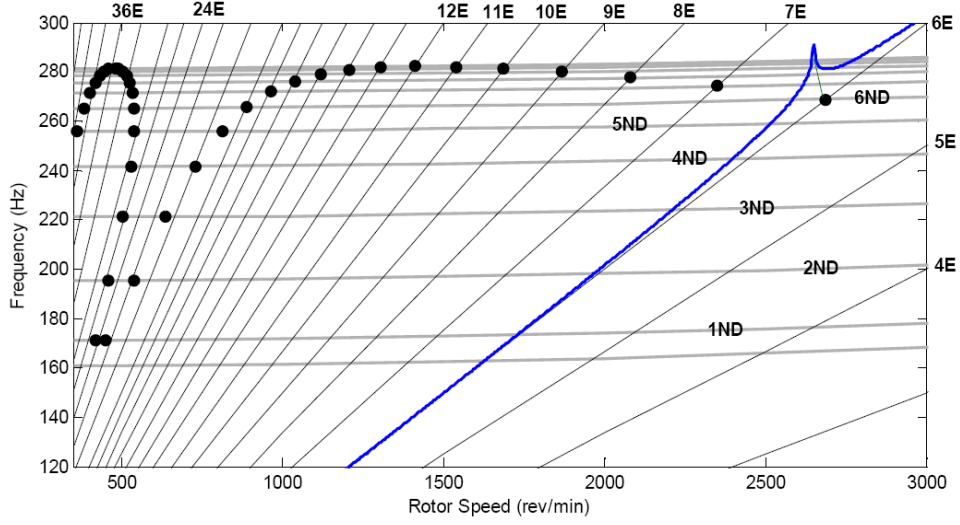


Figure 4.6: A Campbell diagram, after Sever [117].

tribution of the amplification factor and that of mistuning parameters is deterministic. This can be shown by calculating the probability of the amplification factor higher than some threshold amplification factor A_0 . The probability is determined by replacing the function $h_3(\{z\}, \{x\})$ in Equation (4.7)

$$\begin{aligned} H_3 &= p(a(\{z\}, \{x\}, \{f\}) \geq A_0) \\ &= \int_{\hat{x}_N}^{\hat{x}_N} \cdots \int_{\hat{x}_1}^{\hat{x}_1} a_t(\{z\}, \{x\}, \{f\}) f(\{x\}) dx_1 \cdots dx_N \end{aligned} \quad (4.8)$$

with $a_t(\{z\}, \{x\}, \{f\})$ defined in Equation (3.29), which is repeated here:

$$a_t(\{z\}, \{x\}, \{f\}) = \begin{cases} 1 & \text{if } a(\{z\}, \{x\}, \{f\}) \geq A_0 \\ 0 & \text{if } a(\{z\}, \{x\}, \{f\}) < A_0 \end{cases}$$

The function a_t is deterministic because a bladed disc with a particular mistuning pattern corresponds to a single amplification factor. Given the pdf $f(\{x\})$ is also a deterministic function, all terms on the right hand side of Equation (4.8) are deterministic, so is H_3 , which is the inverted cumulative distribution function of the amplification factor distribution. In other words, the amplification factor pdf is defined as the output of the robustness function (a_R) shown in Equation (4.9):

$$\text{pdf}(A) = a_R(\{z\}, \text{pdf}(x), \{f\}) \quad (4.9)$$

Because the shortest fatigue life possible on mistuned bladed discs is of interest, the tail on the right hand side of the amplification factor pdf (with an example shown in Figure 3.6) is observed. This requirement makes the signal-to-noise ratio proposed by Taguchi unsuitable for the blade mistuning problem. The robust optimisation method provides two ways to define input variability and robustness function (i.e. output variability) in the blade mistuning problem:

1. The blade mistuning problem is traditionally dealt with an approach based on *probabilistics*, where the input variability and robustness are defined as the standard deviation of the mistuning parameters of all available blades and the 99.9th (or any other) percentile of the amplification factor pdf, respectively:

$$A_{99.9} = a_{R1}(\{z\}, \sigma(x), \{f\}) \quad (4.10)$$

Robustness of a bladed disc design is defined according to the probabilistic threshold robustness measure in an approach based on probabilistics.

2. The robust counterpart measure of robustness is adopted if the blade mistuning problem is treated according to an approach based on *interval analysis*. Interval analysis is a tool to find the bounds of a function output, given the input parameters to the function are uncertain but bounded. Interval analysis was applied by Sim et al in 2007 [120] to find natural frequency and mode shape bounds under uncertain design parameters.

According to an interval analysis-based approach, the distribution of mistuning parameter is ignored. The input variability and robustness are quantified by the maximum allowable mistune on any blade and the maximum amplification factor, respectively. As a result, the robustness function can be written in the form of Equation (4.11):

$$\hat{A} = a_{R2}(\{z\}, \max(|x|), \{f\}) \quad (4.11)$$

It is discussed in Chapter 3 that the adjusted amplification factor is

bounded from above by the Whitehead Factor even if the mistuning parameters of blades are practically unbounded. Therefore, the maximum amplification factor in Equation (4.11) can be treated as a function of design parameters and the excitation pattern only. Nevertheless, the maximum allowable mistune is kept as an input parameter in Equation (4.11) for two purposes: (i) it prevents non-physical mistuning parameters (e.g. negative blade-alone natural frequencies) being considered, and (ii) it allows the maximum amplification factor under small mistuning to be investigated, as in Section 6.4.

The relationship between input variability and the robustness function according to approaches based on probabilistics and interval analysis are shown in Figures 4.7 (a) and (b), respectively. In previous research in the blade mistuning problem, the curve between input variability and robustness function has a distinct maximum [127]: this is true only if the robustness function is written based on probabilistics. The curve has a non-negative slope if the blade mistuning problem is viewed as an interval analysis problem.

Generally speaking, the interval analysis-based approach to the blade mistuning problem suits practical requirements better, because it provides the worst case scenario under given tolerances, regardless of the distribution of the scatter. However, the robustness of a bladed disc design is more appropriately described using the probabilistics-based approach in some cases. For example, the high amplification factors are less likely to occur (i.e. bladed discs become more robust) by imposing intentional mistuning, even if the worst mistuning pattern remains a possible mistuning pattern.

4.4.3 Outline and approach of investigation

The blade mistuning problem is dealt with as a robust design problem in Chapters 5, 6 and 7. In Chapter 5, the dependence of the robustness on bladed disc design parameters is investigated. In Chapter 6, the effect of controlling the mistuning parameters on robustness is discussed. The issues related to predicting (thus controlling) the forced vibration responses are discussed in Chapter 7.

The terms “input variability” and “robustness” are not used in the discussions in Chapters 5, 6 and 7, because there are two different definitions

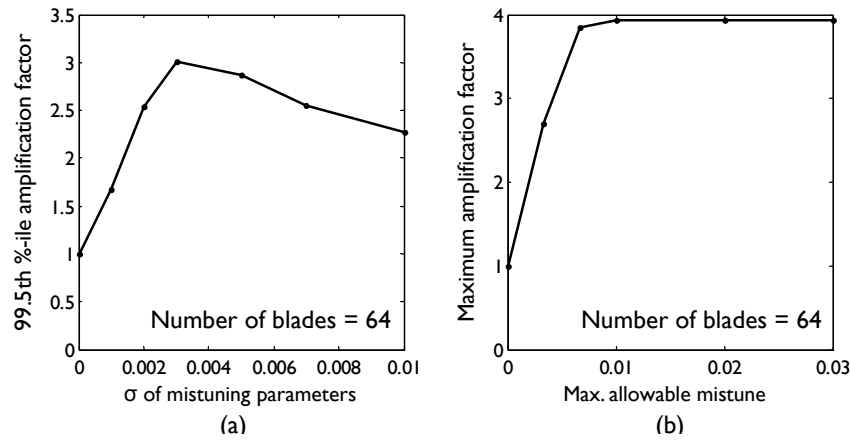


Figure 4.7: Relationship between input variability and output variability in the blade mistuning problem, according to approaches based on (a) probabilistics and (b) interval analysis.

for both “input variability” and “robustness”. Instead, typical terminology in the blade mistuning problem is used: input variability is referred to as “mistuning”, and robustness is referred to as either “maximum amplification factor” or “99.9th percentile amplification factor”.

Although the contents in Chapters 5 and 6 are similar to parameter design and tolerance design of the Taguchi method, respectively, the computational methods in the Taguchi method are not adopted in this thesis because the blade mistuning problem is too complex to be handled using Design of Experiment scheme and the tolerance design procedures. Besides this, while the Whitehead Factor was derived by theoretical means, it seems unlikely to evaluate the robustness function for every combination of design parameters and excitation pattern using the same method.

The robust optimisation method provides two methods of evaluating the robustness function (Section 4.3.2), which are the deterministic and randomised approaches. Kaneko et al [55] and Sinha [121] used the deterministic approach to find the distribution parameters (mean, standard deviation and the pdf approximate) of the peak responses of all blades in mistuned bladed discs.

However, it is impractical to evaluate the robustness function by the deterministic method. According to the probabilistic view of the robustness function (Equation (4.10)), the 99.9th percentile adjusted amplification factor is found by an implicit function (Equation (4.7)). Also, from structural

dynamics principles (Equation (3.1)), the maximum amplification factor is the highest vibration response level across all blades on a mistuned bladed disc, under any excitation frequency in a given resonance region, and in any possible mistuning pattern (Equation (4.12)).

$$\hat{A} = \max_{\{x\}} (A) = \max_{\{x\}} \max_{\Omega} \max_{i=1,2,\dots,N} |u_i(\{z\}, \{x\}, \{f\}, \Omega)| \quad (4.12)$$

Analytical methods are not available to deal with the three extreme value searches involved in finding the maximum amplification factor. As a result, direct search approach, including Direct Monte Carlo simulations and optimisation, is adopted in the analysis to evaluate the robustness functions in the blade mistuning problem.

4.5 Summary

The blade mistuning problem is treated as a robustness problem in this chapter. The robust design approach has been introduced and the two robust design concept, namely the Taguchi method and the robust optimisation method, are discussed. The functions determining the robustness of bladed disc designs and the input parameters to these functions are discussed in detail. Depending on the given mistuning distribution, the blade mistuning problem can be dealt with using approaches either based on probabilistics or interval analysis.

Chapter 5

Improving robustness of bladed discs by parameter design

Blade vibration is an important issue in gas turbine design. Blades suffer from high cycle fatigue (HCF) failure, and the fatigue life of a blade can be halved if the alternating stress experienced on a blade is increased by as little as 4%. By reducing the variation in blade vibration responses related to blade mistuning, the fatigue lives of blades can be extended and the variation of the fatigue lives of blades on the same bladed disc can be reduced.

The potential for reducing the maximum adjusted amplification factor solely by changing the design parameters, but not reducing the maximum allowable mistune, is investigated using three representative models. A 6-DOF cyclic lumped parameter model is analysed to create a “robustness map”, which provides an overview of the dependence of the maximum amplification factor on the levels of interblade coupling and damping. Simulations are carried out on four 64-sector, 2-DOF-per-sector models and six 24-sector integral bladed discs (blisks) to validate the results observed in the 6-DOF models. It is found that the maximum amplification factor can be reduced by changing design parameters, for example, by adding damping to a design with a low level of interblade coupling.

By investigating the distribution of amplification factor in (i) damping mistuned bladed discs, (ii) mistuned bladed discs excited in the veering region and (iii) **apparently-tuned bladed discs**, the adjusted amplification factor distribution was found to be robust under damping mistuning. The adjusted ampli-

fication factor distribution under excitation in the veering region is distinctive because it is bimodal. Also, the scatter of the adjusted amplification factor in apparently tuned bladed discs is much narrower than that in typically mistuned bladed discs.

5.1 Introduction

After the blade mistuning problem is modelled as a robust design problem, potential ways to improve robustness of bladed discs under mistuning are investigated. To avoid the additional costs related to tightening the tolerances of blade dimensions and material properties, a bladed disc design having a low maximum amplification factor under all realistic mistuning patterns is preferred. In the light of the Whitehead Factor, the maximum amplification factor can be cut by reducing the number of blades, N , but this quantity is seldom changed solely due to structural dynamic issues. Previous research [89, 78] reported that only some bladed disc designs are related to maximum amplification factors close to the Whitehead Factor, which indicates the possibility of reducing the maximum amplification factor without changing N .

To begin with, the relationship between high cycle fatigue failure and the extremely high responses due to blade mistuning is explained in Section 5.2. The dependence of the maximum amplification factor on design parameters besides N is investigated in Section 5.3 using three representative models, and the findings are used to explain the variation in the maximum (or the 99th percentile) amplification factor reported in previous research in Section 5.4.

Three less-often-covered topics in previous research are also investigated. The distribution of amplification factor in (i) damping mistuned bladed discs, (ii) mistuned bladed discs excited in the veering region and (iii) apparently-tuned bladed discs are each discussed in Section 5.5.

5.2 Significance of the blade mistuning problem in high cycle fatigue

Blade vibration is a major problem encountered by designers since the early days of gas turbine development [26]. Some blades fail earlier than their

predicted lives due to vibration-induced high cycle fatigue (HCF). Fatigue, together with creep, are the two most important issues related to the material properties of turbine blades [100].

The dynamic stresses of blades due to forced excitation, including that due to the pressure variation behind upstream vanes, are confined within the elastic range of blade materials to avoid low cycle fatigue (i.e. fatigue lives of 10^5 cycles or less) failure. However, bladed discs suffer from high cycle fatigue failure because the alternating stresses leading to high cycle fatigue failure are below the elastic limit of materials. High cycle fatigue failure incur maintenance costs of US\$400 million per year [41], or 30% of all jet engine maintenance costs [131]. There are two goals in bladed disc design:

1. extend the fatigue life of blades
2. prevent some blades failing much earlier than others

The fatigue life (i.e. number of loading cycles before failure) of a blade depends on, *inter alia*, the alternating and the mean stresses experienced on that blade. Wright et al [144] have carried out experiments to determine the relationship between alternating stress $\Delta\sigma$ and the fatigue life L_f in a particular superalloy. Their results on the relationship between fatigue life and alternating stress under zero mean stress are shown in Figure 5.1 in log-log scale. According to Figure 5.1, there is a roughly-linear relationship between $\log L_f$ and $\log(\Delta\sigma)$. By neglecting the single point obtained under a vibration of 0.6 Hz, the relationship between L_f and $\Delta\sigma$ can be written down as

$$L_f = \alpha (\Delta\sigma)^{16.5} \quad (5.1)$$

which means the fatigue life is halved if the alternating stress is increased by 4%. Trivial ways to prolong the fatigue lives of blades are (i) by reducing the alternating stress due to pressure variation, (ii) by designing stiffer blades and (iii) by adding damping elements to bladed discs. However, all three methods involve major design changes, and these methods only tackle the first of the two goals of bladed disc design.

The extremely high responses due to blade mistuning are a major contributor to unexpectedly early high cycle fatigue failure of blades. Some blades in mistuned bladed discs experience twice (or more) the alternating stresses than a blade on a tuned bladed disc, while other blades on the same

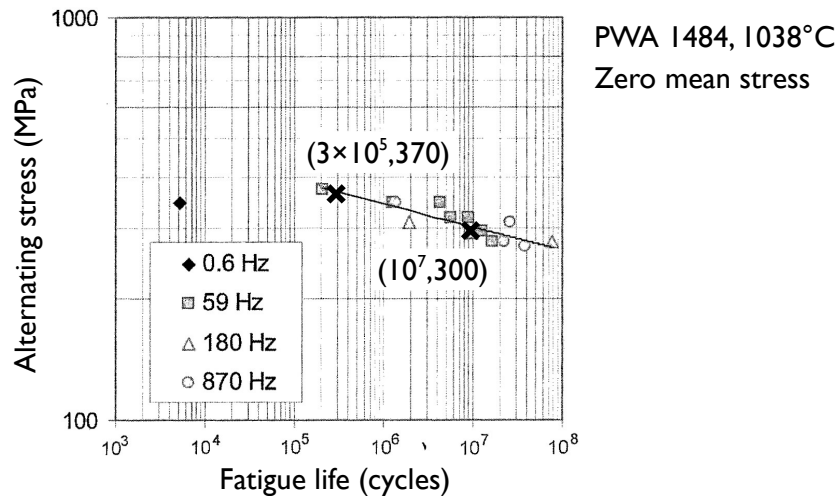


Figure 5.1: Fatigue life of a coated superalloy, after Wright et al [144].

mistuned bladed disc vibrate less heavily than a blade on a tuned bladed disc. This leads to one or both of two issues:

1. some blades on a mistuned bladed disc experience much shorter (e.g. 1/10000) fatigue lives than that of a blade on a tuned bladed disc; and/or
2. many blades on a mistuned bladed disc enjoy very long fatigue lives if a blade design guarantees a certain minimum fatigue life of the blade with the highest response.

It can be seen that the research on finding more robust bladed disc designs is useful in two ways. If a bladed disc design has a lower maximum amplification factor, (i) the fatigue life of a bladed disc due to high cycle fatigue can be extended; and (ii) over-conservative blade designs can be avoided, such that blade designs can be lighter and suit aerodynamic needs better.

5.3 Dependence of robustness on bladed disc design parameters

The derivation of the Whitehead Factor has shown that the upper bound of the maximum amplification factor depends on the number of blades in a bladed disc design. However, amplification factors near to the Whitehead

Factor are seldom encountered in bladed discs. The two examples analysed in Reference [89], listed in Table 5.1, show that the maximum amplification factors of some bladed disc designs are significantly lower than the Whitehead Factor while the others are close to it. If it is possible to reduce the maximum amplification factor solely by changing the design parameters, tight tolerances of blade dimensions and material properties, which are very expensive to implement, can be avoided. The dependence of the maximum amplification factor on interblade coupling and damping is investigated in this section.

Location of the bladed disc	Number of blades N	The Whitehead Factor \hat{A}_{WH}	The max. amp. factor \hat{A}
Fan	26	3.05	1.9
High pressure turbine	92	5.30	5.02

(Maximum allowable mistune in both cases = 5%)

Table 5.1: Whitehead Factors and maximum amplification factors of bladed disc designs investigated by Petrov and Ewins [89].

5.3.1 Models to be used in the analyses

A wide range of bladed disc designs is present in aero engines. For example, the number of blades vary between 26 in fans and up to about 100 in high pressure turbines. The properties of mistuned bladed discs are investigated in Chapters 5, 6 and 7 using three representative bladed disc models described below. Structural damping is present in all three models in the analysis.

1. A simple, cyclic lumped parameter model with 6 degrees of freedom (DOFs), shown in Figure 5.2, is analysed to produce a “robustness map”. A “robustness map” is a contour plot showing the dependence of the maximum amplification factor on the level of interblade coupling and the level of damping loss factor. This map is similar to those presented by Yoo et al [152], who were the first researchers using a contour plot to show the dependence of the amplification factor on the coupling stiffness and the level of damping in a pair of coupled oscillators. Although the results from a 6-DOF model cannot draw practical conclusions because the model is too simple, the results are useful in generalising the findings in more complex bladed disc models.

The level of interblade coupling in the model is controlled by varying the interblade stiffness element K . The responses of the model are measured by the displacement of sector masses u_1 to u_6 .

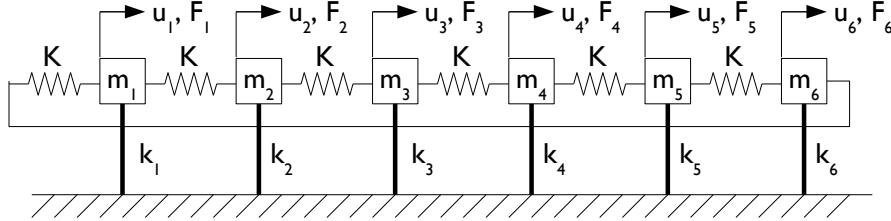


Figure 5.2: Layout of a 6-DOF cyclic lumped parameter model.

2. A 64-sector, 2-DOF-per-sector lumped parameter model shown in Figure 5.3 is used to extend the capability of the results found in the 6-DOF model. The vibration responses are measured by the deformation of the blade stiffness elements Δu_i . A 2-DOF-per-sector model was first used to model mistuned bladed discs by Dye and Henry in 1969 [30], and the parameters used in this thesis are improvised on the 36-bladed disc models used by Afolabi [2] and Yiu [151].

Because lumped parameter models are flexible in assigning parameters, the properties of (i) bladed discs with damping mistuning, (ii) mistuned bladed discs under excitation in the veering region and (iii) apparently-tuned bladed discs are carried out on this model in Sections 5.5.1, 5.5.2 and 5.5.3 respectively.

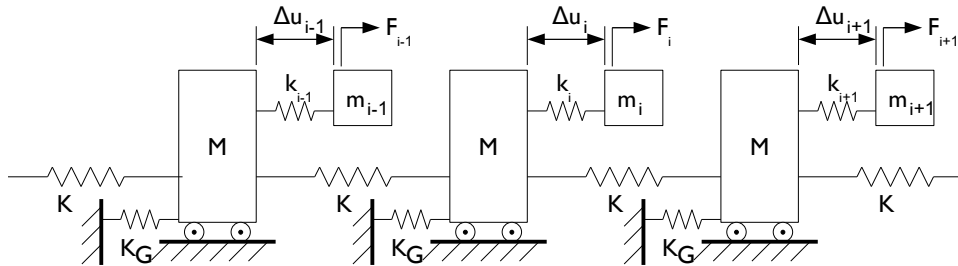


Figure 5.3: Layout of a 64-sector lumped parameter model.

3. The finite element model of a 24-sector blisk is used to demonstrate the findings on the first two models on a realistic bladed disc. The finite element model is based on a blisk test piece prepared by Sever [117]. The outline of the test piece is shown in Figure 5.4, and readers are

referred to Sever [117] for the detailed geometry. The finite element model is reduced using the Fundamental Mistuning Model (FMM) algorithm, which is described in Appendix F, such that only 24 parameters are required to define a mistuning pattern. The responses are measured by the displacements of a selected point on every blade.

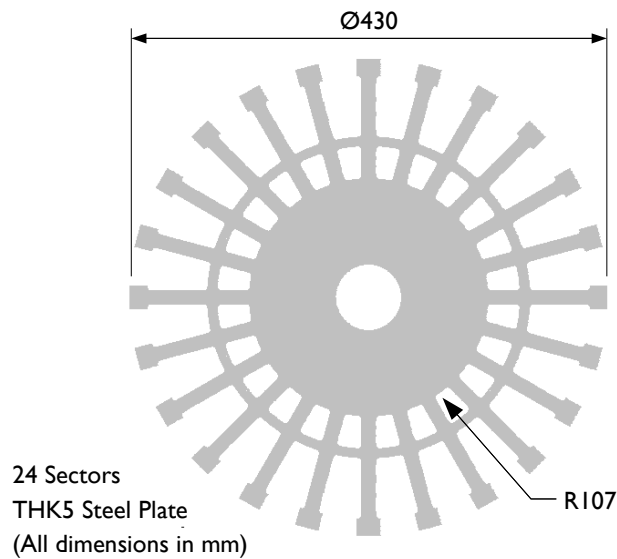
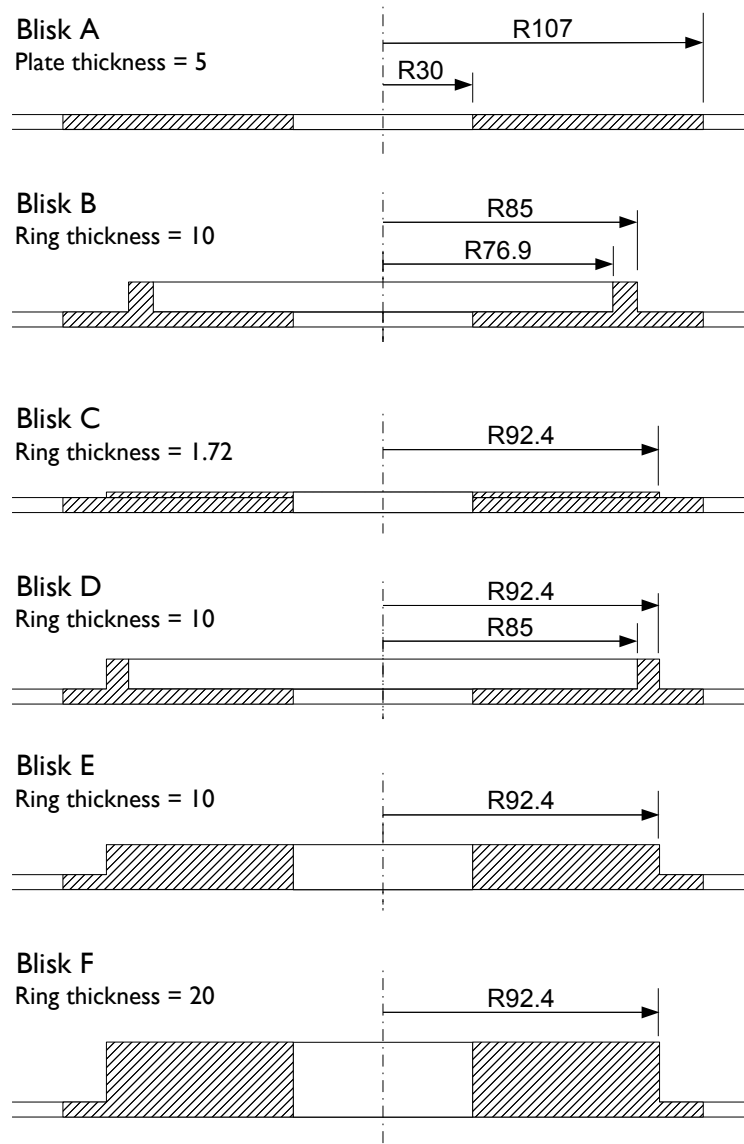


Figure 5.4: Layout of a 24-sector blisk.

The level of interblade coupling in the 24-sector blisk model is adjusted by adding a stiffening ring to the disc part. Six variants of the test piece are investigated in this chapter, with the cross sections of the disc parts shown in Figure 5.5. Within the six blisks, Blisk F is not analysed in Chapter 6 because Blisks E and F behave similarly in tolerance design.

The natural frequencies of the first mode family of the six blisks are plotted in Figure 5.6. Although the disc-to-blade mass ratios in Blisks B, C and D are the same, the levels of interblade coupling are different due to the disc geometries. According to the natural frequency distribution, the level of interblade coupling is decreasing in the order of Blisks A, B, D, E and F, and the level of interblade coupling in Blisk C is similar to that of Blisk B.



(Not to scale, all dimensions in millimetres)

Figure 5.5: Cross sections of the disc part of 24-sector blisk models.

5.3.2 Maximum adjusted amplification factor of a 6-DOF model

The maximum adjusted amplification factors of a 6-DOF cyclic lumped parameter model under 1EO and 3EO excitations are sought by controlling the interblade coupling stiffness, K , and the damping loss factor, η . Contour plots are created by interpolating the maximum adjusted amplification

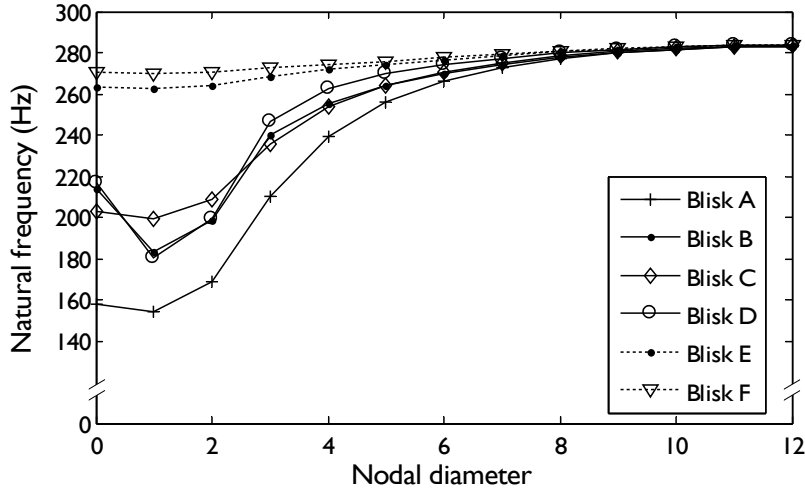


Figure 5.6: Natural frequencies of the first mode family in six blisk models.

factors found under different combinations of K and η . The contour plots related to the two different excitation patterns are expected to be different because the peak response level under an 1EO excitation is normally contributed to by the two distorted 1ND modes, while that of a 3EO excitation is contributed mainly by a single distorted 3ND mode. The nominal values of k and m in the model are equal to 1 Nm^{-1} and 1 kg respectively. The range of interblade coupling stiffnesses and damping loss factors to be tested are listed in Table 5.2.

Quantity	Symbol	Range
Interblade coupling stiffness	K	$0.0002 \text{ Nm}^{-1} - 0.02 \text{ Nm}^{-1}$
Damping loss factor	η	$0.0001 - 0.003$

Table 5.2: Ranges of parameters applied to the 6-DOF model.

The systems are mistuned by perturbing the sector masses and the mistuning parameter of a sector is defined by the difference between the natural frequency of the mistuned sector alone and that of the tuned counterpart. The maximum allowable mistune is set at 20%, which is much higher than the maximum mistune of the worst mistuning pattern.

The contour plots of the maximum adjusted amplification factors under 1EO and 3EO excitations (Figures 5.7 and 5.8) are found to have similar shapes although the exact values are different. The maximum adjusted amplification factors under both excitation patterns are lower in the bottom

right hand corners of Figures 5.7 and 5.8, which refer to designs with high levels of damping and low levels of interblade coupling. The steep slope of the robustness function in that region shows that the maximum adjusted amplification factor can be controlled either

1. by decreasing the level of interblade coupling in a bladed disc design with a high level of damping; or
2. by increasing damping in a bladed disc design with a low level of interblade coupling.

These two possibilities are going to be examined in other bladed disc models. In the analysis in the rest of this thesis, the contour plot created under 1EO excitation (i.e. Figure 5.7) is called the “robustness map” because double n ND modes exist for almost all n EO excitations in practice.

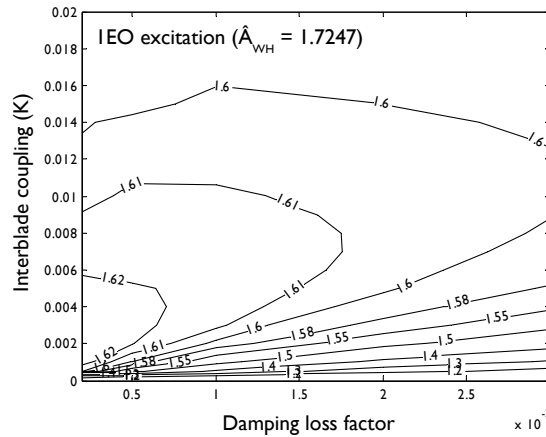


Figure 5.7: Dependence of the maximum adjusted amplification factor on interblade coupling and damping under 1EO excitation.

5.3.3 Maximum adjusted amplification factors of four 64-sector models

The information provided by the robustness map in Section 5.3.2 is validated by a robustness investigation of four 64-sector, 2-DOF-per sector lumped parameter models.

The design parameters of the basic 64-sector model (denoted Model 64A in this thesis) are improvised on the 36-sector model proposed by Afolabi [2],

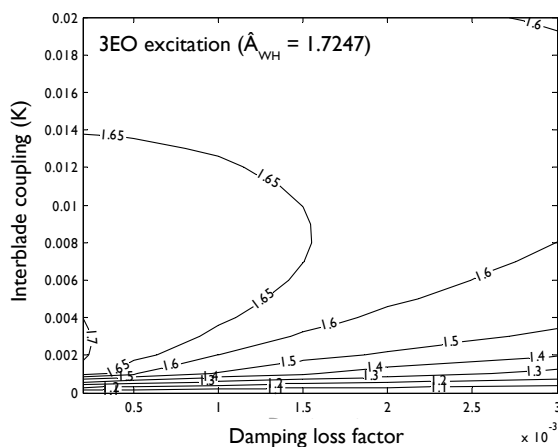


Figure 5.8: Dependence of the maximum adjusted amplification factor on interblade coupling and damping under 3EO excitation.

which is the 2-DOF-per-sector lumped parameter approximation of a bladed disc specimen. Assuming the same disc is used, four properties between Model 64A and the model in Reference [2] are set to be equal, namely (i) the 6ND disc-alone natural frequency, (ii) the total disc mass, (iii) the disc-to-blade mass ratio and (iv) the blade-alone natural frequency of 182 Hz.

Three additional 64-sector models are created by changing the design parameters of Model 64A to investigate the dependence of robustness on design parameters. The two types of design changes considered in this thesis, proposed by Yiu [151], are called the *mass ratio* and *frequency ratio* effects.

- The mass ratio effect simulates the effect of making the disc using different materials. The disc-to-blade mass ratio of the bladed disc is adjusted without changing the disc-alone natural frequencies. Two lumped parameter models, having the disc-to-blade mass ratios 5 and 10 times that of the Model 64A, are created according to the mass ratio effect and are called Models 64B and 64C, respectively. By increasing the sector mass in the order of Models 64A, 64B and 64C, the interblade coupling decreases in terms of the difference between the bladed disc natural frequencies of the 6ND mode in the first family and the blade alone natural frequency.
- The frequency ratio effect simulates the change of the geometry of the disc in a bladed disc design without changing the disc-to-blade mass ratio. According to this effect, Model 64D is created by multiplying

the intersector stiffness of Model 64A by a factor of 10. Similar to that in the mass ratio effect, the level interblade coupling is decreased by stiffening the intersector springs.

The design parameters of the four models employed in this investigation and the 36-sector lumped parameter model used in Reference [2] are listed in Table 5.3. The natural frequencies of the models are normalised against the blade alone natural frequency of 182 Hz and plotted in Figure 5.9, and the natural frequencies in the vicinity of the blade alone natural frequency are plotted in Figure 5.10. The damping loss factor in the models vary between 0.001 and 0.004.

Model	N	K (Nm ⁻¹)	M (kg)	K_G (Nm ⁻¹)	k (Nm ⁻¹)	m (kg)
64A	64	1673834.7	0.10125			
64B	64	8369638	0.50625			
64C	64	16739500	1.0125	36.779	36778.6	0.028125
64D	64	16738347	0.10125			
Ref. [2]	36	941532.0	0.18	65.384	65384.16	0.05

(N = the number of sectors, other variables are defined in Figure 5.3)

Table 5.3: Design parameters of 64-sector models analysed, and those of the 36-sector model after Afolabi [2].

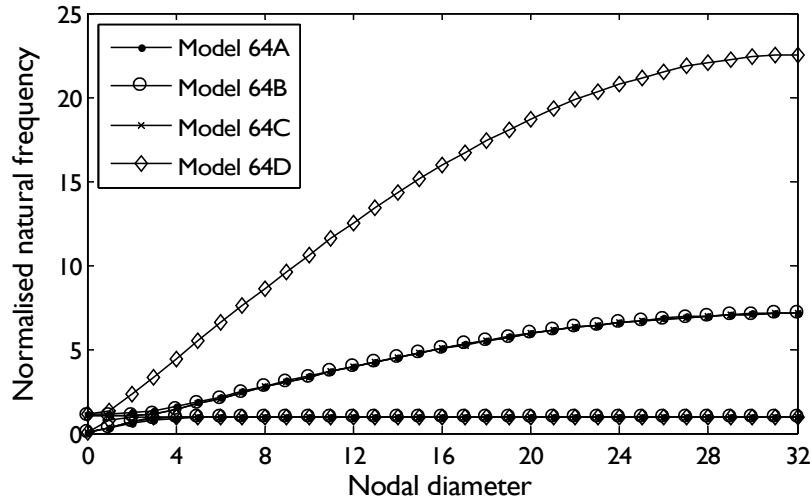


Figure 5.9: Normalised natural frequencies of 64-sector models.

Since the blade designs in the 4 models are identical, the maximum adjusted amplification factor is used to measure robustness. The differences

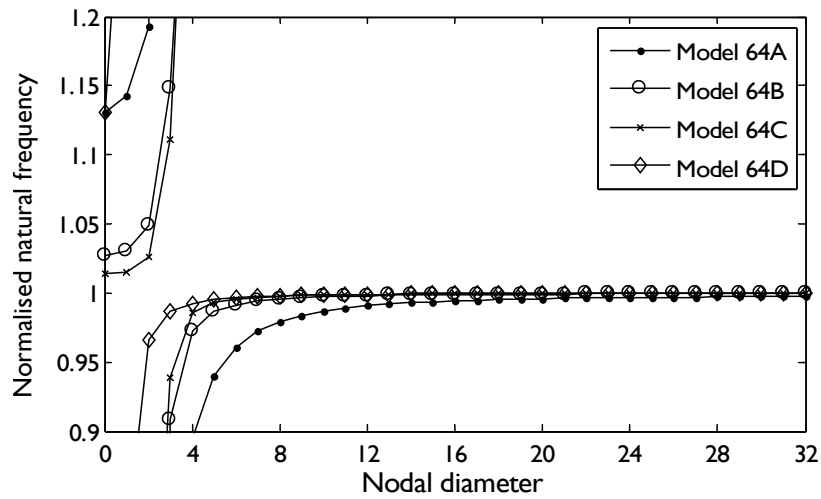


Figure 5.10: Magnified plot of Figure 5.9.

between the maximum amplification factors and the maximum adjusted amplification factors are small in the four models ($\approx 2\%$ in Model 64A and $\approx 0.5\%$ in the other three models). Mistuning is applied to the blades by perturbing the blade masses.

The dependence of the maximum adjusted amplification factor on damping in the four 64-sector models are plotted in Figure 5.11. Similar to the results found in the 6-DOF model, the maximum adjusted amplification factor associated with a bladed disc design is significantly lower than the Whitehead Factor if the level of interblade coupling is low and the level of damping is high.

However, the two proposals to reduce the maximum amplification factor of bladed discs suggested in Section 5.3.2 may have limited application in practice. Firstly, major design changes may be needed to reduce the maximum amplification factor significantly. For example, the maximum adjusted amplification factor reduction of 26% (3.01 in Model 64D against 4.06 in Model 64A, see Figure 5.11) is achieved by multiplying the disc stiffness by a factor of 10.

Also, while adding damping reduces the maximum response level, the problem of variation of blade fatigue life remains, which means some blades will still fail much earlier than others, even if the vibration response levels of all blades are lowered. This is because the maximum vibration response level possible for a mistuned bladed disc is the product of the peak vibration

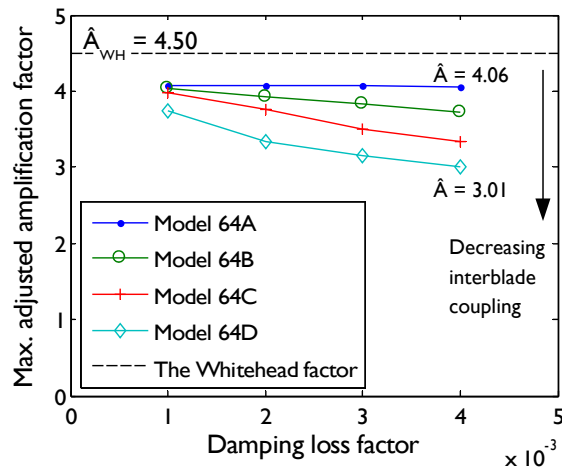


Figure 5.11: Dependence of the adjusted amplification factor on damping loss factor in 64-sector models.

response level of the cantilever blade and the maximum adjusted amplification factor. An example is shown in Figure 5.12: by increasing the damping loss factor in a bladed disc from 0.001 to 0.004, the reduction in the maximum adjusted amplification factor (19% in Model 64D) is not significant compared with that in the tuned peak vibration response (75%).

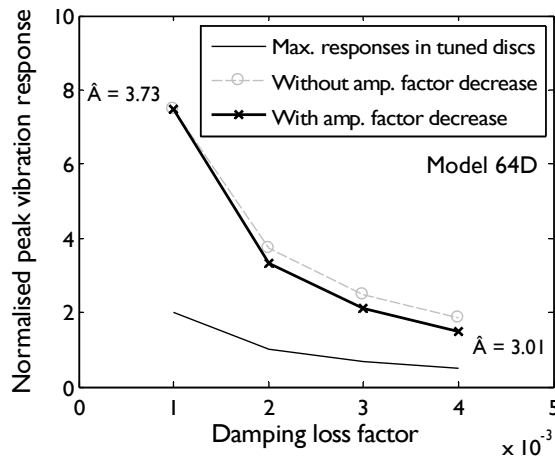


Figure 5.12: Dependence of maximum vibration responses on damping loss factor in tuned and mistuned models.

5.3.4 Maximum amplification factors of six 24-sector blisks

After the analyses carried out on two lumped parameter models in Sections 5.3.2 and 5.3.3, the maximum amplification factors of the six 24-sector blisks

under 6EO excitation are sought. The maximum amplification factors are compared because the responses measured in the FMM reduced order model are not directly proportional to the peak stress encountered in blades. Although the damping loss factor of the bladed disc test piece is determined by properties of the blisk material, the factor is varied between 0.001 and 0.005 in the models to simulate the effect of additional damping devices. Because the blade responses would increase if all blades have negative frequency mistuning, the average of mistuning parameters in a worst mistuning pattern is set at zero such that the amplification factor shows the genuine variation of blade responses. The maximum allowable mistune is 20%.

The dependence of the maximum amplification factor on damping and bladed disc design is shown in Figure 5.13. The biggest difference between the results on blisks and those on 64-sector lumped parameter models is that a heavier bladed disc does not always lead to a lower maximum amplification factor on blisks, especially under a small damping loss factor. Such difference is due to differences between lumped parameter and real blisks models, and the breakdown of the approximations related to the FMM algorithm in flexible bladed discs and bladed discs with large mistuning.

Otherwise, the findings on 24-sector blisks are similar to those on 64-sector lumped parameter models. The maximum amplification factors of blisks with more flexible discs are nearly independent of the damping loss factor. The maximum amplification factor in Blisk D is slightly lower than those in Blisks B and C under a high level of damping because the interblade coupling in Blisk D is lower. The maximum amplification factor in Blisk A is lower than other designs under low damping loss factor as well.

Although the maximum amplification factor in stiff blisks can be reduced by adding damping, the reduction of the maximum amplification factor in Blisk F ($\approx 13\%$) is small compared with that of the reduction in the tuned response ($\approx 80\%$) if the damping loss factor increases from 0.001 to 0.005. The maximum amplification factor also decreases slightly with increasing disc stiffness under a relatively high damping loss factor, but it is not always possible to attach a 20mm-thick stiffening ring to a 5mm-thick blisk to lower the maximum amplification factor by 10%.

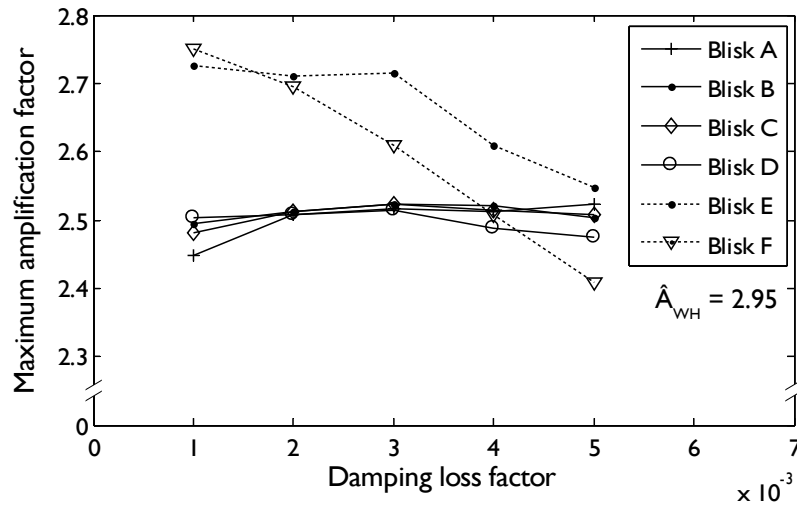


Figure 5.13: Dependence of the maximum amplification factor on damping loss factors in 24-sector blisks.

5.4 Robustness of bladed disc designs in previous research

There are four findings made in the investigation in Sections 5.3, and these are summarised below:

1. The maximum amplification factor of a bladed disc design depends on design parameters other than the number of blades.
2. The maximum amplification factor of a bladed disc design is significantly lower than the Whitehead Factor if the level of damping is high and the level of interblade coupling is low.
3. The maximum vibration response level in a mistuned bladed disc is reduced by adding damping. However the reduction in the maximum amplification factor is insignificant (e.g. 15% in a 64-sector model) compared with the reduction in the tuned peak vibration response level (e.g. 75% in a 64-sector model).
4. The maximum amplification factor of a bladed disc design can be reduced by incorporating a stiffer, or heavier, disc in some situations.

It is timely to check if the four findings above explain the variation of the maximum amplification factors encountered in previous research. Four

bladed discs from Myhre [78] and Petrov and Ewins [89] are examined because the design parameters of the specimen bladed discs and the maximum (or the 99th percentile) amplification factors are explicitly provided in these references. The results reported in these two studies are summarised below.

Myhre investigated the amplification factor distributions of two 30-sector blisk models, called NS and PS, under a 3EO excitation and a modal damping ratio of 1%. Blisk PS is shown in Figure 5.14, and Blisk NS is created from Blisk PS by removing shrouds. The difference of natural frequency distributions in Blisks PS and NS, which are shown in Figures 5.15 and 5.16, respectively, indicate different levels of interblade coupling. Myhre has found that the 99th percentile amplification factor of Blisks PS and NS under a rotation speed of 1500 rev/min are 2.3 and 1.3, respectively, against the Whitehead Factor of 3.24.

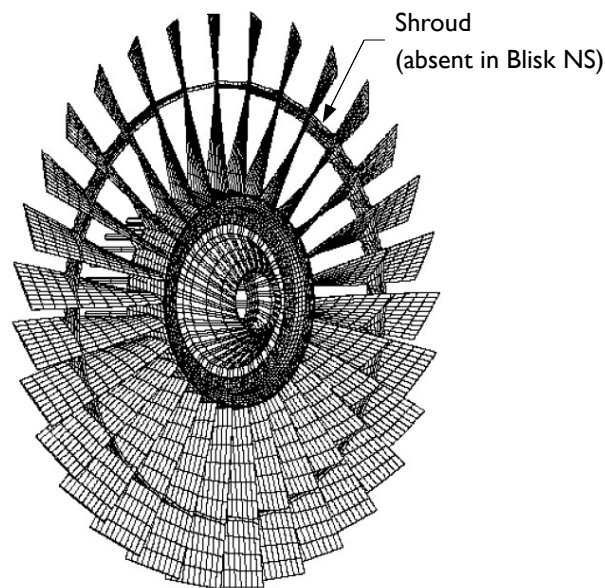


Figure 5.14: Blisk PS, after Myhre [78].

Petrov and Ewins sought the maximum amplification factors on a 26-bladed fan disc and a 92-bladed high pressure turbine disc. The bladed discs are illustrated in Figure 5.17, and selected normalised natural frequencies are plotted in Figure 5.18. Both bladed discs are assumed to have a damping loss factor of 0.003 and under a 6EO excitation. As shown in Table 5.1, the turbine disc experiences a maximum amplification factor close to the Whitehead Factor while the fan disc does not.

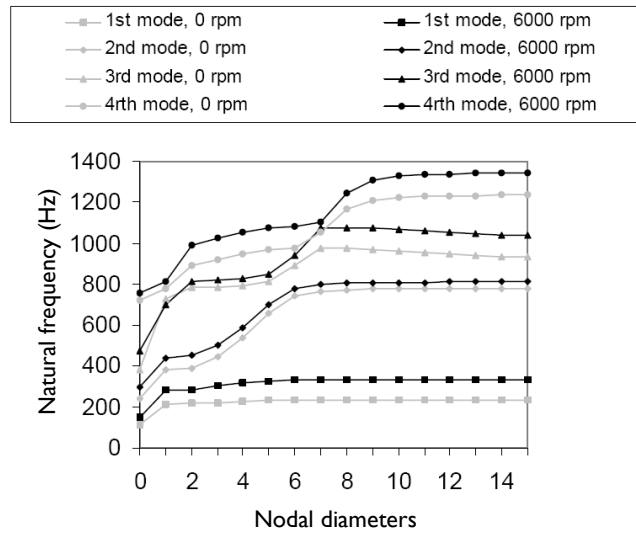


Figure 5.15: Natural frequencies of the first four mode families of Blisk PS, both stationary and rotating, after Myhre [78].

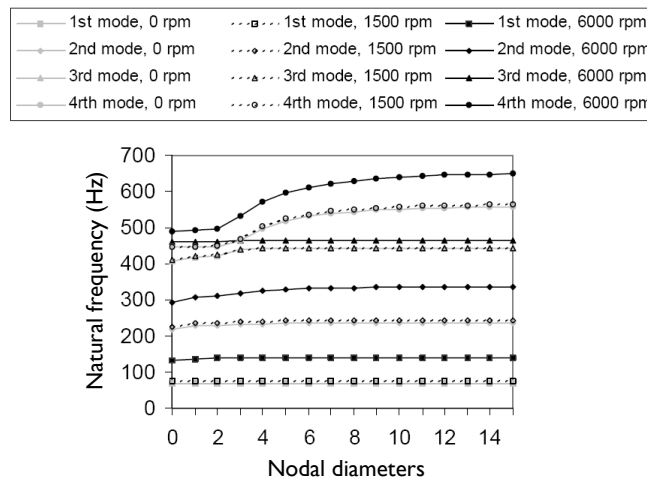


Figure 5.16: Natural frequencies of the first four mode families of Blisk NS, both stationary and rotating, after Myhre [78].

The results in previous research are compared with the robustness analysis carried out in Section 5.3 by locating the bladed disc specimens on the robustness map (Figure 5.7), according to the levels of interblade coupling and damping loss factor of the four bladed disc designs. Although the interblade coupling ratio is defined in Chapter 6, for the moment the level of interblade coupling of a bladed disc design under nEO excitation is assumed to be the smallest fractional difference between the squares of natural fre-

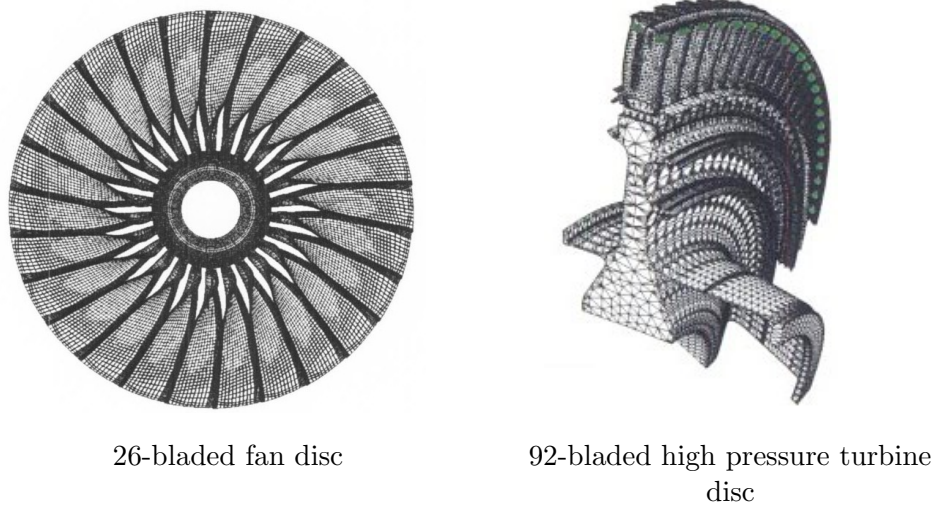


Figure 5.17: Models analysed by Petrov and Ewins [89].

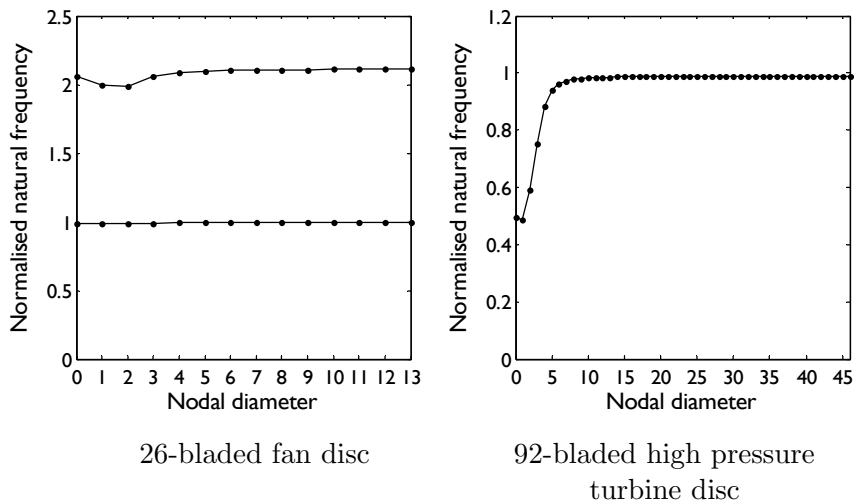


Figure 5.18: Selected normalised natural frequencies of models analysed by Petrov and Ewins [89].

quencies of nND mode and the neighbouring modes. The level of interblade coupling in a 6-DOF model under 1EO excitation is equal to the interblade stiffness K , and those of the bladed disc designs adopted by Myhre and Petrov and Ewins are listed in Table 5.4.

Figure 5.19 shows that the robustness map can explain the robustness behaviour of a wide range of bladed disc designs. The maximum (or the 99th percentile) amplification factors in Blisk NS and the 26-bladed fan bladed disc are relatively low because the level of interblade coupling in these two

Model	Excitation Order	Level of interblade coupling	\hat{A}_{WH}	Reported results
Blisk PS	3	0.0576	3.24	$A_{99} = 2.3$
Blisk NS	3	0.001	3.24	$A_{99} = 1.3$
Fan	6	0.0018	3.05	$\hat{A} = 1.9$
H. Pres. Turbine	6	0.019	5.30	$\hat{A} = 5.02$

Table 5.4: Levels of interblade coupling and maximum (or 99th percentile) amplification factors of bladed disc designs, after References [78] and [89].

models are lower than those in Blisk PS and the 92-bladed turbine bladed disc.

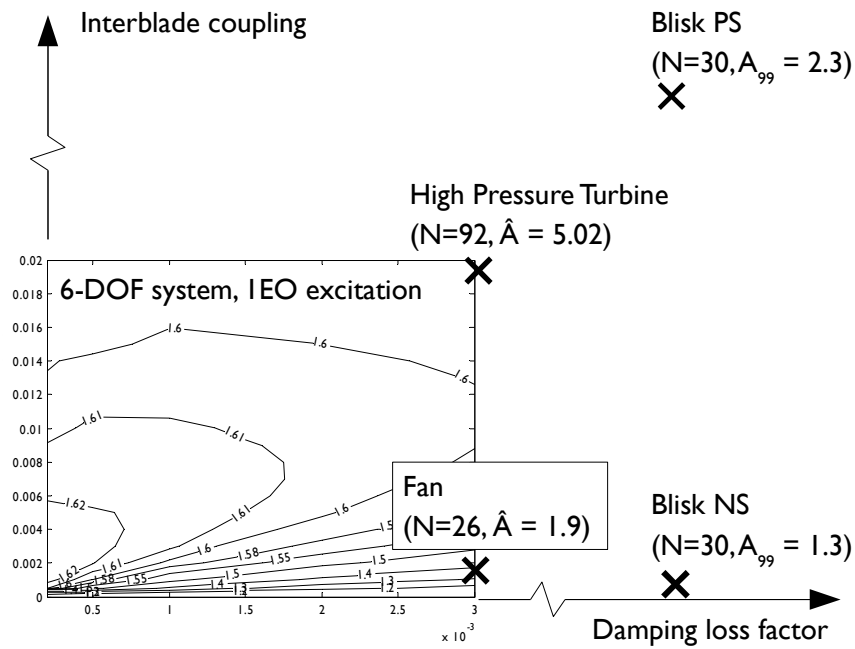


Figure 5.19: Locations of four bladed disc designs adopted in previous research in the robustness map.

5.5 Amplification factor distribution in special situations

5.5.1 Amplification factor distribution in bladed discs with damping mistuning

Although structural damping alone is applied to simulations in Section 5.3, damping in bladed discs mainly comes from friction damping and aerodynamic damping, and both of these can differ across the blades. The variation of damping across blades on a bladed disc is called *damping mistuning*. For example, damping mistuning arises if the properties of friction joints change due to wear, and the extents of wear at joints on a bladed disc are not uniform. The variation of vibration response levels in damping-mistuned bladed discs is investigated below.

The amplification factor has to be defined carefully in dealing with damping mistuned bladed discs. The traditional amplification factor would increase if the levels of damping at all friction joints on a tuned bladed disc are reduced by the same amount because the forced vibration responses of all blades increase, but such an increment does not represent the variation in the peak responses of blades. Therefore, the adjusted amplification factor (Section 3.1) is used to measure the blade responses in damping-mistuned bladed discs, where the vibration response of a mistuned blade is compared with the peak cantilever vibration response of that mistuned blade, under the damping ratio of that blade.

The distribution of the adjusted amplification factor is studied by running three 5000-sample DMC simulations on Model 64B under 6EO excitation. The mistuning parameters of blades are normally distributed with the standard deviation of 1% in all three simulations. The tails of the normal distribution are culled such that the maximum allowable mistune is 3.3%. The damping mistuning of maxima 0%, 20% and 40%, uniformly distributed, are applied to blades, and the adjusted amplification factor pdfs are plotted in Figure 5.20.

The adjusted amplification factor pdf from the simulation with maximum 20% damping mistuning has a very similar shape to that with no damping mistuning, despite the upper bound of the adjusted amplification factor being 5.34 - or 20% higher than the Whitehead Factor - according to Equation (3.19). The similarity between the three curves in Figure 5.20 shows that the

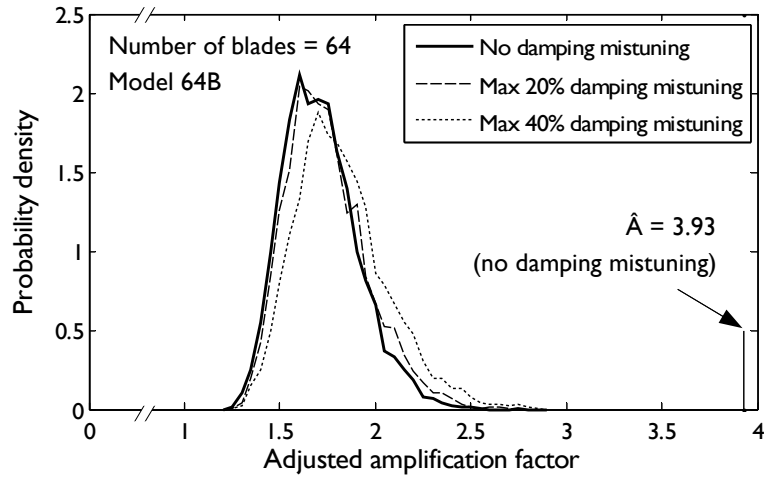


Figure 5.20: Adjusted amplification factor pdfs under various levels of damping mistuning.

vibration responses of bladed discs are more robust to damping mistuning than to blade frequency mistuning.

5.5.2 Amplification factor distribution with excitation of modes in veering regions

Veering regions are the frequency regions where the modes from two different mode families with the same number of nodal diameters have natural frequencies close to each other. The sector mode shape of a mode in a veering region has to be described using more than one blade-alone mode shape, or the combination of a blade-alone mode and a disc mode. The modal properties of bladed discs are presented in Appendix A.

The adjusted amplification factor distributions of two 64-sector, 2-DOF-per-sector lumped parameter models under 4EO excitation are investigated. Model 64E is created by reducing the intersector stiffness of Model 64C such that the disc-alone natural frequency of the 4ND mode is equal to 182 Hz, the blade-alone natural frequency. As a result, the veering region of Model 64E is located at the 4ND mode. The parameters of Models 64C and 64E are listed in Table 5.5 with the normalised natural frequencies in the vicinity of the blade-alone natural frequency plotted in Figure 5.21.

The distinction between the amplification factor and adjusted amplification factor is important in analyses involving responses contributed by mode

Model	K (Nm ⁻¹)	M (kg)	K_G (Nm ⁻¹)	k (Nm ⁻¹)	m (kg)
64C	16739500	1.0125	36.779	36778.6	0.028125
64E	8696691				

(Variables are defined in Figure 5.3, $\eta = 0.002$.)

Table 5.5: Design parameters of Models 64C and 64E.

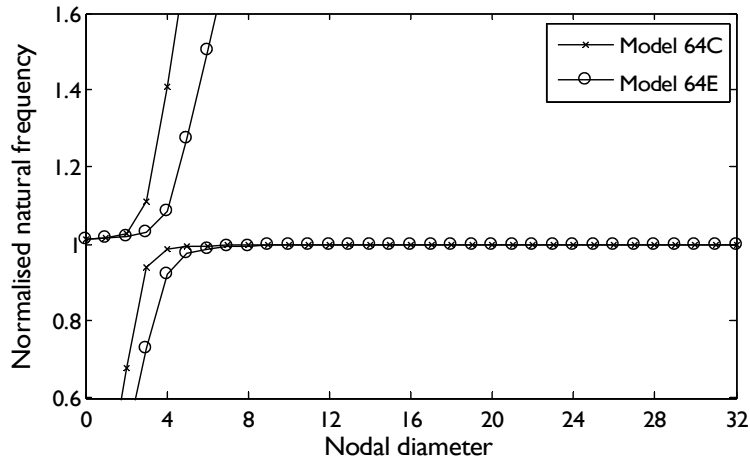


Figure 5.21: Selected normalised natural frequencies of Models 64C and 64E.

shapes in the veering regions. This is because the tuned vibration responses in veering regions are much lower than the responses elsewhere: Figure 5.22 shows that the tuned vibration response of Model 64E under 4EO excitation is only 54% that of the peak cantilever blade vibration response.

A DMC simulation of 10,000 mistuned bladed disc samples was carried out on Model 64E, and an optimisation analysis is carried out afterwards to find the maximum adjusted amplification factor. The blade masses were perturbed such that the mistuning parameters of the blades are normally distributed with $\sigma = 0.04$. The maximum allowable mistune is 0.133. The maximum adjusted amplification factor of Model 64E under 4EO excitation is found to be 3.48, which corresponds to the maximum amplification factor of 6.42. The maximum adjusted amplification factor is below the Whitehead Factor of 4.5 while the maximum amplification factor is not. This finding explains why previous research showed as many as 7% of all bladed discs investigated have amplification factors higher than the Whitehead Factor in this situation [58]: amplification factors appear to be very high, because the tuned peak response level under excitation of modes in the veering region

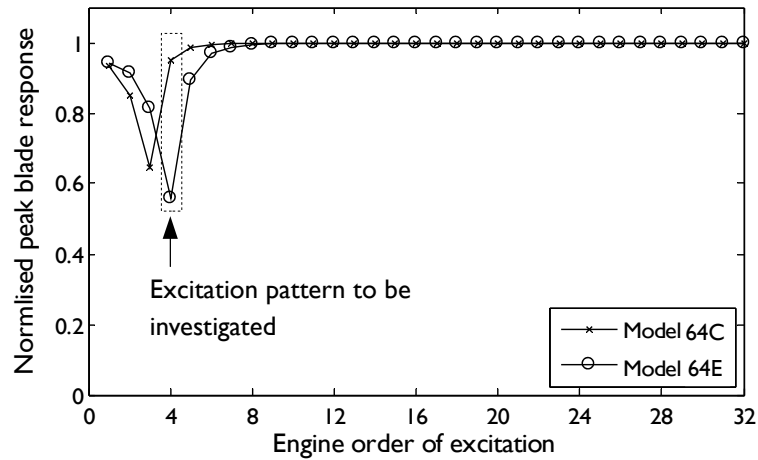


Figure 5.22: Tuned vibration response levels of Models 64C and 64E under various EO excitations.

is lower than that outside the region. By selecting an excitation order-independent response level as a basis, the current simulation shows that the Whitehead Factor can sometimes represent the upper bound of the adjusted amplification factor if the modes in the veering region are excited.

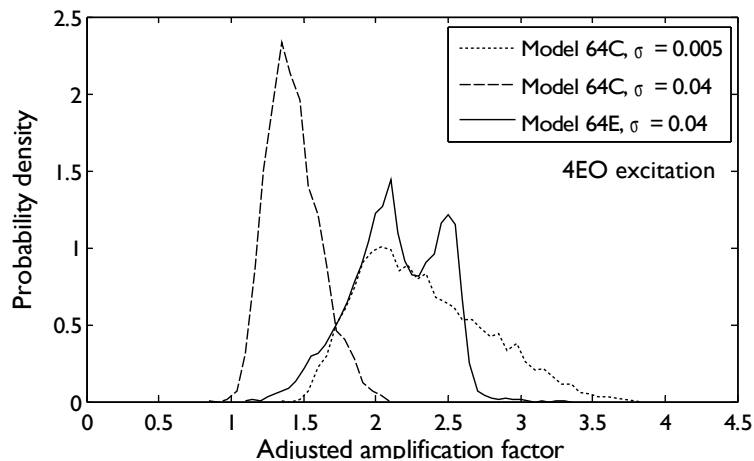


Figure 5.23: Adjusted amplification factor pdfs of Models 64C and 64E.

The adjusted amplification factor pdf from Model 64E are compared with those from two similar 2000-sample DMC simulations on Model 64C in Figure 5.23. One feature of the adjusted amplification factor distribution with excitation of modes in veering regions is its bimodality, and this is investigated by considering the resonance frequency, which is the excitation frequency where the highest response is found. From Figure 5.24, the reso-

nance frequencies of samples form two distinct groups (denoted V1 and V2) scatter around the two tuned 4ND natural frequencies of Model 64E (167 Hz and 197 Hz). By plotting the amplification factor pdf of each group in Figure 5.25, each peak in the amplification factor pdf of all samples is found to be contributed by one group of samples.

Figure 5.25 also shows another feature of the amplification factor distribution in this situation. The amplification factor pdfs of both Groups V1 and V2 are skewed to the right hand side. This is contrary to an amplification factor pdf without excitation of modes in the veering region. Two examples from Model 64C are plotted in Figure 5.23. It means high adjusted amplification factors are more likely to be observed in practice if modes in the veering region are excited.

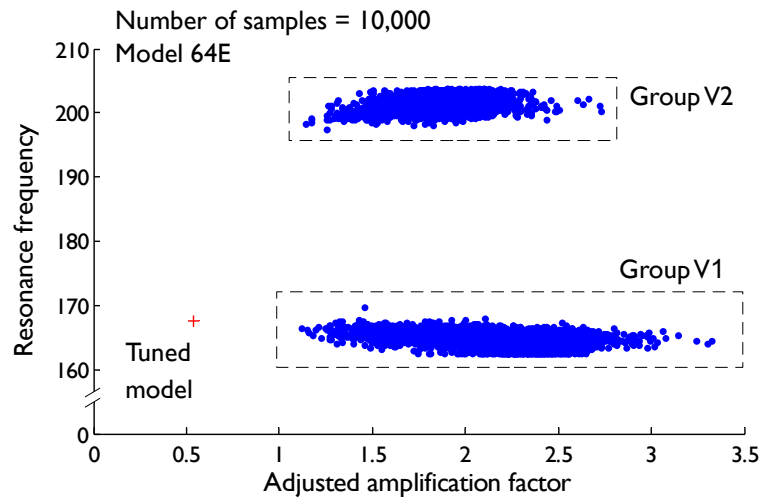


Figure 5.24: Correlation between the adjusted amplification factor and the resonance frequency.

5.5.3 Amplification factor distribution in apparently-tuned bladed discs

Nikolic [80] pointed out that the mistuning parameter in terms of the blade natural frequency is not a physical parameter by itself, but a consequence of the deviation of either the blade stiffness or the blade mass, or both of them, from their respective design values. An extreme example of illustrating this argument is an apparently-tuned bladed disc. Apparently-tuned bladed discs are bladed discs with mistuned blades, but the blade-alone natural

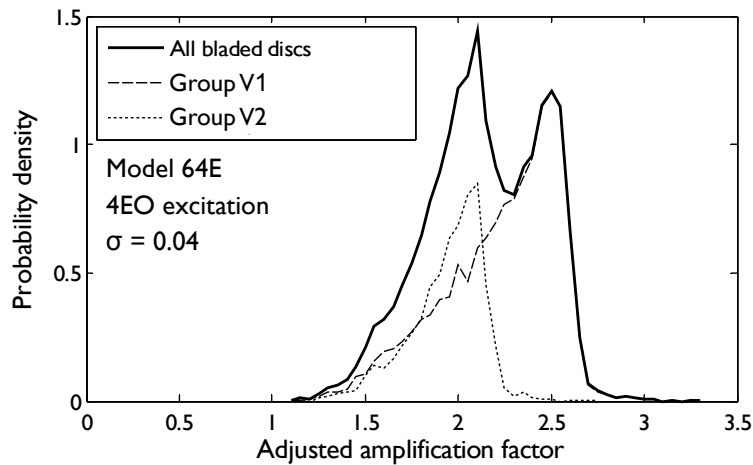


Figure 5.25: Adjusted amplification factor pdfs of all and selected samples.

frequencies on all blades are equal. For example, Sever [117] created an apparently-tuned bladed disc by removing masses at blade tips, in order to reduce the scatter of blade natural frequencies of a mistuned blisk test piece.

A 2000-sample DMC simulation is carried out on Model 64B under 6EO excitation, with blade stiffnesses and masses proportionally mistuned such that the blade natural frequencies of all blades are kept at 182 Hz. Figure 5.26(a) shows the adjusted amplification factor pdf of apparently-tuned bladed disc samples given the standard deviation and maximum fractional blade mass (thus stiffness) perturbation are 0.04 and 0.133 respectively. The scatter in amplification factor (the maximum in 2000 samples being 1.05) is in the same order as that of the perturbation of the masses. This is much narrower than scatter of the adjusted amplification factor if the blades are mistuned in a normal fashion. The adjusted amplification factor pdf in Figure 5.26(b) is generated by mistuning 1000 bladed discs with the standard deviation of blade-alone natural frequency being 0.001. It shows that the commonly-used approach of quantifying mistuning by the blade-alone natural frequency is valid, but a separation of mass and stiffness mistuning elements is preferred if accurate results are sought.

5.6 Summary

Fatigue lives of bladed discs based on a robust bladed disc design are generally longer because a reduction of the alternating stress by 4% can double

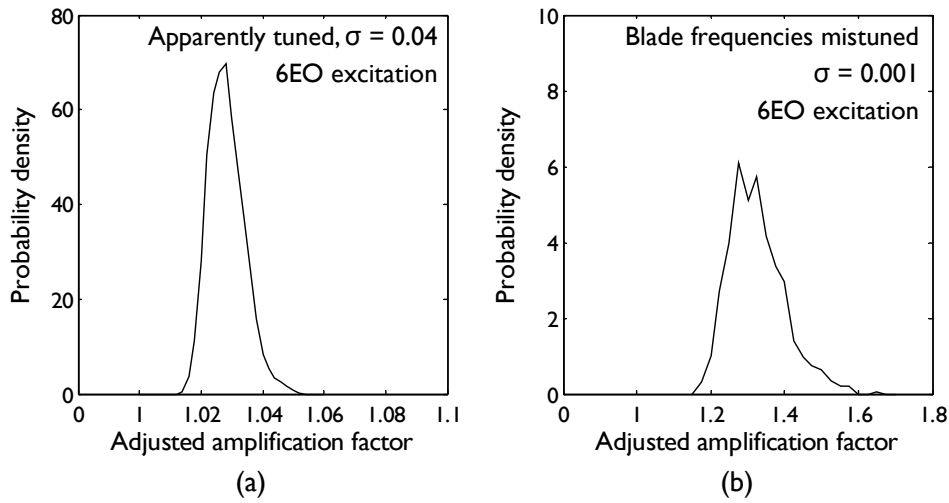


Figure 5.26: Adjusted amplification factor pdfs of (a) apparently tuned bladed discs and (b) mistuned bladed discs.

the fatigue live of blades. Also, the variation of fatigue lives across blades on a single bladed disc can be reduced.

The dependence of robustness of a bladed disc design is investigated using three representative models. It is found that the maximum amplification factor depends on design parameters other than the number of blades. For example, it is found that the maximum amplification factor can be lowered by increasing the level of damping in a bladed disc design, but major design changes are usually involved. The findings in this chapter are used to explain the behaviour of the maximum (or the 99th percentile) amplification factors reported in previous research.

The amplification factor distributions of three special cases are also investigated: firstly, it is found that the adjusted amplification factor distribution is robust under damping mistuning; secondly, high adjusted amplification factors are more likely to be observed in the situation where modes in the veering region are excited, because the pdf is skewed to the right hand side, and thirdly, the scatter of the adjusted amplification factor in apparently-tuned bladed discs is much narrower than that in typically mistuned bladed discs.

Chapter 6

Improving robustness of bladed discs by tolerance design

It has been shown in the previous chapter that the robustness is not always enhanced by small changes of bladed disc designs. In the present chapter, the amplification factor of a mistuned bladed disc is managed by controlling the mistuning pattern on a bladed disc either by (i) imposing a small maximum allowable mistune according to **the small mistuning approach** or (ii) incorporating non-identical blades of specific patterns, known as the **intentional mistuning approach**, which includes the deterministic large mistuning concept investigated in previous research. The probabilistic large mistuning concept proposed previously, which means specifying a large maximum allowable mistune, is not discussed in this thesis.

Because the relationship between robustness and input variability in a bladed disc design forms a continuous curve, the first-order maximum adjusted amplification factor sensitivity in a single-DOF-per-sector system is derived to illustrate the dependence of the robustness sensitivity on design parameters of a bladed disc design. Although the derived maximum amplification factor sensitivity does not estimate the true relationship accurately, the derivation provides a theoretical background for a new definition of the interblade coupling ratio.

By carrying out simulations and optimisation analysis, it is found that reducing the maximum allowable mistune and reducing scatter can lower the maximum amplification factor and the 99.9th percentile amplification factor, respectively, in flexible bladed discs. The maximum allowable mistune and the

scatter can be kept at realistic levels to achieve such reductions if the interblade coupling ratio in a bladed disc design is high.

A tool based on the importance sampling method is used to reduce the computational effort in determining the magnitude of intentional mistuning. The potential of a “linear” mistuning pattern to become an effective intentional mistuning pattern is evaluated by observing the amplification factors of bladed discs with combined intentional mistuning and additional random mistuning. It is found that the median and the 99.9th percentile amplification factor can be reduced, compared with those of the tuned design, by imposing a linear mistuning pattern.

6.1 Introduction

The discussion in Chapter 5 has shown that the robustness of a bladed disc design does not always improve significantly solely by small design changes, and the proposed improvements are effective only in certain bladed disc designs. As a result, the previously less-preferred method of controlling the mistuning pattern on individual bladed discs - using either the small mistuning approach or intentional mistuning approach - is considered in this chapter.

The small mistuning approach involves reducing the maximum amplification factor by controlling the maximum allowable mistune. The investigation of the small mistuning approach begins in Section 6.2 with deriving the sensitivity of the maximum amplification factor of a single-DOF-per-sector lumped parameter system, and verifying the derived sensitivity against the true counterpart in a 6-DOF cyclic lumped parameter model. Based on the sensitivity expression, a new interblade coupling ratio, c , is defined in Section 6.3.

The potential of the small mistuning approach is evaluated in Section 6.4 by using the sensitivity information of the 99.9th amplification factor and the maximum adjusted amplification factor on 24-sector blisks and 64-sector lumped parameter models, respectively.

The intentional mistuning approach [21, 52], which reduces the likelihood of extremely high amplification factors by specifying non-identical blades of specific patterns at the design stage, is discussed in Section 6.5. An importance sampling-based tool is adapted from that described by Fonseca et al [38] (Section 6.5.1) to determine the optimal intentional mistuning strength

efficiently. The effect of the intentional mistuning approach is demonstrated on a 24-sector blisk sample in Section 6.5.2.

The available approaches of improving robustness of bladed discs, based on the findings in Chapters 5 and 6, are presented in the conclusions in Chapter 8.

6.1.1 Issues related to the “large mistuning concept”

Nikolic et al [82] proposed reducing the likelihood of extremely high amplification factors occurring by incorporating mistuning patterns with magnitudes as high as 40%, and this is called the *large mistuning concept*. The concept is motivated by their observation that the highest amplification factor within 1000 mistuned bladed disc samples with a 40% scatter is 1.35, which is 33% lower than 2.02, the highest factor of another 1000 samples with a 0.5% scatter, on the same 26-sector bladed disc design.

Nikolic et al proposed two variants of the large mistuning concept - namely, the probabilistic and the deterministic variants. The *probabilistic large mistuning concept* suggests allowing large (up to 40%) mistune to exist randomly on a bladed disc. On the other hand, the *deterministic large mistuning concept* involves specifying intentional mistuning patterns with magnitudes up to 40% at design stage. They have found that the highest amplification factor of 1000 bladed discs with an intentional mistuning pattern can be as low as 1.04.

The large mistuning concept is not addressed directly in this thesis. The deterministic large mistuning concept is discussed in this chapter as a form of intentional mistuning. The probabilistic large mistuning concept is not discussed in this thesis because of three reasons: (i) the standard deviation of mistuning parameters is determined by the manufacturing processes and it cannot be increased easily; (ii) random large mistune changes the structure of a bladed disc significantly in a random way, and can lead to secondary effects (e.g. unbalanced rotors); and (iii) the bladed discs having the worst mistuning patterns would be considered as “safe” because the maximum mistune of the worst mistuning pattern are much lower than the maximum allowable mistune.

6.2 Maximum amplification factor sensitivity to mass mistune

It is shown in Figure 4.7 that the change of robustness is smooth with respect to the change in input variability, regardless of the approach by which the robustness and input variability are quantified. This means robustness sensitivities to input variability can be found, and the sensitivities are the slopes of the curves at zero input variability in Figure 4.7. This property has been applied (i) to find the sensitivities of the mean and standard deviation of blade responses in mistuned bladed discs [55], and (ii) to specify the maximum allowable mistune, given an allowable maximum amplification factor [114].

In this research, the maximum adjusted amplification factor sensitivity to maximum mass mistune in a single-DOF-per-sector lumped parameter model is derived in Section 6.2.1, assuming only structural damping with a damping loss factor η exists. Only the masses are mistuned in this analysis because the adjusted amplification factor would be equivalent to the amplification factor, and certain terms in mode shape derivatives can be eliminated. The derivation is similar if the stiffness elements in the model are perturbed. The derived expression is analysed in Section 6.2.2, and compared with the actual relationship between the maximum adjusted amplification factor and maximum allowable mistune of a 6-DOF model in Section 6.2.3.

6.2.1 Derivation

The derivation begins with finding the vibration response derivatives with respect to maximum mass mistune of a given mistuning pattern. The extent of mistune is adjusted by a scalar denoted α . Therefore, the mass matrix of a mistuned system is expressed in the form shown in Equation (6.1).

$$[M] = \begin{bmatrix} m & & & 0 \\ & m & & \\ & & \ddots & \\ 0 & & & m \end{bmatrix} + \alpha \begin{bmatrix} \Delta m_1 & & & 0 \\ & \Delta m_2 & & \\ & & \ddots & \\ 0 & & & \Delta m_N \end{bmatrix} \quad (6.1)$$

In a system with natural frequencies, ω_l , and mode shape matrix, $[\Psi]$ excited under an n EO excitation with the force vector $\{f_n\}$ and frequency

Ω , the vibration responses of the DOFs, $\{u\}$, can be found by calculating Equation (6.2):

$$\{u\} = \sum_{l=1}^N \frac{\{\psi_l\}^T \{f\}}{\omega_l^2 - \Omega^2 + j\eta\omega_l^2} \{\psi_l\} \quad (6.2)$$

The vibration responses of a slightly mistuned system under n EO excitation are mainly contributed by the split n -nodal-diameter (n ND) mode pair called $\{\psi_{n_1}\}$ and $\{\psi_{n_2}\}$, such that

$$\{u\} \approx \sum_{l=n_1, n_2} \frac{\{\psi_l\}^T \{f_n\}}{\omega_l^2 - \Omega^2 + j\eta\omega_l^2} \{\psi_l\} \quad (6.3)$$

The response sensitivity vector, written as $\{u'\}$, can be found by taking the derivative of Equation (6.3) with respect to the maximum mistune, α :

$$\begin{aligned} \frac{\partial \{u\}}{\partial \alpha} = \{u'\} \approx & \sum_{l=n_1, n_2} \frac{\left(\{\psi_l\}^T \{f_n\}\right)'}{\omega_l^2 - \Omega^2 + j\eta\omega_l^2} \{\psi_l\} + \sum_{l=n_1, n_2} \frac{\{\psi_l\}^T \{f_n\}}{\omega_l^2 - \Omega^2 + j\eta\omega_l^2} \{\psi'_l\} \\ & + \sum_{l=n_1, n_2} \{\psi_l\}^T \{f_n\} \left(\frac{1}{\omega_l^2 - \Omega^2 + j\eta\omega_l^2}\right)' \{\psi_l\} \end{aligned} \quad (6.4)$$

The equations finding the mode shape and natural frequency derivatives are listed in Appendix C. In slightly mistuned systems, Equation (6.4) can be simplified according to the arguments listed in Appendix D.1 and becomes

$$\frac{\partial \{u\}}{\partial \alpha} = \{u'\} \approx [\psi'_{n_1} \ \psi'_{n_2}] \frac{[\psi_{n_1} \ \psi_{n_2}]^T \{f_n\}}{j\eta\omega_n^2} + \{\psi_{n_2}\} \frac{\{\psi_{n_2}\}^T \{f_n\}}{\omega_n^2} \frac{S'}{\eta^2} \quad (6.5)$$

After finding the vibration response sensitivities, the vibration response *level* sensitivity of DOF i with respect to maximum mass mistune can be found using Equation (6.6) (See [89]):

$$\frac{\partial \{|u|\}_i}{\partial \alpha} = \{|u|\}'_i = \text{Re} \left(\frac{\bar{u}_i}{|u_i|} (u_i)' \right) \quad (6.6)$$

The ratio $\bar{u}_i/|u_i|$ can, again, be simplified according to Appendix D.1. By dividing Equation (6.6) by the peak cantilever blade response, the adjusted amplification factor sensitivity to the maximum mistune with a par-

ticular mistuning pattern can be expressed in terms of Equation (6.7):

$$\frac{\partial A}{\partial \alpha} = \max_{i=1 \dots N} \left(\operatorname{Re} \left(e^{-j \frac{2\pi n(i-1)}{N}} \frac{\partial u_i}{\partial \alpha} \right) \right) \frac{1}{j\eta k} \quad (6.7)$$

The maximum adjusted amplification factor sensitivity to maximum mass perturbation can be found by determining the maximum value of $\frac{\partial A}{\partial \alpha}$ using Equation (6.7).

6.2.2 Analysis

While the maximum adjusted amplification factor sensitivity to the maximum allowable mistune can be sought by calculating Equations (6.7) and (6.5), the components of Equation (6.5) are examined to analyse the cause of high amplification factors in slightly mistuned bladed discs.

First, the factors contributing to the response sensitivity are sought. As it is known that mistuning leads to mode distortion and mode splitting (see Appendix A), the representation of these two effects is identified in Equation (6.5). Because the first term in Equation (6.5) includes mode shape derivatives, and the second term contains the natural frequency derivatives, the first and second terms of this equation refer to the changes of response due to mode distortion and mode splitting, respectively. Moreover, the layout of Equation (6.5) shows that the mode distortion and mode splitting effects are separable in slightly mistuned systems.

Second, the factors behind the maximum adjusted amplification factor sensitivity to the maximum mistune of a mistuning pattern are investigated by evaluating all derivatives appearing in Equation (6.5). It is found in Appendix D.2 that every derivative in this equation can be written as a product of design parameters and a quantity related to this particular mistuning pattern. By separating these two types of variable, the adjusted amplification factor sensitivity with respect to mistuning magnitude under an n EO excitation can be written in the form shown in Equation (6.8):

$$\frac{\partial A}{\partial \alpha} = \left(\sum_{l=1, l \neq n_1, n_2}^N \frac{\operatorname{Re}(b_l) \omega_n^2}{\omega_l^2 - \omega_n^2} + \frac{\operatorname{Re}(b_\eta)}{\eta} \right) \frac{1}{\eta k} \quad (6.8)$$

where n_1 and n_2 refer to the n ND modes of the tuned system, such that $\omega_n = \omega_{n_1} = \omega_{n_2}$. Among all variables appearing in Equation (6.8), only

the coefficients b_l 's and b_η are related to the mistuning pattern. While the relationship between the b_l 's and the mistuning pattern is complicated, the coefficient b_η , which involves to the extent of mode splitting, is proportional to the $\cos 2n\theta$ component of the mistuning pattern as investigated by Ewins [31].

The approach of sensitivity derivation is validated in a 6-DOF model in Section 6.2.3, and the layout of Equation (6.8) is taken to form a new definition of the interblade coupling ratio in Section 6.3. Moreover, this approach is used in Section 6.4.1 to explain the sensitivity of the 99.9th percentile amplification factor and the maximum adjusted amplification factor in 24- and 64-sector systems, respectively.

6.2.3 Demonstration

The validity of the derived first-order maximum adjusted amplification factor sensitivity is examined by calculating the derived sensitivities of three example 6-DOF models under an 1EO excitation, and comparing the results with the actual counterpart. The schematic of a 6-DOF model has been shown in Figure 5.2. As to the analysis carried out in Section 5.3.2, the nominal values of k and m here are equal to 1 Nm^{-1} and 1 kg , respectively, and mistuning is applied to the model by perturbing the masses. Three examples are taken to examine the validity of the derived sensitivity expression:

1. $K = 0.002$ and $\eta = 0.003$ to simulate a lightly coupled system with a relatively high damping loss factor
2. $K = 0.005$ and $\eta = 0.0015$ to simulate a lightly coupled and lightly damped system
3. $K = 0.02$ and $\eta = 0.0015$ to simulate a heavily coupled system

In this demonstration, the maximum adjusted amplification factor sensitivity to maximum allowable mistune in a design refers to the highest adjusted amplification factor sensitivity found in a DMC simulation with 50,000 samples, using Equations (6.5) and (6.7). Simulations with large number of samples are possible in finding sensitivities because the resonant frequency of a slightly mistuned system is assumed to be equal to the natural frequency of the tuned system, and no frequency sweeps are needed.

The actual relationship between the maximum adjusted amplification factor and maximum allowable mistune, the derived sensitivity and the maximum adjusted amplification factor of the three examples are plotted in Figure 6.1 and magnified plots are provided in Figure 6.2.

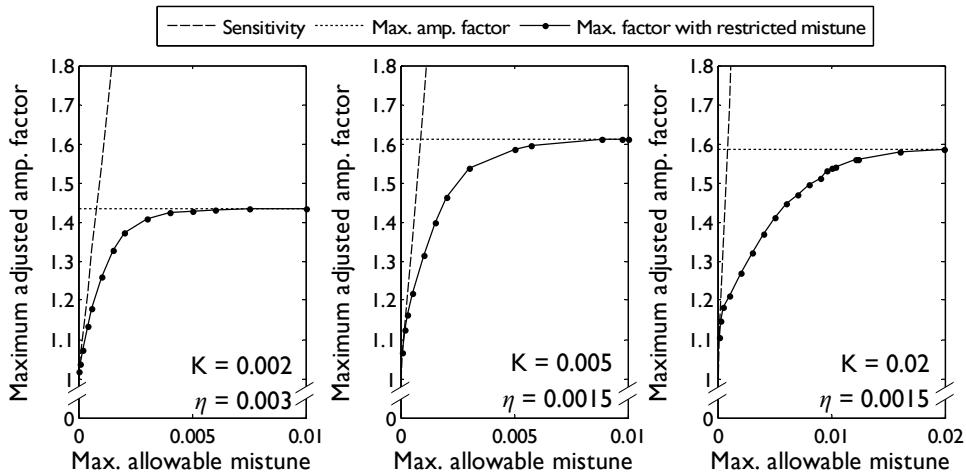


Figure 6.1: Dependence of the maximum adjusted amplification factor on maximum allowable mistune in three 6-DOF examples.

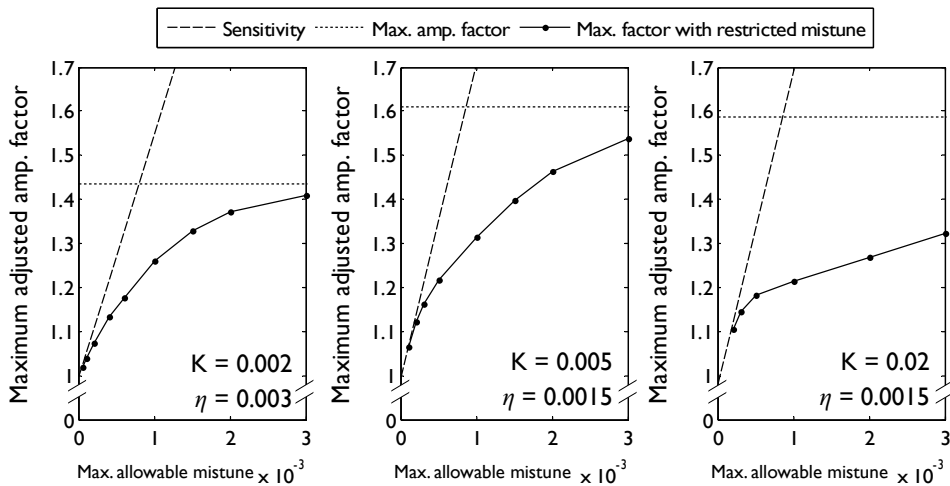


Figure 6.2: A magnified plot of Figure 6.1.

It is found here that the first-order sensitivity and robustness form an upper bound of the actual maximum allowable mistune-maximum adjusted amplification factor curve. The derived sensitivity -

1. shows the slope of the actual relationship with low levels of interblade coupling and high damping. The derived sensitivity does not describe

the actual relationship well because the latter appears as a curve in Figure 6.1. Such deviation from the linear behaviour is due to the contribution to forced vibration responses by mode shapes other than the pair of split n ND modes, and

2. is a good estimate for a model with a high level of interblade coupling and low level of damping where the maximum adjusted amplification factor is between 1 and 1.15. In this situation, the vibration responses of the DOFs are mainly contributed by mode splitting. The results can be compared with those derived by MacBain and Whaley [69], who found the maximum amplification factor to be 1.2.

The derived sensitivity is a conservative estimate in the region where the maximum adjusted amplification factor is higher than 1.2. This is because an adjusted amplification factor higher than 1.2 in this situation is contributed by a combination of mode distortion and mode splitting, which is a second-order effect.

A second-order analysis is not pursued as it does not refine the sensitivity expression. MacBain and Whaley showed [69] that the amplification factor - maximum mistune relationship is not a polynomial, even if only mode splitting is considered, such that the Taylor series expansion does not converge.

The derived maximum adjusted amplification factor sensitivity is used in subsequent analysis in a qualitative sense because it is only a rough estimate of the true counterpart. Nevertheless, the first-order sensitivity analysis provides a useful tool to estimate the contributions of mode splitting and mode distortion effects to high responses in mistuned bladed discs, which are more complex than a 6-DOF model.

6.3 A new definition of interblade coupling ratio

Although the derived sensitivity does not give an accurate approximation of the relationship between the maximum amplification factor and maximum allowable mistune, the sensitivity approach provides new arguments in defining a practically-relevant interblade coupling ratio.

Interblade coupling refers to the influence of the vibration of one blade on all other blades on a bladed disc. For example, a blade disc assembly with

a rigid disc has no interblade coupling, while another assembly of blades and a flexible disc creates a bladed disc with a high level of interblade coupling.

Interblade coupling is considered to be an important design parameter in bladed disc design. It can influence the amplification factor distribution in mistuned bladed discs, and previous research attempted to quantify the complex mechanism of interblade coupling by a single parameter called the *interblade coupling ratio*, written as c . One of three types of quantity of a tuned bladed disc design have been adopted to determine interblade coupling ratio in previous research:

1. off-diagonal terms in stiffness and mass matrices [137, 71]
2. the difference between natural frequencies [78]
3. the difference between squares of natural frequencies [112] (also reported by Srinivasan [127])

It is noted that the interblade coupling ratio can vary in the same bladed disc design according to the number of nodal diameters under consideration, and this has been taken into account in some attempts (e.g. in Reference [78]). As the derivation in Section 6.2 shows that the amplification factor sensitivity depends on the differences of the squares of the tuned natural frequencies, the proposed interblade coupling ratio is defined according to the third quantity above. Precisely speaking, the interblade coupling ratio of a bladed disc to be considered under an n EO excitation is the minimum fractional difference of the squares of the tuned natural frequencies of any mode and the n -ND mode:

$$c = \min_{l \neq n} \frac{|\omega_l^2 - \omega_n^2|}{\omega_n^2} \quad (6.9)$$

For example, the squares of the distinct natural frequencies of a tuned 6-DOF model are $\{\omega^2\} = \{k \quad k + K \quad k + 3K \quad k + 4K\}^T$. If $k = 1\text{Nm}^{-1}$, it follows that the interblade coupling ratio of a 6-DOF model to be considered under 1EO excitation is close to the magnitude of the interblade coupling stiffness:

$$c = \min_{l=0,2,3} \frac{|\omega_{l\text{ND}}^2 - \omega_{1\text{ND}}^2|}{\omega_{1\text{ND}}^2} = \frac{|\omega_{0\text{ND}}^2 - \omega_{1\text{ND}}^2|}{\omega_{1\text{ND}}^2} = \frac{K}{1 + K} \approx K \quad (6.10)$$

The proposed definition is applied to measure the interblade coupling

ratios in the four 64-sector lumped parameter models in Section 5.3.3, the six 24-sector blisk models analysed in Section 5.3.4, and the four bladed discs investigated in previous research (Section 5.4). The interblade coupling ratios of the four 64-sector models and the 6 24-sector blisks are listed in Table 6.1.

Model	n	Interblade coupling ratio, c	Model	n	Interblade coupling ratio, c
Blisk A	6	0.050	Blisk F	6	0.012
Blisk B	6	0.034	Blisk 64A	6	0.023
Blisk C	6	0.034	Blisk 64B	6	0.0052
Blisk D	6	0.023	Blisk 64C	6	0.0026
Blisk E	6	0.014	Blisk 64D	6	0.0017

(n = excitation order, examples shown in Figure 6.3 listed in bold)

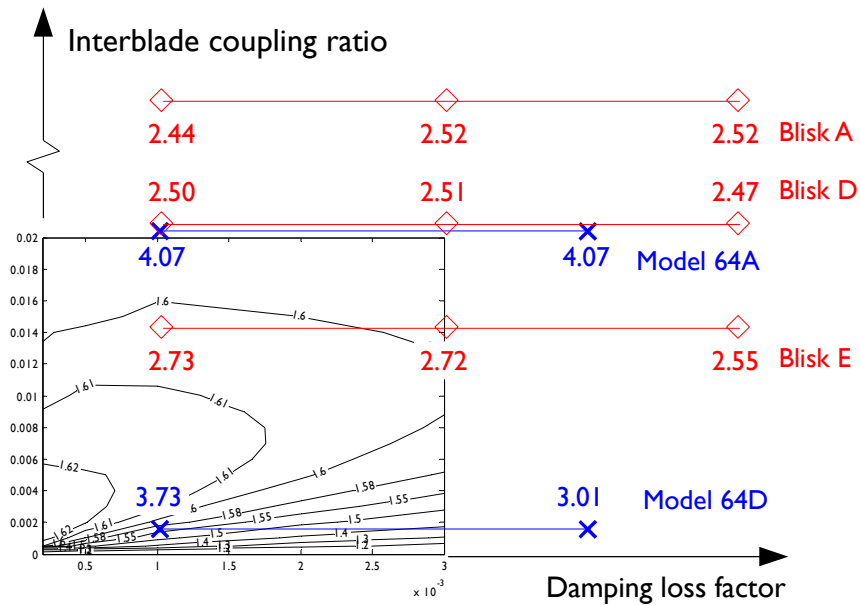
Table 6.1: Interblade coupling ratios of bladed disc designs analysed in Sections 5.3.3 and 5.3.4.

According to the proposed interblade coupling ratio, the robustness map constructed using a 6-DOF model is superimposed with the maximum amplification factors of selected bladed disc designs in Figure 6.3. (A similar comparison of the results from previous research is shown in Figure 5.19.) It is found that the dependence of the maximum amplification factor on the level of damping is nearly the same as the contours in the robustness map, regardless of number of blades.

6.4 Managing blade responses using a small mistuning approach

As the maximum amplification factor increases gradually from unity to the maximum amplification factor by increasing the maximum allowable mistune (Section 6.2), it is possible to reduce the maximum amplification factor by limiting the maximum allowable mistune. This is called the *small mistuning approach* and its potential as a means of controlling the effects of mistuning is investigated in the current section. In this approach, “small mistuning” refers to the region where the slope of the robustness-input variability curve is positive, as shown in Figure 6.4.

The small mistuning approach is not the most preferred approach to manage the extremely high responses, because it is costly in manufacture



(Elements in black: Robustness map generated using 6DOF data, Elements in red: maximum amplification factors of 24-sector blisks, Elements in blue: maximum adjusted amplification factors of 64-sector models)

Figure 6.3: Locations of selected bladed disc designs in the robustness map.

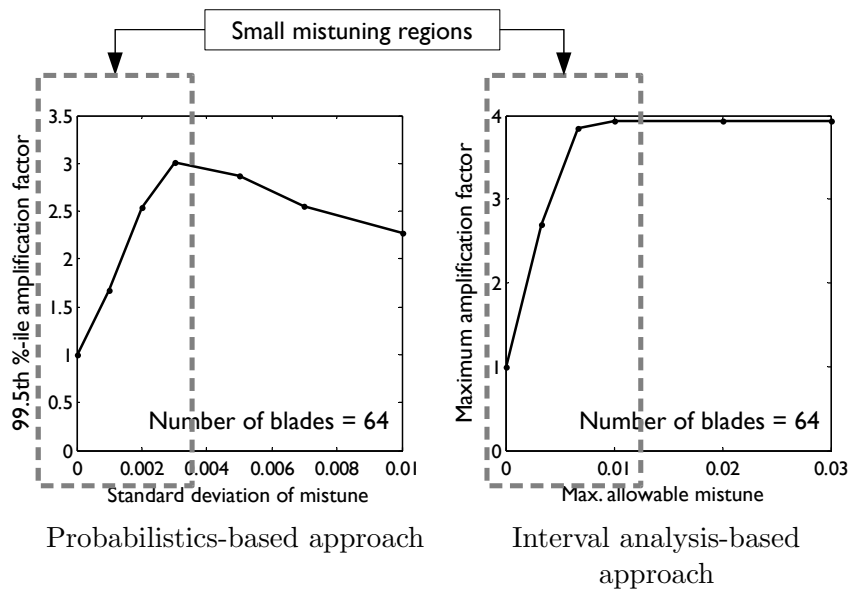


Figure 6.4: Small mistuning regions according to the approaches discussed in Section 4.4.2.

and maintenance:

1. tighter tolerances in blade dimensions lead to a higher rejection rate in manufacture;
2. it may require new and expensive fabrication techniques;
3. it leaves narrow margins for mistuning parameters change due to wear and tear; and
4. accurate measurements are required to ensure an identified mistuning pattern within the small mistuning region is related to a slightly mistuned bladed disc only.

However, the small mistuning approach is investigated because of three reasons:

1. the discussion in Chapter 5 has shown that a cheaper alternative, namely changing the design parameters, does not significantly improve the robustness of a bladed disc design;
2. without considering the cost, a small maximum allowable mistune can be specified to limit the maximum amplification factor to any given value as the slope of the robustness-input variability curve is positive; and
3. the standard deviation of mistuning parameters can currently be controlled to the order of 0.5% at the end of the manufacturing line [60], while small mistuning can refer to much higher standard deviations in some designs.

6.4.1 Dependence of robustness on level of input variability

The small mistuning approach is evaluated by carrying out simulations on five 24-sector blisk designs and three 64-sector, 2-DOF-per-sector lumped parameter systems.

Firstly, the dependence of the 99.9th percentile amplification factor ($A_{99.9}$) on the standard deviation of mistuning parameters under a 6EO excitation is investigated by carrying out DMC simulations on Blisks A, B, C, D and E described in Section 5.3.1, under two levels of damping ($\eta = 0.002$ and $\eta = 0.005$) and seven levels of standard deviation (σ) between 0.005 and 0.05.

In each 10,000-sample DMC simulation, mistuned blisks are created by picking mistuned blades randomly from a collection with a prescribed level of standard deviation, and the maximum mistune is equal to 3.3σ . Therefore, the standard deviations of mistuning patterns in a simulation are not identical. The 99th percentile amplification factors ($A_{99.9}$) of the 5 blisk models are shown in Figure 6.5, and $A_{99.9}$ of Blisks A, B and E under two levels of damping are compared in Figure 6.6.

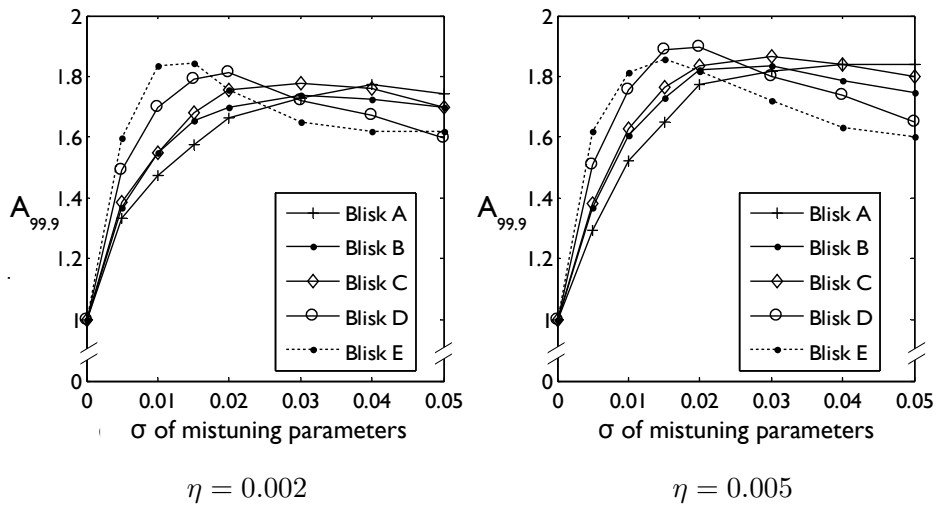


Figure 6.5: Dependence of 99.9th percentile amplification factor on mistuning scatter.

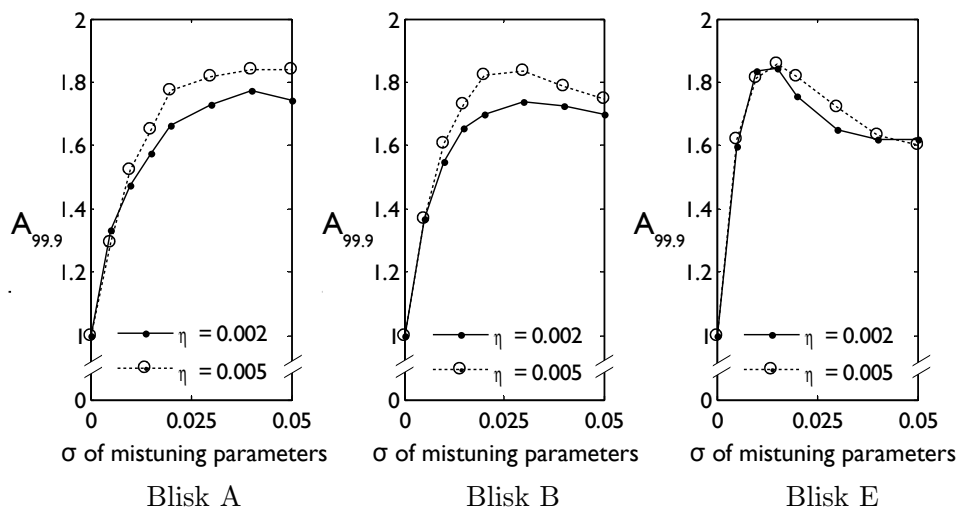


Figure 6.6: Dependence of 99.9th percentile amplification factor on mistuning scatter in various blisks.

Secondly, mistuned systems based on Models 64A, 64B and 64D described in Section 5.3.1, with a damping loss factor between 0.001 and 0.004, are excited under a 6EO excitation. The relationship between the maximum adjusted amplification factor and the maximum allowable mistune of Models 64A, 64B and 64D under a representative damping loss factor of 0.002 are plotted in Figure 6.7, and the same relationship under various damping ratios is shown in Figure 6.8.

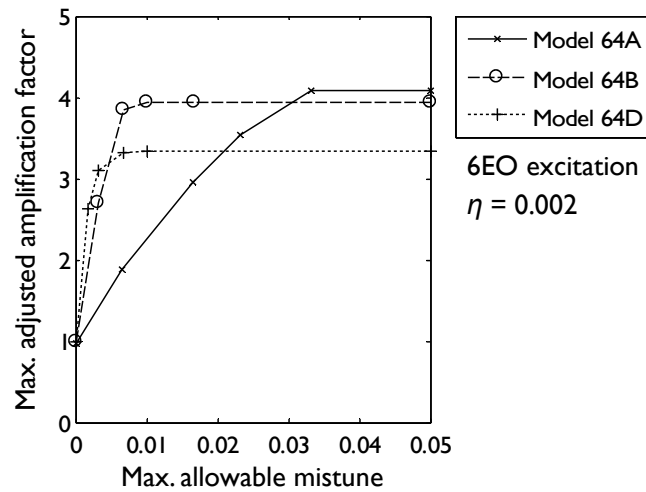


Figure 6.7: Maximum adjusted amplification factors of Models 64A, 64B and 64D under various levels of mistune.

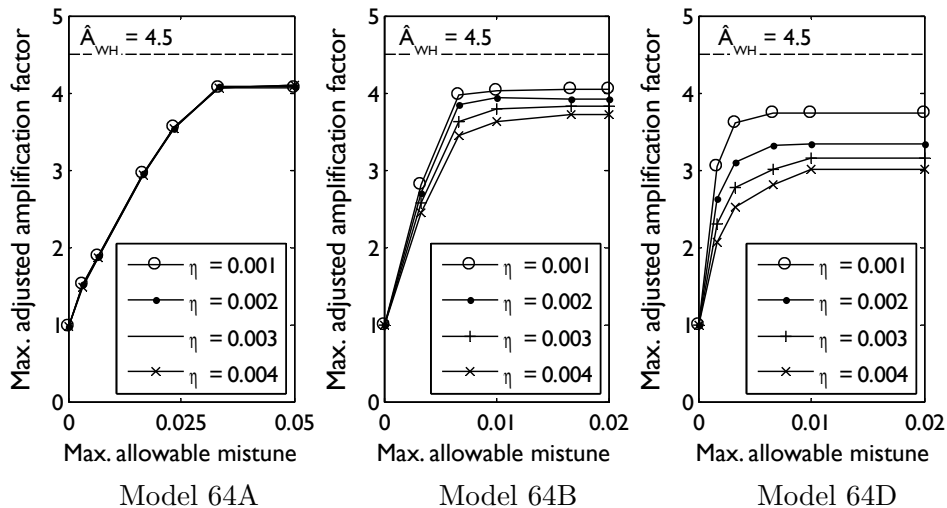


Figure 6.8: Maximum adjusted amplification factors under 6EO excitation, various levels of mistune and damping loss factors.

Since the simulation on the blisk is carried out on a probabilistics-based

approach of robust optimisation and those on the 64-sector models are carried out on the interval analysis-based counterpart, the curves between robustness and the degree of input variability from the two groups of simulations appear differently in two ways. First, the robustness curves from blisks have distinct maxima, and the level of scatter where the highest 99.9th percentile amplification factor is observed is called the *critical level of mistune*. Also, contrary to the maximum amplification factor (Section 5.3.4), the 99.9th percentile amplification factor of a blisk design can rise with increasing damping. With $\sigma = 0.03$, the 99.9th percentile amplification factor of Blisk B rises from 1.6 to 1.8 with the damping loss factor increases from 0.002 to 0.005. However, such an increase is insignificant in terms of response level as the peak response level of the tuned bladed disc decreases by 60% at the same time.

Nevertheless, the slopes of the curves are heavily dependent on the interblade coupling ratio in both simulations (Figures 6.5 and 6.7): the sensitivity is generally negatively-correlated with the interblade coupling ratio of a bladed disc design.

In comparison, the sensitivity is less sensitive to the damping loss factor. The 99.9th percentile amplification factor sensitivities of 24-sector blisks are nearly independent of the damping loss factor, so as the maximum amplification factor sensitivity in Model 64A, which has a high interblade coupling ratio. However, the maximum adjusted amplification factor sensitivity in a lumped parameter model with a low interblade coupling ratio depends on the damping loss factor. In Model 64D, the maximum amplification factor sensitivity at $\eta = 0.001$ is half of that at $\eta = 0.004$. The difference in the maximum amplification factor sensitivity between Models 64A and 64D can be explained by recalling the derivation in Section 6.2:

1. In a model with a high interblade coupling ratio (e.g. Model 64A), the responses of the mistuned system are contributed by the pair of split n ND modes and the maximum adjusted amplification factor sensitivity is expressed as Equation (6.8). In a 64-sector system, there are 62 terms involving interblade coupling parameters (in terms of the natural frequencies) and one term involving the damping loss factor. As the orders of magnitudes of b_l 's and b_η are similar (see Appendix D.2), the effect of changing η is small because the expression is dominated by the terms involving the natural frequencies.

2. In a model with a low interblade coupling ratio (e.g. Model 64D), the natural frequencies are very close to each other (57 of them within ± 1 Hz of the natural frequency of the 6ND mode) such that the vibration responses of the blades are contributed by multiple modes, even in slightly mistuned systems. The high density of natural frequencies invalidates the assumptions made in the derivation. Because the extent of modal superposition depends on the width of the resonance peak, which is proportional to the damping loss factor, the sensitivity of the maximum amplification factor depends on damping.

The dependence of the sensitivity on the interblade coupling ratio shows the viability of the small mistuning approach in bladed discs with high interblade coupling ratios. To begin with, the critical degree of mistune is found to have a positive correlation to the interblade coupling ratio. The critical degree of mistune is as high as 0.05 in Blisk A, with an interblade coupling ratio of 0.05, but that of Blisk E, having an interblade coupling ratio of 0.017, is 0.015. Also, more importantly, the maximum (or the 99.9th percentile) amplification sensitivity in bladed discs with high interblade coupling ratios are so low, that the amplification factor can be reduced by specifying tight tolerances to blade dimensions and material properties, or by reducing the standard deviation of mistuning parameters. For example, by restricting the maximum allowable mistune on Model 64A to 2%, the maximum adjusted amplification factor is reduced by 20%, from 4.07 to 3.2.

However, the small mistuning approach is not applicable to bladed disc designs with small interblade coupling ratios: to achieve a similar reduction of the maximum adjusted amplification factor in Model 64D, the maximum allowable mistune has to be controlled to within 0.3%, which is not achievable in practice.

6.4.2 Excitation of mode shapes in the veering region

The situation of exciting mode shapes in veering regions in a small mistuning context is investigated by exciting Models 64C and 64E (Section 5.5.2) under 4EO excitation with a damping loss factor of 0.002. The maximum allowable mistune is assumed to be 0.1, and the results are plotted in Figure 6.9.

The difference in the shapes of curves related to Models 64C and 64E can be explained by the findings made in the previous analysis on other 64-sector

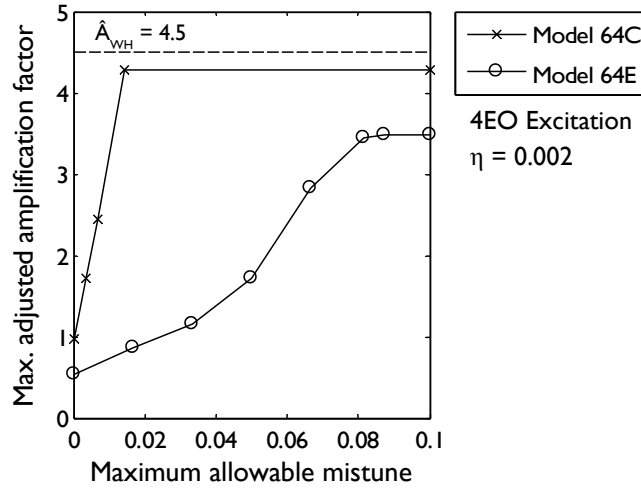


Figure 6.9: Maximum adjusted amplification factor under various levels of mistune.

systems. Firstly, the adjusted amplification factor of the tuned Model 64E is lower than unity as explained in Section 5.5.2. Secondly, the low sensitivity of the curve in Model 64E boils down to the lower natural frequency density around the veering region, which refers to a high interblade coupling ratio, as discussed in Section 6.3.

These two differences lead to a much lower maximum adjusted amplification factor in Model 64E than that in Model 64C with a small, yet achievable, maximum allowable mistune. For example, the maximum adjusted amplification factor of Model 64E is 1.72 if the maximum allowable mistune is kept at 5%, contrary to that of Model 64C of 4.3, with the same tolerances imposed on blade dimensions.

6.5 Feasibility of the intentional mistuning approach

The investigation in Chapter 3 has shown that the extreme amplification factors are only found in bladed discs with particular “problematic” mistuning patterns, which are concentrated in several regions. One of the proposals to manage this problem is the intentional mistuning approach. Under this approach, a designed mistuning pattern (known as an *intentional mistuning pattern*) is incorporated to a bladed disc at design stage, such that the probability of encountering a “problematic” mistuning pattern would be lower than that of a bladed disc design with nominally identical blades. It should

be noted that the maximum amplification factor is not reduced unless the worst mistuning pattern is excluded from combination of all possible mistuning patterns.

Numerous mistuning patterns have been considered as intentional mistuning patterns [21]. Although most patterns proposed in previous research are not associated with high amplification factors, not every mistuning pattern is suitable to become an intentional mistuning pattern.

Identical to the issue experienced on tuned blade disc designs, an intentionally mistuned bladed disc design can suffer from additional mistuning due to variations in manufacture and wear and tear in operation. These are described as *further mistuned bladed discs* (with *further mistuned patterns*) in this analysis. A mistuning pattern becomes a suitable intentional mistuning pattern only if the amplification factors of further mistuned bladed discs are generally lower than the mistuned bladed discs based on the tuned design. In addition to the basic requirement, a good intentional mistuning pattern should comprise (i) few types of blades and (ii) a simple arrangement of blades, because significant additional costs are involved in (i) manufacturing every new type of blade, (ii) controlling over the mistuning parameters of individual blades and (iii) keeping the blade order at installation.

A method is constructed in Section 6.5.1 to determine the consequences of applying an intentional mistuning pattern with various magnitudes efficiently. Using the method, the potential of the linear mistuning pattern [52] as an intentional mistuning pattern is evaluated in Section 6.5.2, using Blistk A as an example.

6.5.1 Determination of the consequences of intentional mistuning using the importance sampling method

Besides the intentional mistuning pattern, the effect of intentional mistuning also depends on the intentional mistuning strength. To decide the optimal intentional mistuning strength, the amplification factor pdf (and the 99.9th percentile amplification factor) can be evaluated by discretising the possible range of intentional mistuning strength and carry out a DMC simulation for each level. However, this process is cumbersome and inefficient because a large amount of samples is needed in each simulation to find a reliable amplification factor pdf, and the samples generated in one simulation cannot be reused in other simulations.

The importance sampling method introduced in Chapter 3 is used again here to tackle such a problem. By using the importance sampling method, the range of intentional mistuning strength is determined. After that, samples are selected randomly from all possible further mistuned patterns under any possible intentional mistuning strength to create a *master*, and the amplification factor pdf under a particular intentional mistuning strength is calculated by reweighting the samples. This approach was first proposed by Fonseca et al [38] to determine the optimal tolerances to be imposed on dimensions of a beam truss structure.

While the basic principles of the importance sampling method are discussed in Chapter 3, the discussion in this section focuses on creating the master. Fonseca et al proposed that each mistuning pattern in the master, $\{x\}$, is the sum of two random mistuning patterns, $\{d\}$ and $\{q\}$. The first pattern, $\{d\}$, refers to an intentional mistuning pattern with the magnitude, δ , a random variable distributed uniformly between δ_1 and δ_2 . The second pattern, $\{q\}$, represents normally-distributed, unculted random mistuning with a predetermined level of scatter, σ .

The pdf of the samples in the master needs to be evaluated to apply the importance sampling method. Provided that the pdf of a normally-distributed variable is written as $f_G(x)$, the pdf of a sample mistuning pattern, $g(\{x\})$, is

$$g(\{x\}) = \frac{1}{\delta_2 - \delta_1} \int_{\delta_1}^{\delta_2} \prod_{i=1}^N f_G(x_i - d_i \delta) d\delta \quad (6.11)$$

Equation (6.11) is solved analytically in Appendix E by examining f_G .

6.5.2 Evaluation of a linear intentional mistuning pattern

The method proposed in Section 6.5.1 is demonstrated by evaluating the optimal magnitude of linear intentional mistuning to be imposed on Blisk A. A sample linear mistuning pattern is shown in Figure 6.10. Jones [52] has shown that that the linear mistuning pattern alone can lead to an amplification factor lower than unity, if (i) the level of damping in the bladed disc is very low ($\eta \approx 0.0002$), and (ii) the order of excitation is near to $N/4$.

However, there are two issues to be resolved before applying the linear mistuning pattern to a blisk design as an intentional mistuning pattern,

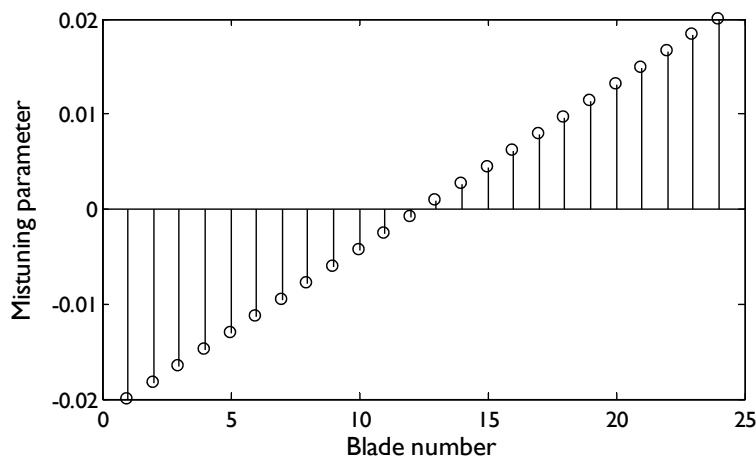


Figure 6.10: Linear mistuning pattern with a mistuning strength of 2%.

which are (i) the robustness of the linear mistuning pattern, which is the amplification factor distribution in further mistuned bladed discs and (ii) the effects of imposing the linear mistuning pattern on bladed discs with much higher level of damping. Although the level of structural damping in a typical blisk can be as low as the level investigated by Jones [52] ($\eta = 0.0002$) because there are no friction joints, the effects of aeroelastic damping and friction dampers have to be taken into account.

The two issues mentioned above are analysed in this section by finding the amplification factor distribution of intentional mistuning strength up to 5% in the presence of further mistuning. The distributions are sought using two methods, both by carrying out repeated DMC simulations at 8 selected intentional mistuning strengths and by carrying out the importance sampling-based algorithm introduced in Section 6.5.1. The additional random mistuning has a standard distribution $\sigma = 2\%$ and a maximum of $3.3\sigma = 6.6\%$. Also, a higher damping loss factor of 0.01 is applied to the model in the current investigation.

The results are presented in Figures 6.11 to 6.13. Although the intentional mistuning pattern alone leads to an amplification factor greater than unity, intentional mistuning can reduce the median of amplification factor compared with the tuned counterpart under a relatively high η . For example, the median of the amplification factor is reduced by 11% if a linear mistuning pattern with the mistuning strength of 5% is imposed. However, only an intentional mistuning strength higher than 0.04 can reduce the 99th and the 99.9th percentile amplification factors in this particular case.

The results show that the linear mistuning pattern can be considered as an intentional mistuning pattern. However, it is not an ideal intentional mistuning pattern because it involves many types of blades.

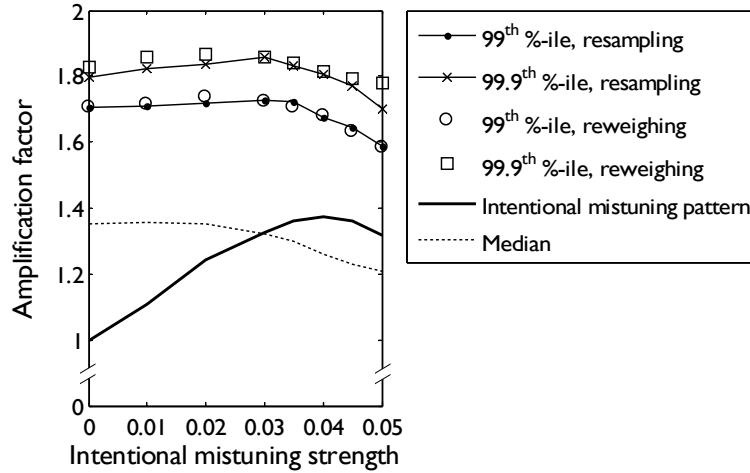


Figure 6.11: Dependence of the 50th, 99th and 99.9th percentiles amplification factor on level of intentional mistuning.

The efficiency of the new method is evaluated next. The cumulative distribution functions sought from DMC simulations and from the new importance sampling-based method are compared in Figure 6.12. The distributions sought from the two methods match well except a significant discrepancy in finding the very small probabilities related to the extremely high amplification factors (Figure 6.13). The 99.9th percentile amplification factors are shown in Figure 6.11 as an example. The results found by using the importance sampling method are significantly higher than those found by using the DMC simulations. There are three possible reasons of the discrepancy:

1. the sample size involved in importance sampling simulation is much higher than that in the DMC simulation;
2. the half-width of the confidence level, Δp , of the probability estimate of 0.1% with 5,000 DMC samples is 0.08% according to Equation (3.31), which means that the DMC estimate is not very reliable; and
3. because the samples taken in the importance sampling method includes the patterns with high amplification factors (e.g. if the intentional mistuning strength = 3%) regardless of the intentional mis-

tuning strength investigated, such that the cumulative distribution function sought from the new method has a longer tail.

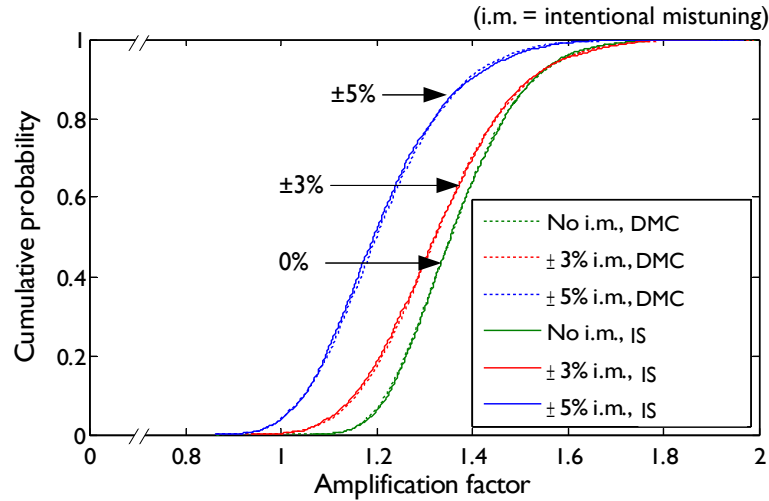


Figure 6.12: Amplification factor cumulative distribution functions under various levels of intentional mistuning.

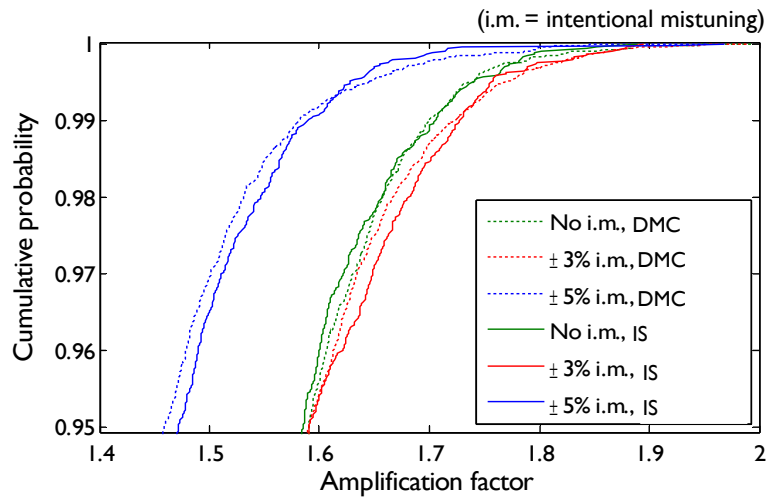


Figure 6.13: A magnified plot of Figure 6.12.

Although the importance sampling method is merely shown as a scheme to reallocate the computational resources in the example, the master can be reweighted to show the amplification factor distribution under other intentional mistuning strengths without additional samples, as long as the magnitude is within the predetermined range. Moreover, the amplification

factor distribution under slightly different intentional mistuning patterns, such as a “stairs” pattern shown in Figure 6.14, can be evaluated without additional simulations.

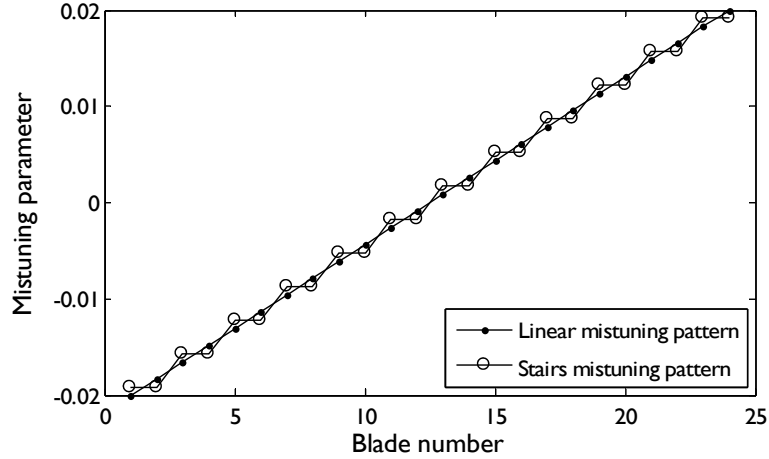


Figure 6.14: Stairs and linear mistuning patterns.

However, the importance sampling-based method cannot be used to describe the dependence of the amplification factor distribution on the maximum allowable mistune, as carried out in Reference [38]. This is because of the number of dimensions involved in the blade mistuning problem. In a univariate (i.e. single-dimension) normal distribution, 95.44% of all random variables are located within the range of $\mu \pm 2\sigma$, where μ and σ are the mean and the standard deviation of the distribution. If a 24-dimensional problem like a 24-sector blisk is considered, only $(0.9544)^{24} = 33\%$ of the mistuning patterns with normally-distributed mistuning parameters would satisfy a maximum allowable mistune of 2σ . As a result, a large portion of blisks samples in the master is excluded from analysis and the quality of the distribution estimate deteriorates.

6.6 Summary

The potential of the small mistuning and intentional mistuning approaches to improve the robustness of bladed discs are investigated in this chapter. The maximum amplification factor sensitivity to the maximum allowable mistune of a single-DOF-per-sector system is derived. Although the derived sensitivity only provides a qualitative description to the true relationship, it gives a theoretical basis on which a new interblade coupling ratio is based,

and explains why the small mistuning approach is more effective in bladed disc designs with high interblade coupling ratios.

It is found that the 99th percentile amplification factor of a bladed disc with a high interblade coupling ratio can be reduced by controlling scatter within a reasonable amount. Similarly, a smaller maximum allowable mistune can be set on this type of bladed disc to reduce the maximum adjusted amplification factor.

The likelihood of extremely high amplification factors can be reduced by the intentional mistuning approach with a linear mistuning pattern. A tool proposed in previous research has been adapted to determine the optimal mistuning strength without repeated DMC simulations.

Chapter 7

Predicting vibration response levels of integral bladed discs (blisks)

A current trend in aero engine compressor design is the wider use of integral bladed discs (blisks) because of the potential weight savings. Because the level of mechanical damping in a blisk is lower than that in a bladed disc assembly, there are challenges in controlling the extreme vibration response levels in a mistuned blisk as both the peak vibration response level in a tuned blisk and the maximum amplification factor are high.

However, as blisks lack the uncertainty and variability of friction properties related to joints, the maximum vibration response level of a blisk test piece in operation can be predicted based on the actual mistuned properties of that blisk prior to installation, or in regular checks during service life.

A previously-proposed procedure for predicting the highest response levels of mistuned blisks is outlined in the current chapter. The procedure is demonstrated experimentally on a test piece with two different mistuning patterns, and the sources of error are analysed. It is found that the procedure can predict the maximum vibration response level of a blisk, and recommendations for improvements to future experiments are presented.

7.1 Introduction

Bladed disc assemblies in aero engine compressors are sometimes replaced by bladed discs manufactured as single components, either by welding blades on rotors or by machining entire bladed discs from single pieces of metal.

As mentioned before, such bladed discs are called integral bladed discs, or blisks. The weight saving by replacing a bladed disc assembly with a blisk can reach 30% [16] because the mass supporting the fir-tree joints can be removed.

The use of blisks in aero engines poses new challenges to managing vibration response levels in mistuned bladed discs. There are fewer joints in a blisk than in a bladed disc assembly, which means the damping loss factors in blisks are lower than in bladed disc assemblies and the vibration responses in tuned blisks are correspondingly higher. Also, the maximum amplification factors of blisks with low levels of damping are typically high (Chapter 5). Therefore, the maximum vibration response level in a mistuned blisk is much higher than that in a mistuned bladed disc assembly. Given the same maximum allowable dynamic stress, the blade responses in a mistuned blisk have to be controlled by one or more of the three approaches:

1. adding dampers (e.g. underplatform dampers [92]) to reduce the vibration response levels of a tuned blisk
2. controlling the high vibration response levels related to mistuning, either by specifying a smaller maximum allowable mistune and/or by changing the blisk design
3. predicting the amplification factors of individual mistuned blisks by testing those blisks before installation, such that the uncertainty of the peak response level is reduced. Moreover, remedial actions can be taken if the peak response level of a given blisk is found to be unacceptable in a test. This way is possible in blisks because no uncertainties and variabilities related to friction properties at joints exist in blisks.

After studying the second approach in Chapters 5 and 6, the third way is investigated in this chapter, first by outlining a possible procedure and the associated tools (Section 7.2), and the proposed procedure is demonstrated in experimental studies in Section 7.3. The potential sources of error identified in the experimental work are discussed in Section 7.4 and the possible improvements to the experimental work are listed in Section 7.5.

7.2 Outline of a response level prediction procedure

The three major factors leading to changes in a mistuning pattern of a blisk are creep, wear (e.g. tip rubbing) and crack growth, and the rate of change of the mistuning pattern due to these effects is likely to be lower than that due to changes in friction properties at joints. To illustrate this argument, a DMC simulation with 100 samples is carried out on Blisk E (Section 5.3.1) to simulate the possible change of the amplification factor upon the changes of mistuning parameters due to crack growth. It is assumed that the rate of change of a mistuning parameter on one blade is proportional to the highest response level of that blade. By perturbing the mistuning parameters of each of the 100 mistuning patterns by a maximum of 1% in 300 steps, the amplification factors before and after the perturbation, compared in Figure 7.1, show that the effects of small changes of the mistuning pattern on the amplification factor of a blisk are likely to be small. As a result, the vibration response levels of blades on a blisk under an EO-type excitation in operating conditions is likely to be predictable by the properties of that particular blisk in a test rig, with a much lower level of uncertainty.

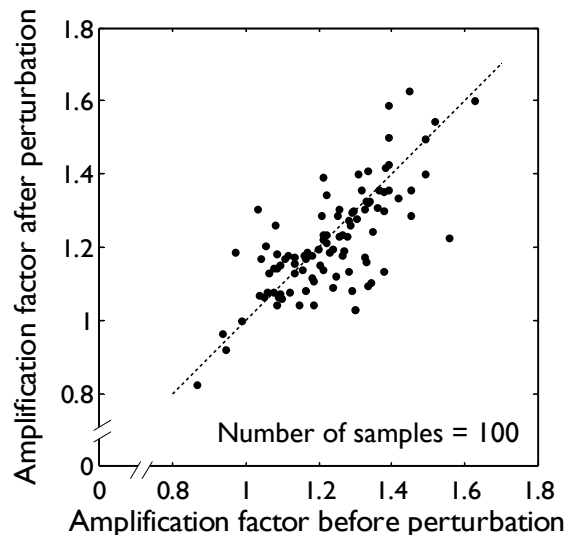


Figure 7.1: Amplification factors before and after perturbation.

The maximum vibration response level of a blisk test piece can be predicted by two methods. In the first method, the test piece is installed on a rotating rig and the responses of a rotating blisk are measured by a scanning

Laser Doppler Vibrometer (LDV) [28]. This method is expensive and very time-consuming.

In the second method, the response levels of the blades in a rotating mistuned blisk test piece are estimated by imposing the mistuning pattern of the blisk on a rotating blisk model. The second method is more versatile, but the mistuning pattern of the blisk test piece has to be known. While the mistuning pattern in a bladed disc assembly can be determined by testing individual blades, the mistuning parameters of blades on a blisk test piece cannot be found in this way. The mistuning pattern in a blisk test piece is estimated using a *mistuning identification algorithm* based on the experimental data sought from that blisk. The experimental data usually refers to natural frequencies and mode shapes, but identification algorithms using FRF information also exist [119].

Griffin and Feiner [43] have proposed a procedure to predict the highest response level of a blisk test piece under an EO-type excitation using a mistuning identification algorithm, called the FMM-ID. The FMM-ID is roughly the reciprocal of the model reduction algorithm, known as the Fundamental Mistuning Model (FMM) [35], and both algorithms are outlined in Appendix F. Their proposed procedure involves finding the mistuning pattern correlated to the identified mode shapes and calculating a set of reconstructed mode shapes using the mistuning pattern. It is arranged as such because (i) it allows arbitrarily-scaled identified mode shapes and (ii) the models involved in the FMM-ID and the FMM algorithms are supposed to be different. If a stationary blisk model is used in the FMM-ID algorithm and a rotating blisk model is used in the FMM algorithm, the peak response level of a rotating blisk test piece can be predicted by carrying out experiments on the same blisk when it is stationary. However, the relationship between the mistuning patterns of a blisk test piece at stationary and rotating states has to be known in advance.

A blisk can be tested either after manufacture or as a part of regular inspection over its service life. Based on the predicted response level, one or more of the three actions below can be performed: (i) reduce the amplification factor by changing the mistuning pattern; (ii) determine the date of the next test and (iii) create a “medical history”, containing the predicted response levels at regular intervals, for every manufactured blisk.

The relationship between the two testing methods and the three possible

actions are shown in Figure 7.2. The response prediction procedure proposed by Griffin and Feiner is demonstrated in Section 7.3.

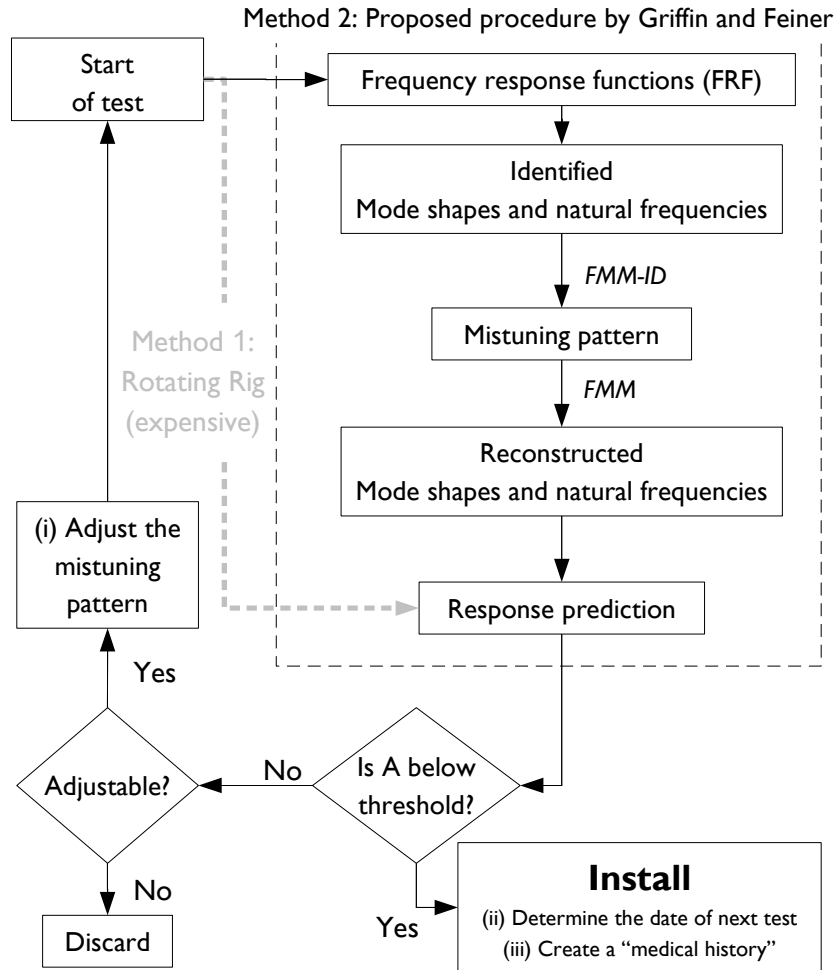


Figure 7.2: Predicting the amplification factor of a mistuned blisk.

7.3 Experimental demonstration of the proposed procedure

(This author acknowledges the assistance from Dr. Dario Di Maio on setting up the experimental equipment.)

Experiments are carried out on the blisk test piece called “Blisk 2” in Reference [117], which is Blisk A in Section 5.3.1, to demonstrate the procedure outlined by Griffin and Feiner [43]. In this analysis, the blade responses of a stationary test piece under a 10EO excitation are predicted, such that

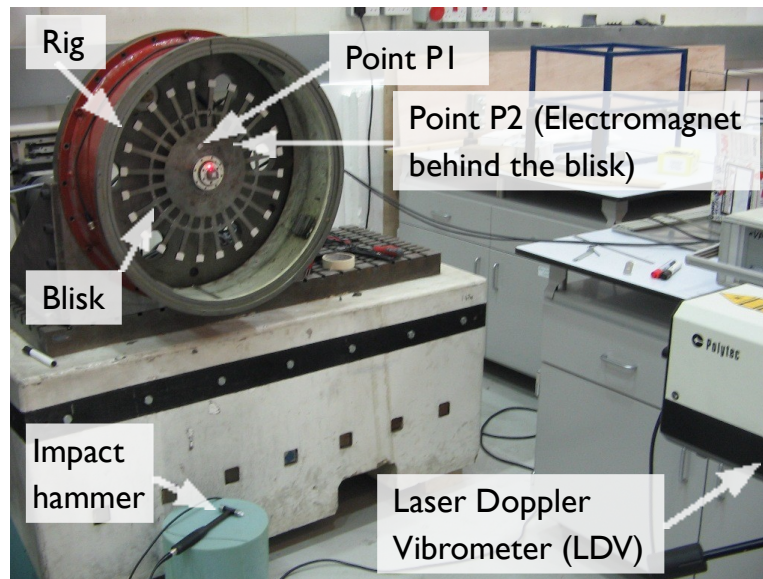


Figure 7.3: Experimental setup.

the blisk models used in the FMM-ID and FMM algorithms are identical. The test piece is supported by a rig, and the experimental set up is shown in Figure 7.3.

Various methods of exciting blisks have been proposed as discussed in Chapter 2. In this analysis, the blisk is excited either by a swept sine excitation using an AC electromagnet or by a hammer impact. Each method has its advantage: an electromagnetic excitation ensures the accuracy of the excitation point, while the level of excitation force can be determined accurately under an impact excitation using a hammer. The test piece is excited at one of two specified positions on the disc, called P1 and P2, with the approximate locations shown in Figure 7.3. The point of electromagnetic excitation, P2, is determined by the construction of the rig, and the points of impact excitation (P1 and P2) are located within the disc part of the blisk to avoid multiple impacts. Multiple impacts (also known as “double-hits”) mean the hammer and the structure come in contact more than once in an impact excitation, usually due to high vibration amplitude of lightly-damped structures, and have to be avoided.

Vibration responses of the blades are measured by using a Laser Doppler Vibrometer (LDV) in the experiment. The captured time histories are converted into frequency response functions (FRFs) and undergo modal analysis - using the line-fit method [34] - to find the natural frequencies, modal damp-

ing ratios and mode shapes of the blisk test piece. Modal analysis is carried out using MODENT, the in-house modal analysis software [50], which is a part of the ICATS software package.

The modal properties of two mistuning patterns on the test piece are measured. Mistuning pattern 1 is the existing mistuning pattern on the test piece, and Mistuning pattern 2 is created by imposing a mistuning pattern - called the *target pattern* - on the blisk test piece by installing screws, nuts and washers of various sizes at blade tips. A picture of three mistuned blades is shown in Figure 7.4, and the detailed arrangement of the attached components are presented in Appendix G.

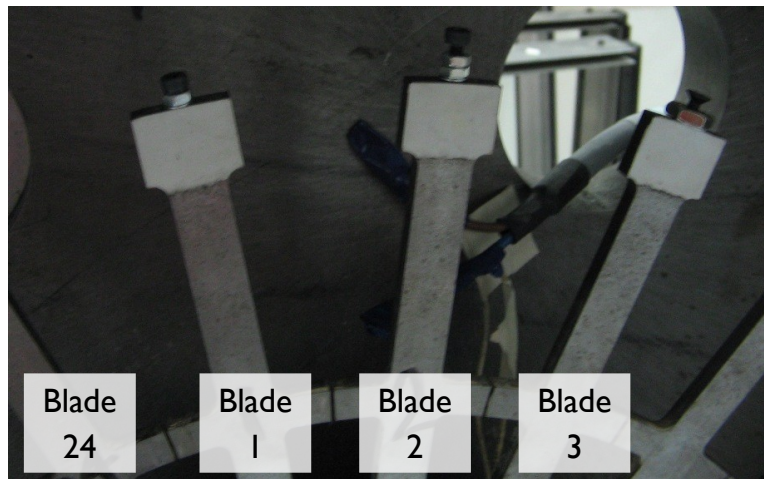


Figure 7.4: Selected mistuned blades of the blisk test piece.

Results from two tests carried out on the test piece with Mistuning pattern 1 and three tests on the test piece with Mistuning pattern 2 are presented in Sections 7.3.1 and 7.3.2, respectively. The key parameters of these tests are listed in Table 7.1.

Test	Mistuning pattern	Method of excitation	Point of excitation	Frequency Range / Resolution (Hz)
1A	1	Hammer impact	P1	0.078-500 / 0.078
1B	1	Electromagnet	P2	275-285 / 0.2
2A	2	Electromagnet	P2	235-285 / 0.0625
2B	2	Hammer impact	P1	0.078-500 / 0.078
2C	2	Hammer impact	P2	0.078-500 / 0.078

Table 7.1: Experimental tests presented in this thesis.

7.3.1 Mistuning pattern 1

Since the test piece was designed to be tuned and has been properly handled, the test piece is a slightly-mistuned blisk. The maximum mistune of Mistuning pattern 1 is very small in such a blisk, and pairs of natural frequencies are extremely close to each other. Although 24 natural frequencies are supposed to be present in a family of modes, only 18 distinct natural frequencies are identified in Test 1A between 100 Hz and 300 Hz. Three pairs of the natural frequencies, corresponding to the 2ND, 6ND and 7ND modes, are 0.16 Hz, 0.03 Hz and 0.05 Hz apart, respectively. Because the natural frequency splits of 6ND and 7ND modes are smaller than the frequency resolution of the FRFs (0.08 Hz), only one mode shape can be identified and the two slightly split natural frequencies are treated as one.

At last, 16 mode shapes are identified in Test 1A between 100 Hz and 300 Hz, and 14 of them belong to the same family. Four mode shapes are identified in Test 1B between 275 Hz and 285 Hz, and the mode shapes represent the 9, 10, 11 and 12 ND modes of the test piece. The natural frequencies from the finite element model and those identified in Test 1A are compared in Figure 7.5.

The discrepancies between the natural frequencies of the lower nodal diameter modes are believed to be due to non-identical boundary conditions (i.e. the clamping mechanism) between the experimental set-up and the finite element model, and the differences between the natural frequencies of the higher nodal diameter modes are due to inaccurate material properties in the finite element model.

The MAC (Modal Assurance Criterion [34]) function between the identified modes in Test 1A and the tuned system travelling modes is computed and the results are shown in Figure 7.6. It can be seen that the mode shapes are only slightly distorted from sinusoidal mode shapes, which are characteristics of the mode shapes in a tuned blisk. The different magnitudes of the MAC functions for the same identified mode shape to backward and forward travelling mode shapes with the same number of nodal diameter mean the identified mode shape is complex, with the 9ND mode identified in Test 1B (Figure 7.7) being a good example.

The mistuning patterns are identified in each test: the mistuning pattern corresponding to Test 1A is identified using all mode shapes except mode shapes 1, 2, 3 and 8 (see Figure 7.6), and that corresponding to Test 1B is

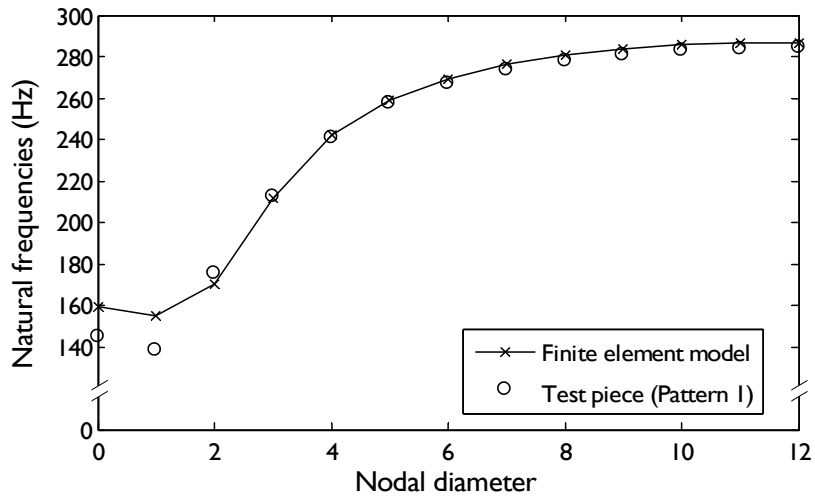


Figure 7.5: Natural frequencies of the model and the test piece.

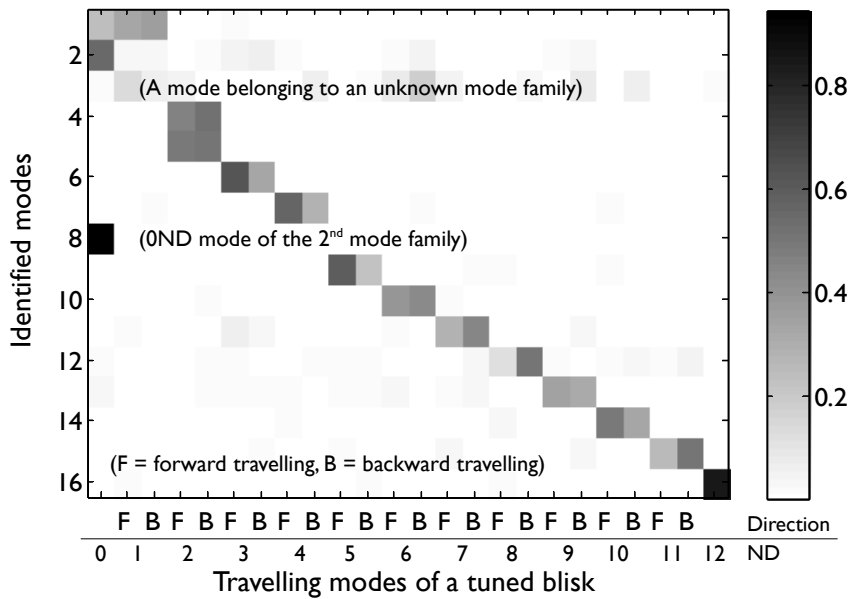


Figure 7.6: MAC function between identified mode shapes from Test 1A and travelling modes of the finite element model.

identified using all 4 mode shapes. Although the mistuning pattern on the actual test piece is not known, the identified mistuning pattern from Test 1A, which is shown in Figure 7.8, is unlikely to be an accurate representation of such, because a maximum mistune of nearly 4% would lead to a maximum natural frequency split of much higher than 0.16 Hz, which is about 0.1% of the natural frequency of the 2ND mode. The error is presumably due to

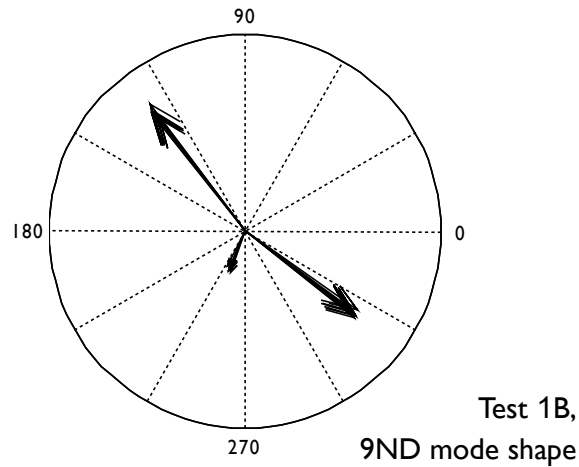


Figure 7.7: Argand diagram of an identified mode shape.

distorted measured mode shapes.

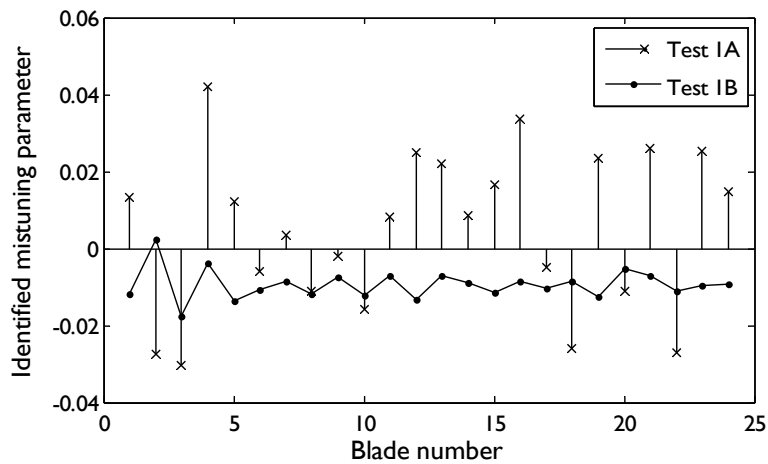


Figure 7.8: Identified mistuning patterns in Tests 1A and 1B.

7.3.2 Mistuning pattern 2

The results from three tests are presented in this section. Test 2A is carried out with a swept sine excitation using an electromagnet and Tests 2B and 2C are carried out with impact excitations at two different excitation points. All identified mode shapes of the test piece with Mistuning pattern 2 are real. The mode shapes from the three tests match well with others: a representative mode shape identified in the three tests is plotted in Figure 7.9, and all mode shapes between Tests 2A, 2B and 2C are compared in

Figure 7.12 by using the MAC function. It is noted that not every mode in the family is identified in a test using impact excitation.

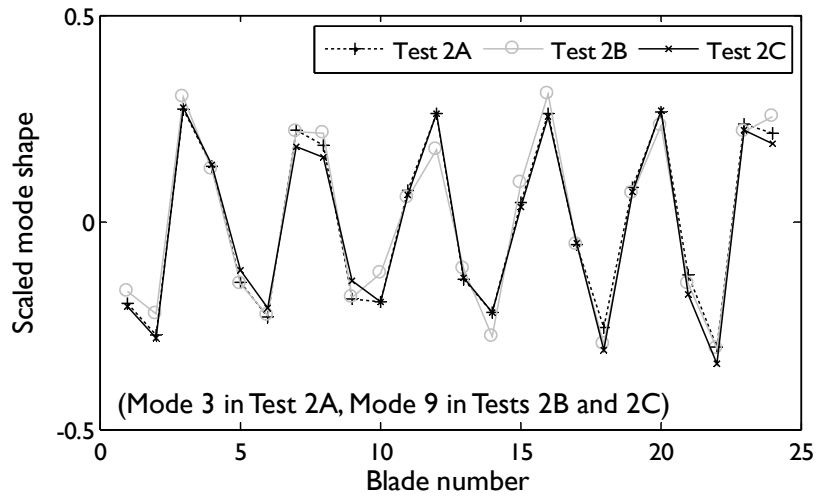


Figure 7.9: Comparison of identified mode shapes.

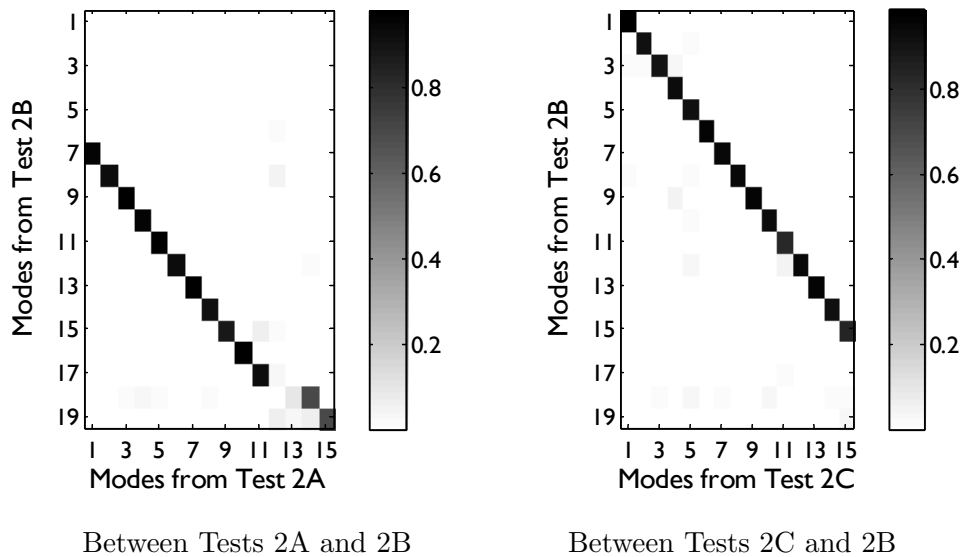


Figure 7.10: MAC function between identified mode shapes from Tests 2A, 2B and 2C.

After the natural frequencies and mode shapes are identified in each test, all identified mode shapes are used to find mistuning patterns with the FMM-ID algorithm. Although the mode shapes between different tests match well in the MAC plots, the identified mistuning patterns from the

three tests are significantly different (Figure 7.11). Only the identified mistuning pattern from Test 2A is reasonably close to the target pattern.

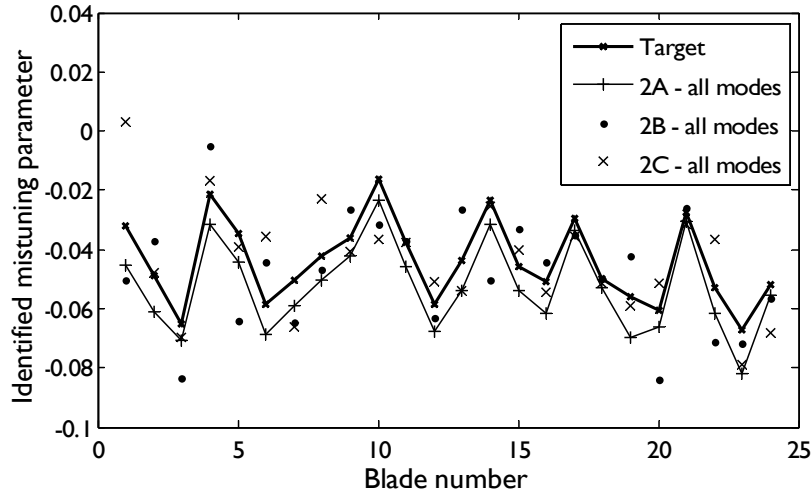


Figure 7.11: Identified mistuning patterns based on all identified modes.

It is suspected that the identified mistuning patterns in Tests 2B and 2C deviate from the target pattern because of errors in modal components. While the impact of such error is investigated in greater detail in Section 7.4.2, a method is developed in this section (i) to check whether the identified mistuning pattern is close to the actual counterpart, and (ii) to remove the mode shapes which contribute significant error to the identified mistuning pattern. The quality the identified mistuning pattern is checked by calculating the reconstructed mode shapes using the identified mistuning pattern and the FMM algorithm, and compute the MAC between the reconstructed and identified mode shapes. If the error in the identified mode shapes is small, the mistuning pattern identified by the FMM-ID algorithm is accurate, and the MAC between the reconstructed mode shapes and the identified counterpart should form a nearly-diagonal matrix as the two sets of mode shapes are nearly identical.

The qualities of the identified mistuning patterns from Tests 2B and 2C are improved by excluding some mode shapes from the FMM-ID algorithm. The results based on Test 2C are shown in Figure 7.12, in which each white dot in the MAC function indicates that an identified mode shape has been included in the FMM-ID algorithm. After trial and error, it can be seen in Figure 7.12 that all identified mode shapes and the reconstructed counterparts match better if the first four identified modes are not considered in

mistuning identification.

It is shown in Figure 7.13 that the identified mistuning patterns based on selected modes are close to the target pattern. The average of mistuning parameters in identified mistuning patterns found in the tests are more negative than that of the target pattern mainly because the screw holes in the blisk are not as deep as indicated in the engineering drawing in Reference [117]. The masses are located further from the blisk centre in the experiment than planned and thus the effective vibrating masses of the blades are higher. In addition to this, the set-up in this experiment is different from the assumption of the FMM-ID algorithm, where only the stiffness matrix is perturbed.

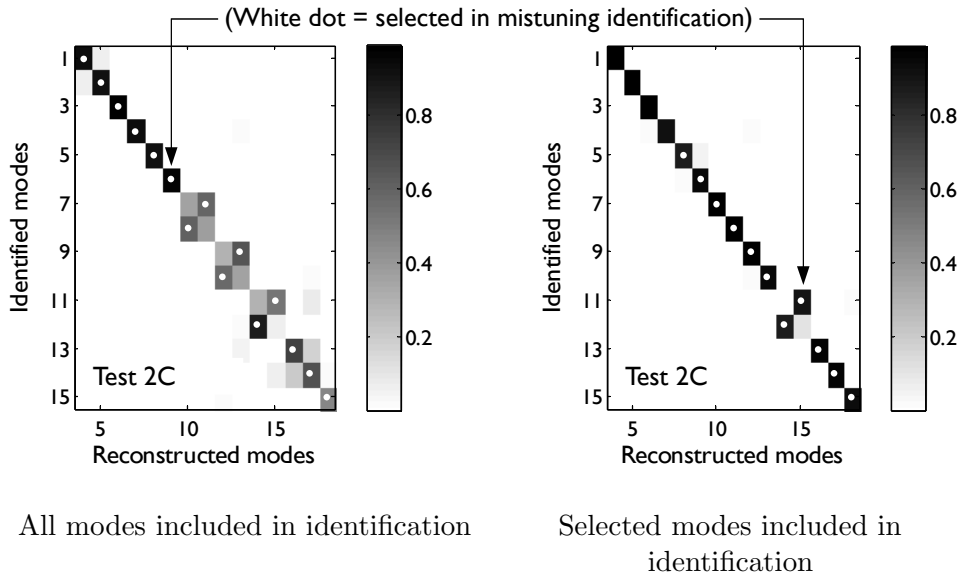


Figure 7.12: MAC function between identified modes and selected reconstructed modes.

After the mistuning patterns are identified, the maximum response of the stationary blisk test piece under 10EO excitation is estimated. Since the software MODENT does not provide a reliable estimate of the modal damping loss factor, η , if η is smaller than 0.01%, η is estimated to be 7.5×10^{-5} according to Sever [117]. The performance of the response prediction is determined by (i) the maximum vibration response level experienced on any blade and (ii) the blade experiencing the maximum vibration level. The parameters are compared in Table 7.2.

The predicted maximum response levels are within 9% of the target pattern, and the blade with the highest response is correctly predicted in

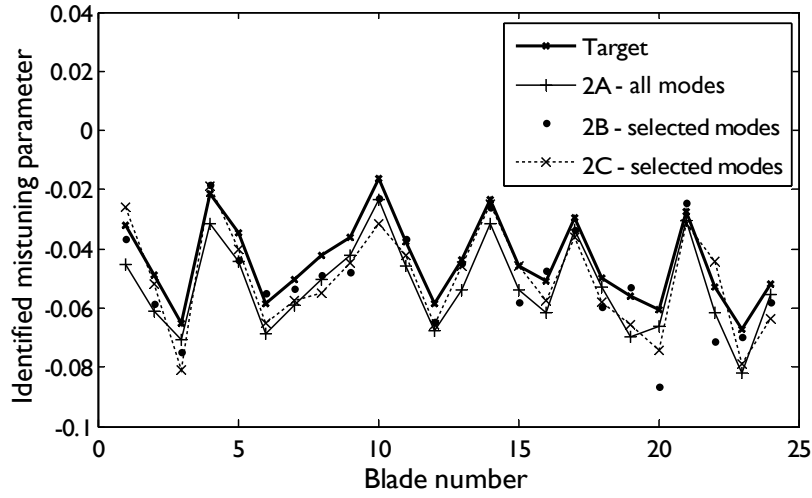


Figure 7.13: Identified mistuning patterns based on selected modes.

	Tuned	Target	Test 2A	Test 2B	Test 2C
Maximum response level	246.6	356.8	374.1	387.3	381.7
Blade	1	1	1	21	10

Table 7.2: Comparison of key identified response parameters.

one test. Every maximum response level in the three tests is higher than that in the target pattern because the mistuning parameters in the identified patterns are more negative than the target pattern on average, which implies the blades are less stiff according to the FMM algorithm (Appendix F). As a result, both the maximum blade alone vibration response, which is inversely proportional to the blade stiffness, and the highest vibration response level of the mistuned blisk increase.

7.4 Robustness of the proposed procedure

The experimental demonstration in Section 7.3 has shown that the proposed procedure can predict the maximum forced vibration response level in a blisk. To improve the quality of response prediction in future experiments, selected sources of error related to carrying out modal testing in blisks are analysed in Section 7.4.1, and their impacts on the identified mistuning pattern with real and complex modes are discussed in Section 7.4.2 and 7.4.3 respectively.

7.4.1 Major sources of error in modal testing

Two major sources of error in the experiments encountered in Section 7.3 - namely (i) inaccurate location of impact and (ii) insufficient frequency resolution in the FRFs - are discussed in this section. Although other sources of error, such as the error related to imperfect swept-sine electromagnetic excitation due to harmonics and the sampling window, are not discussed individually, the impact of noise in experimental data on the predicted response is discussed in Section 7.4.2.

Inaccurate location of impact

An advantage of exciting the blisk with a hammer over an electromagnet is that the accurate level of excitation can be known. This is essential for getting mass-normalised mode shapes, which is required in some mistuning identification algorithms to identify both stiffness and mass mistuning patterns [119], although the identified mode shapes for the FMM-ID algorithm can be arbitrary scaled.

The major issues involved in impact excitation on blisks are (a) multiple impacts, which are considered in Section 7.3, and (b) the sensitivity of the measured FRF to the location of the point of excitation. These two issues cannot be avoided at the same time solely by shifting the point of excitation. On the one hand, if the blisk test piece is excited at one of the blades, multiple impacts are likely to occur because the blades in blisks vibrate at high amplitudes due to a low level of damping. On the other hand, the measured FRFs are very sensitive to the location of the point of excitation if the excitation point is located at the disc part, because nodal lines are very dense there. A perturbed FRF would lead to distorted mode shapes at a particular DOF, and will introduce error to the whole identified mistuning pattern.

Multiple impacts can usually be detected during the test by observing the time history and the power spectrum of the excitation signal. However, the error due to inaccurate point of excitation is more difficult to detect at the same stage. An example showing the sensitivity of a transfer FRF to the location of the excitation point on a tuned finite element model of the test piece is shown in Figures 7.14 and 7.15. Assuming the point of measurement is fixed, the transfer FRF can appear very differently by moving the point

of excitation away from the intended location by as little as 4mm, and the different amplitudes at the resonant peaks (and the formation of new peaks) would result in distorted identified mode shapes.

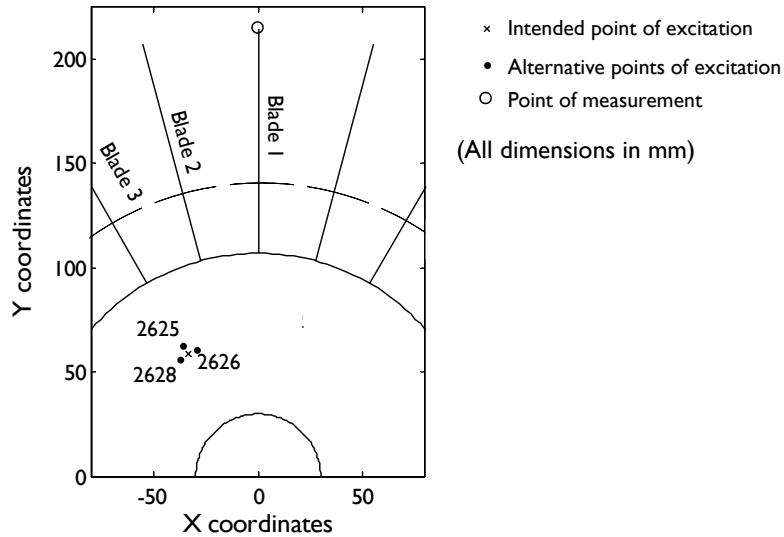


Figure 7.14: Measurement and excitation points in simulations.

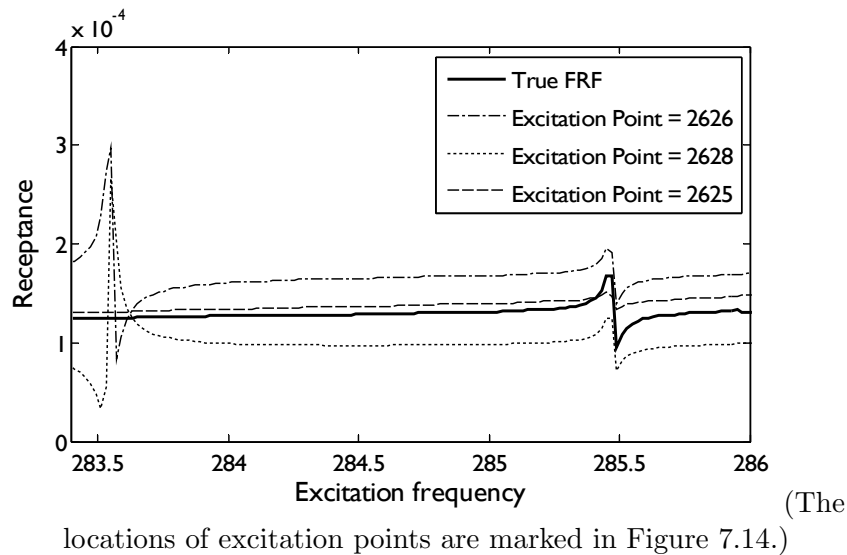


Figure 7.15: Receptance FRFs under various excitation points.

Insufficient frequency resolution in the FRFs

Some of the identified mode shapes of the test piece with Mistuning pattern 1 are complex. Complex modes are unexpected because mode shapes in non-

rotating structures with proportional damping are supposed to be real. A suspected cause of complex modes being observed is that two closely-spaced modes - with a natural frequency split as small as 0.03 Hz - are treated as one mode. Close natural frequencies are typical in bladed disc test pieces because tuned bladed discs have repeated natural frequencies.

By estimating the damping loss factor in the test piece, η , and the natural frequency of a mode, ω , to be 7.5×10^{-5} and 240 Hz, respectively, the width across the half-power points [34] of a single resonance peak in an FRF, $\Delta\omega$, is approximately

$$\Delta\omega = \omega\eta \approx 240 \times 7.5 \times 10^{-5} \approx 0.018 \text{ Hz} \quad (7.1)$$

Equation (7.1) means that two neighbouring resonance peaks of similar modal constants can be identified if (i) the difference between two neighbouring natural frequencies is more than 0.02 Hz, and (ii) the frequency resolution of the FRF is fine enough. Since the estimated natural frequency split is 0.03 Hz in Test 1A, two resonance peaks in Test 1A appear as one peak because the frequency resolutions of the FRFs in Test 1A are too coarse.

To demonstrate the importance of the frequency resolution, the tuned finite element model of the test piece is perturbed by point masses as much as 0.1 g. The natural frequency split of the 4ND modes of this mistuned blisk model is about 0.045 Hz. By assuming the damping loss factor $\eta = 7.5 \times 10^{-5}$, two point FRFs - with frequency resolutions 0.02 Hz and 0.05 Hz - are measured at Blade 1 and shown in Figure 7.16. It can be seen that the two resonance peaks appear to be a single peak if the frequency resolution of the FRF is 0.05 Hz, which is comparable to 0.08 Hz used in Test 1A. Although two natural frequencies can be distinguished with the aid of a modal analysis code like MODENT, the errors in modal constants are significant (Figure 7.17). With the existence of additional error from other sources, slight but genuine natural frequency splits can be obscured.

7.4.2 Robustness of the predicted response

The impact of measurement error on the predicted response is investigated by carrying out eleven 5000-sample DMC simulation runs on the FMM-reduced order model of the test piece finite element model. A pattern cor-

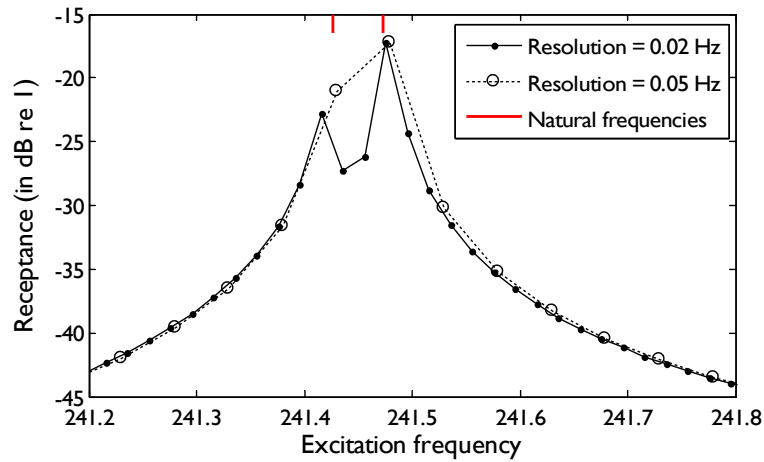


Figure 7.16: Point receptance FRFs around a pair of natural frequencies.

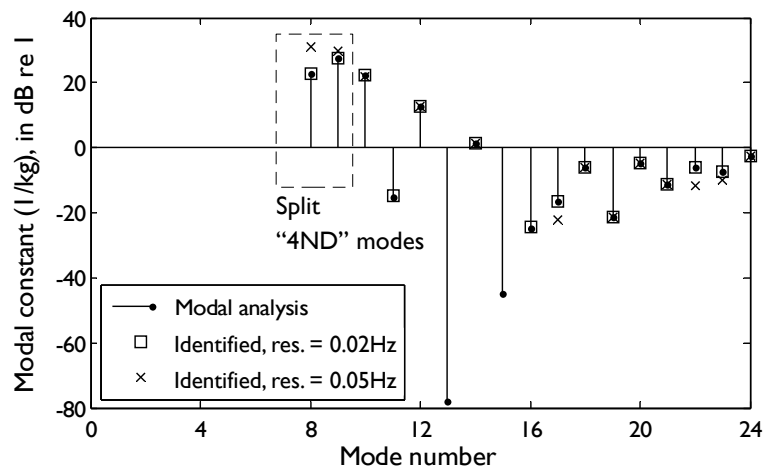


Figure 7.17: Modal constants of a point receptance FRF.

responds to an amplification factor of 1.529 is selected as the unperturbed pattern. Based on observations in the experiment, the sources of error are modelled by the following four ways:

Perturbed natural frequencies. The natural frequencies are perturbed in two ways. Firstly, all natural frequencies are uniformly shifted with a maximum of 0.1 Hz to simulate the effect of temperature change and inaccurate global material properties. Secondly, natural frequencies are perturbed randomly by up to ± 0.03 Hz to simulate the error related to modal analysis.

Distorted mode shapes. Except for simulation run 1, uniformly-distributed

random distortion with the maximum amplitude of either 5% or 10% of an individual modal component is added to each modal component.

Missing modes. Some mode shapes are missing from a set of identified mode shapes because (a) localised mode shapes, which are modes with energy concentrated in few blades, can only be excited from specific points and (b) the qualities of distorted 0ND and 1ND mode shapes are poor due to the interaction between the blisk and the supporting shaft. This effect is modelled in three levels, called L0, L1 and L2, in the simulations. All modes are present in level L0. In level L1, 2 localised modes on average, which are the highest modes in a family, are not considered in the FMM-ID algorithm. In level L2, the 0ND and 1ND mode shapes, plus 4 localised modes on average, are not considered in the FMM-ID algorithm.

Inverted signs. Some modal components with low amplitudes have their phases perpendicular to other components of the same mode because of noise, and wrong signs can be assigned to these components in converting complex modes into real modes. The signs of half of the modal components with the amplitudes smaller than 10% of the largest amplitude in that mode shape are inverted to address this type of error.

While the natural frequencies are perturbed in all eleven simulation runs, these runs include different combinations of the four types of error. The combinations of error types and the quality of response prediction in all eleven simulations are listed in Table 7.3. The quality of the response prediction is measured by using four parameters:

Parameter 1. The 1st percentile of the predicted amplification factor distribution

Parameter 2. The 99th percentile of the predicted amplification factor distribution

Parameter 3. The portion of samples having predicted amplification factors within 5% of that predicted using noiseless natural frequencies and mode shapes

Parameter 4. The portion of samples where the highest response is predicted at the same blade as using noiseless natural frequencies and mode shapes

Run	Noise	Missing modes	Inverted signs	Parameter			
				1	2	3	4
1	0%	L1	×	1.524	1.530	1.00	1.00
2		L0	×	1.246	1.540	0.79	0.98
3		L1	×	1.218	1.536	0.71	0.95
4	5%	L2	×	1.210	1.538	0.70	0.94
5		L0	✓	1.186	1.533	0.57	0.87
6		L1	✓	1.117	1.527	0.43	0.74
7		L0	×	1.133	1.538	0.46	0.83
8		L1	×	1.102	1.530	0.38	0.75
9	10%	L2	×	1.089	1.532	0.38	0.76
10		L0	✓	1.108	1.535	0.41	0.75
11		L1	✓	1.084	1.531	0.32	0.67

Table 7.3: Impact of mode identification error on the predicted peak response level.

The results show that the quality of the response prediction depends strongly on the accuracy of the modal components, including those in localised modes. By introducing 5% error to modal components, only 80% of all samples have predicted amplification factors within 5% of 1.529. Also, efforts should be made to identify all localised modes, as Parameter 3 can drop by as much as 8% if two less mode shapes are identified. If these modes are identified, (i) the scatter of the predicted amplification factor, and (ii) the mistuning identification error, which is the error related to the violation of assumptions in constructing mistuning identification algorithms, can be reduced. Madden et al [70] proposed to reweight the identified mode shapes to minimise the mistuning identification error in a mistuning identification algorithm. They have shown that mode shapes with natural frequencies closest to the blade-alone counterpart should be given high weighting factors because the mistuning identification error with those modes is small.

While it is important to assign correct signs to all modal components, this requirement can be met easily in proportionally-damped blisks if the distortion of modal components is controlled to within 5%.

7.4.3 Identification of the damping mistuning pattern

Besides blisks with frequency mistuning, the procedure proposed by Griffin and Feiner [43] is designed to predict the maximum response levels of blisks

with damping mistuning (Section 5.5.1) as well. According to their proposal, the damping mistuning pattern is identified using the extended FMM-ID algorithm. As complex mode shapes are required to identify damping mistuning patterns, the robustness of the extended FMM-ID algorithm to error in complex mode shapes is analysed below.

Mode shapes of non-proportionally damped systems can be complex, and the complexity is significant if the natural frequencies of a structure are close to each other [34], which is a characteristic of slightly-mistuned blisks. The complexity of a mode can be measured by the MCF2 factor [34].

Although non-proportionality of damping is the only source leading to complexity in true mode shapes, identified mode shapes can be complex due to unidentified mode splits (Section 7.4.1) and measurement error. For example, the natural frequencies of a mode in different FRFs can be slightly different if a mode shape is identified from FRFs generated with non-identical impact excitations.

The robustness of the extended FMM-ID algorithm is checked by perturbing the mode shapes of a damping-mistuned blisk. The finite element model of the test piece is mistuned by attaching two damping tapes of different sizes to Blades 1 and 13. The blisk is otherwise tuned. The first 24 complex modes of such a blisk are found, with the MCF2 factors of these modes vary between 0 and 0.45. The phases of all modal components of all 24 modes are perturbed randomly with a standard deviation of 5 degrees, but the magnitudes of the modal components are unperturbed. This range of perturbation is similar to the scatter found in identified complex modes. A DMC simulation with 5000 samples was carried out, and the distribution of the mistuning parameters and damping mistuning parameters are plotted in Figures 7.18 and 7.19, respectively.

While phase perturbation has a minor impact on the identified damping mistuning pattern, the identified frequency mistuning pattern is not robust to perturbation of phases in modal components, especially on the 2 blades with dampers attached. As a result, extremely accurate complex mode shapes is needed in order to generate reliable mistuning and damping mistuning patterns from the extended FMM-ID algorithm.

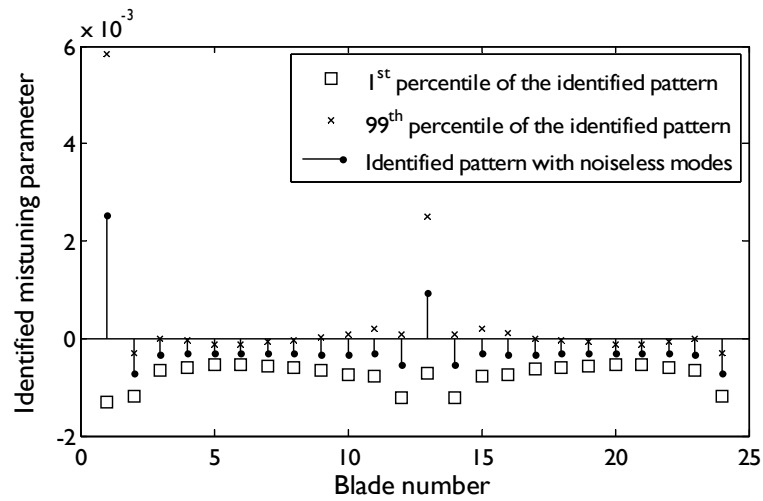


Figure 7.18: Distribution parameters of identified frequency mistuning patterns using noisy modes.

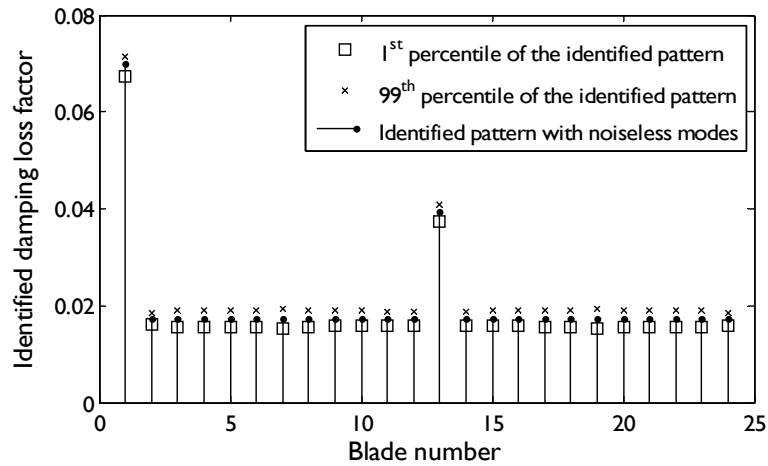


Figure 7.19: Distribution parameters of identified damping mistuning patterns using noisy modes.

7.5 Recommendations for future experimental work

The response prediction method outlined in Section 7.2 can predict the maximum response level of a blisk test piece if the procedure is planned and carried out carefully. After the experimental demonstration and discussion in Sections 7.3 and 7.4, respectively, it is found that good experimental data is of critical importance in the whole procedure. To improve the quality of experimental data, the following four recommendations should be observed:

1. The experimental setup should be capable to fix the point of excitation to avoid mode shapes being distorted
2. The point of excitation is preferred to be away from the centre
3. The frequency resolution of the FRF should be in the order of (or finer than) $\Delta\omega$, the width of the half-power points of a resonance peak. The frequency resolution should be even higher in testing slightly mistuned blisks.
4. More than one excitation point is needed to capture all localised modes, which are needed in the mistuning identification algorithm.

All localised modes should be identified at the modal analysis stage, and the error in amplitudes of modal components should be kept under 5%. On top of this, real modes should be sought if only the frequency mistuning pattern needs to be identified. If the damping mistuning pattern is to be identified, the phases of the components of complex mode shapes need to be accurate to within 5 degrees.

The MAC function between the identified and reconstructed mode shapes, which are mode shapes constructed by the FMM algorithm (or similar) using the identified mistuning pattern, should be calculated. It is recommended that the mode shapes should first be reconstructed assuming the blisk is under the same condition as it is tested, e.g. stationary, such that the quality of the identified mistuning pattern can be controlled. More accurate mode shapes and responses of the test piece under a different condition, such as under rotation, can be determined using a validated mistuning pattern. The flow chart of validation, which forms a part of Figure 7.2, is shown in Figure 7.20.

7.6 Summary

The application of blisk to aero engine compressors has provided the opportunity of predicting the maximum vibration response level of any blisk test piece in a test rig. A procedure for such purpose is demonstrated experimentally and the effects of potential sources of error are analysed. All mode shapes in a family, including the localised ones, need to be identified in modal testing and the error in each modal component needs to be controlled

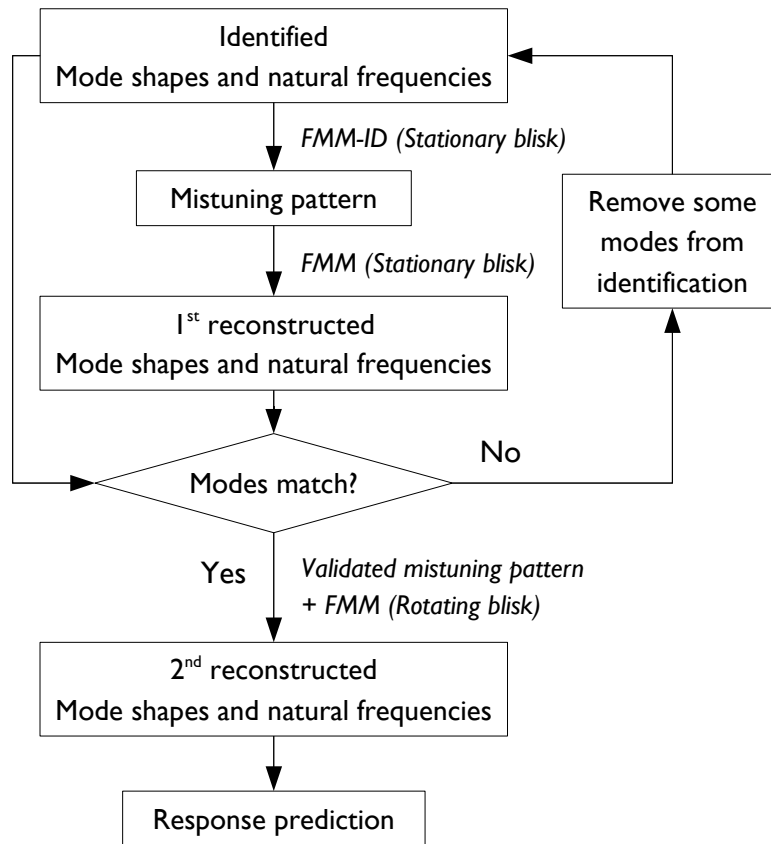


Figure 7.20: Improved response-prediction procedure.

to within 5% for reliable mistuning identification. Also, the error in phase in each modal component should be kept to within 5 degrees if the damping mistuning pattern is to be identified as well.

Chapter 8

Conclusions

The viability of the Mistuning Management Strategy has been shown in the previous chapters of this thesis. More robust bladed disc designs can be produced by the various tools developed. Also, the requirements of predicting peak responses of mistuned bladed discs reliably are specified. In the foreseeable future, the potential of high cycle fatigue failure of mistuned blisks can be determined by regular checks.

The thesis contributes to knowledge in (i) understanding of the amplification factor and the maximum amplification factor, (ii) provision of a new and more efficient algorithm to estimate small probabilities, (iii) description of the blade mistuning problem using a robust design concept, (iv) investigation of robustness of bladed discs, (v) use of the maximum amplification factor sensitivity to construct a new interblade coupling ratio and (vi) the reliability of the forced vibration response prediction approach.

Recommendations are made for future research to refine the Mistuning Management Strategy. These include refinements to the algorithms used in the Strategy, better understanding of the forced vibration response behaviour of mistuned bladed discs, and the experimental techniques.

8.1 Conclusions

The viability of a Mistuning Management Strategy has been evaluated in this thesis by reviewing the previous research and by developing new tools to address existing limitations. The three steps in the strategy are repeated below:

1. Evaluation of the range of response level
2. Achieving a better bladed disc design
3. Monitoring the status of actual hardware

A new procedure has been proposed to carry out Step 1 more efficiently, and a robustness map to help designers to facilitate Step 2. Also, the response-prediction procedure related to Step 3 of the strategy will become practical following the improvements in experimental techniques anticipated in the foreseeable future. The conclusions on the three particular points raised in the Objectives section are listed below.

8.1.1 Efficient estimation of small probabilities

The term “amplification factor” has been clearly defined in Section 3.1 as

the ratio of the highest forced vibration response level found in any blade in the mistuned bladed disc concerned to the peak response level found in every blade on a tuned bladed disc.

New names have been given to the alternative definitions proposed in previous research, including (i) the “partial amplification factor”, where the forced response level is only measured on some of the blades on a mistuned bladed disc, and (ii) the “adjusted amplification factor”, where the response level in a blade on a mistuned bladed disc is normalised with the peak cantilever vibration response level of that blade.

In previous research, the Whitehead Factor $\left(\frac{1 + \sqrt{N}}{2}\right)$ has been shown to be an upper bound of the adjusted amplification factor if an isolated mode family is excited. However, this research has shown that the Whitehead Factor also represents, in some bladed disc designs, an upper bound of the adjusted amplification factor if modes in the veering region are excited. Furthermore, the upper bound of the adjusted amplification factor of damping mistuned bladed discs has been derived.

It has been shown how the maximum amplification factor can be calculated efficiently by an optimisation analysis using the conjugate gradient method. The maximum amplification factor has been defined solely as the value sought from an optimisation analysis. With the knowledge of the worst mistuning patterns, simulations can be carried out by taking more samples

around the worst mistuning patterns according to the importance sampling and cross entropy methods.

A new procedure, based on optimisation analysis and the importance sampling method, has been proposed to estimate the small but significant probabilities of extreme amplification factors. This procedure is up to 1,000 times more efficient than a Direct Monte Carlo simulation, and is capable to find the very small probabilities which are impossible to estimate using Direct Monte Carlo simulations. In the example shown in this thesis, the probability estimates of amplification factors up to 2.15 for a 24-sector blisk can be evaluated, compared with 1.95 from a Direct Monte Carlo simulation. In addition to the advantages listed above, the new procedure can also show the mistuning patterns related to high amplification factors.

8.1.2 Reduction of the variability of responses in blades

By casting the blade mistuning problem as a robustness problem, mistuning and the associated extremely high amplification factors have been defined as input variability and robustness respectively. Two approaches, which are based on probabilistics and interval analysis, have been developed to quantify input variability and robustness. The blade mistuning problem has been dealt with by using the outline of the Taguchi method and the formulations of the robust optimisation method.

To help compare the robustness of different bladed disc designs, each bladed disc design has been characterised by non-dimensional parameters including: number of sectors, level of damping and interblade coupling ratio. Through deriving the first-order maximum amplification factor sensitivity, the most suitable interblade coupling ratio in studying robustness of bladed disc has been found to be the minimum difference between the squares of neighbouring natural frequencies.

Two outstanding questions raised by Nikolic [80], regarding the variations of the maximum amplification factor and the critical degree of mistune in bladed disc designs, respectively, have been answered. The maximum amplification factors of bladed disc designs vary because this factor depends on the interblade coupling ratio and damping, besides the number of sectors. For example, a bladed disc design with a low interblade coupling ratio and a high level of damping is likely to experience a maximum amplification factor much lower than the Whitehead Factor. Also, the critical level of mistune

varies between bladed disc designs because the maximum amplification factor sensitivity depends on the interblade coupling ratio and, to a certain extent, damping of a bladed disc design.

The relationship between the maximum amplification factor and the design parameters (besides number of blades) has been used to create a “robustness map”, and the results from the 64-sector models and 24-sector blisks are consistent with the trend shown in the map. The robustness of a bladed disc design can be improved by any of the four options listed below:

Reducing maximum allowable mistune or mistuning scatter. The maximum and the 99.9th percentile amplification factors can be reduced by imposing small maximum allowable mistune and small mistuning scatter, respectively, in a bladed disc design with a high interblade coupling ratio (e.g. $c \approx 0.02$). For example, the maximum adjusted amplification factor of a 64-sector model is reduced by 20% by lowering the maximum allowable mistune from 4% to 2%, which is realistic in manufacture.

Adjusting the interblade coupling ratio. The interblade coupling ratio can be adjusted by changing the flexibility of discs and shroud geometry. For example, bladed disc designs with more flexible discs usually have higher interblade coupling ratios. Moreover, as Myhre [78] showed, removing shrouds can reduce the interblade coupling ratio significantly.

The interblade coupling ratio of a lightly-coupled bladed disc design (e.g. $c \approx 0.002$) can be lowered further to reduce the maximum amplification factor under a relatively high level of damping. For example, with $\eta = 0.004$, the maximum adjusted amplification factor of Model 64D is 25% lower than that of Model 64A. In contrast, the interblade coupling ratio of a heavily-coupled bladed disc design (e.g. $c \approx 0.02$) can be increased to lower the maximum amplification factor by as much as 17% if the maximum allowable mistune is controlled to within, say, 2%.

However, major design changes may be required to adjust the interblade coupling ratio, such as the increase of disc stiffness by an order from Model 64A to Model 64D.

Imposing an intentional mistuning pattern. The intentional mistun-

ing approach can reduce the likelihood of extremely high amplification factors. In a typical case studied, the 99.9th percentile amplification factor in a 24-sector blisk is reduced by 11% if an linear intentional mistuning pattern of 5% is imposed. The magnitude of intentional mistuning can be determined with the help of the importance sampling-based method shown in Section 6.5.1.

Increasing the level of damping. The vibration response levels of blades are reduced if the level of damping in an bladed disc assembly is increased. A detailed investigation of the relationship between the amplification factor distribution and the level of damping has been carried out. Although the amplification factor distribution changes with additional damping, the magnitude of such is much smaller than the reduction of the tuned response level. As a result, the magnitudes of stresses in blades are lowered by adding dampers, but the variation of dynamic stresses between blades remain. Also, adding friction dampers to bladed discs leads to complex effects in bladed discs and is potentially expensive.

With these conclusions in mind, possible methods to improve robustness for particular bladed disc designs, besides the intentional mistuning approach, are presented below:

Bladed disc designs with high interblade coupling ratios ($c \approx 0.02$).

The maximum amplification factor related to these bladed disc designs can be reduced by specifying a lower maximum allowable mistune (e.g. 2% instead of 4%). Also, the interblade coupling ratio of a bladed disc design can be increased by incorporating a more flexible disc. Although the increase in level of damping does not affect the amplification factor distribution significantly, the maximum stress experienced on a blade is reduced because the tuned vibration response level is lowered.

Bladed disc designs with low interblade coupling ratios ($c \approx 0.002$).

The interblade coupling ratio can be further lowered in some situations to reduce the maximum amplification factor, if the level of damping is high. The level of stresses experienced in blades can be lowered by adding damping because both the tuned vibration response level and the maximum amplification factor are reduced.

The amplification factor distributions under three specific situations have also been discussed. Firstly, although the upper bound of the adjusted amplification factor increases by introducing damping mistuning, the adjusted amplification factor distribution is robust to the magnitude of damping mistuning. The pdf does not change significantly even if the damping mistuning on a bladed disc reach as much as 20%.

Secondly, it is beneficial to excite modes in the veering region if the maximum allowable mistune is small. The response level of a tuned bladed disc excited in the veering region is significantly lower than that of the cantilever blade, and the maximum adjusted amplification factor sensitivity is relatively low. By changing the intersector coupling stiffness, the maximum adjusted amplification factor of a 64-sector model reduces from 4.3 to 1.72 if the maximum allowable mistune is kept at 5%. However, if mistuning scatter is significant (e.g. $\sigma = 4\%$), high response levels are more likely to be encountered if modes in the veering region are excited. The adjusted amplification factor pdf is skewed to the right hand side under such a situation (Figure 5.23).

At last, the current approach of using the deviation of the blade natural frequency as the mistuning parameter is valid because the apparently-tuned bladed discs are robust, but the forced vibration response estimates can become more accurate if mass and stiffness mistuning on a bladed disc are considered separately.

8.1.3 Validation of a response-prediction procedure

The potential of predicting the responses of individual mistuned blisks by testing prior to installation has been investigated experimentally. While the results from the experimental demonstration are within 9% of that given by simulations, the experimental procedure has to be improved to capture the FRFs more accurately, such that the predicted response becomes more reliable.

The consequences of common sources or error on the predicted response have been demonstrated in numerical simulations. The quality of experimental data required for identifying the mistuning pattern, such as (i) identification of all localised modes, (ii) accurate description of the natural frequencies and mode shapes of slightly split pairs of modes and (iii) errors of 5% or smaller in all modal components, are at the limit of the cur-

rent modal testing capabilities. In addition, the error in the phase in every modal component has to be controlled to within 5 degrees of the true value if both the frequency and damping mistuning pattern are to be identified accurately.

8.2 Major contributions to knowledge

The thesis contributes to knowledge in the following areas:

1. A proper discussion and rationalisation of the variants of the amplification factor and the maximum amplification factor created in the past 40 years is carried out. Also, the concepts of the amplification factor and the maximum amplification factor are extended to damping mistuned bladed discs.
2. A novel procedure to calculate the small but significant probabilities of high amplification factors under a given mistuning distribution is presented. This procedure is much more efficient than the commonly-used Direct Monte Carlo simulation in estimating small probabilities, such that the probabilities related to extreme amplification factors can now be evaluated.
3. An attempt of casting the blade mistuning problem as a robust design problem is presented. A novel and unprecedented example of using a mixture of the Taguchi method and the robust optimisation method in a single robust design problem is given.
4. The robustness of bladed disc designs under mistuning is studied, such that (i) a new concept of “robustness map” is created for realistic bladed discs to guide engineers to design more robust bladed discs, (ii) potential methods of improving robustness of bladed discs are presented and (iii) the effect on the robustness of imposing a linear mistuning pattern is evaluated for the first time.
5. A first-order maximum amplification factor sensitivity is derived and its relationship with design parameters of a bladed disc is analysed. For the first time, an interblade coupling ratio applicable to all bladed disc models is developed based on a theoretical analysis.

6. An original experimental demonstration of the reliability of an amplification factor prediction procedure using an impact excitation has been presented. The requirements on experimental data quality are also specified.

The blade mistuning problem may be soon the most critical problem faced by gas turbine designers after other major issues at the moment are solved. This research can contribute to more efficient gas turbine designs in the future.

8.3 Recommendations for future research

Although the Mistuning Management Strategy is proposed and shown to be workable, further refinements can be carried out by solving the following issues:

1. It has to be explained why the highest response level under an nEO excitation is usually observed on blades with blade-alone natural frequencies close to the natural frequency of the nND mode of the bladed disc, and an apparent upper boundary exists among the random data points in Figure 3.3.
2. The new procedure to find the small probabilities related to high amplification factor can be refined by sampling techniques, such as line sampling [116], recently proposed in other disciplines.
3. The effects of imposing intentional mistuning patterns on bladed discs on other than the forced vibration response behaviour should be investigated.
4. The mechanism of mistuning parameter evolution, such as crack growth and tip wear, should be investigated further to facilitate better predictions of the evolution of the amplification factor in service life.
5. Further research is needed in experimental equipments and procedure to achieve the data quality specified in Chapter 7. Also, the correlation between the mistuning parameters of a test piece in stationary and rotating states need to be validated experimentally.

Appendix A

Modal properties of bladed discs

Because a tuned bladed disc is a cyclic symmetric structure, there are some special modal properties related to bladed discs. Every mode shape of a tuned bladed disc vary n times sinusoidally around the annulus, where n is the number of nodal diameters and can be equal to any integer between 0 and $N/2$. Also, the mode shapes can be grouped into families of modes according to the mode shape on a single blade. The number of modes in a family is equal to the number of blades on a bladed disc, N .

There are two n ND modes in each family on a tuned bladed disc. These two *double modes* are independent of each other because the mode shapes are circumferentially separated by a 90° phase shift. These two modes have the same natural frequencies, such that the natural frequencies are *repeated* and as a result, there are less than N distinct natural frequencies in a mode family. A typical plot of natural frequencies of a bladed disc is shown in Figure A.1, where the natural frequencies are grouped according to mode families and the number of nodal diameters in the mode shapes.

If a mode family is isolated (e.g. Mode family 1 in Figure A.1), the magnitude of the mode shape in the disc part is very small to that in the blades, and the mode shape of a single blade is similar to a mode shape of a clamped blade. In other words, the modes of a bladed disc in an isolated mode family are called *blade-dominated modes*. In this situation, the vibration energy (both kinetic and potential) is concentrated in the blades.

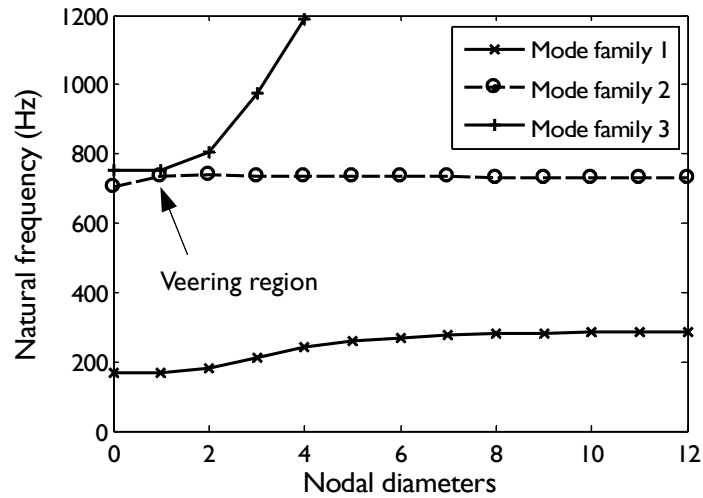


Figure A.1: Natural frequencies of a 24-sector blisk.

The extreme in the contrary to an isolated mode family occurs at the veering region, where mode shapes with the same number of nodal diameters but of different mode families having close natural frequencies. An example of a veering region is marked in Figure A.1. It is called as such because the lines of mode families converge and veer away in a natural frequency plot. A significant portion of modal energy of a mode in the veering region is contained in the disc part of a bladed disc, so it is sometimes called a *disc-dominated mode*. The difference between a blade- and a disc-dominated mode is illustrated in Figure A.2.

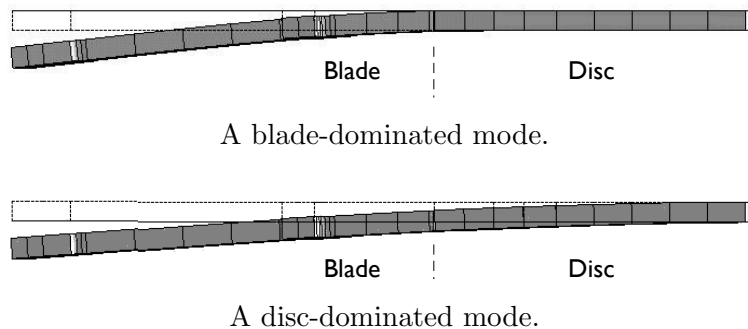


Figure A.2: Two types of modes found on a bladed disc.

Cyclic symmetry is destroyed with the introduction of mistuning. The mode shapes in a mistuned bladed disc are not circumferentially sinusoidal, and a pair of distorted “ n ND” modes in a slightly mistuned bladed disc

have close but distinct natural frequencies. These phenomena are called *mode distortion* and *mode splitting*, respectively. In a mistuned bladed disc, all modes in a mode family are excited under an nEO excitation because all modes contain nND components due to mode distortion. The effects of mode splitting and mode distortion under a particular mistuning pattern in Model 64B (Section 5.3.1) are shown in Figures A.3(a) and (b), respectively. If the maximum mistune in a bladed disc is high, *mode localisation* can occur: the mode shapes can be distorted significantly, such that the modal amplitudes are significant in few blades and nearly zero in others.

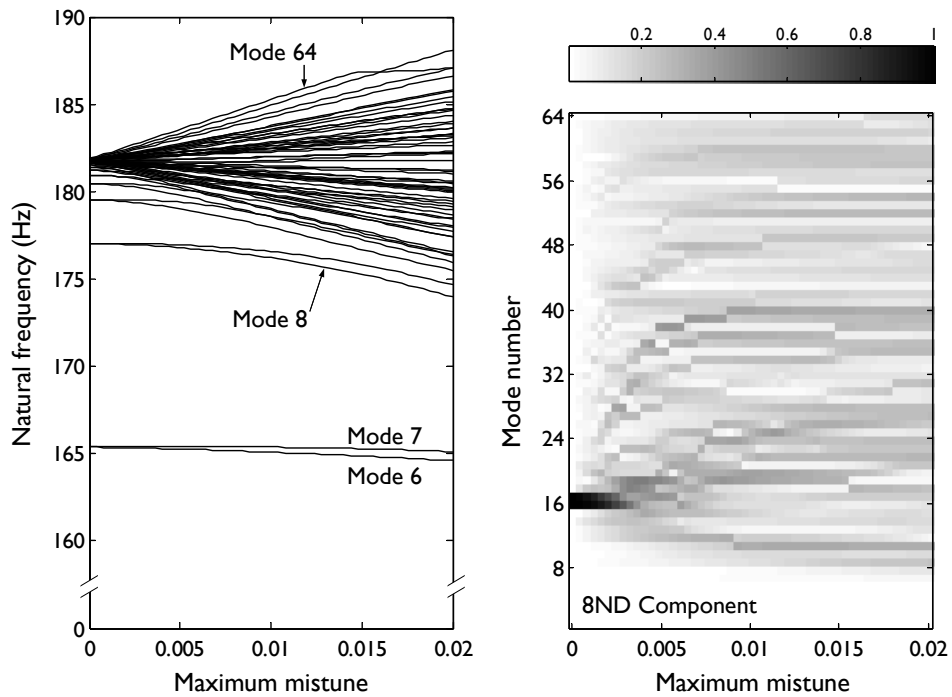


Figure A.3: Effect of mistune on (a) natural frequencies of the bladed disc and (b) nodal diameter components of modes in a family.

Appendix B

Implementation of the cross entropy method

(The algorithm listed below is similar to that provided in Reference [106].)

The sampling distribution in $(k + 1)^{\text{th}}$ iteration, $g_{k+1}(\{x\})$, is found by minimising the distance D between the sampling distribution, $g(\{x\})$, and the ideal distribution defined in Section 3.4.1, $g^*(\{x\})$:

$$\begin{aligned} D(g^*, g) &= E_{g^*} \left(\ln \frac{g^*(\{x\})}{g(\{x\})} \right) \\ &= \int_{\tilde{x}_n}^{\hat{x}_n} \cdots \int_{\tilde{x}_1}^{\hat{x}_1} g^*(\{x\}) (\ln g^*(\{x\}) - \ln g(\{x\})) dx_1 \cdots dx_n \quad (\text{B.1}) \end{aligned}$$

$$\begin{aligned} \min_g (D) &= \min_g \left(\int_{\tilde{x}_n}^{\hat{x}_n} \cdots \int_{\tilde{x}_1}^{\hat{x}_1} g^*(\{x\}) (\ln g^*(\{x\}) - \ln g(\{x\})) dx_1 \cdots dx_n \right) \\ &= \max_g \left(\int_{\tilde{x}_n}^{\hat{x}_n} \cdots \int_{\tilde{x}_1}^{\hat{x}_1} g^*(\{x\}) \ln g(\{x\}) dx_1 \cdots dx_n \right) \quad (\text{B.2}) \end{aligned}$$

As mentioned in Section 3.4.2, the sampling distribution is assumed to be multivariate normal. If the distributions of mistuning parameters of different blades are independent of each other, the pdf of the sampling distribution, $g(\{x\})$, is defined by μ_m and σ_m (where $m = 1, \dots, N$), which are the mean and the standard deviation of the mistuning parameter in blade m , respectively:

$$g(\{x\}) = \prod_{m=1}^N \frac{1}{\sigma_m \sqrt{2\pi}} \exp \left(-\frac{(x - \mu_m)^2}{2\sigma_m^2} \right) \quad (\text{B.3})$$

The sampling distribution can be found by examining Equation (B.2) because the gradient of the integral in Equation (B.2) equals to zero at that distribution:

$$\nabla \int_{\hat{x}_n}^{\hat{x}_n} \cdots \int_{\hat{x}_1}^{\hat{x}_1} g^* (\{x\}) \ln g_{j+1} (\{x\}) dx_1 \cdots dx_n = 0 \quad (\text{B.4})$$

Because the sampling distribution is multivariate normal, the gradient operator, $\nabla g (\{x\})$, refers to a vector with entries being the partial derivatives of the pdf to all $2N$ defining variables:

$$\nabla g (\{x\}) = \left\{ \frac{\partial g}{\partial \mu_1} \quad \frac{\partial g}{\partial \sigma_1} \quad \frac{\partial g}{\partial \mu_2} \quad \cdots \quad \frac{\partial g}{\partial \mu_N} \quad \frac{\partial g}{\partial \sigma_N} \right\}^T \quad (\text{B.5})$$

Equation (3.38), which is $g^* (\{x\}) = |h (\{x\}) f (\{x\})| / p$, is substituted into Equation (B.4) to form

$$\nabla \int_{\hat{x}_n}^{\hat{x}_n} \cdots \int_{\hat{x}_1}^{\hat{x}_1} h (\{x\}) f (\{x\}) \ln g_{j+1} (\{x\}) dx_1 \cdots dx_n = 0 \quad (\text{B.6})$$

According to the importance sampling method (Section 3.4.1), the sampling distribution pdf in j^{th} iteration, $g_j (\{x\})$, can be incorporated:

$$\nabla \int_{\hat{x}_n}^{\hat{x}_n} \cdots \int_{\hat{x}_1}^{\hat{x}_1} h (\{x\}) \frac{f (\{x\})}{g_j (\{x\})} \ln g_{j+1} (\{x\}) g_j (\{x\}) dx_1 \cdots dx_n = 0 \quad (\text{B.7})$$

The fraction $f (\{x\}) / g_j (\{x\})$ in Equation (B.7) can be replaced by a likelihood ratio, $w_j (\{x\})$. Equation (B.6) can be approximated by

$$\nabla \left(\frac{1}{N} \sum_{i=1}^R h (\{x\}) w_j (\{x\}) \ln g_{j+1} (\{x\}) \right) = 0 \quad (\text{B.8})$$

where

$$\ln g (\{x\}) = - \sum_{m=1}^N \ln \left(\sigma_m \sqrt{2\pi} \right) + \frac{(x - \mu_m)^2}{2\sigma_m^2} \quad (\text{B.9})$$

As $h (\{x\}) w_j (\{x\})$ in Equation (B.8) is independent of the sampling distribution in $(j + 1)^{\text{th}}$ iteration, the only unknowns in Equation (B.8) are the derivatives of $\ln g (\{x\})$ with respect to the mean and the standard

deviation the mistuning parameter of each sector:

$$\frac{\partial \ln(g(\{x\}))}{\partial \mu_m} = \frac{x - \mu_m}{\sigma_m^2} \quad (\text{B.10})$$

$$\frac{\partial \ln(g(\{x\}))}{\partial \sigma_m} = \frac{1}{\sigma_m} \left(1 + \frac{(x - \mu_m)^2}{\sigma_m^2} \right) \quad (\text{B.11})$$

By substituting Equations (B.10) and (B.11) into Equation (B.8), the entries of the mean vector, $\{\mu_{j+1}\}$, and the variance vector, $\{\sigma_{j+1}^2\}$, in $(j + 1)^{\text{th}}$ iteration can be found by Equations (B.12) and (B.13) respectively:

$$\{\mu_{j+1}\}_m = \frac{\sum_{i=1}^R h(\{x_i\}) w_j(\{x_i\}) x_{mi}}{\sum_{i=1}^R h(\{x_i\}) w_j(\{x_i\})} \quad (\text{B.12})$$

$$\{\sigma_{j+1}^2\}_m = \frac{\sum_{i=1}^R h(\{x_i\}) w_j(\{x_i\}) x_{mi}^2}{\sum_{i=1}^R h(\{x_i\}) w_j(\{x_i\})} - \{\mu_{j+1}\}_m \quad (\text{B.13})$$

B.1 Outline of the algorithm

An algorithm to find small probabilities using the importance sampling method is outlined below. The algorithm is based on the derivation made in the previous section, and is similar to that provided in Reference [106]. It is assumed that the initial sampling distribution g_1 - with the mean vector $\{\mu_1\}$ and the variance vector $\{\sigma_1^2\}$ - is known. The mean vector of the initial sampling distribution comprises the worst mistuning patterns, and the initial covariance matrix of the distribution is usually a diagonal matrix with entries smaller than the variance of the probability distribution.

The algorithm comprises two stages. At the first stage, iterative simulations with R_1 samples are run to find a good sampling distribution using the cross entropy method. A pass ratio, γ , is set to estimate the quality of the sampling distribution found using the cross entropy method in an iteration. A high pass ratio (e.g. $\gamma = 0.2 - 0.5$) ensures the sampling distribution is close to the best possible counterpart, but lower pass ratios (e.g. $\gamma = 0.01 - 0.1$) can be set if a high pass ratio is not reached in simulations in particular problems. The iteration ends if the mean of the function $h(\{\epsilon_i\})$ in the samples of Iteration k is higher than γ , and the sampling distribution calculated based on Iteration k becomes the sampling distribution at the second stage, the importance sampling simulation.

At the second stage, an importance sampling simulation with R_2 samples

is run. The size of the second simulation, R_2 , is usually higher than R_1 such that a more accurate probability estimate can be found.

1. Set the counter $j = 1$.
2. (The cross entropy method) the following loop is executed:
 - (a) Generate R_1 sets of random variables according to probability distribution $g_j(\{x\})$, which the mean and variance vectors are $\{\mu_1\}$ and $\{\sigma_1^2\}$ respectively.
 - (b) Evaluate each $A_i = a(\{x_i\})$.
 - (c) Evaluate $a_t(\{x_i\})$ for each sample as described in Equation (3.29).
 - (d) Evaluate the weighting ratio $w_i = g_j(\{x_i\})/f(\{x_i\})$.
 - (e) Find the distribution parameters for g_{j+1} by Equations (B.12) and (B.13).
 - (f) If $\sum_{i=1}^{R_1} h_i < \gamma R_1$, set the counter $j = j + 1$ and the loop is repeated, otherwise the loop is terminated.
3. (Importance sampling with the best distribution) importance sampling is carried out with R_2 samples, chosen according to the distribution g_{j+1} . The functions $a(\{x_i\})$, $h(\{x_i\})$ and $w(\{x_i\})$ are evaluated for each sample, in a same way as in Steps 2(b) to 2(d).
4. The probability and variance of $a(\{x\}) > A_0$ are found using equations below:

$$p = \frac{\sum_i h(\{x_i\}) w(\{x_i\})}{R_2} \quad (\text{B.14})$$

$$s^2 = \frac{\sum_i h(\{x_i\}) w(\{x_i\})^2}{R_2} - p^2 \quad (\text{B.15})$$

$$\Delta p = 1.960 \sqrt{\frac{s^2}{R_2}} \quad (\text{B.16})$$

The source of the value 1.960 in Equation (B.16) is explained in Section 3.3 and Reference [61].

Appendix C

First-order derivatives of natural frequencies and mode shapes

The derivation in this section is a simplified form of that provided by Ewins [34] and Friswell [39] by taking account of $\frac{\partial[K]}{\partial\alpha} = 0$, $\frac{\partial^2[K]}{\partial\alpha^2} = 0$ and $\frac{\partial^2[M]}{\partial\alpha^2} = 0$.

C.1 Derivatives of non-repeated natural frequencies

The derivation begins with the equation that finds the natural frequencies of a vibration system:

$$([K] - \omega_l^2 [M]) \{\phi_l\} = \{0\} \quad (\text{C.1})$$

By differentiating Equation (C.1),

$$([K] - \omega_l^2 [M]) \frac{\partial \{\phi_l\}}{\partial \alpha} + \left(\frac{\partial [K]}{\partial \alpha} - \frac{\partial \omega_l^2}{\partial \alpha} [M] - \omega_l^2 \frac{\partial [M]}{\partial \alpha} \right) \{\phi_l\} = \{0\} \quad (\text{C.2})$$

Pre-multiply (C.2) with $\{\phi_l\}^T$,

$$\begin{aligned} \cancel{\{\phi_l\}^T ([K] - \omega_l^2 [M])} \frac{\partial \{\phi_l\}}{\partial \alpha} + \{\phi_l\}^T \left(-\frac{\partial \omega_l^2}{\partial \alpha} [M] - \omega_l^2 \frac{\partial [M]}{\partial \alpha} \right) \{\phi_l\} &= 0 \\ 0 - \frac{\partial \omega_l^2}{\partial \alpha} - \omega_l^2 \{\phi_l\}^T \frac{\partial [M]}{\partial \alpha} \{\phi_l\} &= 0 \end{aligned}$$

Therefore

$$\frac{\partial \omega_l^2}{\partial \alpha} = -\omega_l^2 \{\phi_l\}^T \frac{\partial [M]}{\partial \alpha} \{\phi_l\} \quad (\text{C.3})$$

C.2 Derivative of a mode shape

The derivative of a mode shape can be written as a weighed combination of all mode shapes:

$$\frac{\partial \{\psi_l\}}{\partial \alpha} = \sum_{r=1}^N \{\psi_r\} \beta_{lr} \quad (\text{C.4})$$

Collectively, the mode shape derivative matrix is the product of the mode shape matrix and a weighting matrix, as shown in Equation (C.5).

$$\frac{\partial [\Psi]}{\partial \alpha} = [\Psi]' = [\Psi] [\beta] \quad (\text{C.5})$$

If $r \neq l$ and $\omega_r \neq \omega_l$, the weighting factors β_{rl} are found by differentiating Equation (C.1) with respect to α [34]:

$$\beta_{lr} = -\{\psi_l\}^T \left[\frac{\partial [K]}{\partial \alpha} - \omega_r^2 \frac{\partial [M]}{\partial \alpha} \right] \{\psi_r\} \frac{1}{\omega_l^2 - \omega_r^2} \quad (\text{C.6})$$

If $r = l$, the denominator of the fraction in Equation (C.6) equals to zero. β_{ll} is found by differentiating the equation $\{\psi_l\}^T [M] \{\psi_l\} = 1$ with respect to α , such that

$$\beta_{ll} = -\frac{1}{2} \{\psi_l\}^T \frac{\partial [M]}{\partial \alpha} \{\psi_l\} \quad (\text{C.7})$$

In bladed discs, pairs of distinct mode shapes are found having the same natural frequency. The derivatives of natural frequencies and mode shapes of this case, where $r \neq l$ but $\omega_r = \omega_l$, is discussed in the Section C.3.

C.3 Natural frequency and mode shape derivatives of double modes

By the definition of eigenvalues and eigenvectors, any linear combination of a pair of mode shapes associated with an identical natural frequency is also a mode shape. Although a mode shape in a tuned bladed disc can be any weighted combination of the two sinusoidal and spatially orthogonal mode shapes, mode shapes are unique in mistuned bladed discs. Therefore, we need to find the “correct” mode shapes such that the derivatives of natural frequencies and mode shapes can be calculated accordingly [39].

A pair of correct double modes $\{\psi_{n_1}\}$ and $\{\psi_{n_2}\}$ can be calculated by post-multiplying a pair of arbitrary double modes, denoted $\{\phi_{n_1}\}$ and $\{\phi_{n_2}\}$ by a weighting matrix $[H]$, as shown in Equation (C.8):

$$\begin{bmatrix} \psi_{n_1} & \psi_{n_2} \end{bmatrix} = \begin{bmatrix} \phi_{n_1} & \phi_{n_2} \end{bmatrix} [H] \quad (\text{C.8})$$

The derivatives of natural frequencies and the entries of matrix $[H]$ can be found by solving the eigenvalue-eigenvector problem in Equation (C.9):

$$[\psi_{n_1} \ \psi_{n_2}]^T \begin{bmatrix} \frac{\partial [K]}{\partial \alpha} - \omega_n^2 \frac{\partial [M]}{\partial \alpha} \end{bmatrix} [\psi_{n_1} \ \psi_{n_2}] [H] = \begin{bmatrix} \frac{\partial(\omega_l^2)}{\partial \alpha} & 0 \\ 0 & \frac{\partial(\omega_r^2)}{\partial \alpha} \end{bmatrix} [H] \quad (\text{C.9})$$

The same summation-of-weighted-modes approach is used to find the derivative of the mode shape. While β_{ll} can be found using Equation (C.7), β_{rl} has to be found using the second-order derivative of Equation (C.1). By assuming the stiffness matrix being constant and the second-order derivative of mass being zero,

$$-2 \left(\frac{\partial(\omega_l^2)}{\partial \alpha} [M] + \omega_l^2 \frac{\partial [M]}{\partial \alpha} \right) \{\phi'_l\} - \left(2 \frac{\partial(\omega_l^2)}{\partial \alpha} \frac{\partial [M]}{\partial \alpha} + \frac{\partial^2(\omega_l^2)}{\partial \alpha^2} [M] \right) \{\phi_l\} = 0 \quad (\text{C.10})$$

Appendix C. First-order derivatives of natural frequencies and mode shapes

Pre-multiplying Equation (C.10) with $\{\phi_r\}^T$,

$$2\{\phi_r\}^T \frac{\partial(\omega_l^2)}{\partial\alpha} [M] \{\phi_l'\} + 2\{\phi_r\}^T \omega_l^2 \frac{\partial[M]}{\partial\alpha} \{\phi_l'\} + 2\{\phi_r\}^T \frac{\partial(\omega_l^2)}{\partial\alpha} \frac{\partial[M]}{\partial\alpha} \{\phi_l\} \dots$$

$$+ \{\phi_r\}^T \frac{\partial^2(\omega_l^2)}{\partial\alpha^2} [M] \{\phi_l\} = 0 \quad (C.11)$$

By decomposing all mode shape derivatives and applying (C.14),

$$\beta_{rl} \frac{\partial(\omega_l^2)}{\partial\alpha} - \beta_{rl} \frac{\partial(\omega_r^2)}{\partial\alpha} + \{\phi_r\}^T \frac{\partial(\omega_l^2)}{\partial\alpha} \frac{\partial[M]}{\partial\alpha} \{\phi_l\} = 0 \quad (C.12)$$

As a result,

$$\beta_{rl} = \frac{\partial(\omega_l^2)}{\partial\alpha} \left(\{\phi_r\}^T \frac{\partial[M]}{\partial\alpha} \{\psi_l\} \right) \frac{1}{\frac{\partial(\omega_r^2)}{\partial\alpha} - \frac{\partial(\omega_l^2)}{\partial\alpha}} \quad (C.13)$$

C.4 Summary

Three equations are used to find β_{rl} depending on the relationship between s and r :

1. If $r \neq l$, $\omega_r \neq \omega_l$: β_{rl} is calculated using Equation (C.6).
2. If $r = l$, β_{ll} is calculated using Equation (C.7).
3. If $r \neq l$, $\omega_r = \omega_l$ (i.e. $r = n_1$, $l = n_2$), β_{rl} is calculated using Equation (C.13). However, $\beta_{rl} = 0$ if only the mass matrix is perturbed. By replacing $\begin{bmatrix} \phi_r & \phi_l \end{bmatrix}$ in Equation (C.9) with $\begin{bmatrix} \psi_r & \psi_l \end{bmatrix}$, $[H] = [I]$ such that

$$[\psi_l \ \psi_r]^T \left(-\omega_l^2 \frac{\partial[M]}{\partial\alpha} \right) [\psi_l \ \psi_r] = \begin{bmatrix} \frac{\partial(\omega_l^2)}{\partial\alpha} & 0 \\ 0 & \frac{\partial(\omega_r^2)}{\partial\alpha} \end{bmatrix} \quad (C.14)$$

By matrix algebra, the bracketed term in Equation (C.13) corresponds to off-diagonal terms on the right hand side of Equation (C.14), which is zero.

Appendix D

Sensitivity of the maximum adjusted amplification factor

D.1 Simplifying the vibration responses derivatives vector

The full equation of finding the response derivative vector $\frac{\partial\{u\}}{\partial\alpha}$ is shown in Equation (6.4), and is repeated below:

$$\begin{aligned} \frac{\partial\{u\}}{\partial\alpha} = \{u'\} \approx & \sum_{l=n_1, n_2} \frac{\left(\{\psi_l\}^T \{f_n\}\right)'}{\omega_l^2 - \Omega^2 + j\eta\omega_l^2} \{\psi_l\} + \sum_{l=n_1, n_2} \frac{\{\psi_l\}^T \{f_n\}}{\omega_l^2 - \Omega^2 + j\eta\omega_l^2} \{\psi'_{n_l}\} \\ & + \sum_{l=n_1, n_2} \{\psi_l\}^T \{f_n\} \left(\frac{1}{\omega_l^2 - \Omega^2 + j\eta\omega_l^2}\right)' \{\psi_l\} \end{aligned} \quad (\text{D.1})$$

Equation (D.1) is simplified by considering each term separately.

The first term is simplified by using Equation (C.4), where the mode shape derivative can be written as the weighed sum of mode shapes:

$$\frac{\partial\{\psi_r\}}{\partial\alpha} = \sum_{l=1}^N \{\psi_l\} \beta_{lr}$$

It is noted that β_{lr} is proportional to $\omega_r^2 / (\omega_r^2 - \omega_l^2)$ if $r \neq l$ (Equation (C.6)), and β_{ll} is proportional to unity (Equation (C.7)), if we assume the

expression

$$\{\phi_r\}^T \frac{\partial [M]}{\partial \alpha} \{\phi_l\} \quad (\text{D.2})$$

for different pairs of r and l are in the same order of magnitude. Because the natural frequencies in bladed discs are generally close to each other, β_{ll} is negligible. Also, $\{\psi_l\}^T \{f\} = 0$ if $\{\psi_l\}$ corresponds to an m ND mode and $m \neq n$. As a result, the first term in Equation (D.1) can be approximated to zero.

The second term in Equation (D.1) can be simplified because the two slightly split modes form a single resonant peak in slightly mistuned systems because natural frequencies are close to each other. In this case, the resonant frequency, Ω , can be taken as either ω_{n_1} or ω_{n_2} , and both can be approximated to ω_n , the natural frequency of the tuned n ND mode. For example, if $\Omega = \omega_{n_1}$, the denominator of the second term in (6.4) can be simplified:

$$\begin{aligned} \omega_{n_1}^2 - \omega_{n_1}^2 + j\eta\omega_{n_1}^2 &= j\eta\omega_{n_1}^2 \approx j\eta\omega_n^2 \\ \omega_{n_2}^2 - \omega_{n_1}^2 + j\eta\omega_{n_2}^2 &\approx j\eta\omega_{n_2}^2 \approx j\eta\omega_n^2 \end{aligned}$$

The third term of Equation (D.1) is simplified by introducing a dimensionless mode split parameter S . The parameter S and its derivative with respect to α are defined in Equations (D.3) and (D.4):

$$S = \frac{\omega_{n_2}^2 - \omega_{n_1}^2}{\omega_n^2} \quad (\text{D.3})$$

$$\frac{\partial S}{\partial \alpha} = S' \approx \frac{1}{\omega_n^2} \left(\frac{\partial (\omega_{n_2}^2)}{\partial \alpha} - \frac{\partial (\omega_{n_1}^2)}{\partial \alpha} \right) \quad (\text{D.4})$$

In addition, four assumptions are made:

1. $\omega_{n_1}^2$ and $\omega_{n_2}^2$ diverge with similar magnitudes but in opposite directions, such that $\omega_{n_1}^2 \approx (1 - S/2)\omega_n^2$ and $\omega_{n_2}^2 \approx (1 + S/2)\omega_n^2$
2. $\Omega = \omega_{n_1}$
3. the damping loss factor η is small
4. the mode splitting parameter S is smaller than η in magnitude

Given the mode split parameter and the four assumptions, the two

derivatives appearing in the third term of Equation (D.1) are simplified in Equations (D.5) and (D.6):

$$\frac{\partial}{\partial \alpha} \left(\frac{1}{\omega_{n_1}^2 - \Omega^2 + j\eta\omega_{n_1}^2} \right) = \frac{1}{j\eta\omega_n^2} \frac{\partial}{\partial \alpha} \left(\frac{1}{1 - \frac{S}{2}} \right) \approx \frac{1}{j\eta\omega_n^2} \frac{S'}{2} \quad (\text{D.5})$$

$$\begin{aligned} \frac{\partial}{\partial \alpha} \left(\frac{1}{\omega_{n_2}^2 - \Omega^2 + j\eta\omega_{n_2}^2} \right) &= \frac{1}{\omega_n^2} \frac{\partial}{\partial \alpha} \left(\frac{1}{S + j\eta \left(1 + \frac{S}{2}\right)} \right) \\ &= \frac{1}{\omega_n^2} \frac{-1}{\left(S + j\eta \left(1 + \frac{S}{2}\right)\right)^2} \left(S' + \frac{j\eta S'}{2} \right) \\ &\approx \frac{S'}{\eta^2 \omega_n^2} \left(1 + \frac{j\eta}{2} \right) \approx \frac{S'}{\eta^2 \omega_n^2} \end{aligned} \quad (\text{D.6})$$

Equation (D.5) is approximated to zero because the magnitude of the result in Equation (D.6) is much higher than that in Equation (D.5) under small η . By combining the simplification efforts above, Equation (6.4) becomes Equation (D.7) (which is Equation (6.5)):

$$\frac{\partial \{u\}}{\partial \alpha} = \{u'\} = [\psi'_{n_1} \ \psi'_{n_2}] \frac{[\psi_{n_1} \ \psi_{n_2}]^T \{f_n\}}{j\eta\omega_n^2} + \{\psi_{n_2}\} \frac{\{\psi_{n_2}\}^T \{f_n\}}{\omega_n^2} \frac{S'}{\eta^2} \quad (\text{D.7})$$

Given the response derivative vector to the maximum mass mistune is known, the response level derivative vector can be found by using Equation (6.6). The ratio $\bar{u}_i/|u_i|$ in this equation can be simplified by assuming DOF 1 has a zero phase. This can be achieved by shifting the phase of the force vector.

The phase difference between neighbouring DOFs is $\frac{2\pi n}{N}$, and is denoted θ . By writing $e^{j\theta}$ as $\angle\theta$, the response vector can be written down as

$$\{u\} = |u| \left\{ 1 \quad \angle\theta \quad \dots \quad \angle(N-1)\theta \right\}^T \quad (\text{D.8})$$

The conjugate of the response vector, $\{\bar{u}\}$, equals to

$$\{u\} = |u| \left\{ 1 \quad \angle-\theta \quad \dots \quad \angle-(N-1)\theta \right\}^T \quad (\text{D.9})$$

As a result, $\bar{u}_i/|u_i| = e^{-j\frac{2\pi n(i-1)}{N}}$.

D.2 Analysing the adjusted amplification factor sensitivity

Although the amplification factor sensitivity and design parameters do not form a straightforward relationship, the dependence of the amplification factor sensitivity on design parameters can be analysed qualitatively by considering the response sensitivities. By substituting the weighted sum of mode shapes for the mode shape derivatives in Equation (D.7),

$$\begin{aligned} \{u'\} &= [\Psi] \begin{bmatrix} \beta_{1n_1} & \beta_{1n_2} \\ \vdots & \vdots \\ \beta_{Nn_1} & \beta_{Nn_2} \end{bmatrix} \left[\frac{[\psi_{n_1} \ \psi_{n_2}]^T \{f_n\}}{j\eta\omega_n^2} + \{\psi_{n_2}\} \frac{\{\psi_{n_2}\}^T \{f_n\} S'}{\omega_n^2 \eta^2} \right] \\ &= \sum_{l=1}^N \{\psi_l\} \{\beta_{ln_1} \ \beta_{ln_2}\} \left[\frac{[\psi_{n_1} \ \psi_{n_2}]^T \{f_n\}}{j\eta\omega_n^2} + \{\psi_{n_2}\} \frac{\{\psi_{n_2}\}^T \{f_n\} S'}{\omega_n^2 \eta^2} \right] \end{aligned} \quad (\text{D.10})$$

All variables present in Equation (D.10) are design parameters of the tuned bladed disc design, except the matrix $[\beta]$ and the mode splitting parameter derivative S' . Actually, $[\beta]$ and S' are dependent on design parameters as well:

- each β_{ln} , except if $\omega_l = \omega_n$, is calculated using Equation (C.6):

$$\beta_{ln} = \frac{\omega_n^2}{\omega_l^2 - \omega_n^2} \{\psi_l\}^T \left(\frac{\partial [M]}{\partial \alpha} \right) \{\psi_n\} \quad (\text{D.11})$$

The terms β_{ln} if $\omega_l = \omega_n$ are negligible as discussed in Section 6.2.1. By expanding the coefficient β_{ln} for other values of l ,

$$\{\psi_l\} \{\beta_{ln_1} \ \beta_{ln_2}\} = \frac{\omega_n^2}{\omega_l^2 - \omega_n^2} \{\psi_l\} \{\psi_l\}^T \left(\frac{\partial [M]}{\partial \alpha} \right) [\psi_{ln_1} \ \psi_{ln_2}] \quad (\text{D.12})$$

- The derivative of the mode splitting parameter S' is proportional to ω_n^2 (Equation (D.4)).

Appendix D. Sensitivity of the maximum adjusted amplification factor

Suppose the highest response level in a slightly mistuned model is observed at DOF 1, the response sensitivity of DOF 1 to maximum mistune can be written as

$$\frac{\partial u_1}{\partial \alpha} = \sum_{l=1, l \neq n_1, n_2}^N \frac{b_l \omega_n^2}{\omega_l^2 - \omega_n^2} + \frac{b_\eta}{\eta} \quad (\text{D.13})$$

where

$$\begin{aligned} b_l &= -j \psi_{1l} \{\psi_l\}^T \frac{\partial [M]}{\partial \alpha} [\psi_{1n_1} \ \psi_{1n_2}] [\psi_{n_1} \ \psi_{n_2}]^T \{f_n\} \\ b_\eta &= \psi_{1n_2} \left(\frac{\partial \omega_{n_2}^2}{\partial \alpha} - \frac{\partial \omega_{n_1}^2}{\partial \alpha} \right) \{\psi_{n_2}\}^T \{f_n\} \\ &= \psi_{1n_2} \left(\{\psi_{n_2}\}^T \frac{\partial [M]}{\partial \alpha} \{\psi_{n_2}\} - \{\psi_{n_1}\}^T \frac{\partial [M]}{\partial \alpha} \{\psi_{n_1}\} \right) \{\psi_{n_2}\}^T \{f_n\} \end{aligned} \quad (\text{D.14})$$

$$(\text{D.15})$$

It can be seen that the coefficients b_l and b_η are dependent on the exact mistuning pattern, and the maxima of both of them have the same order of magnitude. Finally, the adjusted amplification factor sensitivity can be written in a similar form:

$$\frac{\partial A}{\partial \alpha} = \left(\sum_{l=1, l \neq n_1, n_2}^N \frac{\text{Re}(b_l) \omega_n^2}{\omega_l^2 - \omega_n^2} + \frac{\text{Re}(b_\eta)}{\eta} \right) \frac{1}{\eta k} \quad (\text{D.16})$$

For the mistuning pattern corresponding to the sensitivity of the maximum adjusted amplification factor, b_l is probably negative if $\omega_l < \omega_n$ and positive otherwise.

Appendix E

Pdf of the sum of random numbers of different distributions

(The derivation below is carried out with the kind help of Dr. Roy Jacobs.)

If a mistuning pattern $\{x\}$, with N elements, is the sum of random vectors $\{d\}$ and $\{q\}$ as described in Section 6.5.1, the pdf of $\{x\}$ is expressed in Equation (6.11):

$$g(\{x\}) = \frac{1}{\delta_2 - \delta_1} \int_{\delta_1}^{\delta_2} \prod_{i=1}^N f_G(x_i - d_i\delta) d\delta$$

where δ is the magnitude of intentional mistuning, and f_G refers to the pdf of a normally-distributed variable with zero mean:

$$f_G(x) = \frac{1}{\sigma\sqrt{2\pi}} \exp\left(-\frac{x^2}{2\sigma^2}\right) \quad (\text{E.1})$$

The sampling distribution pdf (Equation (6.11)) can be evaluated by substituting Equation (E.1) into the integrand of (6.11):

$$\prod_{i=1}^N f_G(x_i - d_i\delta) = \underbrace{\left(\frac{1}{\sigma\sqrt{2\pi}}\right)^N}_{A^N} \exp\left(-\frac{1}{2\sigma^2} \sum_{i=1}^N (x_i - d_i\delta)\right) \quad (\text{E.2})$$

Equation (E.2) can be derived further:

$$\begin{aligned}
 \text{(E.2)} &= A^N \exp \left(-\frac{1}{2\sigma^2} \sum_{i=1}^N (x_i^2 - 2x_i d_i \delta + d_i^2 \delta^2) \right) \\
 &= A^N \underbrace{\exp \left(-\frac{\sum_{i=1}^N x_i^2}{2\sigma^2} \right)}_B \underbrace{\exp \left(-\frac{-2\delta \sum_{i=1}^N (x_i d_i) + \delta^2 \sum_{i=1}^N d_i^2}{2\sigma^2} \right)}_C
 \end{aligned} \tag{E.3}$$

As A and B are independent of δ , the terms can be taken out of the integral in Equation (6.11). The variable C is evaluated by completion of squares, such that it becomes a form similar to that of the normal distribution pdf.

$$\begin{aligned}
 C &= \exp \left(-\frac{1}{2\sigma^2} \left(\frac{\left(\sum_{i=1}^N x_i d_i \right)^2}{\sum_{i=1}^N d_i^2} - 2\delta \sum_{i=1}^N (x_i d_i) + \delta^2 \sum_{i=1}^N d_i^2 - \frac{\left(\sum_{i=1}^N x_i d_i \right)^2}{\sum_{i=1}^N d_i^2} \right) \right) \\
 &= \exp \left(\frac{\left(\sum_{i=1}^N x_i d_i \right)^2}{2\sigma^2 \sum_{i=1}^N d_i^2} \right) \exp \left(-\frac{\sqrt{\sum_{i=1}^N d_i^2}}{2\sigma^2} \left(\frac{\sum_{i=1}^N x_i d_i}{\sum_{i=1}^N d_i^2} - \delta \right)^2 \right) \\
 &= \frac{1}{A} \exp \left(\frac{\left(\sum_{i=1}^N x_i d_i \right)^2}{2\sigma^2 \sum_{i=1}^N d_i^2} \right) f_G \left(\sqrt{\frac{1}{\sum_{i=1}^N d_i^2}} \left(\sum_{i=1}^N x_i d_i - \sum_{i=1}^N d_i^2 \delta \right) \right) \tag{E.4}
 \end{aligned}$$

By substituting Equations (E.3) and (E.4) into Equation (6.11),

$$\begin{aligned}
 g(\{x\}) &= \frac{1}{\delta_2 - \delta_1} \left(\frac{1}{\sigma\sqrt{2\pi}} \right)^{N-1} \exp \left(-\frac{\sum_{j=1}^N x_j^2}{2\sigma^2} + \frac{\left(\sum_{i=1}^N x_i d_i \right)^2}{2\sigma^2 \sum_{i=1}^N d_i^2} \right) \cdots \\
 &\quad \int_{\delta_1}^{\delta_2} f_G \left(\frac{\sum_{i=1}^N (x_i d_i) - \sum_{i=1}^N d_i^2 \delta}{\sqrt{\sum_{i=1}^N d_i^2}} \right) d\delta \tag{E.5}
 \end{aligned}$$

The integrand in Equation E.5 can be calculated using the values of the cumulative distribution function of the normal distribution at $\delta = \delta_1$ and δ_2 .

Appendix F

The Fundamental Mistuning Model (FMM) and FMM-ID algorithms

(The derivation in this section is based on Reference [35].)

F.1 The Fundamental Mistuning Model (FMM) algorithm

The Fundamental Mistuning Model (FMM) algorithm was first developed to find the natural frequencies and mode shapes of an isolated mode family of a mistuned blisk, denoted ω_M and $\{\beta_M\}$, respectively, using three pieces of information:

1. A diagonal matrix with the entries being the tuned natural frequencies of the mode family considered in the tuned blisk design, $[\omega]$
2. The tuned mode shapes of the mode family considered in the tuned blisk design, $[\Psi]$. Travelling modes are required in the FMM algorithm, which means $[\Psi]$ is complex:

$$[\Psi] = [\{\psi_0\} \{\psi_{1F}\} \{\psi_{2F}\} \cdots \{\psi_{2B}\} \{\psi_{1B}\}] \quad (\text{F.1})$$

$\{\psi_{nF}\}$ and $\{\psi_{nB}\}$ refer to n ND forward- and backward-travelling modes, respectively.

3. The mistuning pattern of the mistuned blisk, in terms of the natural frequency deviation of a sector, $\{x\}$

A good example of an isolated mode family is the first mode family shown in Figure A.1, as the natural frequencies of an isolated mode family are well separated from those of other mode families. The FMM algorithm can represent the properties of a mistuned blisk by using a system of N equations. There exists a second, but implicit, assumption, that mistuning in a blisk perturbs the stiffness matrix only.

The derivation begins with dividing both stiffness and mass matrices in a mistuned blisk into the tuned and the mistuned parts. The natural frequencies and mode shapes of a mistuned blisk can be found by evaluating Equation (F.2):

$$([K] + [\Delta K] - \omega_M^2 ([M] + [\Delta M])) \{\psi_M\} = \{0\} \quad (\text{F.2})$$

Because the family of modes is isolated, the behaviour of a mistuned blisk within the natural frequency range of that family of modes can be approximated by the properties related to these N modes in a family, denoted $[\Psi]$. As a result, a mistuned mode is approximated by the weighted sum of the N modes:

$$\{\psi_M\} = [\Psi] \{\beta_M\} \quad (\text{F.3})$$

Equation (F.2) is pre-multiplied by the Hermitian transpose of $[\Psi]$, denoted $[\Psi]^H$, to become

$$[\Psi]^H ([K] + [\Delta K] - \omega_M^2 ([M] + [\Delta M])) [\Psi] \{\beta_M\} = \{0\} \quad (\text{F.4})$$

Because $[\Psi]^H [K] [\Psi] = [\omega^2]$, which is a diagonal matrix with squares of natural frequencies of the tuned blisk, and $[\Psi]^H [M] [\Psi] = [I]$, Equation (F.4) becomes

$$\begin{aligned} \left([\omega^2] + [\Psi]^H [\Delta K] [\Psi] - \omega_M^2 [I] - \omega_M^2 [\Psi]^H [\Delta M] [\Psi] \right) \{\beta_M\} &= \{0\} \\ \left([\omega^2] + [\Psi]^H [\Delta K] [\Psi] - \omega_M^2 [\Psi]^H [\Delta M] [\Psi] \right) \{\beta_M\} &= \omega_M^2 \{\beta_M\} \end{aligned} \quad (\text{F.5})$$

The FMM algorithm treats Equation (F.5) as an eigenvalue-eigenvector problem, with natural frequencies of the mistuned blisk, ω_M^2 , and weighting factors, $\{\beta_M\}$, being the eigenvalues and eigenvectors of the matrix in the parentheses. Such an eigenvalue-eigenvector analysis implicitly assumes that

only the stiffness matrix is perturbed. In a normal eigenvalue-eigenvector analysis, every eigenvector is normalised such that $\{\beta_M\}^H \{\beta_M\} = 1$. Also, the modal mass of the mistuned blisk related to any particular mode delivered by the FMM algorithm, $\{\psi_M\}$, is

$$\begin{aligned} \{\psi_M\}^H [M_M] \{\psi_M\} &= \{\beta_M\}^H [\Psi]^H ([M] + [\Delta M]) [\Psi] \{\beta_M\} \\ &= \{\beta_M\}^H [\Psi]^H [M] [\Psi] \{\beta_M\} + \{\beta_M\}^H [\Psi]^H [\Delta M] [\Psi] \{\beta_M\} \\ &= \underbrace{\{\beta_M\}^H \{\beta_M\}}_{=1} + \{\beta_M\}^H [\Psi]^H [\Delta M] [\Psi] \{\beta_M\} \end{aligned} \quad (\text{F.6})$$

As a result, the mode shapes delivered by the FMM algorithm are true mode shapes of the blisk only if $[\Delta M] = [0]$, i.e. mistuning perturbs the entries in the stiffness matrix only.

If the matrix product $[\Psi]^H [\Delta K] [\Psi]$ in Equation (F.6) is denoted $[A]$, Equation (F.6) becomes

$$([\omega^2] + [A]) \{\beta_M\} = \omega_M^2 \{\beta_M\} \quad (\text{F.7})$$

The remainder of the derivation is dedicated to finding the structure of the matrix $[A]$. If the perturbation of the stiffness matrix is confined within individual sectors (e.g. within blades), $[\Delta K]$ is a block diagonal matrix. The m^{th} -row, n^{th} -column entry in matrix $[A]$ can be written as

$$A_{mn} = \{\psi_m\}^H \begin{bmatrix} \Delta K_0 & & & 0 \\ & \Delta K_1 & & \\ & & \ddots & \\ 0 & & & \Delta K_{(N-1)} \end{bmatrix} \{\psi_n\} \quad (\text{F.8})$$

It is assumed that i , m and n are counted from 0 to $(N - 1)$ in this analysis. To simplify Equation (F.8), the entries in each tuned mode shape $\{\psi\}$ can be divided into N groups according to the location of the DOF:

$$\{\psi\}^H = \left\{ \{\psi_{(0)}\}^H, \{\psi_{(1)}\}^H, \dots, \{\psi_{(N-1)}\}^H \right\} \quad (\text{F.9})$$

By substituting Equation (F.9) into Equation (F.8), and considering only the perturbation in one sector (e.g. Sector 0) only,

$$\{\psi_m\}^H \begin{bmatrix} \Delta K_0 & & & 0 \\ & 0 & & \\ & & \ddots & \\ 0 & & & 0 \end{bmatrix} \{\psi_n\} = \{\psi_{m(0)}\}^H [\Delta K_0] \{\psi_{n(0)}\} \quad (\text{F.10})$$

By repeating the approach in Equation (F.10) in every sector,

$$A_{mn} = \sum_{i=0}^{N-1} \{\psi_{m(i)}\}^H [\Delta K_i] \{\psi_{n(i)}\} \quad (\text{F.11})$$

Because travelling modes are used in the FMM algorithm, the mode shape over Sector i , $\{\psi_{(i)}\}$, is the phase shift of the mode shape over Sector 0, $\{\psi_{(0)}\}$. Equation (F.11) can be simplified to become Equation (F.12):

$$A_{mn} = \sum_{i=0}^{N-1} \exp\left(\frac{j2\pi(m-n)i}{N}\right) \{\psi_{m(0)}\}^H [\Delta K] \{\psi_{n(0)}\} \quad (\text{F.12})$$

The existence of two different modal quantities - $\{\psi_m\}$ and $\{\psi_n\}$ - in Equation (F.12) can be eliminated because any sector mode shape in an isolated mode family can be replaced by a blade-alone mode, denoted $\{\psi_b\}$, as they are of similar shapes. The difference between the magnitudes of a blade-alone mode and a sector mode of the whole blisk is the product of $1/\sqrt{N}$ and a scaling factor, which is determined as the ratio of the tuned natural frequency for Mode m (or n) to the sector-alone natural frequency, ω_b . After the replacement, Equation (F.12) becomes

$$A_{mn} = \sum_{i=0}^{N-1} \exp\left(\frac{j2\pi(m-n)i}{N}\right) \frac{\omega_m \omega_n}{N \omega_b^2} \{\psi_b\}^H [\Delta K_i] \{\psi_b\} \quad (\text{F.13})$$

The relationship between the sector frequency deviation of Sector i , x_i , and the stiffness perturbation of that sector, $[\Delta K_i]$, is found by calculating

the Rayleigh quotient of Sector i :

$$\begin{aligned} (\omega_b (1 + x_i))^2 &= \frac{\{\psi_b\}^H ([K_b] + [\Delta K_i]) \{\psi_b\}}{\{\psi_b\}^H [M_b] \{\psi_b\}} \\ 2\omega_b^2 x_i &\approx \{\psi_b\}^H [\Delta K_i] \{\psi_b\} \end{aligned} \quad (\text{F.14})$$

Matrices $[K_b]$ and $[M_b]$ in Equation (F.14) are the sector-alone stiffness and mass matrices respectively. Substituting Equation (F.14) into Equation (F.13) gives

$$A_{mn} = \frac{2\omega_m \omega_n}{N} \sum_{i=0}^{N-1} \exp\left(\frac{j2\pi(m-n)i}{N}\right) x_i \quad (\text{F.15})$$

It can be seen that the summation in Equation (F.15) is identical over a diagonal of $[A]$ and is the discrete Fourier transform of the mistuning pattern. By writing

$$\tilde{x}_n = \frac{1}{N} \sum_{i=0}^{N-1} \exp\left(\frac{-j2\pi ni}{N}\right) x_i \quad (\text{F.16})$$

The matrix $[A]$ can be written as

$$[A] = 2 [\omega] \begin{bmatrix} \tilde{x}_0 & \tilde{x}_1 & \dots & \tilde{x}_{(N-1)} \\ \tilde{x}_{(N-1)} & \tilde{x}_0 & & \tilde{x}_{(N-2)} \\ \vdots & & \ddots & \vdots \\ \tilde{x}_1 & \tilde{x}_2 & \dots & \tilde{x}_0 \end{bmatrix} [\omega] = 2 [\omega] [\tilde{x}] [\omega] \quad (\text{F.17})$$

As a result, Equation (F.7) becomes

$$([\omega^2] + 2 [\omega] [\tilde{x}] [\omega]) \{\beta_M\} = \omega_M^2 \{\beta_M\} \quad (\text{F.18})$$

F.2 The FMM-ID algorithm

Feiner and Griffin [35] created an mistuning identification algorithm on top of the FMM algorithm and called it the FMM-ID algorithm. The fundamental FMM-ID algorithm, called the *basic FMM-ID*, identifies the mistuning pattern of a blisk, $\{x\}$, using

1. all N' identified natural frequencies of a mode family in the mistuned blisk, $[\omega_M]$;
2. all N' identified mode shapes of a mode family in the mistuned blisk, $[\Psi_M]$;
3. the natural frequencies of a mode family in the tuned blisk design, $[\omega]$; and
4. the mode shapes of a mode family in the tuned blisk design, $[\Psi]$. This is not required in the original derivation shown in Reference [36], but inclusion of mode shape information can improve the quality of the identification.

On top of the basic FMM-ID, they have created three additional variants of the algorithm: basic-extended FMM-ID, advanced FMM-ID and advanced-extended FMM-ID. In the FMM-ID-related terminology, “extended” means the capability of identifying the variation of the level of damping on blades, and “advanced” refers to the capability of identifying the mistuning pattern without the use of the tuned natural frequencies. All variants of the FMM-ID algorithms can identify the mistuning pattern if not all N modes in a family are identified.

To conform to the context of this thesis, only the basic and the basic-extended FMM-ID algorithms are discussed in the current section. The derivations of the two algorithms are largely identical except at the final stage.

The derivation begins with finding the relationship between one identified mode shape (with the corresponding natural frequency) and the mistuning pattern. The terms in Equation (F.18) are rearranged into the following form:

$$2[\omega][\tilde{x}][\omega]\{\beta_M\} = (\omega_M^2[I] - [\omega^2])\{\beta_M\} \quad (\text{F.19})$$

where the vector $\{\beta_M\}$ is evaluated by carrying out Equation (F.3) in an opposite direction:

$$\{\beta_M\} = [\Psi]^{-1}\{\psi_M\} \quad (\text{F.20})$$

The unknown in Equation (F.19) is the Fourier transform of the mistuning pattern, $[\tilde{x}]$. The left hand side of Equation (F.19) is rewritten in two steps:

1. A new vector, $\{\gamma_M\}$, is created:

$$\{\gamma_M\} = [\omega] \{\beta_M\} \quad (\text{F.21})$$

such that the left hand side of Equation (F.19) becomes

$$2 [\omega] [\tilde{x}] \{\gamma_M\} \quad (\text{F.22})$$

2. The product between a circulant matrix, $[\tilde{x}]$, and a vector, $\{\gamma_M\}$, in Equation (F.22) is transformed into a product between a Hankel matrix, $[\Gamma_M]$, and a vector, $\{\tilde{x}\}$, where

$$[\Gamma_M] = \begin{bmatrix} \gamma_{M0} & \gamma_{M1} & \cdots & \gamma_{M(N-1)} \\ \gamma_{M1} & \gamma_{M2} & \cdots & \gamma_{M0} \\ \vdots & \vdots & & \vdots \\ \gamma_{M(N-1)} & \gamma_{M0} & \cdots & \gamma_{M(N-2)} \end{bmatrix} \quad \{\tilde{x}\} = \begin{Bmatrix} \tilde{x}_0 \\ \tilde{x}_1 \\ \cdots \\ \tilde{x}_{(N-1)} \end{Bmatrix}$$

After the two-step rearrangement, Equation (F.19) becomes

$$2 [\omega] [\Gamma_M] \{\tilde{x}\} = (\omega^2 [I] - [\omega^2]) \{\beta_M\} \quad (\text{F.23})$$

Equation (F.23) gives the relationship between the mistuning pattern of a blisk to one identified mode on a blisk test piece. Usually, more than one measured mode is available, and those modes are also needed to reduce the error. Equation (F.23) is constructed using every identified mode, and all equations are assembled to form Equation (F.24):

$$\begin{bmatrix} 2 [\Omega] [\Gamma_1] \\ 2 [\Omega] [\Gamma_2] \\ \vdots \\ 2 [\Omega] [\Gamma_{N'}] \end{bmatrix} \{\tilde{x}\} = \begin{Bmatrix} (\omega_1^2 [I] - [\Omega^2]) \{\beta_{M1}\} \\ (\omega_2^2 [I] - [\Omega^2]) \{\beta_{M2}\} \\ \vdots \\ (\omega_{N'}^2 [I] - [\Omega^2]) \{\beta_{MN'}\} \end{Bmatrix} \quad (\text{F.24})$$

The number of Equations in Equation (F.24), which is (NN') , exceeds the number of variables in $\{\tilde{x}\}$, N . As a result, a least-squares fit of $\{\tilde{x}\}$ can be found. The identified mistuning parameter of Sector i , x_{Ii} , is found

by calculating the inverse discrete Fourier transform of $\{\tilde{x}\}$:

$$x_{\mathbb{I}i} = \sum_{n=0}^{N-1} \exp\left(\frac{j2\pi ni}{N}\right) \tilde{x}_n \quad (\text{F.25})$$

In the basic FMM-ID algorithm, all identified mistuning parameters $x_{\mathbb{I}i}$ represent the natural frequency deviations of blades. The identified mistuning parameters are supposed to be real, and the imaginary part of each $x_{\mathbb{I}i}$ is removed. However, the basic extended FMM-ID algorithm makes use of the imaginary part of mistuning parameters to find the damping on a blade. The nominal sector-alone natural frequency, ω_b , the natural frequency deviation of Blade i , x_i , and the damping ratio of Blade i , η_i , are related to the identified mistuning parameter in the following way:

$$\omega_b (1 + x_i) (1 + j\eta_i) = \omega_b (1 + \text{Re}(x_{\mathbb{I}i}) + j\text{Im}(x_{\mathbb{I}i})) \quad (\text{F.26})$$

Rearranging the terms gives

$$x_i = \text{Re}(x_{\mathbb{I}i}) \quad (\text{F.27})$$

$$\eta_i = \frac{\text{Im}(x_{\mathbb{I}i})}{1 + \text{Re}(x_{\mathbb{I}i})} \quad (\text{F.28})$$

Appendix G

Parameters of an intentionally-mistuned blisk test piece

Mistuning pattern 2 is imposed on a blisk test piece by installing screws, nuts and washers at blade tips. This is possible as one M3 threaded hole was drilled at each blade tip as part of the original specifications [117]. Before listing the target pattern and the component installed on the blades, it is appropriate to explain the process of finding the components to be installed at blade tips from a mistuning pattern.

Representative components used in the experiment and the masses of those components are listed in Table G.1, where “L” stands for the length of the screw thread in a cap screw, or the full length of a countersunk screw.

Component	Mass (g)	Component	Mass (g)
M3 screws:		M3 washer	0.067
- Countersunk, L12	0.80	M4 washer	0.14
- Cap, L8	0.74	M3 nut	0.33
- Cap, L16	1.07	M6 thin brass nut	1.5

Table G.1: Masses of representative components installed at blade tips.

The relationship between a particular assembly of components and the frequency deviation (i.e. the mistuning parameter) of a blade is found by observing the natural frequency changes of a blisk finite element model with such an assembly added to every blade. It is noted that the exact mass to be installed at a blade tip depends on the assembly.

Illustrations of two representative mistuning assemblies are shown in Figure G.1. Countersunk screws are used on the blade with lightest mistuning mass (Blade 10) and every blade with mistuning mass more than 1.9 g, and cap screws are used in other blades. Threads in all M6 nuts are removed, such that every M6 nut can be attached to an M3 nut by a press fit.

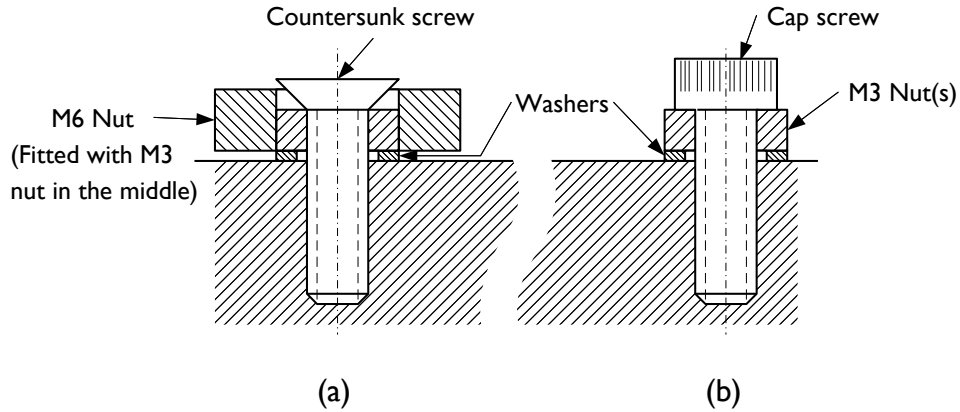


Figure G.1: Mistuning assemblies with (a) countersunk and (b) cap screws.

The combination of components to be installed on a blade tip is chosen such that the total masses of the components is slightly higher than the designed added mass. Extra mass is removed either by filing the M6 screw or by slightly shortening the screw, such that the actual mass is within 0.15g of the designed counterpart.

The details of the components installed at blade tips are listed in Table G.2, and “L” and “C/s” stand for “length of screw” and “countersunk” respectively.

Appendix G. Parameters of an intentionally-mistuned blisk test piece

Table G.2: Masses and components installed in Mistuning pattern 2.

Blade	Frequency deviation	Added mass (g)		Components		
		Designed	Actual	Screw	Nuts	Washers
1	-0.0320	1.178	1.180	Cap, L10	M3	1×M3
2	-0.0488	1.785	1.790	Cap, L16	2×M3	1×M3
3	-0.0650	2.601	2.587	C/s, L16	M3+M6	1×M4
4	-0.0214	0.763	0.775	Cap, L8	-	1×M3
5	-0.0346	1.287	1.296	Cap, L12	M3	1×M3
6	-0.0585	2.305	2.289	C/s, L12	M3+M6	1×M3
7	-0.0503	1.940	1.944	C/s, L10	M3+M6	1×M3
8	-0.0422	1.511	1.520	Cap, L16	M3	2×M3
9	-0.0362	1.359	1.367	Cap, L12	M3	1×M3
10	-0.0165	0.582	0.597	C/s, L8	-	2×M3
11	-0.0375	1.407	1.396	Cap, L12	M3	2×M3
12	-0.0586	2.306	2.306	C/s, L12	M3+M6	1×M3
13	-0.0436	1.661	1.663	Cap, L12	2×M3	1×M3
14	-0.0236	0.848	0.865	Cap, L8	-	2×M3
15	-0.0460	1.673	1.674	Cap, L16	2×M3	1×M3
16	-0.0511	1.982	1.976	C/s, L10	M3+M6	1×M3
17	-0.0293	1.070	1.079	Cap, L12	-	2×M3
18	-0.0496	1.913	1.922	C/s, L10	M3+M6	1×M3
19	-0.0561	2.191	2.199	C/s, L12	M3+M6	1×M3
20	-0.0606	2.400	2.393	C/s, L12	M3+M6	1×M3
21	-0.0274	0.990	1.001	Cap, L12	-	1×M3
22	-0.0529	2.054	2.056	C/s, L8	M3+M6	1×M3
23	-0.0672	2.696	2.685	C/s, L16	M3+M6	2×M3
24	-0.0519	2.009	2.014	C/s, L8	M3+M6	1×M3

References

- [1] AFOLABI, D., AND ALABI, B. Catastrophe theory, curve veering and the vibration of bladed discs. *Proceedings of the Institution of Mechanical Engineers, Part C: Mechanical Engineering Science* 206, 2 (1992), 143–144.
- [2] AFOLABI, D. H. *Vibration of Mistuned Bladed Disc Assemblies*. PhD thesis, University of London, 1982.
- [3] ARMSTRONG, E. K. *An investigation into the coupling between turbine disc and blade vibrations*. PhD thesis, University of Cambridge, 1955.
- [4] ASMUSSEN, S., AND GLYNN, P. W. *Stochastic Simulation*. Springer, New York, USA, 2007.
- [5] AYERS, J. P., FEINER, D. M., AND GRIFFIN, J. H. Reducing mistuning effects by optimally switching blades. In *Proceedings of the 10th National Turbine Engine High Cycle Fatigue Conference* (2005).
- [6] BAH, M. T., BHASKAR, A., AND KEANE, A. J. Model-order reduction and pass-band based calculations for disordered periodic structures. *Journal of Sound and Vibration* 256, 4 (2002), 605–627.
- [7] BAH, M. T., NAIR, P. B., BHASKAR, A., AND KEANE, A. J. Forced response statistics of mistuned bladed disks: a stochastic reduced basis approach. *Journal of Sound and Vibration* 263, 2 (2003), 377–397.
- [8] BAIK, S., CASTANIER, M. P., AND PIERRE, C. Mistuning sensitivity prediction of bladed disks using eigenvalue curve veerings. In *Proceedings of the 9th National Turbine Engine High Cycle Fatigue Conference* (Pinehurst, NC, 2004).

REFERENCES

- [9] BEIROW, B., KÜHHORN, A., AND SCHRAPE, S. Influence of air flow on blisk vibration behaviour. In *1st CEAS European Air and Space Conference (2007)*.
- [10] BENDIKSEN, O. Localization phenomena in structural dynamics. *Chaos, Solitons and Fractals* 11, 10 (2000), 1621 – 1660.
- [11] BEYER, H.-G., AND SENDHOFF, B. Robust optimization - a comprehensive survey. *Computing methods in applied mechanics and engineering* 196 (2007), 3190–3218.
- [12] BLADH, R., CASTANIER, M. P., AND PIERRE, C. Reduced order modeling and vibration analysis of mistuned bladed disk assemblies with shrouds. *Transactions of the ASME. Journal of Engineering for Gas Turbines and Power* 121, 3 (1999), 515–522.
- [13] BLADH, R., CASTANIER, M. P., AND PIERRE, C. Component-mode-based reduced order modeling techniques for mistuned bladed disks- Part I: Theoretical models. *Transactions of the ASME. Journal of Engineering for Gas Turbines and Power* 123, 1 (2001), 89–99.
- [14] BLADH, R., CASTANIER, M. P., AND PIERRE, C. Effects of multi-stage coupling and disk flexibility on mistuned bladed disk dynamics. *Transactions of the ASME. Journal of Engineering for Gas Turbines and Power* 125, 1 (2003), 121–130.
- [15] BLADH, R., PIERRE, C., CASTANIER, M. P., AND KRUSE, M. J. Dynamic response predictions for a mistuned industrial turbomachinery rotor using reduced-order modeling. *Transactions of the ASME. Journal of Engineering for Gas Turbines and Power* 124, 2 (2002), 311–324.
- [16] BUSSMANN, M., AND BAYER, E. Market-oriented blisk manufacturing A challenge for production engineering. In *the 1st European Air and Space Conference (CEAS 2007) (2007)*.
- [17] CAMBRIDGE UNIVERSITY PRESS. *Cambridge Advanced Learner’s Dictionary*. Cambridge University Press, 2008.
- [18] CAPIEZ-LERNOUT, E., SOIZE, C., LOMBARD, J. P., DUPONT, C., AND SEINTURIER, E. Blade manufacturing tolerances definition for a mistuned industrial bladed disk. *Transactions of the ASME. Journal of Engineering for Gas Turbines and Power* 127, 3 (2005), 621–628.

REFERENCES

- [19] CASTANIER, M. P., OTTARSSON, G., AND PIERRE, C. Reduced order modeling technique for mistuned bladed disks. *Transactions of the ASME. Journal of Vibration and Acoustics* 119, 3 (1997), 439–447.
- [20] CASTANIER, M. P., AND PIERRE, C. Individual and interactive mechanisms for localization and dissipation in a mono-coupled nearly-periodic structure. *Journal of Sound and Vibration* 168, 3 (1993), 479 – 505.
- [21] CASTANIER, M. P., AND PIERRE, C. Consideration on the benefits of intentional blade mistuning for the forced response of turbomachinery rotors. In *American Society of Mechanical Engineers, Aerospace Division (Publication) AD* (Dallas, TX, USA, 1997), vol. 55, ASME, Fairfield, NJ, USA, pp. 419–425.
- [22] CASTANIER, M. P., AND PIERRE, C. Predicting localization via lyapunov exponent statistics. *Journal of Sound and Vibration* 203, 1 (1997), 151 – 157.
- [23] CASTANIER, M. P., AND PIERRE, C. Modeling and analysis of mistuned bladed disk vibration: Status and emerging directions. *Journal of Propulsion and Power* 22, 2 (2006), 384–396.
- [24] CHEN, W., ALLEN, J., TSUI, K.-L., AND MISTREE, F. Procedure for robust design: Minimizing variations caused by noise factors and control factors. *Journal of Mechanical Design, Transactions of the ASME* 118, 4 (1996), 478 – 485.
- [25] CHOI, B. K., LENTZ, J., RIVAS-GUERRA, A. J., AND MIGNOLET, M. P. Optimization of intentional mistuning patterns for the reduction of the forced response effects of unintentional mistuning: Formulation and assessment. *Transactions of the ASME. Journal of Engineering for Gas Turbines and Power* 125, 1 (2003), 131–140.
- [26] CONSTANT, H. *Development of the British Gas Turbine Unit*. ASME, 1947.
- [27] DEHNAD, K., Ed. *Quality Control, Robust Design, and the Taguchi Method*. Wadsworth & Brooks/Cole, 1989.
- [28] DI MAIO, D. *SLDV technology for measurement of mistuned bladed disc vibration*. PhD thesis, Imperial College London, 2007.

REFERENCES

- [29] DU, X., AND CHEN, W. Towards a better understanding of modeling feasibility robustness in engineering design. *Transactions of the ASME. Journal of Mechanical Design* 122 (2000), 385–394.
- [30] DYE, R., AND HENRY, T. Vibration amplitudes of compressor blades resulting from scatter in blade natural frequencies. *Journal of Engineering for Power* 91 (1969), 182 – 188.
- [31] EWINS, D. J. Effects of detuning upon forced vibrations of bladed disks. *Journal of Sound and Vibration* 9, 1 (1969), 65–79.
- [32] EWINS, D. J. Vibration characteristics of bladed disc assemblies. *Journal of Mechanical Engineering Science* 15, 3 (1973), 165 – 186.
- [33] EWINS, D. J. The effects of blade mistuning on vibration response: A survey. In *IFTToMM 4th International Conference on Rotordynamics* (Prague, Czech Republic, 1991).
- [34] EWINS, D. J. *Modal testing: Theory, practice and application*, 2 ed. Research Studies Press, 2000.
- [35] FEINER, D. M., AND GRIFFIN, J. H. Mistuning identification of bladed disks using a fundamental mistuning model - Part I: Theory. *Transactions of the ASME. Journal of Turbomachinery* 126, 1 (2004), 150–158.
- [36] FEINER, D. M., AND GRIFFIN, J. H. Mistuning identification of bladed disks using a fundamental mistuning model - Part II: Application. *Transactions of the ASME. Journal of Turbomachinery* 126, 1 (2004), 159–165.
- [37] FISHER, R. A. *Design of experiments*. Oliver & Boyd, 1951.
- [38] FONSECA, J. R., FRISWELL, M. I., AND LEES, A. W. Efficient robust design via monte carlo sample reweighting. *International Journal for Numerical Methods in Engineering* 69 (2007), 2279–2301.
- [39] FRISWELL, M. I. The derivatives of repeated eigenvalues and their associated eigenvectors. *Transactions of the ASME. Journal of Vibration and Acoustics* 118 (1996), 390–397.
- [40] GANINE, V., LEGRAND, M., MICHALSKA, H., AND PIERRE, C. A sparse preconditioned iterative method for vibration analysis of

REFERENCES

- geometrically mistuned bladed disks. *Computers and Structures* 87 (2009), 342–354.
- [41] GARRISON, B. High cycle fatigue (HCF) science and technology program 2000 annual report. Tech. Rep. AFRL-PR-WP-TR-2001-2010, Propulsion Directorate, Air Force Research Laboratory, Air Force Material Command, Wright-Patterson AFB, 2000.
- [42] GHANEM, R. G., AND SPANOS, P. D. *Stochastic Finite Elements: A Spectral Approach*. Dover Publications, 1991.
- [43] GRIFFIN, J. H., AND FEINER, D. M. Determination of damping in bladed disk systems using the fundamental mistuning model. US Patent 7,206,709, 2007.
- [44] GRIFFIN, J. H., AND HOOSAC, T. M. Model development and statistical investigation of turbine blade mistuning. *Journal of Vibration, Acoustics, Stress, and Reliability in Design* 106, 2 (1984), 204 – 210.
- [45] HAN, J. S., AND KWAK, B. M. Robust optimal design of a vibratory microgyroscope considering fabrication errors. *Journal of micromechanics and microengineering* 11 (2001), 662–671.
- [46] HE, Z., EPUREANU, B. I., AND PIERRE, C. Fluid-structural coupling effects on the dynamics of mistuned bladed disks. *AIAA Journal* 45, 3 (2007), 552–561.
- [47] HOLDEN, A. V. *Chaos*. Manchester University Press, 1986.
- [48] HUANG, B., AND KUANG, J. Mode localization in a rotating mistuned turbo disk with coriolis effect. *International Journal of Mechanical Sciences* 43, 7 (2001), 1643 – 1660.
- [49] HUNTER, W. A., AND GRIMMER, G. A. T700 blisk and impeller manufacturing process development program. Tech. Rep. ADA093877, General Electric Company, November 1979.
- [50] ICATS. *MODENT users guide*, February 2006.
- [51] IMREGUN, M., AND EWINS, D. J. Aeroelastic vibration analysis of tuned and mistuned bladed systems. In *Proceedings of the 2nd Symposium on Unsteady Aerodynamics of Turbomachines and Propellers* (Cambridge, UK, 1984).

REFERENCES

- [52] JONES, K. Minimizing maximum modal force in mistuned bladed disk forced response. *Transactions of the ASME. Journal of Turbomachinery* 130 (April 2008), 011011.
- [53] JUDGE, J. A., CECCIO, S. L., AND PIERRE, C. Traveling-wave excitation and optical measurement techniques for non-contacting investigation of bladed disk dynamics. *Shock and Vibration Digest* 35, 3 (May 2003), 183–190.
- [54] KAHL, G. Mistuning and coupling effects in turbomachinery bladings. In *Unsteady aerodynamics, aeroacoustics and aeroelasticity of turbomachines*, K. C. Hall, R. E. Kielb, and J. P. Thomas, Eds. Springer Netherlands, 2006, pp. 119–131.
- [55] KANEKO, Y., MASE, M., FUJITA, K., AND NAGASHIMA, T. Vibrational response analysis of mistuned bladed disk. *JSME International Journal, Series C: Dynamics, Control, Robotics, Design and Manufacturing* 37, 1 (1994), 33–40.
- [56] KENYON, J. A., AND GRIFFIN, J. H. Forced response of turbine engine bladed disks and sensitivity to harmonic mistuning. *Transactions of the ASME. Journal of Engineering for Gas Turbines and Power* 125, 1 (2003), 113–120.
- [57] KENYON, J. A., GRIFFIN, J. H., AND FEINER, D. M. Maximum bladed disk forced response from distortion of a structural mode. *Transactions of the ASME. Journal of Turbomachinery* 125, 2 (2003), 352–63.
- [58] KENYON, J. A., GRIFFIN, J. H., AND KIM, N. E. Sensitivity of tuned bladed disk response to frequency veering. *Transactions of the ASME. Journal of Engineering for Gas Turbines and Power* 127, 4 (2005), 835–42.
- [59] KIELB, R. E., FEINER, D. M., GRIFFIN, J. H., AND MIYAKOZAWA, T. Probabilistic analysis of mistuned bladed disks and blisks with aerodynamic and fmm structural coupling. In *9th National Turbine Engine HCF Conference* (Pinehurst, NC, March 2004).
- [60] KLAUKE, T., KÜHHORN, A., BEIROW, B., AND GOLZE, M. Numerical investigations of localized vibrations of mistuned blade integrated

REFERENCES

- disks blisks. *Transactions of the ASME. Journal of Turbomachinery* 131 (2009), 031002.
- [61] LAW, A. M. *Simulation modeling and analysis*. McGraw-Hill, 1982.
- [62] LAXALDE, D., THOUVEREZ, F., SINOU, J.-J., LOMBARD, J.-P., AND BAUMHAUER, S. Mistuning identification and model updating of an industrial blisk. *International Journal of Rotating Machinery Article ID 17289* (2007), 10pp. doi:10.1155/2007/17289.
- [63] LEE, K.-H., EOM, I.-S., PARK, G.-J., AND LEE, W.-I. Robust design for unconstrained optimization problems using the Taguchi method. *AIAA Journal* 37, 5 (1996), 1059–1063.
- [64] LEE, K.-H., AND PARK, G.-J. Robust optimization considering tolerances of design variables. *Computers and Structures* 79 (2001), 77–86.
- [65] LIM, S.-H., BLADH, R., CASTANIER, M. P., AND PIERRE, C. A compact, generalized component mode mistuning representation for modeling bladed disk vibration. *Collection of Technical Papers - AIAA/ASME/ASCE/AHS/ASC Structures, Structural Dynamics and Materials Conference 2* (2003), 1359 – 1380.
- [66] LIM, S.-H., CASTANIER, M. P., AND PIERRE, C. Intentional mistuning design space reduction based on vibration energy flow in bladed disks. *Proceedings of the ASME Turbo Expo 2004 6* (2004), 373 – 384.
- [67] LIM, S. H., CASTANIER, M. P., AND PIERRE, C. Predicting mistuned blade amplitude bounds and stress increases from energy formulations. In *9th National Turbine Engine HCF Conference* (2004).
- [68] LIN, C. C., AND MIGNOLET, M. P. Effects of damping and damping mistuning on the forced vibration response of bladed disks. *Journal of Sound and Vibration* 193, 2 (1996), 525–543.
- [69] MACBAIN, J. C., AND WHALEY, P. W. Maximum resonant response of mistuned bladed disks. *Journal of Vibration, Acoustics, Stress, and Reliability in Design* 106, 2 (1984), 218 – 223.
- [70] MADDEN, A. C., CASTANIER, M. P., AND EPUREANU, B. I. Reduced-order model construction procedure for robust mistuning identification of blisks. *AIAA Journal* 46, 11 (2008), 2890–2898.

REFERENCES

- [71] MARTEL, C., AND CORRAL, R. Asymptotic description of maximum mistuning amplification of bladed disk forced response. *Transactions of the ASME. Journal of Engineering for Gas Turbines and Power* 131 (2009), 022506.
- [72] MIGNOLET, M. P., HU, W., AND JADIC, I. On the forced response of harmonically and partially mistuned bladed disks. Part I: Harmonic mistuning. *International Journal of Rotating Machinery* 6, 1 (2000), 29–41.
- [73] MIGNOLET, M. P., HU, W., AND JADIC, I. On the forced response of harmonically and partially mistuned bladed disks. Part II: Partial mistuning and applications. *International Journal of Rotating Machinery* 6, 1 (2000), 43–56.
- [74] MIGNOLET, M. P., AND LIN, C.-C. Identification of structural parameters in mistuned bladed disks. *Transactions of the ASME. Journal of Vibration and Acoustics* 119, 3 (1997), 428–438.
- [75] MULVEY, J. M., VANDERBEI, R. J., AND ZENIOS, S. A. Robust optimization of large-scale systems. *Operations Research* 43 (1995), 264–281.
- [76] MURPHY, T. E., TSUI, K.-L., AND ALLEN, J. K. A review of robust design methods for multiple responses. *Research in Engineering Design* 16 (2005), 118–132.
- [77] MUSZYNSKA, A., AND JONES, D. I. G. On tuned bladed disk dynamics: some aspects of friction related mistuning. *Journal of Sound and Vibration* 86, 1 (1983), 107–128.
- [78] MYHRE, M. *Numerical investigation of the sensitivity of forced response characteristics of bladed disks to mistuning*. Licentiate thesis, KTH The Royal Institute of Technology, Sweden, 2003.
- [79] NAIR, V. N., ABRAHAM, B., MACKAY, J., NELDER, J. A., BOX, G., PHADKE, M. S., KACKER, R. N., SACKS, J., WELCH, W. J., LORENZEN, T. J., SHOEMAKER, A. C., TSUI, K. L., LUCAS, J. M., TAGUCHI, S., MYERS, R. H., GEOFFREY VINING, G., AND WU, C. F. J. Taguchi's parameter design: A panel discussion. *Technometrics* 34, 2 (May 1992), 127–161.

REFERENCES

- [80] NIKOLIC, M. *New insights into the blade mistuning problem*. PhD thesis, Imperial College London, 2006.
- [81] NIKOLIC, M., PETROV, E. P., AND EWINS, D. J. Coriolis forces in forced response analysis of mistuned bladed disks. *Transactions of the ASME. Journal of Turbomachinery* 129, 4 (2007), 730–739.
- [82] NIKOLIC, M., PETROV, E. P., AND EWINS, D. J. Robust strategies for forced response reduction of bladed disks based on large mistuning concept. *Transactions of the ASME. Journal of Engineering for Gas Turbines and Power* 130 (2008), 022501.
- [83] ÓTTARSSON, G., AND PIERRE, C. A transfer matrix approach to free vibration localization in mistuned blade assemblies. *Journal of Sound and Vibration* 197, 5 (1996), 589–618.
- [84] ÓTTARSSON, G. S. *Dynamic modeling and vibration analysis of mistuned bladed disks*. PhD thesis, University of Michigan, 1994.
- [85] PARK, G.-J., LEE, T.-H., LEE, K. H., AND HWANG, K.-H. Robust design: an overview. *AIAA Journal* 44, 1 (2006), 181–191.
- [86] PEASE, B. What’s all this Taguchi stuff, anyhow? *Electronic design* 83 (25 June 1992).
- [87] PETROV, E. P. A method for forced response analysis of mistuned bladed discs with aerodynamic effects included. In *Proceedings of ASME Turbo Expo 2009: Power for Land, Sea and Air* (Orlando, FL, USA, 2009), no. GT2009-59634.
- [88] PETROV, E. P., AND EWINS, D. J. Search for the best blade arrangement in a mistuned bladed disc assembly. In *Proceedings of the 7th National Turbine Engine HCF Conference* (Palm Beach Gardens, Florida, USA, 2002). 11pp.
- [89] PETROV, E. P., AND EWINS, D. J. Analysis of the worst mistuning patterns in bladed disk assemblies. *Transactions of the ASME. Journal of Turbomachinery* 125, 4 (2003), 623–631.
- [90] PETROV, E. P., AND EWINS, D. J. Method for analysis of nonlinear multiharmonic vibrations of mistuned bladed disks with scatter of contact interface characteristics. *Transactions of the ASME. Journal of Turbomachinery* 127, 1 (2005), 128–136.

REFERENCES

- [91] PETROV, E. P., AND EWINS, D. J. Effects of damping and varying contact area at blade-disk joints in forced response analysis of bladed disk assemblies. *Transactions of the ASME. Journal of Turbomachinery* 128, 2 (2006), 403–410.
- [92] PETROV, E. P., AND EWINS, D. J. Advanced modeling of underplatform friction dampers for analysis of bladed disk vibration. *Transactions of the ASME. Journal of Turbomachinery* 129, 1 (2007), 143 – 50.
- [93] PETROV, E. P., AND IGLIN, S. P. Search of the worst and best mistuning patterns for vibration amplitudes of bladed disks by the optimization methods using sensitivity coefficients. In *Proceedings of the 1st ASSMO UK Conference. Engineering Design Optimization* (Ilkley, UK, 1999), pp. 303–310.
- [94] PETROV, E. P., SANLITURK, K. Y., AND EWINS, D. J. A new method for dynamic analysis of mistuned bladed disks based on the exact relationship between tuned and mistuned systems. *Transactions of the ASME. Journal of Engineering for Gas Turbines and Power* 124, 3 (2002), 586–597.
- [95] PETROV, E. P., VITALI, R., AND HAFTKA, R. T. Optimization of mistuned bladed discs using gradient-based response surface approximations. In *Collection of Technical Papers - AIAA/ASME/ASCE/AHS/ASC Structures, Structural Dynamics and Materials Conference* (Atlanta, GA, USA, 2000), vol. 1, American Inst. Aeronautics and Astronautics Inc., Reston, VA, USA, pp. 1129–1139.
- [96] PICHOT, F., LAXALDE, D., SINOUE, J.-J., THOUVEREZ, F., AND LOMBARD, J.-P. Mistuning identification for industrial blisks based on the best achievable eigenvector. *Computers and Structures* 84 (2006), 2033–2049.
- [97] PIERRE, C., AND MURTHY, D. V. Aeroelastic modal characteristics of mistuned blade assemblies: mode localization and loss of eigenstructure. *AIAA Journal* 30, 10 (1992), 2483–2496.
- [98] PIERRE, C., SMITH, T. E., AND MURTHY, D. V. Localization of aeroelastic modes in mistuned high-energy turbines. *Journal of Propulsion and Power* 10, 3 (1994), 318 – 328.

REFERENCES

- [99] PRESS, W. H., TEUKOLSKY, S. A., VETTERLING, W. T., AND FLANNERY, B. P. *Numerical recipes: the art of scientific computing*, 3rd ed. Cambridge University Press, 2007.
- [100] REED, R. C. *The Superalloys: Fundamentals and Applications*. Cambridge University Press, New York, USA, 2006.
- [101] RIVAS-GUERRA, A. J., AND MIGNOLET, M. P. Maximum amplification of blade response due to mistuning: localization and mode shape aspects of the worst disks. *Transactions of the ASME. Journal of Turbomachinery* 125, 3 (2003), 442–54.
- [102] ROLLS-ROYCE PLC, Ed. *The jet engine*, 4th ed. Rolls-Royce plc, 1986.
- [103] ROLLS-ROYCE PLC. BR725: Clean, efficient power for ultra-long-range business jets, April 2008.
- [104] ROLLS-ROYCE PLC. Trent XWB: Optimised for the Airbus A350 XWB family, May 2009.
- [105] ROSSI, M., FEINER, D., AND GRIFFIN, J. Experimental study of the fundamental mistuning model (FMM) for probabilistic analysis. In *Proceedings of the 9th National Turbine Engine HCF Conference* (2004).
- [106] RUBINSTEIN, R. Y., AND KROESE, D. P. *Simulation and the Monte Carlo method*, 2nd ed. ed. Wiley-interscience, 2008.
- [107] RUFFLES, R. C. The future of aircraft propulsion. *Proceedings of the Institution of Mechanical Engineers Part C* 214 (2000), 289–305.
- [108] RZADKOWSKI, R. General model of free vibrations of mistuned bladed discs. part I: Theory. *Journal of Sound and Vibration* 173, 3 (1994), 377–393.
- [109] RZADKOWSKI, R. General model of free vibrations of mistuned bladed discs. part II: Numerical results. *Journal of Sound and Vibration* 173, 3 (1994), 395–413.
- [110] SALHI, B., LARDIES, J., BERTHILLIER, M., VOINIS, P., AND BODEL, C. Modal parameter identification of mistuned bladed disks using tip timing data. *Journal of Sound and Vibration* 314 (2008), 885–906.

REFERENCES

- [111] SANDGREN, E., AND CAMERON, T. M. Robust design optimization of structures through consideration of variation. *Computers and Structures* 80 (2002), 1605–1613.
- [112] SANLITURK, K. Y. *Vibration Analysis of Mistuned Bladed Systems*. PhD thesis, University of London, 1992.
- [113] SANLITURK, K. Y., AND EWINS, D. J. Modelling two-dimensional friction contact and its application using harmonic balance method. *Journal of Sound and Vibration* 193 (1996), 511–523.
- [114] SANLITURK, K. Y., AND IMREGUN, M. Vibration analysis of mistuned bladed-disk assemblies - inverse approach. *AIAA Journal* 32, 4 (1994), 857–865.
- [115] SCARSELLI, G., AND LEECE, L. Non deterministic approaches for the evaluation of the mistune effects on the rotor dynamics. In *AIAA 2004 Conference* (Palm Springs, California, 19 - 22 April 2005).
- [116] SCHUËLLER, G., PRADLWARTER, H. J., AND KOUTSOURELAKIS, P. S. A critical appraisal of reliability estimation procedures for high dimensions. *Probabilistic Engineering Mechanics* 19 (2004), 463–474.
- [117] SEVER, I. A. *Experimental validation of turbomachinery blade vibration predictions*. PhD thesis, University of London, March 2004.
- [118] SHAPIRO, B. Solving for mistuned forced response by symmetry. *Journal of Propulsion and Power* 15, 2 (1999), 310 – 325.
- [119] SHENG, X. Model identification and order response prediction for bladed wheels. *Journal of Sound and Vibration* 323, 1-2 (2009), 194–213.
- [120] SIM, J., QIU, Z., AND WANG, X. Modal analysis of structures with uncertain-but-bounded parameters via interval analysis. *Journal of Sound and Vibration* 303, 1-2 (2007), 29 – 45.
- [121] SINHA, A. Computation of the statistics of forced response of a mistuned bladed disk assembly via polynomial chaos. *Transactions of the ASME. Journal of vibration and acoustics* 128 (2006), 449–457.
- [122] SINHA, A. Reduced-order model of a mistuned multi-stage rotor. In *Proceedings of GT2007: ASME Turbo Expo 2007: Power for Land, Sea and Air* (2007).

REFERENCES

- [123] SINHA, A. Reduced-order model of a bladed rotor with geometric mistuning. *Transactions of the ASME. Journal of Turbomachinery*. 131 (2009), 031007.
- [124] SINHA, A., AND CHEN, S. A higher order technique to compute the statistics of forced response of a mistuned bladed disk. *Journal of Sound and Vibration* 130, 2 (1989), 207–221.
- [125] SLADOJEVIĆ, I. *Forced response analysis of aero-elastically coupled mistuned bladed disks*. PhD thesis, University of London, 2006.
- [126] SONG, S. H., CASTANIER, M. P., AND PIERRE, C. System identification of multistage turbine engine rotors. In *Proceedings of GT2007: ASME Turbo Expo 2007: Power for Land, Sea and Air* (2007).
- [127] SRINIVASAN, A. V. Flutter and resonant vibration characteristics of engine blades. *Transactions of the ASME. Journal of Engineering for Gas Turbines and Power* 119, 4 (1997), 742 – 775.
- [128] TAGUCHI, G. *Design of Experiments*, vol. 1. Maruzen, Tokyo, 1957.
- [129] TAGUCHI, G., CHOWDBURY, S., AND WU, Y. *Taguchi's quality engineering handbook*. John Wiley & Sons, 2004.
- [130] TANG, J., AND WANG, K. W. Vibration delocalization of nearly periodic structures using coupled piezoelectric networks. *Transactions of the ASME. Journal of Vibration and Acoustics* 125 (2003), 95–108.
- [131] THOMSON, D. E., AND GRIFFIN, J. T. The national turbine engine high cycle fatigue program. *Global Gas Turbine News* 39 (1999), 14–17.
- [132] TOBIAS, S. A., AND ARNOLD, R. N. Influence of dynamical imperfection on vibration of rotating disks. *Institution of Mechanical Engineers – Proceedings* 171, 22 (1957), 669–690.
- [133] TROSSET, M. W. Taguchi and Robust Optimization. Tech. Rep. 96-31, Department of Computational & Applied Mathematics, Rice University, Houston, TX, 1996.
- [134] TROSSET, M. W. Managing uncertainty in robust design optimization. In *SNL Workshop on Optimization Under Uncertainty* (January 2004).

REFERENCES

- [135] VAKAKIS, A. F. Dynamics of a nonlinear periodic structure with cyclic symmetry. *Acta Mechanica* 95, 1-4 (1992), 197–226.
- [136] WATSON, B. C., AND KAMAT, M. P. Analysis of mistuned cyclic systems using mistune modes. *Applied Mathematics and computation* 67 (1995), 61–79.
- [137] WEI, S.-T., AND PIERRE, C. Localization phenomena in mistuned assemblies with cyclic symmetry. part I: Free vibrations. *Journal of Vibration, Acoustics, Stress, and Reliability in Design* 110, 4 (1988), 429 – 438.
- [138] WEI, S.-T., AND PIERRE, C. Localization phenomena in mistuned assemblies with cyclic symmetry. part II: Forced vibrations. *Journal of Vibration, Acoustics, Stress, and Reliability in Design* 110, 4 (1988), 439 – 449.
- [139] WELCH, W. J., AND SACKS, J. A system for quality improvement via computer experiments. *Communications in Statistics - Theory and Methods* 20, 2 (1991), 477–495.
- [140] WHITEHEAD, D. S. Effect of mistuning on vibration of turbomachine blades induced by wakes. *Journal of Mechanical Engineering Science* 8, 1 (1966), 15–21.
- [141] WHITEHEAD, D. S. Research note: Effect on mistuning on forced vibration of blades with mechanical coupling. *Journal of Mechanical Engineering Science* 18 (1976), 306–307.
- [142] WHITEHEAD, D. S. The maximum factor by which forced vibration of blades can increase due to mistuning. *Transactions of the ASME. Journal of Engineering for Gas turbines and Power* 120 (1998), 115–119.
- [143] WOLFE, M. A. *Numerical methods for unconstrained optimization - an introduction*. van Nostrand Reinhold, 1978.
- [144] WRIGHT, P. K., JAIN, M., AND CAMERON, D. High cycle fatigue in a single crystal superalloy: time dependence at elevated temperature. In *Superalloys 2004* (Warrendale, PA, 2004), K. A. Green, T. M. Pollock, H. Harada, and et al., Eds., The Minerals, Metals and Materials Society (TMS).

REFERENCES

- [145] XIAO, B. *Blade model identification and maximum amplification of forced response due to mistuning*. PhD thesis, Arizona State University, 2005.
- [146] XIAO, B., RIVAS-GUERRA, A. J., AND MIGNOLET, M. P. Maximum amplification of blade response due to mistuning in multi-degree-of-freedom blade models. *Proceedings of the ASME Turbo Expo 2004 6* (2004), 427 – 438.
- [147] XIE, W.-C., AND ARIARATNAM, S. T. Vibration mode localization in disordered cyclic structures, i: Single substructure mode. *Journal of Sound and Vibration 189*, 5 (1996), 625–645.
- [148] YANG, M.-T., AND GRIFFIN, J. Exploring how shroud constraint can affect vibratory response in turbomachinery. *Transactions of the ASME. Journal of Engineering for Gas Turbines and Power 117*, 1 (1995), 198 – 206.
- [149] YANG, M. T., AND GRIFFIN, J. H. A reduced order approach for the vibration of mistuned bladed disk assemblies. *Transactions of the ASME. Journal of Engineering for Gas Turbines and Power 119*, 1 (1997), 161–167.
- [150] YANG, M. T., AND GRIFFIN, J. H. A reduced-order model of mistuning using a subset of nominal system modes. *Transactions of the ASME. Journal of Engineering for Gas Turbines and Power 123*, 4 (2001), 893–900.
- [151] YIU, H. *Vibration characteristics of mistuned bladed disc assemblies*. PhD thesis, University of London, 1995.
- [152] YOO, H. H., KIM, J. Y., AND INMAN, D. J. Vibration localization of simplified mistuned cyclic structures undertaking external harmonic force. *Journal of Sound and Vibration 261* (2003), 859–870.
- [153] ZANG, C., FRISWELL, M. I., AND MOTTERSHEAD, J. E. A review of robust optimal design and its application in dynamics. *Computers and Structures 83*, 4-5 (2005), 315–326.